

**Faculty of Science  
Department of Imaging and Applied Physics**

**Design of Nanostructured Polymeric Materials for Radiation Shielding of Ionizing  
Radiations**

**Nurul Zahirah Binti Noor Azman**

**This thesis is presented for the Degree of  
Doctor of Philosophy  
of  
Curtin University**

**September 2013**

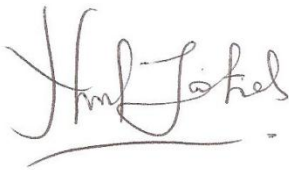
## DECLARATION

---

“To the best of my knowledge and belief this thesis contains no materials previously published by any other person except where due acknowledgement has been made. This thesis contains no material which has been for the award of any other degree or diploma in any thesis.”

Nurul Zahirah Binti Noor Azman

Signature:

A handwritten signature in black ink, appearing to read 'Nurul Zahirah', with a horizontal line underneath.

Date: 5<sup>th</sup> September 2013

## ABSTRACT

---

X-rays were first discovered and studied in the year 1895 by Wilhelm Röntgen, a German physicist. The hazards of X-rays became apparent within a year of their discovery. During the early part of the twentieth century, the potential hazards from X-rays were recognized and the need for an X-ray shield in any application where X-rays are used is now a common knowledge. Without a proper X-ray shield, a person is in a state of very high danger. It is estimated that approximately 0.4% of all diagnosed cancers are due to exposure to X-rays, typically in CT scans and medical applications. While there is background radiation all around us, the exposure to X-rays' investigative apparatus, especially repeated over time, poses the highest risk of cancers and other health complications.

Since then, X-ray shielding requirements have become more stringent with regard to standards for exposure of personnel and the general public. Lead glass is the best known transparent form of X-ray shield, and, with increased understanding of the required density of the lead shields, virtually complete protection can be provided to those who work with X-rays or those who are required to have X-rays. However, glass is heavy, expensive and breakable, and thus more dangerous to handle. Therefore in recent times, polymers have gained much attention from the X-ray shielding technologists as the replacement to lead glass due to their unique properties such as: the ability to form intricate shapes, optical transparency, low manufacturing cost and toughness. In addition, the magnitude of polymer properties has been improved with filler addition during the synthesis process. This study seeks to provide a novel approach for producing technologically viable new radiation shielding materials to meet the safety requirements for use in medical X-ray imaging facilities, based upon the dispersion of heavy element fillers into polymeric materials by different filler dispersion methods. Such a product has high potential application for shielding of X-rays.

The preliminary study aimed to investigate the X-ray attenuation ability of composites prepared from the dispersion of different wt% (10, 30, 50 and 70 wt%) of lead oxides (PbO and Pb<sub>3</sub>O<sub>4</sub>) filler within an epoxy matrix by a traditional method, specifically, the melt-mixing method. A comprehensive literature survey reveals that the X-ray shielding

characteristics of filler-reinforced epoxy resins have not yet been attempted. The effect of the composite's density on the attenuation ability of the composites for radiation shielding purposes was studied using a calibrated general radiology unit. Characterization of the microstructure properties of the synthesized composites was performed using synchrotron radiation diffraction (SRD), optical microscopy (OM) and scanning electron microscopy (SEM). Results indicate that the attenuation ability of the composites increased with an escalation in the composite's density. The phase compositions of PbO and Pb<sub>3</sub>O<sub>4</sub> used were single-phase pure. Meanwhile, microstructural analyses have confirmed the existence of fairly uniform dispersion of fillers within the epoxy matrix with the average particle size of 1–5 μm for composites with filler loading of ≤30 wt% and 5–15 μm for composites with filler loading of ≥50 wt%.

Further investigation was performed using the same procedure for lead chloride (PbCl<sub>2</sub>), bismuth oxide (Bi<sub>2</sub>O<sub>3</sub>) and tungsten oxide (WO<sub>3</sub>) filled epoxy composites of 8 mm thickness, but with extra study added by comparing the X-ray attenuation ability with the 10 mm thickness of commercial lead glass. In addition, this work demonstrates how the mechanical properties of the composites were tested during which their flexural properties and hardness were investigated. As expected, the X-ray transmission by the composite was decreased by the increment of the filler loading, Bi<sub>2</sub>O<sub>3</sub>-epoxy composite having 70 wt% of Bi<sub>2</sub>O<sub>3</sub>. As a result, this gave nearly the same X-ray attenuation ability as compared with lead glass. Meanwhile, the flexural modulus and hardness of the composites were increased through an increase in filler loading. However, the flexural strength showed a marked decrease with the increment of filler loading (≥30 wt%). Some agglomerations were observed for composites having ≥50 wt% of filler.

With the same filler dispersion method as performed by melt-mixing, deeper investigation was undertaken to study the effect of particle size (<100 nm and ~20 μm), filler loadings (5, 10, 20, 30, 35 wt%) and X-ray tube voltage operated by mammography (25-49 kV) and general radiology (40-100 kV) units on the X-ray transmission in 7 mm thickness of WO<sub>3</sub>-epoxy composites. Results indicate that nano-sized WO<sub>3</sub> has a better ability to attenuate the X-ray beam generated by lower tube voltages (25–35 kV) when compared with micro-sized



WO<sub>3</sub> of the same filler loading. However, the effect of particle size on X-ray transmissions was negligible at the higher X-ray tube voltages (40–120 kV).

A similar study was performed for 2 mm thickness of WO<sub>3</sub>-epoxy composites and the X-ray transmission was investigated using X-ray Absorption Spectroscopy (XAS) at the energy of 10-40 keV. Further, in this work, the mechanical properties of the composites were tested, during which their flexural properties and hardness were investigated. The results obtained were used to determine the equivalent X-ray energies for X-ray tube voltages operated by a mammography unit and general radiology unit. The results confirmed the superior attenuation ability of nano-sized WO<sub>3</sub>-epoxy composites in the energy range of 10-25 keV when compared with their micro-sized counterparts. However, at higher energy (i.e. 30-40 keV), the X-ray transmission was similar with no size effect for both nano-sized and micro-sized WO<sub>3</sub>-epoxy composites. The equivalent X-ray energies for X-ray tube voltages operated by a mammography unit (25-49 kV) were in the range 15-25 keV. Similarly, for the general radiology unit of 40-60 kV, the range was 25-40 keV; for voltages greater than 60 kV (i.e. 70-100 kV), the equivalent energy was in excess of 40 keV. The mechanical properties of epoxy composites increased initially with an increase in the filler loading, but increased further in the WO<sub>3</sub> loading, resulting in deterioration of flexural strength, modulus and hardness.

Following that, a new approach for fabricating filler-epoxy matrix by ion-implantation method was conducted. Epoxy samples having 2 mm thickness were implanted with heavy ions (tungsten W, gold Au and lead Pb) in order to investigate the attenuation characteristics of ion-implanted epoxy composites. Near-surface composition depth profiling of the implanted composites was studied using Rutherford Backscattering Spectroscopy (RBS). The effect of implanted ions on the X-ray attenuation was studied with a general radiology unit (40 to 100 kV). Results of the X-ray mass attenuation coefficient ( $\mu_m$ ) for implanted epoxy with ions W, Au and Pb respectively show distinguishably higher ratings than the  $\mu_m$  for the unimplanted epoxy.

This work was continued by implanting W and Pb ions on acrylic and glass so as to investigate their X-ray attenuation characteristics. The results were compared with previous work on ion-implanted epoxy. As predicted, the RBS results and X-ray attenuation for both

ion-implanted acrylic and glass increase with the type of ions implanted when compared with the controls. However, since glass is denser than either epoxy or acrylic, it has provided the higher X-ray attenuation property and higher RBS ion implanted concentration with a shorter range of the ion depth profile when compared to epoxy and acrylic. A prolonged time is necessary for implanting acrylic with a very high nominal dose in order to minimize a heightened possibility of acrylic melting during the process.

Finally, a novel electrospinning method was performed to fabricate the filler-nanofibre mats. Poly lactic acid (PLA) was used as the matrix for nanofibre mat synthesis due to the advantages of PLA in the electrospinning process; while  $\text{Bi}_2\text{O}_3$  particles of sizes 90–210 nm and 10  $\mu\text{m}$  were used as a filler for synthesizing electrospun  $\text{Bi}_2\text{O}_3/\text{PLA}$  nanofibre mats. The characteristics of the X-ray attenuation in electrospun nano(n)- and micro(m)-  $\text{Bi}_2\text{O}_3/\text{PLA}$  nanofibre mats with different  $\text{Bi}_2\text{O}_3$  loadings ( 24, 28, 34 and 38 wt%) were compared as a function of energy using mammography (i.e. tube voltages of 22–49 kV) and X-ray absorption spectroscopy (XAS) (7–20 keV). Results indicate that X-ray attenuation by electrospun n- $\text{Bi}_2\text{O}_3/\text{PLA}$  nanofibre mats is distinctly higher than that of m- $\text{Bi}_2\text{O}_3/\text{PLA}$  nanofibre mats at all energies investigated. In addition, with increasing filler loading (n- $\text{Bi}_2\text{O}_3$  or m- $\text{Bi}_2\text{O}_3$ ), the porosity of the nanofibre mats decreased, thus increasing the X-ray attenuation, except for the sample containing 38 wt%  $\text{Bi}_2\text{O}_3$  (the highest loading in the present study). The latter showed higher porosity, with some beads having formed, thus resulting in a sudden decrease in the X-ray attenuation.

The success in this project indicated that all such final products produced have high potential as candidates for shielding applications of X-rays in diagnostic radiology purposes.

## ACKNOWLEDGEMENTS

---

First and foremost, I would like to express my heartfelt gratitude to my supervisor, Professor Jim Low, for the continuous support of my Ph.D study and research; for his patience, motivation, enthusiasm and immense knowledge. He is one of the smartest and most low-profile persons I know. His guidance helped me during the entire time of research and writing of this thesis. I could not have imagined having a better supervisor and mentor for my Ph.D study. I also admire his personal characteristics, especially his ability to balance research interests and personal pursuits. Despite being extremely busy, he still had time to respond promptly to my emails as early as he could.

In addition, I am deeply grateful to my co-supervisor, Dr. Salim Ahmed Siddiqui, for his expert guidance on radiation protection. The opportunity of working with him has been a great pleasure to me. He has been a steady influence throughout my Ph.D. career; having oriented and supported me with promptness and care, as well as always being patient and encouraging in times of new ideas and difficulties. He has listened to my ideas and discussions with him frequently led to key insights.

My sincere thanks also go to Dr. Mihail Ionescu, as my second co-supervisor, who has helped with all the ion-implantation works and the data collections for ion-beam analyses at Australian Nuclear Science and Technology Organisation (ANSTO). Even though we have not met for a long period of time, his inspiration, enthusiasm and love for helping is contagious. His encouragement in helping me to improve my English has always been remembered.

The financial support for my Ph.D study was provided by the Ministry of Higher Education (MOHE) in Malaysia and also Universiti Sains Malaysia (USM). Without their support, I may not have had the opportunity to further my study and gain more experience in Australia.

This thesis was also co-funded by the Australian Synchrotron and the Australian Institute of Nuclear Science and Engineering (AINSE), and I would like to thank both organisations for

their generous support. I acknowledge their funding for the travel and access costs for many experiments conducted at Australian Synchrotron and ANSTO.

At Australian Synchrotron, I would like to thank Dr. Justin Kimpton, who helped me with Powder Diffraction data collection and analysis. Next, I would like to acknowledge the valuable assistance of Dr. Bernt Johannessen on the collection and analysis of X-ray attenuation data using X-ray Absorption Spectroscopy (XAS).

I will forever be thankful to Dr. Robin Hart and Carolyn Mandeley who gave permission to use the general diagnostic radiography and mammography unit at Royal Perth Hospital. All the X-ray attenuation data collected there has been invaluable in completing my project.

I would also like to express my gratitude to my wonderful colleagues; Dr. Pang Wei Kong, Dr. Hatem Al-Amri, Abdullah Al-Huthali, Julie Andrianny Murshidi and Teoh Ying Jia for guiding me to study, as well as sharing their opinions and suggestions on how to explore new ideas. Without these people, I may still be on the wrong path to finish this study.

I would like to express my appreciation for my husband, Mohd Shafiq bin Mohd Ismail, for his infinite love, support, encouragement and understanding during the course of this research project. These past several years have not been an easy ride, both academically and personally. I truly thank him for sticking by my side, even when I was irritable and depressed. I feel that we both learned a lot about life and strengthened our commitment and determination to each other and to live life to the fullest. Thank you for your sacrifice in babysitting our kids during all these times.

Finally, I would like to thank my beloved family in Malaysia for their infinite support throughout the course of my PhD study

## LIST OF PUBLICATIONS INCLUDED AS PART OF THE THESIS

---

(Listed in order as found in this thesis)

**Noor Azman, N.Z.**, Siddiqui, S.A., Hart, R., Low, I.M., Microstructured design of lead oxide-epoxy composites for radiation shielding purposes, *Journal of Applied Polymer Science*, 128 (2013) 3213-3219

**Noor Azman, N.Z.**, Siddiqui, S.A., Low, I.M., Synthesis and characterization of epoxy composites filled with Pb, Bi or W compound for shielding of diagnostic X-rays, *Applied Physics A: Materials Science & Processing*, 110 (2013) 137-144

**Noor Azman, N.Z.**, Siddiqui, S.A., Hart, R., Low, I.M., Effect of particle size, filler loadings and X-ray energy on the X-ray attenuation ability of tungsten oxide – epoxy composites, *Applied Radiation and Isotopes*, 71 (2013) 62-67

**Noor Azman, N.Z.**, Siddiqui, S.A., Low, I.M., Characterisation of micro-sized and nano-sized tungsten oxide-epoxy composites for radiation shielding of diagnostic X-rays, *Materials Science and Engineering C*, In press

**Noor Azman, N.Z.**, Siddiqui, S.A., Ionescu, M., Low, I.M., Synthesis and characterization of ion-implanted epoxy composites for X-ray shielding, *Nuclear Instruments and Methods in Physics Research B: Beam Interactions with Materials and Atoms*, 287 (2012) 120–123

**Noor Azman, N.Z.**, Siddiqui, S.A., Ionescu, M., Low, I.M., A comparative study of X-ray shielding capability in ion-implanted acrylic and glass, *Radiation Physics and Chemistry*, 85 (2013) 102-106

**Noor Azman, N.Z.**, Siddiqui, S.A., Haroosh, H.J., Albetran, H.M.M., Johannessen, B., Dong, Y., Low, I.M., Characteristics of X-ray attenuation in electrospun bismuth oxide / poly-lactic acid nanofibre mats, *Journal of Synchrotron Radiation*, 20 (2013) 741-748

## STATEMENT OF CONTRIBUTION OF OTHERS

---

Nurul Zahirah Binti Noor Azman's input into this project and the associated papers include the execution of all the experimental work, as well as a dominant contribution to the intellectual input involved in the project. Other scientists made contributions to the current work, as is almost always the case in the physical sciences. These contributions were significant enough to warrant co-authorship on the resulting journal articles. These are specified as below:

Prof. I.M. Low, who provided project supervision and manuscript editing.

Dr. S.A. Siddiqui, who provided specialist technical advice and instrument usage (general diagnostic radiology machine at Department of Imaging and Applied Physics, Curtin University) and also manuscript editing.

Dr. R. Hart, who provided specialist technical service advice and instrument usage (general radiography and mammography unit at Royal Perth Hospital) as well as manuscript editing.

Dr. M. Ionescu, who provided specialist technical service advice and instrument usage (ion-implantation, IBA and RBS at ANSTO) and manuscript editing.

Dr B. Johannessen, who provided specialist technical service advice and instrument usage (XAS at Australian Synchrotron) and also manuscript editing.

Dr. Y. Dong, who provided specialist technical service advice and instrument usage (electrospinning machine) as well as manuscript editing.

H.J. Haroosh, who provided specialist technical service advice and samples for electrospinning experiments.

H.M.M. Albetran, who provided specialist technical service advice and samples for electrospinning experiments.



---

Nurul Zahirah Binti Noor Azman



---

Prof. It-Meng Low



# TABLE OF CONTENTS

---

ABSTRACT .....	i
ACKNOWLEDGEMENTS .....	v
LIST OF PUBLICATIONS INCLUDED AS PART OF THE THESIS .....	vii
STATEMENT OF CONTRIBUTION OF OTHERS .....	ix
TABLE OF CONTENTS .....	xi
LIST OF FIGURES.....	xiv
LIST OF TABLES .....	xvii
LIST OF ABBREVIATIONS .....	xviii
1. INTRODUCTION AND OVERVIEW .....	1
1.1 Background.....	1
1.2 Objective and Scope of Work.....	2
1.3 Thesis overview .....	3
2. LITERATURE REVIEW.....	6
2.1 Historical foundations of X-ray shielding .....	6
2.2 X-ray attenuation.....	6
2.3 X-ray interactions with matter.....	9
2.3.1 Photoelectric effect .....	11
2.3.2 Compton scattering effect.....	12
2.4 X-ray energy.....	13
2.5 Effect of particle-size on X-ray attenuation .....	14
2.6 Advantages and disadvantages of commercial lead glass .....	17
2.7 Other commercial polymer composites for X-ray shielding .....	19
2.7.1 Lead acrylic.....	19
2.7.2 X-ray lead vinyl .....	20
2.7.3 Poly tungsten.....	21
2.7.4 Hybrid polymer X-ray shielding material.....	22
2.7.5 Other polymer composites fabricated by researchers .....	23
2.8 Ion-implantation .....	24
2.9 Electrospinning.....	27

3.	DISPERSION OF THE MICRO-SIZED FILLER INTO THE EPOXY MATRIX BASED ON THEIR X-RAY ATTENUATION ABILITY .....	32
3.1	Microstructured Design of Lead Oxide-Epoxy Composites for Radiation Shielding Purposes .....	33
3.2	Synthesis and Characterization of Epoxy Composites Filled with Pb, Bi or W Compound for Shielding of Diagnostic X-rays .....	41
4.	PARTICLE SIZE EFFECT ON THE X-RAY ATTENUATION ABILITY OF WO <sub>3</sub> FILLER-EPOXY COMPOSITES .....	50
4.1	Effect of Particle Size, Filler Loadings and X-ray Energy on the X-ray Attenuation Ability of Tungsten Oxide – Epoxy Composites .....	51
4.2	Characterisation of Micro-sized and Nano-sized Tungsten Oxide-Epoxy Composites for Radiation Shielding of Diagnostic X-rays .....	58
5.	FILLER DISPERSION WITHIN EPOXY, ACRYLIC AND GLASS BY ION-IMPLANTATION METHOD .....	65
5.1	Synthesis and Characterization of Ion-Implanted Epoxy Composites for X-ray Shielding .....	66
5.2	A Comparative Study of X-ray Shielding Capability in Ion-Implanted Acrylic and Glass.....	71
6.	CHARACTERISTICS OF X-RAY ATTENUATION IN ELECTROSPUN BISMUTH OXIDE/POLY-LACTIC ACID NANOFIBRE MATS .....	77
7.	CONCLUSIONS AND FUTURE WORK.....	87
7.1	Conclusions .....	87
7.1.1	Filler dispersion within epoxy resins by melt-mixing method .....	87
7.1.2	Filler dispersion within epoxy, acrylic and glass by ion-implantation method .....	89
7.1.3	Filler dispersion within PLA nanofibre mats by electrospinning method .....	90
7.2	Recommendation for Future Work.....	91
8.	APPENDICES .....	93
8.1	APPENDIX A: Supplementary Information for Publication .....	93
8.1.1	Appendix A-1: Supplementary Information for Chapter 5.1 .....	93
8.1.2	Appendix A-2: Supplementary Information for Chapter 6.....	96
8.2	APPENDIX B: Statement of Contributions of Others .....	98

8.2.1 Appendix B-1: Statement of Contribution of Others for “Microstructured Design of Lead Oxide-Epoxy Composites for Radiation Shielding Purposes”	98
8.2.2 Appendix B-2: Statement of Contribution of Others for “Synthesis and Characterization of Epoxy Composites Filled with Pb, Bi or W Compound for Shielding of Diagnostic X-rays”	102
8.2.3 Appendix B-3: Statement of Contribution of Others for “Effect of Particle Size, Filler Loadings and X-ray Energy on the X-ray Attenuation Ability of Tungsten Oxide – Epoxy Composites”	105
8.2.4 Appendix B-4: Statement of Contribution of Others for “Characterisation of micro-sized and nano-sized tungsten oxide-epoxy composites for radiation shielding of diagnostic X-rays”	109
8.2.5 Appendix B-5: Statement of Contribution of Others for “Synthesis and Characterization of Ion-Implanted Epoxy Composites for X-ray Shielding”	112
8.2.6 Appendix B-6: Statement of Contribution of Others for “A comparative study of X-ray shielding capability in ion-implanted acrylic and glass”	116
8.2.7 Appendix B-7: Statement of Contribution of Others for “Characteristics of X-ray attenuation in electrospun bismuth oxide / Poly-lactic acid nanofibre mats”	120
8.3 APPENDIX C: Copyright Forms	127
8.3.1 Appendix C-1: Elsevier Journal Articles	127
8.3.2 Appendix C-2: John Wiley and Sons Articles	131
8.3.3 Appendix C-3: Springer	133
8.3.4 Appendix C-4: (IUCr) Synchrotron Radiation Online	135
9 BIBLIOGRAPHY	138

## LIST OF FIGURES

---

Figure 2.1: A narrow beam geometry setup for measurement of X-ray attenuation ( <i>X-ray absorption</i> ). .....	7
Figure 2.2: Determination of linear attenuation coefficients (Hussain, Haq & Mohammad 1997). .....	8
Figure 2.3: X-ray transmission measured for X-ray beams generated at 25, 30 and 60 kV tube voltages and transmitted through the nanosized samples with 5%, 10% and 30% CuO powder concentration in an epoxy resin (Künzel & Okuno 2012). .....	9
Figure 2.4: Possible X-ray interactions within a material showing (1) scattering; (2) absorption; and (3) no interaction ( <i>X-ray Interaction (Part I)</i> ). .....	10
Figure 2.5: Illustrations of the region of photon energy ( $h\nu$ ) and the atomic number ( $Z$ ) of absorbing material for three major photon interactions with matter, specifically: photoelectric effect $\tau$ , Compton scattering effect $\sigma$ , and pair production $\kappa$ . The curves show where two kinds of interaction are equally probable ( $\tau=\sigma$ ) and ( $\sigma=\kappa$ ) (Abdel-Rahman & Podgorsak 2010; Attix 1986). .....	11
Figure 2.6: Process of the photoelectric effect in an atom of absorbing material ( <i>X-ray Interactions</i> ). .....	12
Figure 2.7: Process of Compton scattering in an atom of absorbing material. The outgoing X-ray photon has a lower energy with a longer wavelength compared to the incoming X-ray photon ( <i>Chapter 6 Modern Technology</i> 2012). .....	13
Figure 2.8: Comparison of the X-ray spectra transmitted through 10.3 mm samples composed of 30% CuO of both particle sizes incorporated to a polymeric resin for beams generated at 25, 30, 60 and 120 kV tube voltages. Solid lines stand for the microstructured material; whereas the dashed ones correspond to the nanostructured samples (Künzel & Okuno 2012). .....	16
Figure 2.9: Total mass attenuation coefficients ( $\mu/\rho$ ) as a function of atomic number ( $Z$ ) (the solid line is the calculated data, filled circles present experimental data and open circles result from Baltaş et al. 2005 and Teli et al. 2000) (Akkurt et al. 2005). .....	18
Figure 2.10: X-ray lead glass and lead acrylic (a) side view thickness comparison; and (b) face view comparison ( <i>Control Windows</i> 2000-2010). .....	20

Figure 2.11: Lead vinyl curtain used for patient's changing room ( <i>Other ray-bar products</i> 2000-2010). .....	21
Figure 2.12: (a) Poly tungsten sheets; and (b) poly tungsten as radiation-protective clothing ( <i>Tungsten Products: Poly Tungsten</i> ). .....	22
Figure 2.13: Hybrid polymer X-ray shielding material ( <i>Hybrid polymer X-ray shielding material</i> 2010). .....	23
Figure 2.14: Physical principles of IBA techniques: PIXE, RBS and NRA (Koen, Janssens & Van Grieken 2004). .....	27
Figure 2.15: TEM images of PbS nanoparticles formed in PVP fibres (Lu, Zhao & Ce 2005). .....	28
Figure 2.16: Schematic illustration of electrospinning processes. A polymer solution held in a syringe (A) is fed to a metal needle (B). High voltage supply (C) is connected to the needle, producing a fine jet of polymer solution (D). This dries out in transit, resulting in fine fibres which are collected on collector target (E) ( <i>Technology: Electrospinning</i> 2007-2012). .....	29
Figure 2.17: Relationship between the fibre diameter and applied voltage, showing the average fibre diameter for 12 kV, 15 kV and 18 kV (Chowdhury & Stylios 2010). .....	30
Figure 2.18: Relationship between the fibre diameter and needle-collector distance, showing the average fibre diameter for 5 cm, 8 cm and 11 cm (Chowdhury & Stylios 2010). .....	31
Figure 8.1: Backscattered micrograph for epoxy implanted with W (white patches) at $1.4 \times 10^{15}$ ions/cm <sup>2</sup> (Sample B2). .....	94
Figure 8.2: EDS result of Spectrum 1 obtained from Figure 8.1. ....	94
Figure 8.3: EDS result of Spectrum 2 obtained from Figure 8.1. ....	95
Figure 8.4: Backscattered micrograph for epoxy implanted with Pb at $1.4 \times 10^{15}$ ions/cm <sup>2</sup> (side view) (Sample B6). .....	95
Figure 8.5: Electrospinning experimental set up to perform the electrospinning process. ....	96

Figure 8.6: Final product collected on the aluminium foil after the process was completed. The product on the left side is the control PLA nanofibre mat; while at the right side is the Bi<sub>2</sub>O<sub>3</sub>/PLA nanofibre mat..... 97

## LIST OF TABLES

---

Table 1:	The applied X-ray tube voltage and the target material used to produce X-rays vary depending on the particular application ( <i>X-rays</i> 2012).....	14
Table 2:	Lead equivalencies, thickness and densities of lead acrylic used as X-ray shielding ( <i>Control Windows</i> 2000-2010).....	20
Table 3:	Lead equivalence shielding value for a specified lead vinyl thickness ( <i>Other ray-bar products</i> 2000-2010).....	21

## LIST OF ABBREVIATIONS

---

AINSE	Australian Institute of Nuclear Science and Engineering
ANSTO	Australian Nuclear Science and Technology Organisation
Bi <sub>2</sub> O <sub>3</sub>	Bismuth (III) oxide
IBA	Ion Beam Analysis
keV	Kiloelectron volt
kV	Kilovoltage
mAs	Miliampere second
OM	Optical Microscopy
PbO	Lead (II) oxide
Pb <sub>3</sub> O <sub>4</sub>	Lead (II,IV) oxide
PD	Powder Diffraction
PLA	Poly lactic acid
RBS	Rutherford Backscattering Spectroscopy
SEM	Scanning Electron Microscopy
WO <sub>3</sub>	Tungsten (VI) oxide
XAS	X-ray Absorption Spectroscopy



# 1. INTRODUCTION AND OVERVIEW

---

## 1.1 Background

Radiation (X-ray/gamma-ray) shielding is an ongoing problem and has been studied in great detail up until now, since they are used extensively in many applications such as in medical fields (i.e. diagnostic imaging and therapy), industrial or other applications. X-rays/gamma-rays are the most penetrating of the ionizing radiation that is known to be harmful to human health and heredity. X-ray photons are produced by the interaction of energetic electrons with matter at the atomic level. As an X-ray beam passes through an object, the following effects occur, specifically: (i) it can penetrate the section of the matter with an interaction but with no change of energy to the atoms or X-ray (i.e. Thompson scattering); (ii) it can interact with the matter and be totally absorbed by the atoms of the matter (i.e. photoelectric effect), or (iii) it can interact partially with the matter and be scattered from its original course in all directions (i.e. Compton scattering). Hence, there is no doubt that X-ray shielding requirements have become more stringent with regard to standards for exposure of personnel (patients and radiography workers) and the general public while carrying out of diagnosis examination procedures.

To overcome the danger of X-rays, it is vitally important for the material chosen for X-ray shielding to be able to totally absorb the transmitted and scattered X-rays, so as to minimise the exposure to personnel and general public. Hitherto, lead glass is the best-known transparent material for X-ray shielding either for diagnostic or therapeutic examinations; however it is heavy, expensive and extremely brittle. Thus, it is not surprising that the application of polymers in X-ray shielding technology is increasing steadily since polymers also have an enormous potential in many crucial applications that glass could not meet. This is largely due to their unique properties, such as the ability to form intricate shapes, optical transparency, low manufacturing cost and toughness.

With this thesis being a conclusion of the doctoral research program, a variety of research efforts were conducted which aimed at developing and understanding the fabrication of new

polymer composites with good filler dispersion for usage as an X-ray shielding. This research program led to in-depth analysis of synthesis methods, X-ray attenuation ability and characterization of these polymer composites respectively. The synthesis methods used were melt-mixing, ion-implantation, solution casting and electrospinning which comprise different approaches. Meanwhile, the X-ray attenuation ability of the fabricated composites was studied by means of X-ray transmission or attenuation coefficient determination for the X-ray energy ranges used in the diagnostic examination. This was performed by three separate pieces of equipment, i.e.: general radiography unit, mammography unit and X-ray Absorption Spectroscopy (XAS).

## **1.2 Objectives and scope of work**

This project mainly focused on the nanotechnology advances involved in designing electromagnetic radiation (focused on X-ray) shielding materials. It combined viable processing methodologies, with the new material's design concept intended to enhance radiation shielding purposes so as to meet the safety requirements for use in medical X-ray imaging facilities.

The sample preparation was based upon the dispersion of different types of micro-sized and nano-sized particles into polymeric materials by different methods such as melt-mixing, ion-implantation and an electrospinning method. An accurate and effective melt-mixing method was becoming increasingly important so that a uniform mixture could be produced; whilst ion-implantation technology is capable of precisely controlling the number of implanted ions into the material. Meanwhile, electrospinning is a method which provides advantageous use of the nanofibre webs in a layered structure together with a suited substrate material and offers sufficient strength and durability. All such final products generated have high potential applications for shielding of ionizing radiations such as X-rays and gamma-rays

### 1.3 Thesis overview

The present work incorporates seven manuscripts, all have been peer reviewed and published or are in press in academic journals as indicated below:

- [1] **Noor Azman, N.Z.**, Siddiqui, S.A., Hart, R., Low, I.M., Microstructured design of lead oxide-epoxy composites for radiation shielding purposes, *Journal of Applied Polymer Science*, 128 (2013) 3213-3219.
- [2] **Noor Azman, N.Z.**, Siddiqui, S.A., Low, I.M., Synthesis and characterization of epoxy composites filled with Pb, Bi or W compound for shielding of diagnostic X-rays, *Applied Physics A: Materials Science & Processing*, 110 (2013) 137-144.
- [3] **Noor Azman, N.Z.**, Siddiqui, S.A., Hart, R., Low, I.M., Effect of particle size, filler loadings and X-ray energy on the X-ray attenuation ability of tungsten oxide – epoxy composites, *Applied Radiation and Isotopes*, 71 (2013) 62-67.
- [4] **Noor Azman, N.Z.**, Siddiqui, S.A., Low, I.M., Characterisation of micro-sized and nano-sized tungsten oxide-epoxy composites for radiation shielding of diagnostic X-rays, *Materials Science and Engineering C*. In press.
- [5] **Noor Azman, N.Z.**, Siddiqui, S.A., Ionescu, M., Low, I.M., Synthesis and characterization of ion-implanted epoxy composites for X-ray shielding, *Nuclear Instruments and Methods in Physics Research B: Beam Interactions with Materials and Atoms*, 287 (2012) 120–123.
- [6] **Noor Azman, N.Z.**, Siddiqui, S.A., Ionescu, M., Low, I.M., A comparative study of X-ray shielding capability in ion-implanted acrylic and glass, *Radiation Physics and Chemistry*, 85 (2013) 102-106.
- [7] **Noor Azman, N.Z.**, Siddiqui, S.A., Haroosh, H.J., Albetran, H.M.M., Johannessen, B., Dong, Y., Low, I.M., Characteristics of X-ray attenuation in electrospun bismuth oxide / poly-lactic acid nanofibre mats, *Journal of Synchrotron Radiation*, 20 (2013) 741-748.

The peer-reviewed publications listed above comprise the individual chapters of this thesis. The text that appears in these chapters is unchanged from that of the original manuscripts. Formatting and numbering of headings, subheadings, figures, tables and equations have been

altered for the purposes of amalgamation to form the present thesis. The underlying theme that has guided the research shown in this thesis has been the development of X-ray shielding materials.

The first manuscript presented in Chapter 3, which forms Chapter 3.1 of this thesis, is the preliminary investigation of the filler dispersion within an epoxy matrix. A comprehensive literature survey reveals that the gamma/X-ray shielding characteristics of the filler (PbO and Pb<sub>3</sub>O<sub>4</sub>)-reinforced epoxy resins have not been attempted to date. This analysis allowed for the discussion of the effects of filler loadings to the density, phase composition, and morphology of the epoxy composites. Moreover, the X-ray attenuation by the samples was performed using a calibrated general diagnostic radiology machine. In Chapter 3.2, further analyses of filler-reinforced epoxy resins are reported. This work comprises similar characterizations of the synthesized different species of filler (PbCl<sub>2</sub>, WO<sub>3</sub> and Bi<sub>2</sub>O<sub>3</sub>)-epoxy composites as in Chapter 3.1, including the discussion of their mechanical properties. In addition, the feasibility of these composites for use in X-ray shielding is compared with that of commercial lead glass.

Meanwhile, Chapter 4 reveals the effect of particle size, filler loadings and X-ray tube voltage on the X-ray transmission in WO<sub>3</sub>-epoxy composites. For the study in Chapter 4.1, a mammography unit and a diagnostic radiology machine were used; these comprised variable X-ray tube voltages 25- 120 kV. Thus, Chapter 4.2 is the continuous analysis of Chapter 4.1, which provides the X-ray transmission results from XAS and also includes some mechanical and microstructural analyses.

Chapter 5 (5.1 and 5.2) reports the fabrication of filler-polymers matrix (epoxy, acrylic and glass) using ion-implantation. Pb, W and Au ions were implanted on the polymer matrix since they are well-known candidates for X-ray shielding. A comparative study of the near surface composition depth profiling of the samples was performed using ion beam analysis (Rutherford backscattering spectroscopy). Further, the comparative X-ray attenuation analysis of the samples was performed using a calibrated general diagnostic radiology machine.

The final episode of this thesis concerns the presentation of a novel electrospinning method to fabricate the filler-nanofibre mats. Poly lactic acid (PLA) was used as the matrix for nanofibre mat synthesis due to the advantages of PLA in relation to the electrospinning process. This work presents the performance of the PLA mat together with different particle sizes for X-ray transmission. A better understanding was gained by the comparative study using a solution casting method to synthesize the same composites, but in a thin film form.

## 2. LITERATURE REVIEW

---

### 2.1 Historical foundations of X-ray shielding

During the early part of the 20th century, the hazards from ionizing radiation were recognized and the use of lead and other materials became commonplace for shielding against X-rays. Once the dangers of X-rays were considered, lead became an important material for radiation protection. Since then, protection has evolved into an elaborate infrastructure of controls and disciplines specifying how this shield should be deployed (Archer 1995, 2005; Archer, Thornby & Bushong 1983). Recently, shielding requirements have become more stringent as standards relating to exposure of personnel and the general public have been reviewed. X-ray technologists practise a principle called ‘as-low-as-reasonably-achievable dose’ when dealing with X-rays, so that the radiation dose received by personnel and the general public can be as low as possible (Edward 1966; Erdem et al. 2010; Kurudirek et al. 2010; Okunade 2002).

In addition, as a consequence of the extensive use of nuclear energy and radioactive isotopes in various fields such as reactors, nuclear power plants, nuclear engineering and space technology respectively, the issue of radiation shielding became an important concern. It was increasingly realised that proper precautions were required in order to avoid harm from the radiation hazards (Archer 1995).

### 2.2 X-ray attenuation

Several researchers have focused their efforts on studying how to measure the X-ray attenuation of an absorbing material. Whereas most researchers who examine this issue tried to measure and calculate the photon attenuation coefficient of the absorbing material and made a comparison with the theoretical value tabulated from NIST XCOM (Baltaş et al. 2007; Gerward 1992; Gowda et al. 2004; Harish, Nagaiah & Harish Kumar 2012; Harish et al. 2009; İçelli, Erzeneoglu & Boncukçuoğlu 2003, 2004; Tran, Chantler & Barnea 2003), others take the direct X-ray transmission results as an approach (Berger et al. 2010; Botelho et al. 2011; Künzel & Okuno 2012). In particular, the former can be measured for specific X-ray energy

for a narrow beam geometry setup, as shown in Figure 2.1. For the same absorbing material, the transmitted X-ray intensity ( $I$ ) was recorded as a function of the thickness of the material. The linear attenuation coefficient ( $\mu$ ) of the material can be evaluated from a linear graph of  $\ln(I/I_0)$  versus thickness ( $t$ ) of the absorbing material, where ( $I_0$ ) is the incoming X-ray intensity or the X-ray intensity without absorbing material. In order to quantify attenuation of a material independent of its physical state (i.e. density), the mass attenuation coefficient ( $\mu/\rho$ ) is commonly being used by providing thicknesses in mass per unit area ( $\rho t$ ) in  $[\text{g}/\text{cm}^2]$  where  $\rho t$  is known as mass thickness or areal thickness of the absorbing material (*Interaction of radiation with matter:attenuation coefficients* 2010; Attix 1986).

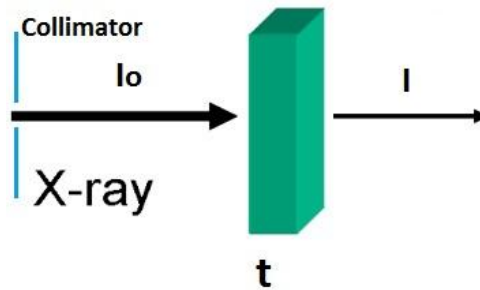


**Figure 2.1:** A narrow beam geometry setup for measurement of X-ray attenuation (*X-ray absorption*).

For instance, Hussain et al. (1997) have studied the shielding properties of poly ethylene glycol-lead oxide composite for Co-60 gamma-ray source. They calculated the linear attenuation coefficient from the plot of log of the count rate versus the composite thickness, as shown in Figure 2.2 where the equation for the plot is:

$$\text{Log } I(t) = \text{Log } I_0 - \mu t$$

where  $I(t)$  = count rate for the radiation that has not been involved in any collision during passage through a shield of thickness  $t$ ,  $I_0$  = count rate in the absence of shielding material and  $\mu$  = linear attenuation coefficient. This can be seen to be the slope of the plot (Hussain, Haq & Mohammad 1997). In their case, they did not compare the attenuation coefficient results with the theoretical tabulated data from XCOM (Berger et al. 2010). Meanwhile, using a similar method, Harish et al. (2012) have investigated the radiation shielding properties of gamma-

rays from Ba-133, Cs-137 and Co-60 point sources of lead oxide (PbO, PbO<sub>2</sub> and Pb<sub>3</sub>O<sub>4</sub>) with different concentrations of filled isophthalic resin polymer composites. They found that their experimental attenuation coefficient results for the composites at the specific value of gamma-rays energy were in agreement with the theoretical results (Berger et al. 2010) with an acceptable error (Harish, Nagaiah & Harish Kumar 2012).

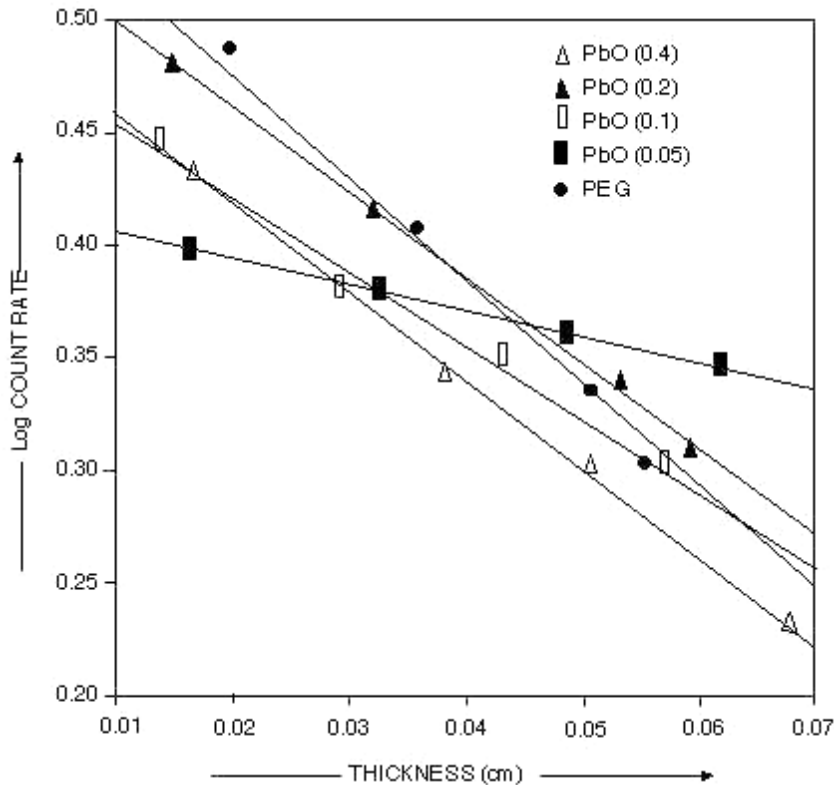


**Figure 2.2:** Determination of linear attenuation coefficients (Hussain, Haq & Mohammad 1997).

It would be much more useful to present the X-ray transmission (i.e. measured intensities through absorbing material divided by the measured intensity in the same configuration with absorbing material absent) over the full energy range (weighted by an appropriate model for X-ray tube spectrum) if the thickness of the absorbing materials is fixed. Absolute intensities obviously depend on the mAs setting, distance from source to detector, detector calibration etc. (Tickner 2000). Usually, these direct transmission measurements were performed for the polychromatic X-ray energies, since quoting these measurements would be correct for all the effects (Al-Maamori, Al-Bodairy & Saleh 2012; Botelho et al. 2011; Künzel & Okuno 2012; Tickner 2000). Figure 2.3 shows the example for X-ray transmission  $(K_{\mu}/K_n)_{air}$  through the



nanosized CuO-epoxy resin samples studied by Künzel and Okuno (2012) versus X-ray tube voltages containing polychromatic X-ray energies (Künzel & Okuno 2012).

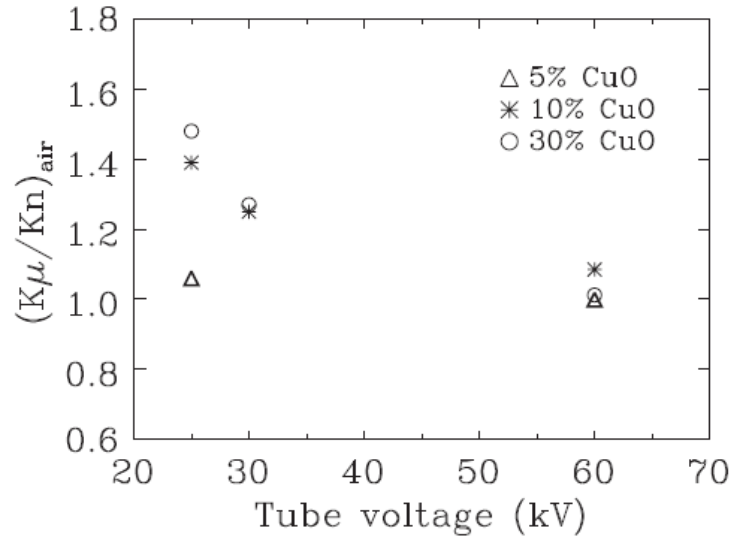


**Figure 2.3:** X-ray transmission measured for X-ray beams generated at 25, 30 and 60 kV tube voltages and transmitted through the nanosized samples with 5%, 10% and 30% CuO powder concentration in an epoxy resin (Künzel & Okuno 2012).

### 2.3 X-ray interactions with matter

Generally, there are three possible X-ray interactions occurring in an absorbing material. These are shown in Figure 2.4 and consist of:

- (1) Scattering – An X-ray photon will interact with an atom of absorbing material and it will be deflected. Depending on the case, it may or may not result in loss of energy.
- (2) Absorption – An X-ray photon will interact with an atom of absorbing material and will lose all of its energy to the atom accordingly.
- (3) No interaction – An X-ray photon merely passes through the absorbing material without interacting with any atoms of absorbing material

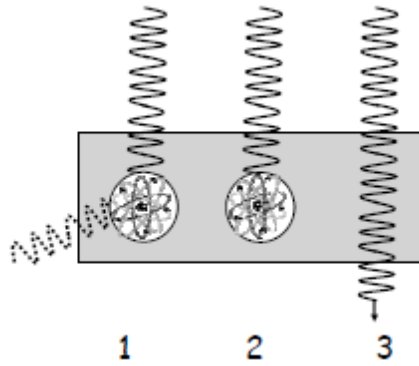


**Figure 2.4:** Possible X-ray interactions within a material showing (1) scattering; (2) absorption; and (3) no interaction (*X-ray Interaction (Part I)*).

These possible interactions have been categorized into five different types of X-ray interaction which must be considered in radiological physics. They are as listed as below:

- i. Photoelectric effect
- ii. Compton scattering effect
- iii. Pair production
- iv. Rayleigh scattering
- v. Photonuclear interactions

The first three are the most important, since their interactions result in the transfer of energy to electrons and are then imparted to matter along their tracks. These interactions depend on both photon energy  $E$  and atomic number  $Z$  of the absorbing material. Figure 2.5 shows the region of  $E$  ( $h\nu$ ) and  $Z$  together with the domination for each interaction. The photoelectric effect is dominant at the lower photon energies, while the Compton scattering effect takes over at medium energies. Pair production is leading at the higher photon energies. Compton scattering effect domination is very broad for low  $Z$  of absorbing material and gradually narrows with increasing  $Z$ .

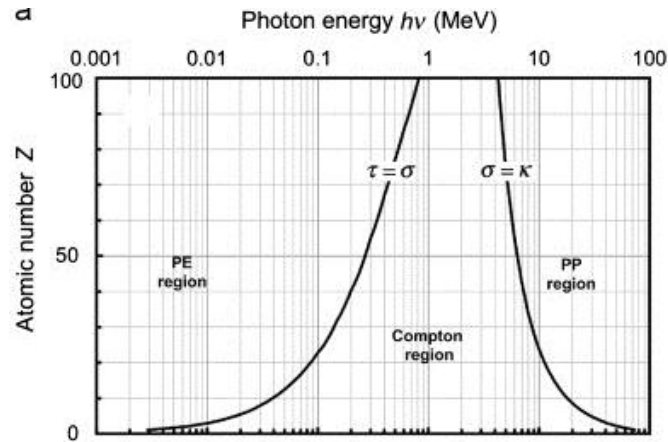


**Figure 2.5:** Illustrations of the region of photon energy ( $h\nu$ ) and the atomic number ( $Z$ ) of absorbing material for three major photon interactions with matter, specifically: photoelectric effect  $\tau$ , Compton scattering effect  $\sigma$ , and pair production  $\kappa$ . The curves show where two kinds of interaction are equally probable ( $\tau=\sigma$ ) and ( $\sigma=\kappa$ ) (Abdel-Rahman & Podgorsak 2010; Attix 1986).

The Rayleigh scattering is an elastic interaction in which the photon is merely redirected through a small angle with no energy loss. The last interaction (photonuclear) is only significant for photon energies above a few MeV.

Further discussions are only related to photoelectric effect and Compton scattering effect since both of them take part in the photon energy ranges studied for this thesis project.

### 2.3.1 Photoelectric effect

Photoelectric effect is the most important interaction of concern during the interaction of low energy photons with matter (Figure 2.6). During photoelectric interaction, an inelastic collision occurs between the incident X-ray photon with an orbiting electron (inner shell electron). The photon gives up all of its energy and therefore disappears (absorbed by the electron). The electron is then ejected from an atom and flies off into space as a photoelectron which may undergo another interaction with the atom. The vacancy left is immediately filled by an electron from the outer shell. The quantum ‘jumps’ of the electron produce a characteristic radiation which is equal to the energy difference between shells. The photoelectric effect always yields three end products, namely: (1) characteristic radiation; (2)

a negative ion (photoelectron) and (3) a positive ion (an atom deficient one electron) (*X-ray Interaction (Part I); X-Ray Interactions; Attix 1986; Thomas, James & Robert 1990*).

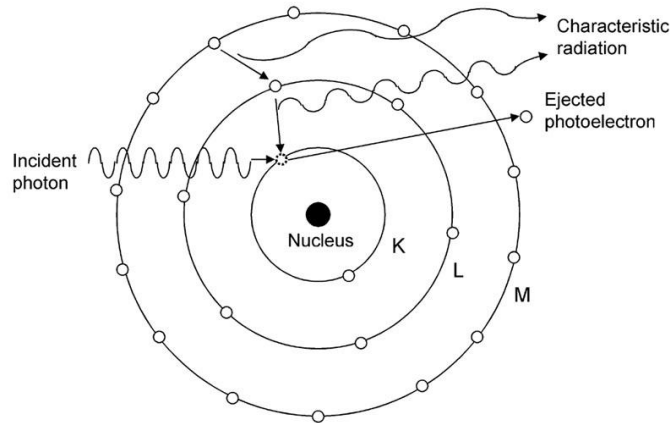


**Figure 2.6:** Process of the photoelectric effect in an atom of absorbing material (*X-ray Interactions*).

The probability of the photoelectric effect is inversely proportional to the cube of the X-ray energy  $(1/E)^3$  and directly proportional to the cube of the atomic number of the absorbing material  $Z^3$  (*Interactions of Photons with Matter*).

### 2.3.2 Compton scattering effect

Almost all the scatter radiation that is encountered in diagnostic radiology comes from Compton scattering. During this interaction, an incident photon of relatively high energy strikes a loosely bound outer shell electron, ejecting it from its orbit. The photon is then deflected by the electron and travels in a new direction as scatter radiation with part of its original energy. Since the scattered X-ray photon has less energy, it has a longer wavelength and is less penetrating than the incident/incoming X-ray photon. The reaction produces an ion pair of a positive atom and a negative outgoing/recoil electron. Figure 2.7 shows the process of Compton scattering interaction (*Chapter 6 Modern Technology 2012*).

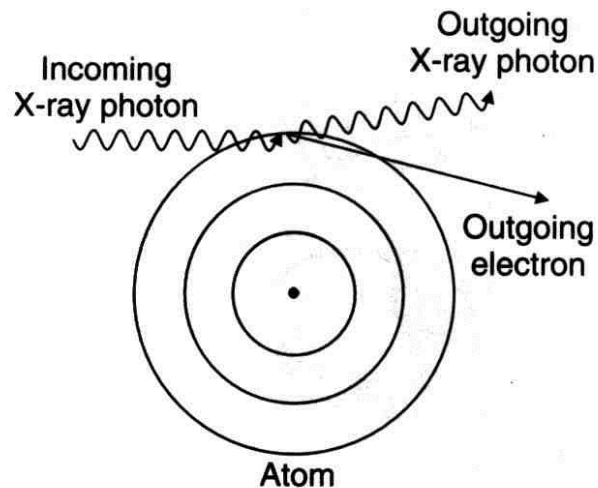


**Figure 2.7:** Process of Compton scattering in an atom of absorbing material. The outgoing X-ray photon has a lower energy with a longer wavelength compared to the incoming X-ray photon (*Chapter 6 Modern Technology* 2012).

The Compton scattering probability is almost independent of the atomic number of the absorbing material ( $Z$ ) and will decrease as the photon energy ( $E$ ) increases. In addition, it is directly proportional to the number of electrons per gram, which only varies by 20% from the lightest to the heaviest elements (except for hydrogen) (*Interactions of Photons with Matter*).

## 2.4 X-ray energy

X-rays are the most penetrating of ionizing radiation following gamma-rays that are known to be harmful to human health and heredity. They are emitted by excited atoms in the process of de-excitation to a ground state by means of electrons changing atomic energy levels (characteristic or fluorescence X-rays); or by an ion or a charged particle when a negative acceleration is applied to it (i.e., slowing down in a Coulomb force field or changing direction). In addition, X-rays can be generated by high energy gamma ray interaction with matter. Most commonly, the energy ranges of X-rays are classified as follows (in terms of the generating applied X-ray tube voltage) (Attix 1986):

- 0.1-20 kV Low energy or “soft” X-rays
- 20-140 kV Diagnostic-range X-rays
- 140-300 kV Orthovoltage X-rays

- 300 kV-1 MV Intermediate-energy X-rays
- 1 MV upward Megavoltage X-rays

Table 1 provides the applied X-ray tube voltage as well as the target material used to produce X-rays which vary depending on the particular application for the diagnostic-range X-ray tube voltages (20-140 kV), since these tube voltages are related to this thesis project.

**Table 1:** The applied X-ray tube voltage and the target material used to produce X-rays vary depending on the particular application (*X-rays* 2012).

	Use	X-ray tube voltage	Target	Source type	Average photon energy
<b>Diagnostic X-rays</b>	<b>Mammography</b>	20 - 30 kV	Rhodium Molybdenum	Tube	20 keV
	<b>Dental</b>	60 kV	Tungsten	Tube	30 keV
	<b>General</b>	40 - 140 kV	Tungsten	Tube	40 keV
	<b>CT</b>	80 - 140 kV	Tungsten	Tube	60 keV

Basically, these X-ray energy ranges (produced by the applied X-ray tube voltages) are classified as polychromatic and monochromatic X-rays. Polychromatic X-rays are a broad spectrum of X-ray energies having various wavelengths, the expected form of X-ray generated in clinical practice. Meanwhile, a monochromatic X-ray is an X-ray with a single exclusive wavelength (Hoheisel et al. 2006; Martínez Ripoll & Félix Hernández 2013). As for the diagnostic X-rays, average photon energy was measured using a half-value layer (HVL) experiment (Suk, Wei & Harun 2012) for each of the accelerating voltages used for the particular application. This average photon energy is an important parameter for further attenuation coefficient comparison between the measured value of the experiment and the tabulated data NIST XCOM (Berger et al. 2010).

## 2.5 Effect of particle-size on X-ray attenuation

Currently, it has been demonstrated that materials at the nanoscale have unique physical and chemical properties compared to their bulk counterparts and, further, these properties are

highly promising for a variety of technological applications. Numerous analytical methods have been developed to investigate the effect of particle size of a material on the X-ray attenuation for various incoming X-ray energy ranges (including the scattered gamma-rays and X-rays) (Chen et al. 2013; El Haber & Froyer 2008; Granmayeh Rad, Abbasi & Afzali 2011; Hołyńska 1969; Huang & El-Sayed 2010; Jackson et al. 2011; Patra et al. 2010; Popov 2009; Sahare et al. 2007; Van Den Heuvel, Locquet & Nuyts 2010; Wang et al. 2013). Some X-ray technologists believe that nano-sized particles will disperse more uniformly within the matrix with less agglomeration when compared to micro-sized particles. Moreover, they believe that this will consequently affect the density and composition that modify the attenuation ability of the material (Botelho et al. 2011; El Haber & Froyer 2008; Steinhart 2004). In addition, nanomaterials have unique material properties that can be exploited to develop novel lead-free radiation-protection materials.

For instance, Hołyńska (1969) found that the intensity of scattered radiation escalates with increasing grain size. This size-effect has been observed in a sand matrix and with samples containing heavy elements such as iron or barium (Hołyńska 1969). Moreover, the latest study undertaken by Buyuk et al. (2012) proved that decreasing the titanium diboride particle size in the titanium diboride reinforced boron carbide-silicon carbide composites results in a higher linear attenuation coefficient for the energy of 0.662 MeV emitted by a Cs-137 gamma source (Buyuk et al. 2012). In a complementary finding, a recent study by Botelho et al. (Botelho et al. 2011) showed that nanostructured copper oxide (CuO) is more effective in attenuating X-ray beams generated from lower tube voltages (i.e. 26 and 30kV), whilst no significant variation in the attenuation of the X-ray beams generated from higher tube voltages (i.e. 60 and 102 kV) was observed.

Künzel and Okuno (2012) also provided similar results, showing that the X-ray beam attenuation is greater for a nanostructured CuO compound incorporated to a polymeric resin compared with the microstructured counterpart for low energies of tube voltages (25 and 30 kV) for a range of 5%, 10% and 30% CuO concentrations incorporated into polymeric resins. Figure 2.8 shows the X-ray spectra transmitted through 10.3 mm samples composed of 30% CuO of both particles sizes incorporated to a polymeric resin for beams generated in 25, 30, 60 and 120 kV tube voltages respectively. The incident X-ray beams on the samples were

absorbed only by the inherent X-ray tube filtration. The transmitted X-ray beams spectra through the microsized material were normalized to unity at the maximum of the spectra. The normalization of the transmitted X-ray beams through the nanosized material was performed using the normalization factor of the corresponding spectra transmitted through the microsized sample. The comparison of the relative number of photons for each measured spectra at 25 and 30 kV tube voltages reveals that the nanostructured material absorbs lower energy photons relative to the microstructured ones. Meanwhile, for the X-ray beams produced at 60 and 120 kV tube voltages, a minimal difference, less than 2%, in the X-ray transmission through the nanostructured and microstructured materials is observed (Künzel & Okuno 2012).

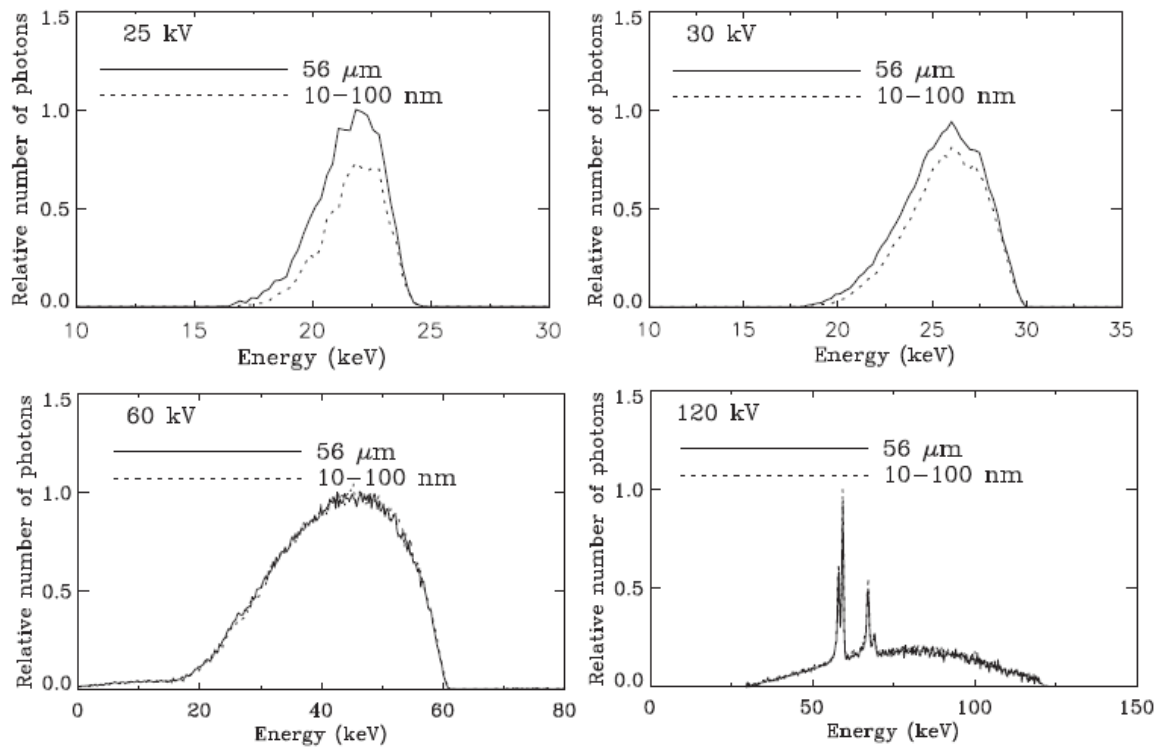


**Figure 2.8:** Comparison of the X-ray spectra transmitted through 10.3 mm samples composed of 30% CuO of both particle sizes incorporated to a polymeric resin for beams generated at 25, 30, 60 and 120 kV tube voltages. Solid lines stand for the microstructured material; whereas the dashed ones correspond to the nanostructured samples (Künzel & Okuno 2012).



## 2.6 Advantages and disadvantages of commercial lead glass

X-ray shielding lead glass is utilized in medical and industrial applications so that the operator can view the part or patient without being exposed to X-rays or gamma-rays. To provide viewing of the patient in the X-ray room while providing protection to the operator, lead glass viewing windows can be furnished in the barrier. In most cases, the X-ray attenuation of the glass must be at least equal to the wall or barrier in which the window is installed. It can be installed in multiple layers so as to provide the same lead equivalency as the wall (*Data sheet lead glass (X-ray protection); Lead glass for X-ray / radiation shielding 2009; Lead X-ray glass vs. lead plastic acrylic 2013*).

Lead glass ensures excellent protection against gamma rays and X-rays. Its effectiveness for X-ray shielding increases the attenuation of ionizing photons emitted by X-ray equipment, because this property increases dramatically as the atomic number of the attenuating material increases. Lead has a high atomic number ( $Z$ ) which further intensifies the density of lead glass, thus increasing the attenuation of X-ray photons. X-rays used in medicine, specifically diagnostic X-rays, often have lower energies on the ionizing radiation spectrum, which are easily shielded by leaded glass (*Lead glass for X-ray / radiation shielding 2009; Leaded glass for X-ray shielding*). Figure 2.9 shows the dependence of mass attenuation coefficients ( $\mu/\rho$ ) on the atomic number ( $Z$ ) of absorbing material for photon energy of 0.66 and 1.33 MeV studied by Akkurt et al. (Akkurt et al. 2005). The calculated ( $\mu/\rho$ ) were compared with the experimental results of this work and some other experiments (Baltaş et al. 2005; Teli, Nathuram & Mahajan 2000). The comparison between calculated and experimental works gives a good agreement. It can be seen that ( $\mu/\rho$ ) depend on the photon energies and decrease with the increasing photon energy. It can also be seen that ( $\mu/\rho$ ) decrease sharply in low atomic numbers ( $Z \leq 10$ ) and have a smooth structure in the middle  $Z$  number region ( $10 \leq Z \leq 60$ ) for both photon energies. In the case of a high  $Z$  number of elements ( $Z \geq 60$ ); ( $\mu/\rho$ ) start to increase for both photon energies, while it slightly increases in one (Figure 2.9(b)), it sharply increases in the other (Figure 2.9(a)).

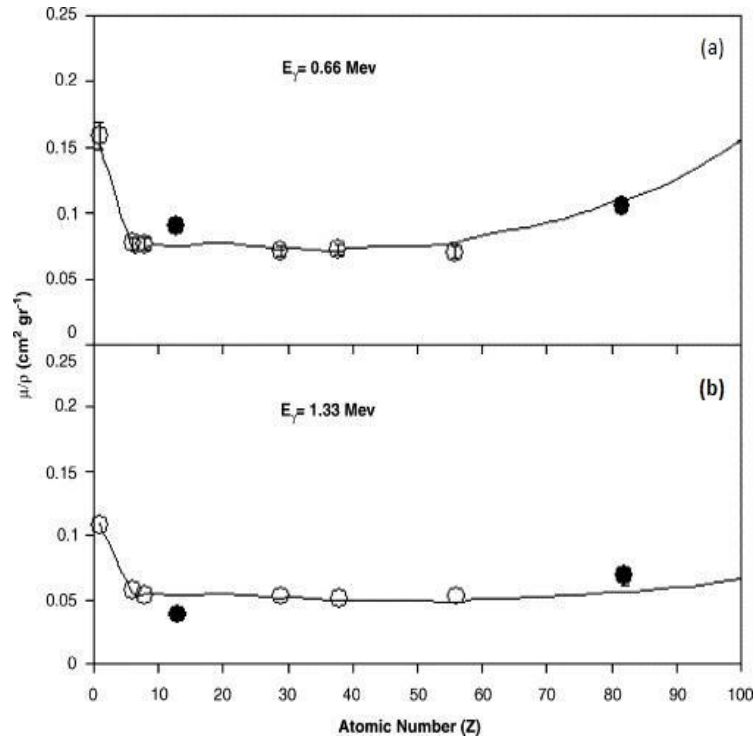


**Figure 2.9:** Total mass attenuation coefficients ( $\mu/\rho$ ) as a function of atomic number ( $Z$ ) (the solid line is the calculated data, filled circles present experimental data and open circles result from Baltaş et al. 2005 and Teli et al. 2000) (Akkurt et al. 2005).

Lead glass utilizes lead in the form of more than 65% lead oxide into a glass during the manufacturing process. It is transparent and easy to see through for observation purposes since it is made of high quality optical grade material. It also offers a high refractive index and high light transmission with little to no distortion, even in the thickest available varieties, delivers superior visual clarity and does not discolor due to radiation. One important advantage during everyday use is that the glass resists scratches much better than plastic since it has both hard and polished surfaces (using Mohs' hardness scale tests at Level 6 which is compatible to feldspar, a constituent of granite) (*Leaded glass for X-ray shielding*). It is also an incombustible material and has a high chemical resistance as well (*Data sheet lead glass (X-ray protection)*; *Lead glass for X-ray / radiation shielding 2009*; *Lead X-ray glass 2013*; *Lead X-ray glass vs. lead plastic acrylic 2013*; *Leaded glass for X-ray shielding*).

Even though lead glass provides good X-ray attenuation ability, it still has some disadvantages or limitations. Lead glass transmits more light; thereby it will create more annoying reflections, causing eye strain to medical personnel. Moreover, it is very fragile and

easily breakable and can shatter into sharp pieces if not handled with care. It is also a heavy and very expensive material. In addition, it cannot be tempered, as this is physically impossible due to its low melting temperature and surface characteristics. During shipment, it is more prone to breakage, so it must be shipped on its edge and never laid flat. Crates must not be stacked upon or dropped (*Lead X-ray glass vs. lead plastic acrylic* 2013).

## **2.7 Other commercial polymer composites for X-ray shielding**

Recently, several significant research efforts have been focused towards designing efficient, stronger, lightweight, cost-effective, and flexible shielding materials for protection against radiation encountered in medical X-ray procedures, either for diagnosis or treatment. In this regard, polymer composites have become attractive candidates for developing materials that can be designed to effectively attenuate photon or particle radiation. The following are some commercial polymer composites used nowadays for X-ray shielding purposes.

### **2.7.1 Lead acrylic**

Lead acrylic is made from an acrylic copolymer resin into which lead is chemically introduced as an organo-lead salt compound. It is a unique, versatile, transparent plastic that contains 30% lead weight and has a constant density of  $1.6 \text{ gm/cm}^3$  with a refractive index of 1.54. It combines superb light transmission with effective radiation protection. Recently, it has been widely used as a substitution for lead glass in observation viewing windows and intercommunication windows, door glazing, panoramic glazing, mobile shielding protection or protection panels for check-up systems respectively (*Lead Acrylic* 2013; Wardray 2005-2011). Lead equivalencies, thickness and densities of lead acrylic are summarized in Table 2 (*Control Windows* 2000-2010).

**Table 2:** Lead equivalencies, thickness and densities of lead acrylic used as X-ray shielding (*Control Windows 2000-2010*).

Lead Equivalency (mm)	Thickness (mm)	Weight (lb./ft)
0.3	7	2.3
0.5	12	3.9
0.8	18	5.9
1.0	22	7.2
1.5	35	11.5
2.0	46	13.7

For the same lead equivalent, lead acrylic has to be approximately 5 times thicker than lead glass, significantly reducing observation capabilities (Figure 2.10). For example, 2.0 mm lead glass would be 5/16” thick and lead acrylic would be approximately 1-1/2” thick for the same protection.

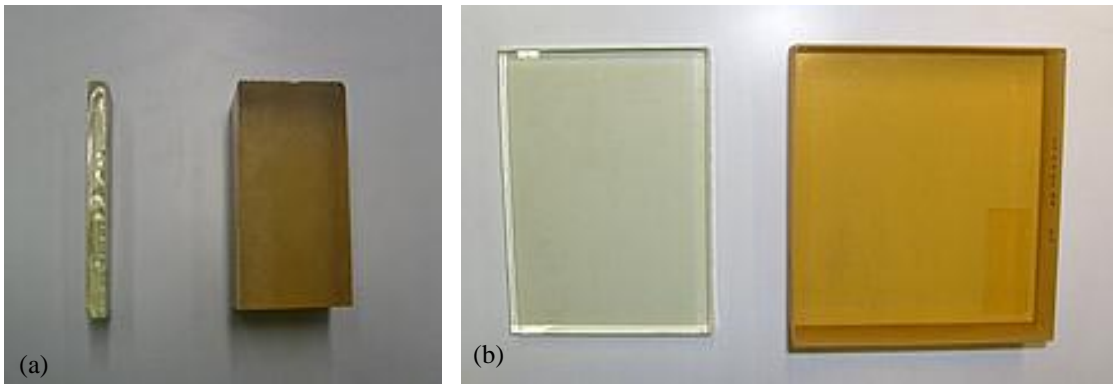


**Figure 2.10:** X-ray lead glass and lead acrylic (a) side view thickness comparison; and (b) face view comparison (*Control Windows 2000-2010*).

### 2.7.2 X-ray lead vinyl

X-ray lead vinyl is more suitable for use in low energy X-ray / gamma radiation reduction. It is flexible and pliable for a wide variety of applications such as a lead vinyl curtain (Figure 2.11) since it has uniform density for a consistently dependable shielding value and is very

durable and abrasion-resistant for everyday use. Moreover, it has a high acid/ alkali resistance and is also smooth and, hence, cleaning its surfaces on both sides is relatively easy (*Other ray-bar products 2000-2010*). Table 3 shows the lead equivalence shielding value for a specified lead vinyl thickness.



**Figure 2.11:** Lead vinyl curtain used for patient’s changing room (*Other ray-bar products 2000-2010*).

**Table 3:** Lead equivalence shielding value for a specified lead vinyl thickness (*Other ray-bar products 2000-2010*).

Lead Vinyl Thickness (mm)	Lead Equivalence Shielding Value (mm)
0.8	0.25
1.6	0.50
3.2	1.00

### 2.7.3 Poly tungsten

Poly tungsten (Figure 2.12(a)) (also known as tungsten - filled polymer) is a composition of various resins and tungsten powder which are mixed together through a special metallurgical technology. The resins may include acrylonitrile butadiene styrene (ABS), polypropylene (PP), polybutylene terephthalate (PBT), polyamide (PA), polyurethane (PU), and thermoplastic elastomer (TPE) respectively. Poly tungsten has a high density of more than  $11.34 \text{ g/cm}^3$  which provides a good radiation shielding performance, since tungsten has

comparable radiation shielding ability to lead, but is less hazardous. The Poly tungsten is made of non-toxic and recyclable materials and produces no pollution to the environment. To date, many manufacturers, especially those in the medical industry, are trying to replace lead radiation shielding products with poly tungsten products. Furthermore, it has good flexibility and excellent workability in which the poly tungsten sheets can be cut or holed with household scissors and formed into shapes with various curved surfaces (*Poly tungsten radiation shielding 1997-2013; Tungsten Products: Poly Tungsten*).

Tungsten-filled polymers can replace lead in radiation shielding applications such as: X-ray equipment and CT scanning devices, tungsten poly syringe, tungsten poly collimator, radiation-protective clothing (Figure 2.12(b)), etc. Testing, both on prototypes and actual products already in use, has proven that our tungsten-filled polymer products provide radiation shielding more efficiently than lead material radiation shielding and without leakage or hot spots (*Poly tungsten radiation shielding 1997-2013*).

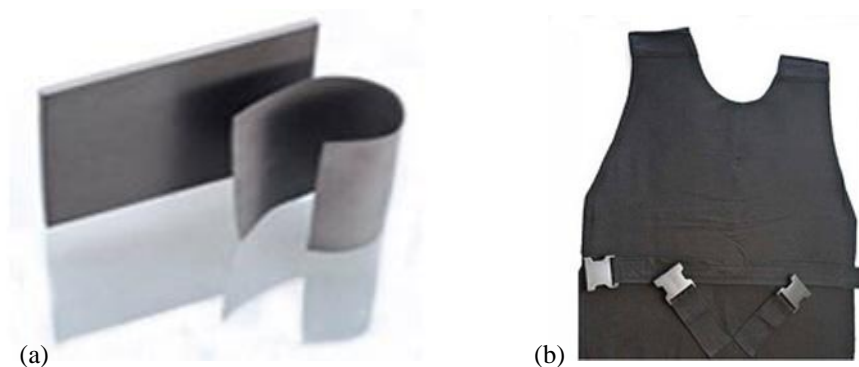


**Figure 2.12:** (a) Poly tungsten sheets; and (b) poly tungsten as radiation-protective clothing (*Tungsten Products: Poly Tungsten*).

#### 2.7.4 Hybrid polymer X-ray shielding material

The hybrid polymer X-ray shielding material (Figure 2.13) is a chemical compound of many organic and inorganic materials enabling it to shield X-ray radiation. This X-ray radiation shielding material can be used in many areas such as: research laboratories, or in medicine, industry, agriculture or the military. It has many advantages over lead shielding plates. Apart from being able to stop the X-ray, it is lighter and can shape more easily than lead plates, in

addition to being economic. Another important specification of this hybrid polymer X-ray shielding material is that it is not toxic to human beings or to the environment (*Hybrid polymer X-ray shielding material* 2010).



**Figure 2.13:** Hybrid polymer X-ray shielding material (*Hybrid polymer X-ray shielding material* 2010).

### 2.7.5 Other polymer composites fabricated by researchers

In the meantime, many researchers also tried to prepare new polymer composites for X-ray shielding purposes. For instance, Harish et. al. have prepared lead monoxide-polyester (Harish et al. 2009) and also lead oxide-isophthalic resin (ISO) (Harish, Nagaiah & Harish Kumar 2012) for gamma radiation shielding applications. The lead monoxide-polyester composites were observed to exhibit excellent percentages of heaviness and half value layer (HVL) in comparison with other conventional materials (Harish et al. 2009). Meanwhile, the lead monoxide-ISO composites, when compared with conventional shielding materials, perform as strong contenders to barite, steel and concrete at low gamma ray energies. Even at higher gamma ray energies, they perform satisfactorily and are very much comparable to steel and concrete (Harish, Nagaiah & Harish Kumar 2012).

Nambiar et. al (Nambiar, Osei & Yeow 2011) have prepared polydimethylsiloxane (PDMS) composites with different weight percentages (wt%), together with the following high atomic-number (Z) materials: (i) bismuth tungsten oxide (BTO) and (ii) bismuth oxide (BO). X-ray attenuation tests were performed using the diagnostic X-ray machine (Ysio, Siemens) for

voltages from 40 kV to 150 kV. PDMS composite with 36.36 wt% of BTO shows an overall increase of 18.3% and 50% attenuation relative (absolute differential between the % attenuation) to that achieved by 18.18 wt% of BTO and pure PDMS (no BTO) respectively. A composite sample with 60.6 wt% of BO (thickness of 2.67 mm) has shown the best result by far, with 92.5% attenuation of the beam at 60 kV (Nambiar, Osei & Yeow 2011).

Furthermore, polymer nanocomposite-based materials for shielding against diagnostic X-rays were developed. For instance, Nambiar et. al. (Nambiar, Osei & Yeow 2013) succeeded in fabricating polydimethylsiloxane / bismuth oxide (PDMS/BO) nanocomposites by using different weight percentages (wt %) of bismuth oxide (BO) nanopowder. The attenuation properties of the nanocomposites were characterized using diagnostic X-ray energies from 40 to 150 kV tube potential and were compared to the attenuation characteristics of 0.25-mm-thick pure lead sheet. The PDMS/BO nanocomposite (44.44 wt% of BO and 3.73-mm thick) was capable of attenuating the scattered X-rays generated at a tube potential of 60 kV, which is the beam energy commonly employed in interventional radiological IVR (Nambiar, Osei & Yeow 2013).

## **2.8 Ion-implantation**

There are several new techniques that are being explored towards polymer surface modifications; these are necessary to enhance their surface properties for various applications in industry. A polymer surface modification by ion implantation is an effective technique which uses energetic ions to alter the outermost surfaces of polymers without affecting their bulk properties. Since ion bombardment leads to a significant change in the polymer structure, it alters not only electrical properties but also polymer's optical, mechanical and tribological characteristics. This occurs due to the ease and readability of controlling some parameters during the irradiation such as: the choice of ions, the ion fluence, the depth of ion implantation, etc. This subsequently allows various organic-based devices to be fabricated (Anders 1997; Chen et al. 2001; Dworecki et al. 2004; Lopatin et al. 1998; Popok 2012; Rodríguez et al. 2007; Soares et al. 2004; Wu et al. 2000). However, by using ion implantation, polymer properties can be changed not only due to the irradiation-related



phenomena, but one also can embed some impurity and fabricate a composite material. Implantation of metal ions to high fluencies leads to the formation of nanoparticles (NPs). Hence, composite metal/polymer nanostructured materials can be produced, which are of great interest for a number of practical applications (Popok 2012).

During the process, ion implantation uses a series of high voltage grids to extract the ions from a plasma and accelerate them as an ion beam toward a target material in a low pressure environment. Medium (100 eV-100 keV) and high energy (>100 keV) ions implant beneath the surface, affecting the target material in a number of different ways. Since polymers are a relatively soft material, composed of around 20% free space, implanted ions travel a comparatively large distance before coming to rest. It can strongly modify the polymer chains along the track. High doses of low energy ions can adsorb on or near the surface, congregating together to form islands, eventually resulting in thin film growth. Also, a more important consideration for polymers, rather than the presence of implanted ions or atoms, is the “damage” to the polymer molecules that the ions cause before they come to rest. Damage events such as ionisation and recoil displacement result in the modification of the original polymer structure.

Di Girolamo et al. have successfully irradiated polycarbonate substrates at room temperature with low-energy metal ions ( $\text{Cu}^+$  and  $\text{Ni}^+$ ) of fluences in the range between  $1 \times 10^{16}$  and  $1 \times 10^{17}$  ions/cm<sup>2</sup> for strain gauge applications. They concluded that the experimental results show that low-energy metal ion implantation is suitable for the fabrication of polymer-based nanocomposites that are attractive and promising structures for the development of innovative strain gauges characterized by high reliability and sensitivity (Di Girolamo et al. 2010). However, with the increase of ion fluence, a formation of a continuous nanocrystalline Cu subsurface film near the polymer surface, together with a damaged and structurally disordered film, were obtained (aggregation of dispersed Cu nanoparticles occurs) (Di Girolamo et al. 2008; Di Girolamo et al. 2010). Meanwhile, Umeda et al. have implanted  $\text{Cu}^+$  ions of 60 keV into high-density polyethylene (HDPE), polystyrene (PS) and polycarbonate (PC) at  $1 \mu\text{A}/\text{cm}^2$  up to a total dose of  $1.5 \times 10^{17}$  ions/cm<sup>2</sup>. They reported that optical absorption spectra showed surface plasmon resonance, indicating formation of Cu nanoparticles for all the polymers, but the onset dose depended on the polymer species. The FTIR-ATR results showed that low-

energy Cu ion implantation did not cause serious damage to polymers and that Cu atoms implanted into the polymers cause nanoparticle precipitation to have promising results for optical application (Umeda et al. 2003).

Ion beam analysis (IBA) has been applied for ions depth profiling after the implantation process, where the interest is in the surface or near-surface region up to a fraction of a mm in thickness. It comprises various methods, such as: Rutherford backscattering spectrometry (RBS), nuclear reaction analysis (NRA) and particle-induced X-ray emission (PIXE) methods respectively. IBA techniques rely on the interaction of light ions of energy in the MeV range with the constituent atoms of materials and the detection of secondary products which can be either photons or ions and have an energy characteristic of the target atom. Figure 2.14 shows the physical principle process for PIXE, RBS and NRA. PIXE is a two-step process: an inner-shell electron of the target atom is expelled by the impinging ion then follows an electronic rearrangement accompanied by X-ray emission. RBS relies on a purely elastic process based upon the electrostatic repulsion between a positively charged projectile and target nuclei. NRA occurs when the projectile and the target nuclei come close enough to undergo a nuclear reaction with emission of characteristic photons or charged particles (Koen, Janssens & Van Grieken 2004).

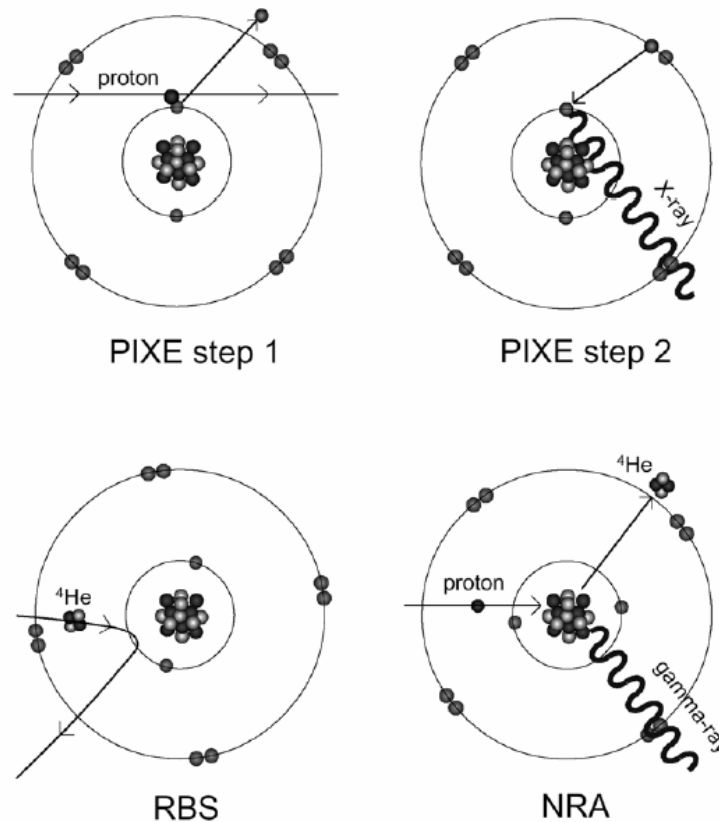


**Figure 2.14:** Physical principles of IBA techniques: PIXE, RBS and NRA (Koen, Janssens & Van Grieken 2004).

## 2.9 Electrospinning

In recent years, electrospinning has gained significant popularity as a manufacturing technique because it is a highly versatile method that can consistently produce different types of polymer fibres that range from microscale (10  $\mu\text{m}$ ) to nanoscale (<1000 nm) in diameter, resulting in materials with very high surface areas. These multilayer polymer fibres are widely used in applications such as: drug delivery, tissue engineering and protective clothing (Faccini, Vaquero & Amantia 2012; Fuh & Lien 2013; Haroosh, Chaudhary & Dong 2012; Hu, Huang & Liu 2010; Huang et al. 2012; Molamma et al. 2008; Rajeswari et al. 2012; Russo & Lamberti 2011; Sill & von Recum 2008; Yu et al. 2009). This technique provides many benefits to industry, with perhaps the most important one being its versatility and simplicity, meaning that it is a very time-efficient way to fabricate a variety of continuous

nanofibrous structures. Despite its limitations, such as relatively low productivity, the electrospinning method remains a promising and intriguing method that enables the preparation of nanofibres as a commercial process (*Technology: Electrospinning 2007-2012*; Hu, Huang & Liu 2010) since it also has been used to fabricate different types of nanocomposites by incorporating nanomaterials into various polymer matrices (Faccini, Vaquero & Amantia 2012; Lu, Zhao & Ce 2005). For instance, a study by Lu et al. succeeded in producing semiconductors of lead acetate (PbS) nanoparticles in polyvinylpyrrolidone (PVP)-fibre matrices by the electrospinning process (Figure 2.15) (Lu, Zhao & Ce 2005).

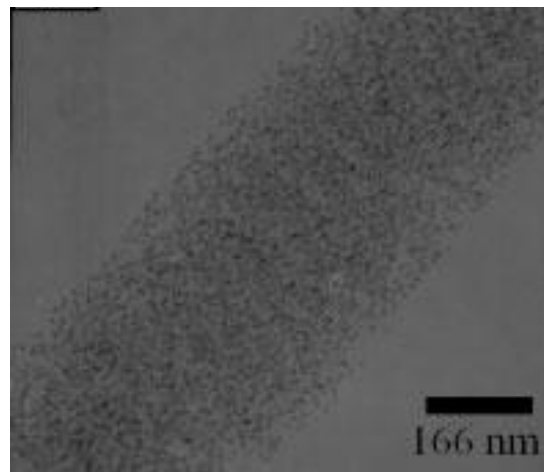


**Figure 2.15:** TEM images of PbS nanoparticles formed in PVP fibres (Lu, Zhao & Ce 2005).

Electrospinning involves the application of a high voltage electric field to a polymer solution or melt, so that mutual charge repulsion on the surface of the liquid overcomes the surface tension and causes a thin liquid jet to be ejected from the syringe through the needle. As the jet travels towards a collector target (at a different electric potential), electrostatic repulsion from charges on the surface causes the jet diameter to narrow. Continuous solid polymer fibres are formed as the jet dries or cools; they then accumulate on the collector to form a non-woven material. A schematic of the system is found in Figure 2.16.

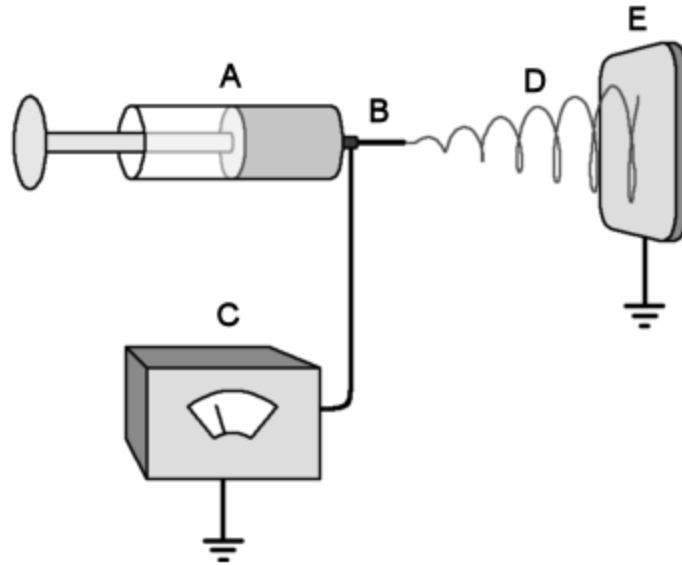


**Figure 2.16:** Schematic illustration of electrospinning processes. A polymer solution held in a syringe (A) is fed to a metal needle (B). High voltage supply (C) is connected to the needle, producing a fine jet of polymer solution (D). This dries out in transit, resulting in fine fibres which are collected on collector target (E) (*Technology: Electrospinning 2007-2012*).

In order to form a Taylor Cone and eventually a fibre, three parameters must be balanced. The first one is the flow rate of the polymer solution through the needle, which can influence both the fibre size and the shape. It has been shown that only the consistent replacement of the polymer solution that is withdrawn into nanofibres can maintain the shape of the Taylor Cone at the tip of needle (Deitzel et al. 2001; Haroosh, Chaudhary & Dong 2012; Taylor 1969). Chowdhury et al. reported that for a Nylon 6 electrospinning system, increasing the flow rate too much causes fibres to be collected without sufficient solvent evaporation, leading to an increase in the number of beads reaching the collector. This incomplete drying process causes the formation of ribbon-like fibres (fibres with many beads). Optimally, a lower solution flow rate, while maintaining the Taylor Cone, is preferable since it permits time for solvent evaporation and produces better fibres. However, a solution flow rate below the threshold for a given voltage causes evaporation at the needle tip, thus preventing electrospinning. Overall, it was found that the higher the polymer flow rate, an increase in the fibre diameter can be found up to the point where bead formation begins (Chowdhury & Stylios 2010).

The next parameter to control is that of the applied voltages which determine the Taylor Cone quality and jet whipping. The electrospinning process produces fibres only if the applied voltage is above a given limiting value required to overcome the surface tension of the solution. Too high applied voltage will result in electrospray or sparking; similarly, too little applied voltage will fail to form a Taylor Cone and jet altogether (Chowdhury & Stylios 2010; Deitzel et al. 2001; Haroosh, Chaudhary & Dong 2012). A study by Chowdhury et al. on the relationship between voltage and fibre diameter of Nylon 6 demonstrated that increasing the voltage from 12 kV to 18 kV at the same distance decreased the fibre diameter accordingly (Figure 2.17) (Chowdhury & Stylios 2010).

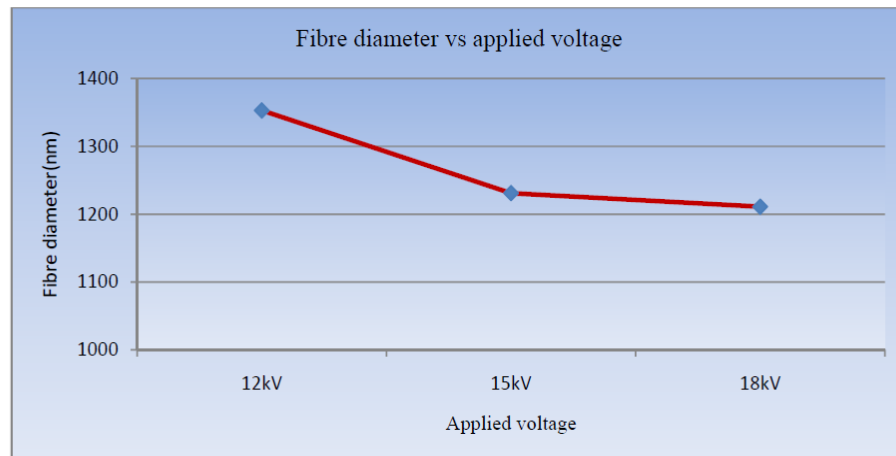


**Figure 2.17:** Relationship between the fibre diameter and applied voltage, showing the average fibre diameter for 12 kV, 15 kV and 18 kV (Chowdhury & Stylios 2010).

The last parameter of concern is in relation to the needle to collector distance which affects the jet flight time and the electric field strength across the jet. A decrease in this distance shortens jet flight times and solvent evaporation time, but increases the electric field strength, which results in an increase in bead formation. The effect of decreasing needle-collector distance is almost the same as increasing applied voltage (Chowdhury & Stylios 2010; Deitzel et al. 2001; Haroosh, Chaudhary & Dong 2012). For instance, the work by Chowdhury et al. reveals that at greater distances from the needle to the collector of 8 cm and 11 cm, electrospun Nylon 6 fibres of 1000 nm and 900 nm in diameter were produced (Figure 2.18) (Chowdhury & Stylios 2010).

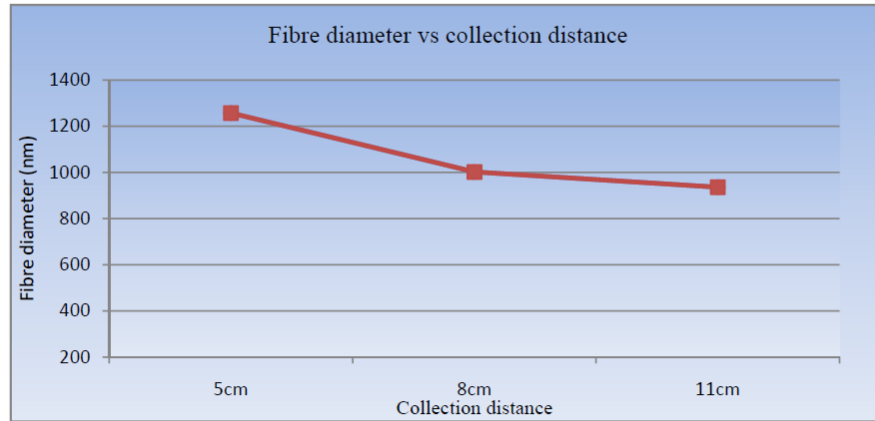


**Figure 2.18:** Relationship between the fibre diameter and needle-collector distance, showing the average fibre diameter for 5 cm, 8 cm and 11 cm (Chowdhury & Stylios 2010).

### **3. DISPERSION OF THE MICRO-SIZED FILLER INTO THE EPOXY MATRIX BASED ON THEIR X-RAY ATTENUATION ABILITY**

---

This chapter reports the fabrication of micro-sized filler-epoxy composites by using a melt-mixing method. It presents the preliminary investigation of the filler dispersion within an epoxy matrix, since the comprehensive literature survey reveals that the gamma/X-ray shielding characteristics of the fillers reinforced epoxy resins have not been attempted. This analysis allowed for discussion on the effects of filler loadings to the density, phase composition, and morphology of the epoxy composites respectively. Moreover, the X-ray attenuation by the samples was performed using a calibrated general diagnostic radiology machine.



### 3.1 Microstructured Design of Lead Oxide-Epoxy Composites for Radiation Shielding Purposes

---

This study details the fabrication of lead oxides-epoxy composites by using a melt-mixing method as published in the *Journal of Applied Polymer Science*, volume 128, pages 3213-3219 in the year 2013.

#### **Key findings:**

- The attenuation ability of the composites increased with the escalation in the composite's density.
- The calculated mass attenuation coefficient for all the composites were a few percent lower than the values interpolated from NIST for the given X-ray tube voltages.
- Epoxy composites having 50 wt% of PbO or Pb<sub>3</sub>O<sub>4</sub> provided better radiation shielding than the 50 wt % of PbO reinforced isophthalate resin composite fabricated by Harish and coworkers.
- PbO and Pb<sub>3</sub>O<sub>4</sub> compounds used were confirmed as a single-phase pure.
- Fairly uniform dispersion of fillers was found within the epoxy matrix.
- The average particle size for composite with filler loading of  $\leq 30$  wt% is 1–5  $\mu\text{m}$  and 5–15  $\mu\text{m}$  for composites with filler loading of  $\geq 50$  wt%.

## Microstructural Design of Lead Oxide-Epoxy Composites for Radiation Shielding Purposes

Nurul Zahirah Noor Azman,<sup>1,2</sup> Salim Ahmed Siddiqui,<sup>1</sup> Robin Hart,<sup>3</sup> It Meng Low<sup>1</sup>

<sup>1</sup>Department of Imaging and Applied Physics, Faculty of Science and Engineering, Curtin University, Perth, Western Australia 6845, Australia

<sup>2</sup>School of Physics, Universiti Sains Malaysia, 11800 Penang, Malaysia

<sup>3</sup>Department of Radiology, Royal Perth Hospital, East Perth, Western Australia 6001, Australia

Correspondence to: I. M. Low (E-mail: j.low@curtin.edu.au)

**ABSTRACT:** Composite epoxy samples filled with PbO and Pb<sub>3</sub>O<sub>4</sub> were fabricated to investigate the mass attenuation characteristics of the composites to X-rays in the diagnostic imaging energy range. The effect of density on the attenuation ability of the composites for radiation shielding purposes was studied using a calibrated X-ray machine. Characterization of the microstructure properties of the synthesized composites was performed using synchrotron radiation diffraction, optical microscopy, and scanning electron microscopy. The results indicate that the attenuation ability of the composites increased with an increase in density. The particle size of WO<sub>3</sub> fillers has a negligible effect on the value of mass attenuation coefficient. Microstructural analyses have confirmed the existence of fairly uniform dispersion of fillers within the matrix of epoxy matrix with the average particle size of 1–5 μm for composites with filler loading of ≤ 30 wt % and 5–15 μm for composites with filler loading of ≥ 50 wt %. © 2012 Wiley Periodicals, Inc. *J. Appl. Polym. Sci.* 128: 3213–3219, 2013

**KEYWORDS:** radiation; radiation shielding; resins; composites; density; microscopy

Received 25 June 2012; accepted 25 August 2012; published online 20 September 2012

**DOI:** 10.1002/app.38515

### INTRODUCTION

During the early part of the 20th century, the hazards from ionizing radiation were recognized, and the use of lead and other materials became commonplace for shielding against X-rays.<sup>1–3</sup> Once the dangers of X-rays are considered, lead has become an important material for radiation protection. Since then protection has evolved into an elaborate infrastructure of controls and disciplines specifying how this shield should be deployed.<sup>4–6</sup> Recently, shielding requirements have become more stringent as standards for exposure of personnel and the general public. X-ray technologists practice a principle called as-low-as-reasonably-achievable dose when dealing with X-rays, so that radiation dose received by personnel and the general public can be as low as possible.<sup>3,7</sup>

The shielding for radiation purposes are based on the type and energy of the radiation itself. Gamma and X-rays are the most penetrating radiations as compared to other ionizing radiations. Their interaction depends on the probability of their collision with the atoms of the materials during the interaction. To increase the probability, they will interact the density of the material they are passing through needs to be increased which

means the materials should have a lot of atoms with an assumption that the materials are free from voids. If dealing with a material having a lot of pores, porosity needs to be taken into account, because it will affect the interaction of the radiations with the atoms within the material.<sup>8</sup>

Lead-glass is one example of the material used as shielding materials for ionizing radiations, but it is heavy, expensive, and very brittle. So, it is not surprising that polymers have made inroads into markets that were in the beginning dominated by glass. Polymers also have a great potential in many important applications that glass could not meet because of their unique properties, such as a low density, ability to form intricate shapes, optical transparency, low manufacturing cost, and toughness. However, the use of polymers is still limited, because of their inherent softness and low thermal stability.<sup>9,10</sup> One modern example of the filler-reinforced polymer used for radiation shielding is lead-acrylic.<sup>11,12</sup> Moreover, many researchers tried to create new lead-based composites for this radiation shielding purposes such as lead-polyester composites,<sup>13</sup> lead-styrene butadiene rubber,<sup>14</sup> lead-polystyrene,<sup>15</sup> and similar materials.

**Table I.** List of Composites Prepared with Different Weight Fractions of Filler and Epoxy System and Corresponding Designations Used in This Study

Composite by weight fraction (wt %)			Composite designation
Filler	Epoxy system		
PbO	10	90	A1
	30	70	A2
	50	50	A3
	70	30	A4
Pb <sub>3</sub> O <sub>4</sub>	10	90	B1
	30	70	B2
	50	50	B3
	70	30	B4

Rudraswamy et al.<sup>16</sup> have shown that some lead compounds such as PbO, PbO<sub>2</sub>, PbNO<sub>3</sub>, and PbCl<sub>2</sub> have an adequate mass attenuation coefficient,  $\mu_m$  for use in radiation shielding purposes. Unfortunately, the usage of either lead or lead compounds alone will cause certain health risks to human, animals, and also to the surroundings.<sup>17</sup> Moreover, lead or lead compounds themselves are also not really malleable and lack in mechanical strength.<sup>18</sup>

Additionally, there are many methods available to achieve a good dispersion of fillers within a polymeric matrix. One of the traditional methods for dispersing fillers in polymer matrices is melt-mixing method of the fillers into the polymer. The fillers are weighted and added straightly into the polymer for mixing. In many works done, many researchers used a static mixer with constant speed during the mixing process to achieve homogeneously dispersion of fillers within the polymers.<sup>13,19</sup>

It is expected that lead oxide–epoxy composites will be a good material to be used as radiation shielding in diagnostic radiology purposes. This is because lead oxide can be easily dispersed within a polymer matrix.<sup>13</sup> Besides, an epoxy system is a thermoset material that is generally stronger and better suited to higher temperatures than thermoplastics, so it can withstand the high energetic X-rays bombardment during the diagnostic imaging.<sup>20</sup> Hence, the purpose of this study is to prepare and characterize a composite that is made of an epoxy system filled with lead oxides. The feasibility of this material for use in X-ray shielding is discussed.

## EXPERIMENTAL METHODS

### Samples Preparation

To prepare PbO–epoxy composite samples, micron-sized PbO powder (Chem Supply, Gillman, South Australia, product number LL021) was added into the FR251 epoxy resin (Bisphenol-A diglycidyl ether polymer) before the FR251 hardener (isophoronediamine) was mixed into it. The ratio of epoxy resin to hardener used was 2 : 1. The mixing of PbO powder in epoxy resin was done through gentle stirring with a wooden stick within a beaker with constant speed for 10 min to ensure fairly uniform dispersion of the powder in epoxy matrix. The well-mixed mixture was then cast in a 4 × 6 cm<sup>2</sup> rectangular silicon rubber mold with a thickness of 5 mm and was allowed to set over-

night at room temperature. The list of samples with different weight percentages of PbO are shown in Table I.

The same procedure was used to prepare epoxy composites filled with micron-sized Pb<sub>3</sub>O<sub>4</sub> powder (Chem Supply, Gillman, South Australia, product number LL027). The list of samples is also shown in Table I.

### Density Measurements

The apparent density  $\rho$  of prepared samples was measured using the Archimedes method and calculated using eq. (1).<sup>21</sup> A calibrated single pan electrical balance, ethanol, and toluene were used for this purpose.

$$\rho = \frac{m_1}{m_2 - m_3}(\rho_l) \quad (1)$$

where  $m_1$ ,  $m_2$ , and  $m_3$  are the mass of the sample weighted on the balance, the mass of the sample hanging on balance arm in the air, and the mass of the sample hanging on the balance arm immersed in ethanol or toluene, respectively, whereas  $\rho_l$  is the density of the immersion liquid.

The measured densities were compared with the theoretical values,  $\rho_c$  (with an assumption that the samples were free from voids) which are determined according to eq. (2)<sup>13</sup>:

$$\rho_c = \frac{100}{\left[\frac{F}{\rho_f} + \frac{E}{\rho_e}\right]} \quad (2)$$

where  $F$  is the wt % of the filler,  $E$  is the wt % of epoxy,  $\rho_f$  is the density of filler, and  $\rho_e$  is the density of epoxy.

### Measurement of X-ray Mass Attenuation Coefficients

To determine the initial dose ( $D_0$ ), the generated X-rays were directly exposed to the DIADOS diagnostic detector connected to DIADOS diagnostic dosimeter (PTW-Freiburg, Germany) without having passed through any sample. The distance between the X-ray tube and the detector was set to 100 cm, and the X-ray beam was well collimated according to the size of the sample. This experiment was done using a calibrated X-ray machine in Royal Perth Hospital, Western Australia. The final dose ( $D$ ) was taken with the sample placed on the detector. The exposure was set at 10 mA s, where the X-ray tube voltage was started at 40 kV<sub>p</sub> with 10 kV<sub>p</sub> increment up to 100 kV<sub>p</sub>. Next, the linear attenuation coefficient,  $\mu$ , for each sample was determined by eq. (3), where  $x$  is the thickness of the sample. This  $\mu$  is divided by the calculated  $\rho_c$  to determine  $\mu_m$  [eq. (4)].

$$\mu = \frac{(\ln \frac{D_0}{D})}{x} \quad (3)$$

The observed results of  $\mu_m$  were compared with the theoretical values evaluated from Hubbell's database, NIST XCOM.

$$\mu_m = \frac{\mu}{\rho_c} \quad (4)$$

### Powder Diffraction

Powder diffraction measurements were performed at the Australian Synchrotron in Melbourne to identify the crystalline phases

**Table II.** Comparison of Measured and Theoretical Density Values for the Composites

Composite designation	Density of composite, $\rho_{comp}$ (g/cm <sup>3</sup> )	
	Theoretical	Measured
A1	1.26	1.26 ± 0.01
A2	1.56	1.53 ± 0.01
A3	2.06	2.05 ± 0.02
A4	3.00	2.93 ± 0.03
B1	1.26	1.26 ± 0.01
B2	1.55	1.55 ± 0.01
B3	2.02	2.00 ± 0.03
B4	2.90	2.83 ± 0.03

present in the samples. This work was conducted on the Powder Diffraction beamline, and the diffraction patterns were recorded in the  $2\theta$  range of 10–60° at a fixed wavelength of 1.37 Å.

### Optical Microscopy

Optical microscopy was done using Nikon ME600 optical microscope. The samples were polished using diamond pastes from 15 to 1.0  $\mu\text{m}$  to obtain mirror-like surface finish.

### Scanning Electron Microscopy

The surface of the samples was also examined using a Zeiss Evo 40XVP scanning electron microscope. Samples were Pt-coated

**Table III.** Equivalent Energy for the Various X-ray Tube Voltages Used

X-ray tube voltage (kV <sub>p</sub> )	Equivalent energy (keV)
40	29.9
50	34.3
60	38.5
70	42.5
80	46.2
90	49.7
100	52.9

to prevent any charging on the samples during the imaging process. The backscattered electron technique was chosen to gain better contrast because of different atomic number between epoxy and lead. A pure epoxy sample was also examined as a control.

## RESULTS AND DISCUSSION

### Density of Samples

As can be seen from Table II, the values of apparent density for samples obtained from the Archimedes' technique did not totally agreed with the theoretical values because of experimental uncertainties. The porosity calculated for each sample was less than 1%. Besides, the higher the wt % of the filler within the composite, the higher the value of  $\rho_c$  as also been observed by Harish et al.<sup>13,22</sup>

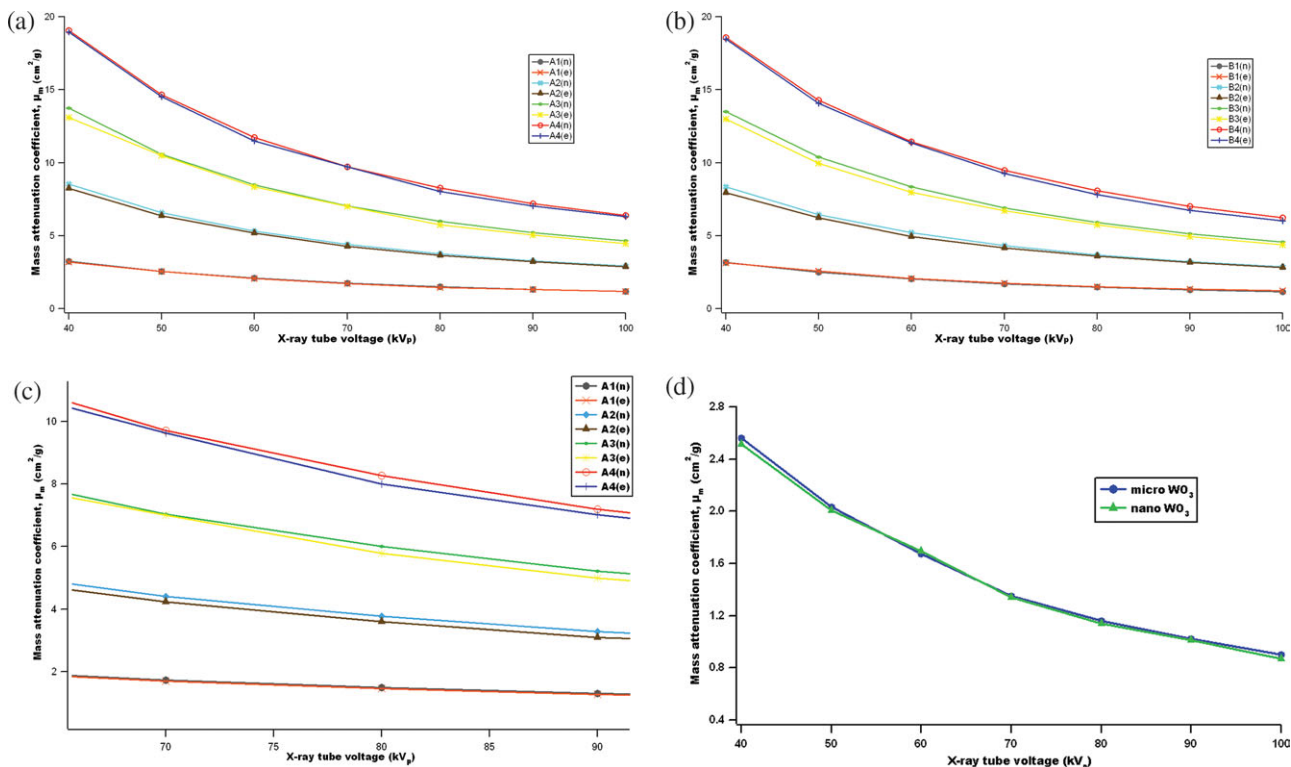


**Figure 1.** Mass attenuation coefficients as a function of kV<sub>p</sub> as obtained from NIST (n) and experiment (e) for samples of (a) PbO–epoxy composite, (b) Pb<sub>3</sub>O<sub>4</sub>–epoxy composite, (c) close-up view of (a), and (d) micro- and nano-WO<sub>3</sub> epoxy composites. [Color figure can be viewed in the online issue, which is available at [wileyonlinelibrary.com](http://wileyonlinelibrary.com).]



**Table IV.** Mass Attenuation Coefficients Interpolated from NIST Databases for Gamma Rays of Energy 0.662 MeV from Cs-137 Point Source

Composite designation	Mass attenuation coefficient, $\mu_m$ (cm <sup>2</sup> /g)
A1	0.0871
A2	0.0924
A3	0.0978
A4	0.1055
B1	0.0871
B2	0.0922
B3	0.0974
B4	0.1025

### X-ray Mass Attenuation Coefficients

The  $\mu_m$  values given in NIST are specifically measured for characteristic photon energy, whereas in this experiment; the X-ray tube voltages used are in continuous spectrum. So, the equivalent energies for the X-ray tube voltages used within the experiment must be taken into account for comparing the value of  $\mu_m$  between NIST and experiment. The equivalent energies for the X-rays tube voltages used are shown in Table III. These values were calculated using the equation fitted as an exponential function<sup>23</sup>:

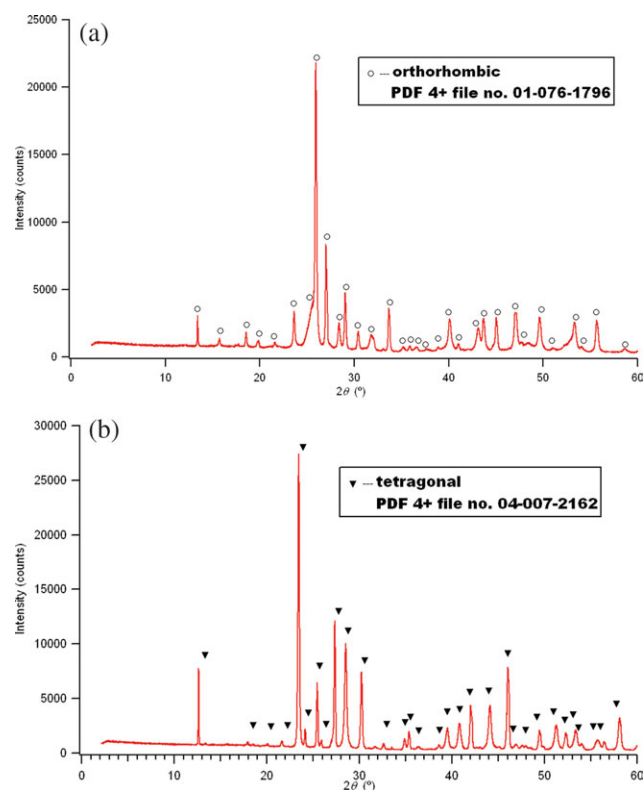


**Figure 2.** Typical powder diffraction patterns for (a) PbO-epoxy composite and (b) Pb<sub>3</sub>O<sub>4</sub>-epoxy composite. [Color figure can be viewed in the online issue, which is available at wileyonlinelibrary.com.]

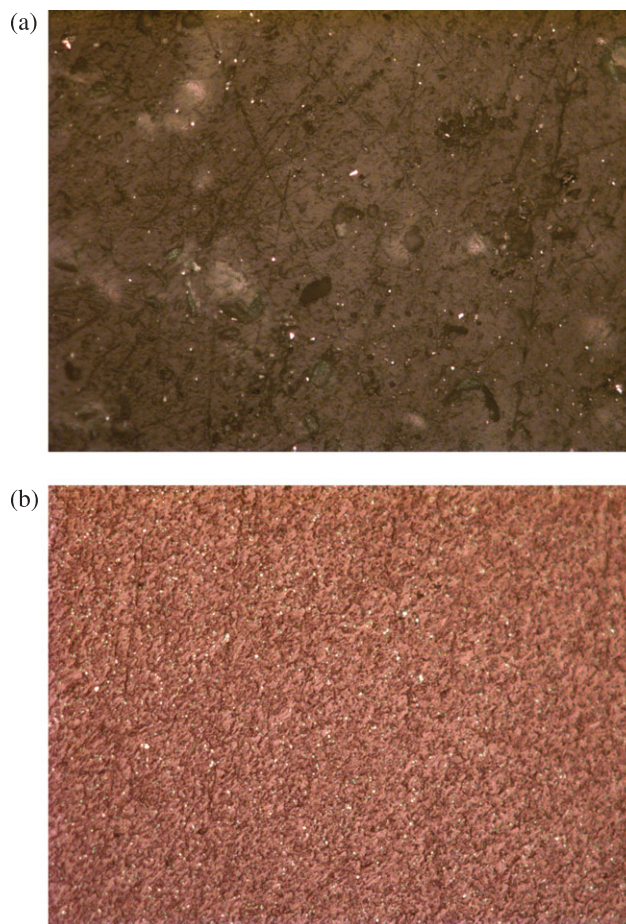


**Figure 3.** Optical micrographs showing the typical uniform dispersion of fillers in the matrix of epoxy for two composite samples: (a) A3 and (b) B2. 50 × magnification. [Color figure can be viewed in the online issue, which is available at wileyonlinelibrary.com.]

$$y = a_{\text{exp}} \left(\frac{x}{c}\right) + b \quad (5)$$

where  $a$ ,  $b$ , and  $c$  in the eq. (5) are constants with values of  $-97.535$ ,  $106.857$ , and  $168.672$ , respectively, whereas  $y$  is the equivalent energy and  $x$  is the X-ray tube voltage.

For composites, the value of  $\mu_m$  was calculated using eq. (6):

$$\mu_m = \sum w_i \mu_{m_i} \quad (6)$$

where  $\mu_m$  is the mass attenuation coefficient of the composite, whereas  $w_i$  and  $\mu_{m_i}$  are the weight fraction and the mass attenuation coefficient of each compound used to make the composite, respectively.

The plots in Figure 1(a–c) show that almost all the lines for the  $\mu_m$  experimental values were a few percent lower than the  $\mu_m$  values interpolated from NIST for the given X-ray tube voltages. These results are similar to the work done by Gerward et al., which they have found that tabulated X-ray mass attenuation coefficients are commonly a few percent higher than the measured values.<sup>24,25</sup> İçelli et al.<sup>26</sup> obtained very similar results

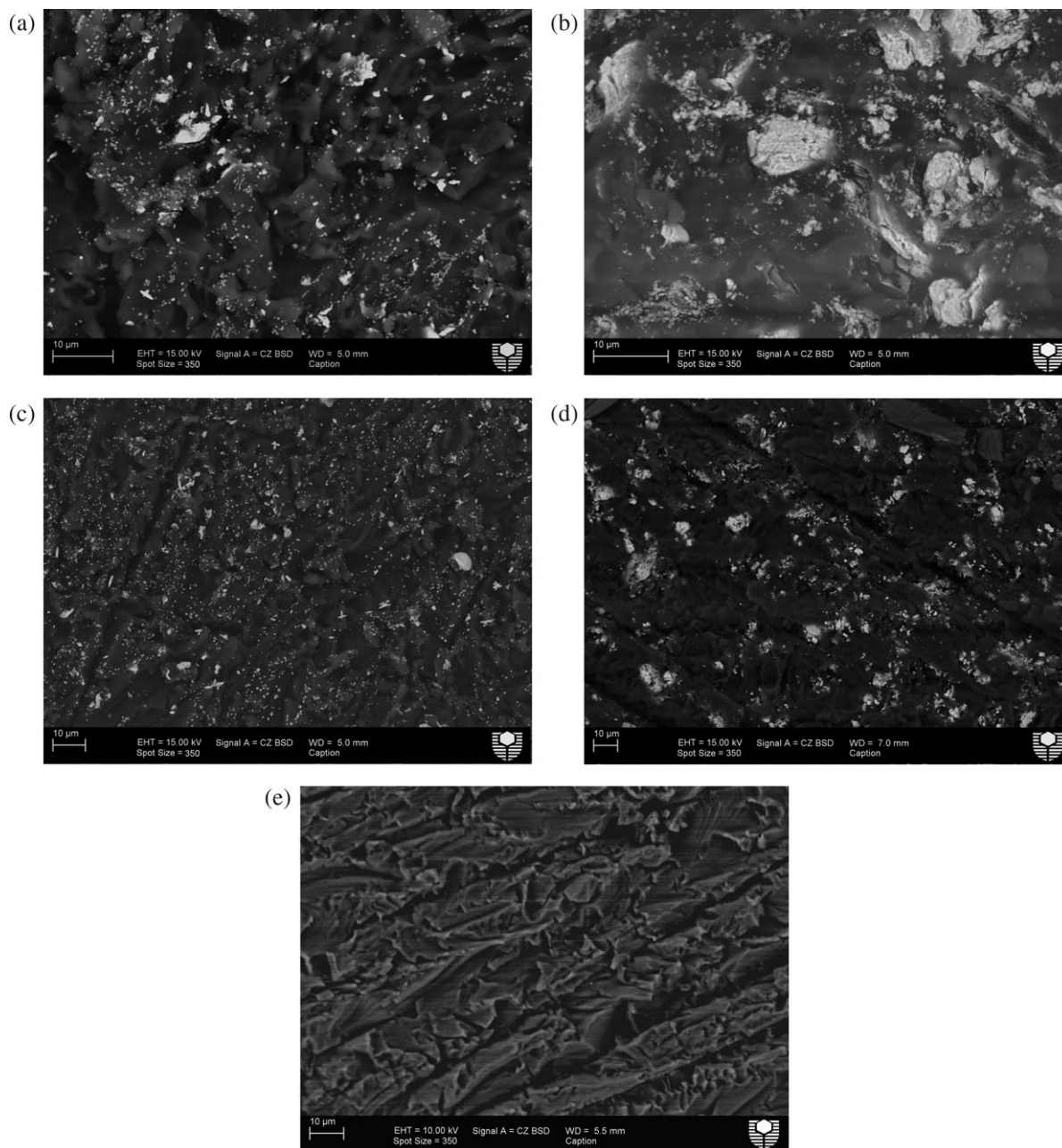


**Figure 4.** SEM micrographs showing the uniform dispersion of PbO or Pb3O4 particles within the epoxy matrix in various composite samples: (a) A3, (b) A4, (c) B2, (d) B3, and (e) pure epoxy.

where the higher the density of the material, the higher the value of  $\mu_m$ .

However, the relationship between mass attenuation coefficient ( $\mu_m$ ) and particle size of lead oxide remains unknown. In particular, would the use of nanosized lead oxide increase or decrease the value of  $\mu_m$ ? As nanosized lead oxide was not available, the effect of particle size of  $WO_3$  filler (purchased from Sigma-Aldrich, Castle Hill, NSW, Australia) on  $\mu_m$  was studied. The procedure to prepare this composite was similar to that for preparing PbO-epoxy samples. Figure 1(d) shows the effect of particle size on the mass attenuation coefficient in epoxy composite filled with either microsized ( $\sim 20 \mu m$ ) or nanosized

( $< 100 \text{ nm}$ )  $WO_3$ . It is clearly shown that particle size has a negligible effect on the value of  $\mu_m$  of a material for this range of X-ray energy 40–100 kV<sub>p</sub>. However, it should be noted that nanosized particles (e.g., CuO) have been reported to show better X-ray attenuation at the lower X-ray beam energy (i.e., 26–30 kV).<sup>27,28</sup> As photoelectric absorption dominates at low photon energies, the probability of an X-ray with low energy to interact and to be absorbed is higher for nanosized particles, in addition to maximization of the surface/volume ratio. However, as photon energy increases, the probability of Compton scattering increases, and hence the attenuation by the material decreases, as this interaction is weakly dependent on atomic

number of the element and the photon energy. Hence, the probability of an X-ray with higher energy to interact and to be absorbed becomes similar for both nanosized and microsized particles. It appears that the use of nanosized particles only helps in providing a fairly uniform dispersion within the epoxy matrix but has no direct effect on the value of  $\mu_m$  as clearly indicated in eq. (4). Only the abundance of  $\text{WO}_3$  dispersed in the composite will influence the value of  $\mu_m$ .

The mass attenuation coefficient,  $\mu_m$  is the rate of photon interactions within 1-unit of mass per 1-unit of area ( $\text{g}/\text{cm}^2$ ). It depends on the energy of the photon and the concentration of electrons in the material. Its value will decrease rapidly with the increment of photon energy. Further the chance of a photon coming close enough to an electron is higher when the concentration of electrons within the material is higher, because it is absorbed by the material. Electron concentration was determined by the physical density of the material. Thus, composites with a fine dispersion of high density material provide more interaction probability for photons and also better radiations shielding properties.<sup>13,29</sup>

To ascertain the shielding ability of the composites, calculations of  $\mu\mu_m$  were done to compare the 50 wt % of PbO reinforced isophthalate resin composite performed by Harish et al.<sup>13</sup> The value of  $\mu_m$  for their composite was calculated to be 0.0948  $\text{cm}^2/\text{g}$ , whereas the values of  $\mu_m$  for samples A3 and B3 in this study, which also have 50 wt % of the fillers, were 0.0978 and 0.0974  $\text{cm}^2/\text{g}$ , respectively. The calculation of  $\mu_m$  was done by interpolating NIST databases for gamma rays of energy 0.662 MeV from a Cs-137 point source. These results show that samples A3 and B3 in this study provided better radiation shielding than the composite fabricated by Harish and coworkers. Moreover, the usage of lead oxides for radiation shielding can be minimal in the fabrication of composites and thus reduce the health risks associated with lead oxides. The results for other samples at the same energy range are shown in Table IV.

#### Phase Compositions

The reference for phase-fitting the peaks were taken from International Centre for Diffraction Data PDF-4 + 2009 database. The wavelength for all of these databases was chosen to be the same as the wavelength of the synchrotron radiation used.

From Figure 2(a), all the peaks belong to orthorhombic PbO crystal structures (PDF-4 + files 01-076-1796). While for composite filled with  $\text{Pb}_3\text{O}_4$  powder, all the peaks were identified as tetragonal  $\text{Pb}_3\text{O}_4$  crystal structures (PDF-4 + file 04-007-2162) as shown in Figure 2(b). These indicate that the powders of PbO and  $\text{Pb}_3\text{O}_4$  used were single-phase pure.

#### Microstructures

The typical fracture surfaces for the samples are shown in Figure 3. The scratches seen in the images were due to the polishing process. These images have shown that the fractured surfaces were quite rough, and the fillers (white patches) were well dispersed and firmly embedded in the epoxy matrix due to their relatively small particle size and good compatibility with the epoxy matrix. Although the fillers have a greater weight fraction than epoxy, they were dispersed quite uniformly with only some

agglomerations to be found. As can be seen in Figure 3(a), the blurry white patches are clear indications of some minor filler agglomerations.

The scanning electron microscopy (SEM) images in Figure 4 have provided results that agreed with the optical images shown in Figure 3. The bright regions represent the filler particles (lead-oxide) dispersed in the dark epoxy matrix. The fillers were seen to be quite uniformly dispersed in the composites, although minor agglomerations can be observed. The average particle size obtained from the SEM images was  $\sim 1\text{--}5\ \mu\text{m}$  for composites with filler loading of  $\leq 30\ \text{wt}\%$  and  $\sim 5\text{--}15\ \mu\text{m}$  for composites with filler loading of  $\geq 50\ \text{wt}\%$ .

#### CONCLUSIONS

Epoxy composites filled with fairly dispersed lead oxide particles of  $1\text{--}5\ \mu\text{m}$  for composites with filler loading of  $\leq 30\ \text{wt}\%$  and  $5\text{--}15\ \mu\text{m}$  for composites with filler loading of  $\geq 50\ \text{wt}\%$  have been successfully fabricated. These composites showed good X-ray attenuation properties and could be considered as a potential candidate for radiation shielding in diagnostic radiology purposes. The particle size of  $\text{WO}_3$  fillers has a negligible effect on the value mass attenuation coefficient ( $\mu_m$ ) for the X-ray energy of  $40\text{--}100\ \text{kV}_p$ . In addition, the lead oxide-epoxy composites in this study are superior to the lead oxide-isophthalate resin composite previously investigated.

#### ACKNOWLEDGMENTS

The funding for the collection of synchrotron powder diffraction data at the Australian Synchrotron in this work was provided by Grant Number AS111/PD3509 and AS111\_PDFI3181.

#### REFERENCES

1. Archer, B. R.; Thornby, J. I.; Bushong, S. C. *Health Phys.* **1983**, *44*, 507.
2. Archer, B. R. *Health Phys.* **1995**, *69*, 750.
3. Archer, B. R. *Health Phys.* **2005**, *88*, 579.
4. Hessenbruch, A. *Endeavour* **2002**, *26*, 137.
5. Okunade, A. A. *Appl. Radiat. Isotopes* **2002**, *57*, 819.
6. Okunade, A. A. *Med. Phys.* **2004**, *31*, 513.
7. Dixon, R. L.; Simpkin, D. J. *Health Phys.* **1998**, *74*, 181.
8. Lorenzen, W. MadSci Network: Engineering, **2000**.
9. Polymer versus Glass, POLYMICRO Newsletter, 2004. Available at: <http://www.polymicro-cc.com>. Accessed on 24 June 2011.
10. Lee, E. H., Rao, G. R., Lewis, M. B., Mansur, L. K. *Nucl. Instrum. Methods Phys. Res. Sect. B: Beam Interact. Mater. Atoms* **1993**, *74*, 326.
11. Premac Lead Acrylic, Part of the Wardray Premise Total Radiation Shielding Package, Wardray Premise Ltd. Available at: <http://wardray-premise.com/structural/materials/premac.html>. Accessed on 4 May 2011.
12. Radiation Safety & Consumable Products. Available at: [http://www.lablogic.com/moreinfo/PDF/consumables/lablogic\\_consumables\\_brochure.pdf](http://www.lablogic.com/moreinfo/PDF/consumables/lablogic_consumables_brochure.pdf). Accessed on 4 May 2011.



13. Harish, V.; Nagaiah, N.; Prabhu, T. N.; Varughese, K. T. *J. Appl. Polym. Sci.* **2009**, *112*, 1503.
14. Abdel-Aziz, M. M.; Badran, A. S.; Abdel-Hakem, A. A.; Helaly, F. M.; Moustafa, A. B. *J. Appl. Polym. Sci.* **1991**, *42*, 1073.
15. Pavlenko, V. I.; Lipkanskii, V. M.; Yastrebinskii, P. N. *J. Eng. Phys. Thermophys.* **2004**, *77*, 11.
16. Rudraswamy, B.; Dhananjaya, N.; Manjunatha, H. *Nucl. Instrum. Methods Phys. Res. Sect. A: Accelerators Spectrometers Detectors Associated Equipment* **2010**, *619*, 171.
17. Robert, R. D. High Density Composites Replace Lead; Eco-mass Technologies, Austin, Texas, USA **2005**.
18. Spinks, J. W. T.; Wood, R. J. An Introduction to Radiation Chemistry, Wiley-Interscience: New York, **1976**.
19. Tanahashi, M. *Materials* **2010**, *3*, 1593.
20. Material Guide, Archos LLC. Available at: [http://www.archos-llc.com/Material\\_Guide\\_2.html](http://www.archos-llc.com/Material_Guide_2.html). Accessed on 20 June 2011.
21. Australian Standards 1774.5, Method 5. The Determination of Density, Porosity and Water Absorption, 1989.
22. Berger, M. J.; Hubbell, J. H.; Seltzer, S. M.; Chang, J.; Coursey, J. S.; Sukumar, R.; Zucker, D. S.; Olsen, K. XCOM: Photon Cross Section Database (version 1.5), National Institute of Standards and Technology, Gaithersburg, MD, **2010**. Available at: <http://physics.nist.gov/xcom>. Accessed on 20 June 2011.
23. Mincong, C.; Hongmei, L.; Ziyu, C.; Ji, S. *Appl. Radiat. Isotopes* **2008**, *66*, 1387.
24. Gerward, L. *Nuclear Inst. Methods Phys. Res. B* **1992**, *69*, 407.
25. Midgley, S. M. *Radiat. Phys. Chem.* **2005**, *72*, 525.
26. İçelli, O.; Erzeneoglu, S.; Boncukçuoğlu, R. *Ann. Nuclear Energy* **2004**, *31*, 97.
27. Botelho, M. Z.; Künzel, R.; Okuno, E.; Levenhagen, R. S.; Basegio, T.; Bergmann, C. P. *Appl. Radiat. Isotopes* **2011**, *69*, 527.
28. Künzel, R.; Okuno, E. *Appl. Radiat. Isotopes* **2012**, *70*, 781.
29. Sprawls, P. The Physical Principles of Medical Imaging, Aspen Publishers: Gaithersburg, Md **1993**.



## 3.2 Synthesis and Characterization of Epoxy Composites Filled with Pb, Bi or W Compound for Shielding of Diagnostic X-rays

---

In this work, further analyses of filler-reinforced epoxy resins by melt-mixing method are reported as published in the *Applied Physics A: Materials Science & Processing*, volume 110, pages 137-144 in the year 2013.

This work comprises similar characterizations of the synthesized different species of filler (PbCl<sub>2</sub>, WO<sub>3</sub> and Bi<sub>2</sub>O<sub>3</sub>)-epoxy composites. These are detailed in Chapter 3.1, with a discussion of their mechanical properties. In addition, the feasibility of these composites for use in X-ray shielding is compared with that of commercial lead glass.

### Key findings:

- The measured density of the composites did not agree very well with the theoretical values, especially when the filler loading was more than 30 wt% due to lack of epoxy to fully cover the surfaces of filler powder.
- For the same filler type and at the same X-ray tube voltage, X-ray transmission value was decreased by the increment of the filler loading.
- Bi<sub>2</sub>O<sub>3</sub>-epoxy composite of 8 mm thickness having 70 wt% of Bi<sub>2</sub>O<sub>3</sub> gave nearly the same X-ray transmission value as compared with 10 mm thickness of lead glass which contained 56 wt% of Pb, despite being thinner than lead glass.
- PbCl<sub>2</sub>, Bi<sub>2</sub>O<sub>3</sub> and WO<sub>3</sub> compounds used were single-phase pure without impurities.
- Uniform dispersion of fillers within the epoxy matrix for the composite having low filler loading.
- Filler agglomerations can be seen in the composites with  $\geq 50$  wt% of filler.
- The flexural strength has improved for composites with 10 wt% filler loading and then decreased for filler loading  $\geq 30$  wt%.
- Both the flexural modulus and hardness of the composites increased with a subsequent escalation in filler loading.

\*\*In Table 1 (page 44), the unit of the density is g/cm<sup>3</sup>; not cm<sup>3</sup>/g.

# Synthesis and characterization of epoxy composites filled with Pb, Bi or W compound for shielding of diagnostic x-rays

Nurul Z. Noor Azman · Salim A. Siddiqui · It M. Low

Received: 2 October 2012 / Accepted: 20 November 2012 / Published online: 5 December 2012  
© Springer-Verlag Berlin Heidelberg 2012

**Abstract** Lead chloride, bismuth oxide and tungsten oxide filled epoxy composites with different weight fractions were fabricated to investigate their x-ray transmission characteristics in the x-ray diagnostic imaging energy range (40–127 kV) by using a conventional laboratory x-ray machine. Characterizations of the microstructure properties of the synthesized composites were performed using synchrotron radiation diffraction, backscattered electron imaging microscopy, three-point bend test and Rockwell hardness test. As expected, the x-ray transmission was decreased by the increment of the filler loading. Meanwhile, the flexural modulus and hardness of the composites were increased through an increase in filler loading. However, the flexural strength showed a marked decrease with the increment of filler loading ( $\geq 30$  wt%). Some agglomerations were observed for the composites having  $\geq 50$  wt% of filler.

## 1 Introduction

X-rays/gamma-rays are the most penetrating of ionizing radiation that is known to be harmful to human health and heredity. Hence there is no doubt that the attenuation of them through composite materials has attracted much attraction amongst the researchers especially for medical studies

[1–3]. The most important quantity to characterize the attenuation of photons (x-rays/gamma-rays) within the extended material they pass through is the linear attenuation coefficient ( $\mu$ ) or mass attenuation coefficient ( $\mu/\rho$ ). This quantity is needed in solving various problems such as in radiation dosimetry and radiation shielding application [1, 4, 5].

Lead-glass is one of the materials used for shielding of ionizing radiations, but it is heavy, expensive and very brittle. So, it is not surprising that the application of polymers in x-ray shielding technology is increasing steadily. This is due to a number of advantages that glass could not meet because of their unique properties, such as low manufacturing cost and rugged shatter-resistant material. In addition, the improved dispersion of fillers within polymer will enable the formation of mechanically stable materials and the possibility to modify both chemical composition and the related physical properties of polymers by easy-to-control fabrication parameters [6–10]. However, the use of polymers is still limited because of their inherent softness and low thermal stability [11–13].

Recently, many researchers have tried to synthesize new filler-reinforced polymer composites for radiation shielding and as the replacement for lead glass which is heavy and very fragile [14–17]. The x-ray shielding properties of the filler-reinforced polymer composites generally increase with a good dispersion degree of the filler within the polymer [18]. One modern example of the filler-reinforced polymer used for radiation shielding is lead-acrylic [19, 20]. The lead acrylic of the same size of lead glass with equal lead equivalence, the lead acrylic has nearly twice the weight of lead glass, and it is even thicker than lead glass if just looking for the same lead equivalent factor, hence reducing the observation capabilities.

The comprehensive literature survey reveals that the gamma/x-ray shielding characteristics of filler-reinforced

---

N.Z. Noor Azman · S.A. Siddiqui · I.M. Low (✉)  
Department of Imaging & Applied Physics, Curtin University,  
GPO Box U1987, Perth, WA 6845, Australia  
e-mail: [j.low@curtin.edu.au](mailto:j.low@curtin.edu.au)  
Fax: +618-9266-2377

N.Z. Noor Azman  
School of Physics, Universiti Sains Malaysia, 11800 Penang,  
Malaysia

epoxy resins have not been attempted. In a recent work on WO<sub>3</sub>-filled epoxy composites [21], we investigated only the effect of nano-sized and micro-sized fillers on x-ray attenuation in the energy range of 22–127 kV, but the mechanical properties of these composites were not investigated. The results showed that nano-sized WO<sub>3</sub> was more effective than micro-sized WO<sub>3</sub> in x-ray attenuation only at the low energy range of 22–35 kV, but this size effect was not apparent at the higher energy range of 40–120 kV.

Thus, the aim of this study was to prepare, characterize and compare the physical, mechanical and x-ray transmission properties of epoxy composites filled with Pb, Bi or W compound. The feasibility of these composites for use in x-ray shielding is compared with the commercial lead glass.

## 2 Experimental procedure

### 2.1 Samples preparation

Powders of lead chloride (~10 μm, PbCl<sub>2</sub>) (Chem Supply), bismuth oxide (~10 μm, Bi<sub>2</sub>O<sub>3</sub>) and tungsten oxide (~20 μm, WO<sub>3</sub>) (Sigma Aldrich) were used as fillers for synthesizing filler-reinforced epoxy composites. Commercial FR251 epoxy resin (Bisphenol-A diglycidyl ether polymer) and FR251 hardener (Isophoronediamine) were used for the preparation of composites.

PbCl<sub>2</sub>-epoxy composite samples were prepared by mixing the epoxy resin with four different weight percentages (10, 30, 50 and 70 %) of PbCl<sub>2</sub> using a mechanical stirrer at constant speed for 15 minutes to ensure uniform dispersion of the powder in an epoxy matrix. After that, the hardener was added to the mixture and then manually stirred slowly to minimize the formation of air bubbles within the sample. The well-mixed mixture was then cast in a 4 cm × 6 cm rectangular silicon rubber mold with a thickness of 8 mm and left for 24 hours at room temperature for curing. The same procedure was used to prepare epoxy composites filled with Bi<sub>2</sub>O<sub>3</sub> and WO<sub>3</sub>.

### 2.2 Density measurements

The Archimedes method was used for determining the apparent density ( $\rho_s$ ) of prepared samples by using Eq. (1) [22]. A calibrated single pan electrical balance and ethanol were used for this purpose.

$$\rho_s = \frac{m_1}{m_2 - m_3}(\rho_e), \quad (1)$$

where  $m_1$ ,  $m_2$  and  $m_3$  are the mass of the sample weighted in the balance, the mass of the sample hanging on the balance arm in the air and the mass of the sample hanging on the balance arm immersed in ethanol respectively, and  $\rho_e$  is the density of ethanol.

### 2.3 X-ray transmission measurements

The x-ray transmission through the prepared samples was studied using beams generated from a diagnostic x-ray machine (Shimadzu, model Circlex 0.6/1.2 P364DK-100SF) in the range from 40 to 127 kV tube voltages. For all beams, the exposure was set at 10 mAs. The distance between the x-ray tube (tungsten anode) and the detector was set at 100 cm, and the x-ray beam was well collimated at 0° angle relative to the center of the detector for a dimension of about 5 cm × 7 cm according to the sample size to minimize the scattered x-rays produced by the sample arriving to the detector.

The primary x-ray beam ( $I_o$ ) and the transmitted x-ray beam ( $I$ ) were measured using a DIADOS diagnostic detector connected to the DIADOS diagnostic dosimeter (PTW-Freiburg, Germany). The dosimeter is a universal dosimeter for measuring simultaneous dose and dose rate for radiography, fluoroscopy, mammography, dental X-ray and CT with a sensitivity of 0.01 microRoentgen (μR). The exposure produced by the primary x-ray beam was measured in the absence of sample between the x-ray tube and the detector. Meanwhile, the transmitted x-ray beam ( $I$ ) was measured with the sample placed on the detector. All the x-ray transmissions ( $I/I_o$ ) were compared with the results measured for commercial lead glass (Gammasonics Institute for Medical Research Pty Ltd). For each composite sample, the measurements were performed three times.

### 2.4 Powder diffraction (PD)

Powder diffraction measurements were conducted to identify the crystalline phases present in the samples. This was done at the Australian Synchrotron in Melbourne, on the Powder Diffraction beamline. Mythen detectors were used to record the diffraction patterns in the  $2\theta$  range of 10°–60° at a fixed wavelength of 1.13 Å.

### 2.5 Backscattered electron microscopy (BSEM)

The microstructures of polished samples were observed using a backscattered electron imaging technique (Zeiss Evo 40XVP scanning electron microscope). All surfaces were coated with carbon to minimize the charging effect and to enhance resolution during imaging.

### 2.6 Flexural tests

Rectangular bars of approximate size 60 mm × 10 mm × 8 mm were cut from the fully cured samples for three-point bend tests in order to evaluate the flexural strength ( $\sigma_f$ ) and flexural modulus ( $E_f$ ) of the samples. Flexural testing was carried using the 3-point bend configuration according to the ASTM D790-03 standard [23] on a universal testing machine (LLOYD Instruments) equipped with

**Table 1** Density of filler-epoxy composite samples

% Weight	Density (cm <sup>3</sup> /g)					
	PbCl <sub>2</sub> -epoxy		Bi <sub>2</sub> O <sub>3</sub> -epoxy		WO <sub>3</sub> -epoxy	
	(e)	(t)	(e)	(t)	(e)	(t)
10	1.24 ± 0.02	1.25	1.26 ± 0.01	1.26	1.24 ± 0.03	1.26
30	1.47 ± 0.05	1.52	1.55 ± 0.03	1.56	1.50 ± 0.02	1.54
50	1.85 ± 0.03	1.92	2.00 ± 0.03	2.04	1.87 ± 0.06	1.98
70	2.54 ± 0.06	2.63	2.68 ± 0.07	2.95	2.71 ± 0.03	2.79

Notes: (e) = experiment, (t) = theory

an adjustable-span flexural test fixture. Flexural testing was carried out utilizing a span-to-depth ratio of 16 together with a crosshead speed of 1.0 mm/min. A minimum of three samples was tested for each composite, and the average results were taken. In these measurements, the samples were tested to the applied load with the results calculated by the NEXY-GEN Plus software.

2.7 Indentation hardness test

The indentation hardness of polished samples was carried out using the Avery Rockwell hardness tester according to Rockwell hardness scale H. The measurements of Rockwell hardness were conducted using the indentation load of 588.4 N and ball indenter of 0.3 cm. Five measurements were conducted for each sample in order to obtain an average value.

3 Results and discussion

3.1 Density

From Table 1, the apparent density of each sample of the same filler type increased with the increment of filler content, a phenomenon which was also observed by Harish et al. [14]. However, the results did not agree very well with the theoretical values, especially when the filler loading was more than 30 wt% due to lack of epoxy to fully cover the surfaces of filler powder, resulting in the concomitant increase in the number of pores and thus reducing the density of the composite. Equation (2) was used to compute the relative errors for density measurements relative to the theoretical density values:

$$\delta\rho_s = \left( \frac{\delta m_1}{m_1} + \frac{\delta m_2 + \delta m_3}{m_2 - m_3} + \frac{\delta\rho_e}{\rho_e} \right) \times \rho_s, \tag{2}$$

where  $\delta\rho_s$  is the apparent density uncertainty of the sample,  $\delta m_1$ ,  $\delta m_2$  and  $\delta m_3$  are the mass uncertainty of the sample weighted in the balance, the sample hanging on the balance arm in the air and the sample hanging on the balance arm

immersed in ethanol respectively.  $\delta\rho_e$  is the density uncertainty of ethanol calculated from the error of its measured density and its accepted density.

The theoretical density values ( $\rho_{comp}$ ) were calculated from Eq. (3) with an assumption of the samples being void-free:

$$\rho_{comp} = \frac{100}{\left[ \frac{F}{\rho_{filler}} + \frac{E}{\rho_{epoxy}} \right]}, \tag{3}$$

where  $F$  is the wt% of the filler,  $E$  is the wt% of epoxy,  $\rho_{filler}$  is the density of filler,  $\rho_{epoxy}$  is the density of epoxy system. The computed errors for density values relative to the theoretical density values are in the acceptable limit (i.e. <10.0 %).

3.2 Effect of filler loading on the x-ray transmission ( $I/I_o$ ) by epoxy-based composites

The plots in Fig. 1a show that for the same filler type and at the same x-ray tube voltage, x-ray transmission value was decreased by the increment of the filler loading. For example (Fig. 1b), at 60 kV x-ray tube voltage, x-ray transmission for the 10 wt% of Bi<sub>2</sub>O<sub>3</sub>-epoxy composite is about 57 times greater than the x-ray transmission value for the 70 wt% of Bi<sub>2</sub>O<sub>3</sub>-epoxy composite. This was due to the amplification of elemental composition of the composite with the increment of filler loading in the epoxy base which play an important role in absorbing the x-ray passing through them. A similar result in x-ray transmission as a function of filler loading was obtained for epoxy composites filled with PbCl<sub>2</sub> and WO<sub>3</sub>.

In order to ascertain the shielding ability of the composites, these results were compared with commercial lead glass (thickness 10 mm) which contained 56 wt% of Pb (information provided by Gammasonics Institute for Medical Research Pty Ltd) (see Fig. 1a). Bi<sub>2</sub>O<sub>3</sub>-epoxy composite having 70 wt% of Bi<sub>2</sub>O<sub>3</sub> gave nearly the same ( $I/I_o$ ) value as compared to lead glass and other composite samples even though it is thinner than lead glass. Hence the usage of lead in x-ray shielding can be substituted by Bi<sub>2</sub>O<sub>3</sub>

**Fig. 1** (a) X-ray transmission ( $I/I_0$ ) as a function of x-ray tube voltage for all composites and commercial lead glass; (b) X-ray transmission ( $I/I_0$ ) as a function of  $\text{Bi}_2\text{O}_3$  loading (wt%) showing that ( $I/I_0$ ) was decreased by the increment of the filler loading; and (c) X-ray transmission ( $I/I_0$ ) as a function of x-ray tube voltage for epoxy composites filled with 70 wt% of  $\text{PbCl}_2$ ,  $\text{Bi}_2\text{O}_3$  and  $\text{WO}_3$

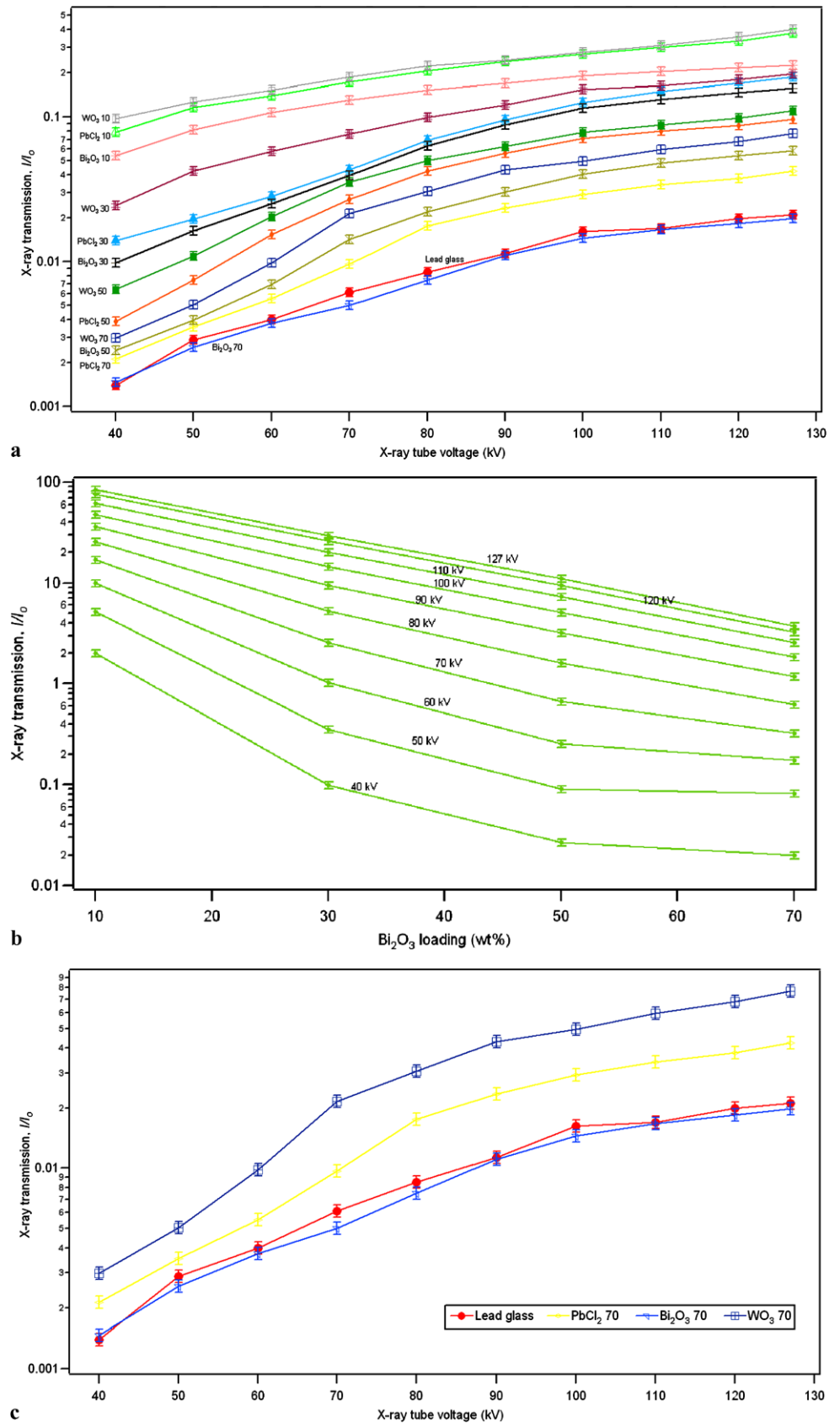


**Fig. 2** Typical powder diffraction pattern of (a)  $\text{PbCl}_2$ -epoxy composite; (b)  $\text{Bi}_2\text{O}_3$ -epoxy composite and (c)  $\text{WO}_3$ -epoxy composite

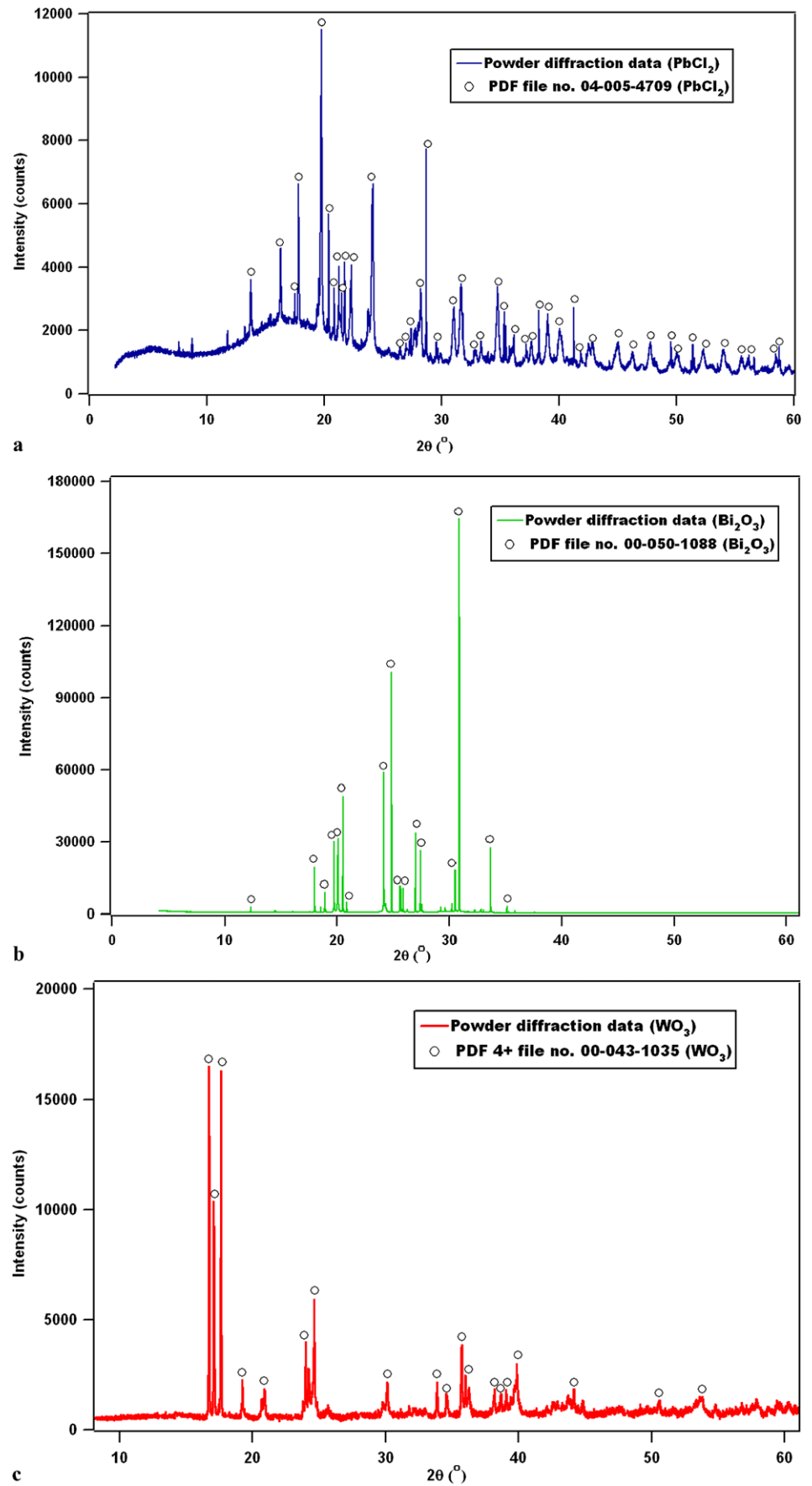
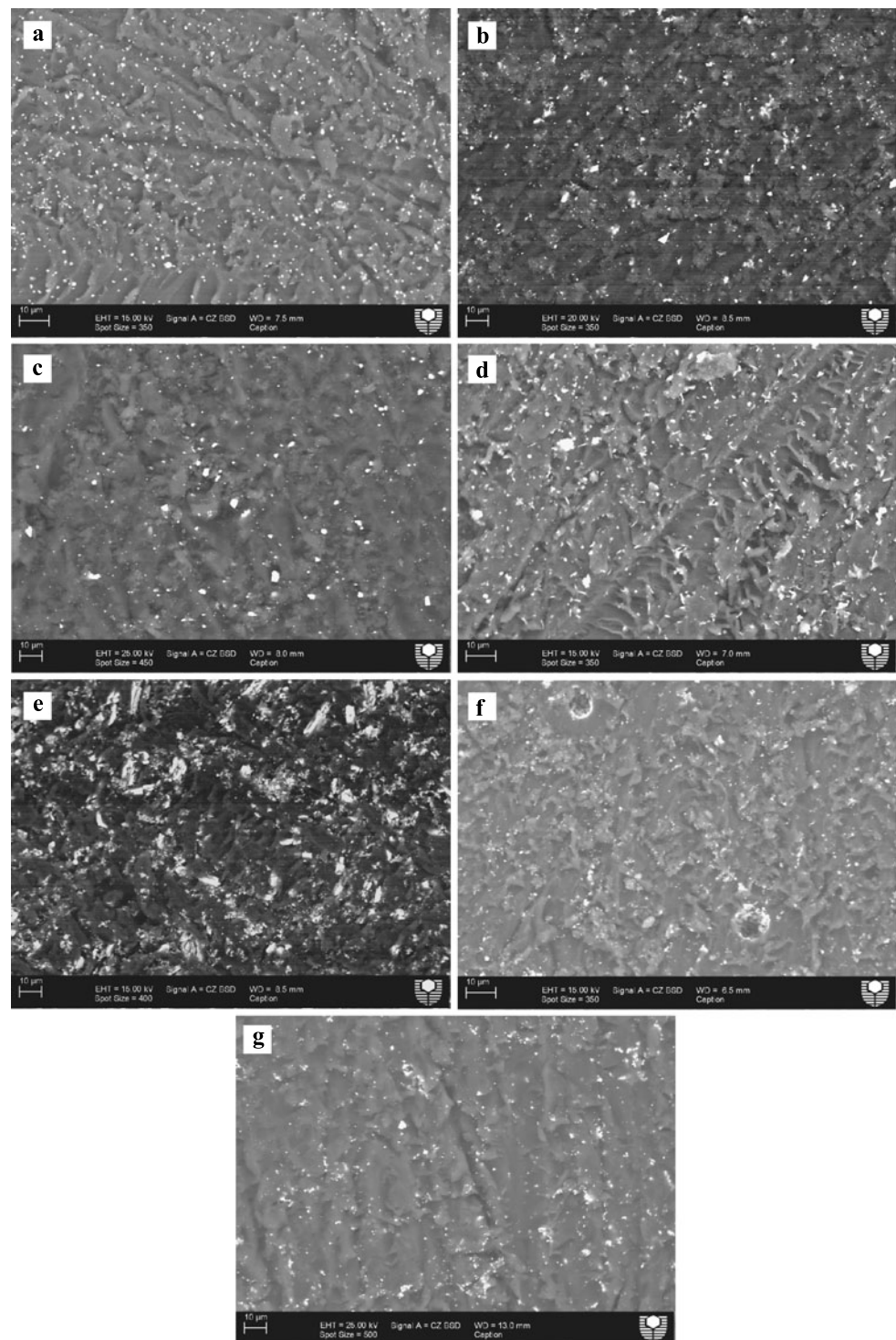




**Fig. 3** Backscattered electron micrographs showing the dispersion of fillers in epoxy composites containing (a) 10 wt%  $\text{PbCl}_2$ ; (b) 30 wt%  $\text{Bi}_2\text{O}_3$ ; (c) 30 wt%  $\text{WO}_3$ ; (d) 50 wt%  $\text{PbCl}_2$ ; (e) 50 wt%  $\text{Bi}_2\text{O}_3$ ; (f) 70 wt%  $\text{PbCl}_2$ ; and (g) 70 wt%  $\text{WO}_3$



whereby Bi is classified as least toxic compared to Pb. In addition, even though the 70 wt%  $\text{WO}_3$ -epoxy composite with 8 mm thickness shows higher ( $I/I_0$ ) values when compared to lead glass (Fig. 1c),  $\text{WO}_3$ -epoxy composite also can be a substitute material for Pb in x-ray shielding by increasing its thickness so that it can provide similar x-ray transmission characteristic as lead glass. The usage of  $\text{PbCl}_2$ -epoxy

composite with larger thickness can also be considered as a lighter alternative for lead glass in x-ray shielding.

### 3.3 Phase compositions

The reference for fitting the peaks was taken from International Centre for Diffraction Data (ICDD) PDF-4+ 2009

database. The wavelength for all of these databases was chosen to be the same as the wavelength of the synchrotron radiation used.

The Powder Diffraction (PD) pattern in Fig. 2a shows that all the peaks belong to orthorhombic  $\text{PbCl}_2$  (PDF files 04-005-4709). For composite filled with  $\text{Bi}_2\text{O}_3$ , all the peaks were identified as monoclinic  $\text{Bi}_2\text{O}_3$  (PDF file 00-050-1088) as shown in Fig. 2b, and the diffraction peaks shown in Fig. 2c belong to monoclinic  $\text{WO}_3$  (PDF file 00-043-1035). These results indicate that  $\text{PbCl}_2$ ,  $\text{Bi}_2\text{O}_3$  and  $\text{WO}_3$  were single-phase pure without impurities.

### 3.4 Microstructure analyses

The surface features of samples in Fig. 3, which uses atomic number contrast to differentiate between low and high atomic number elements, show that the fillers appear brighter (higher atomic number) than the surrounding epoxy (low atomic number). The fillers (white patches) are seen to be dispersed uniformly in the epoxy matrix with low filler loading (Fig. 3a–c). However, the dispersion of the fillers within the matrix becomes less uniform with the increment of filler loading, resulting in some agglomerations. These filler agglomerations can be seen in composites with  $\geq 50$  wt% of filler (Fig. 3d–g). To minimize the occurrence of these agglomerations, higher shear forces through faster stirring are required to achieve a fine dispersion in the polymer matrix. Alternatively, the use of ultrasonication can be used to prevent or minimize filler agglomerations. These methods promote the “peeling off” of individual particles located at the outer part of the particle bundle, or agglomerates, and thus results in the separation of individualized particles from the bundles.

### 3.5 Mechanical properties

Figure 4 shows the effect of filler loading on flexural strength, flexural modulus and Rockwell hardness of epoxy composites. The flexural strength has improved for composite with 10 wt% filler loading. For instance, the flexural strength of epoxy has improved by 48 % in the composite with 10 wt%  $\text{WO}_3$  loading. However, the addition of more filler ( $\geq 30$  wt%) caused a marked decrease in flexural strength due to the filler not well dispersed within the epoxy matrix. In addition, the porosity for the samples was between 1 %–10 % with more pores for filler  $\geq 30$  wt% because of air-bubbles trapped in the samples which act as stress-concentrators and thus the resultant weakening. On the other hand, the flexural modulus increased with an increase in filler loading which suggests that the stiffness of the composites obey the rule-of-mixtures. In comparison, the flexural strength and flexural modulus of lead glass are  $\sim 90$  MPa and  $\sim 6500$  MPa respectively, thus indicating that

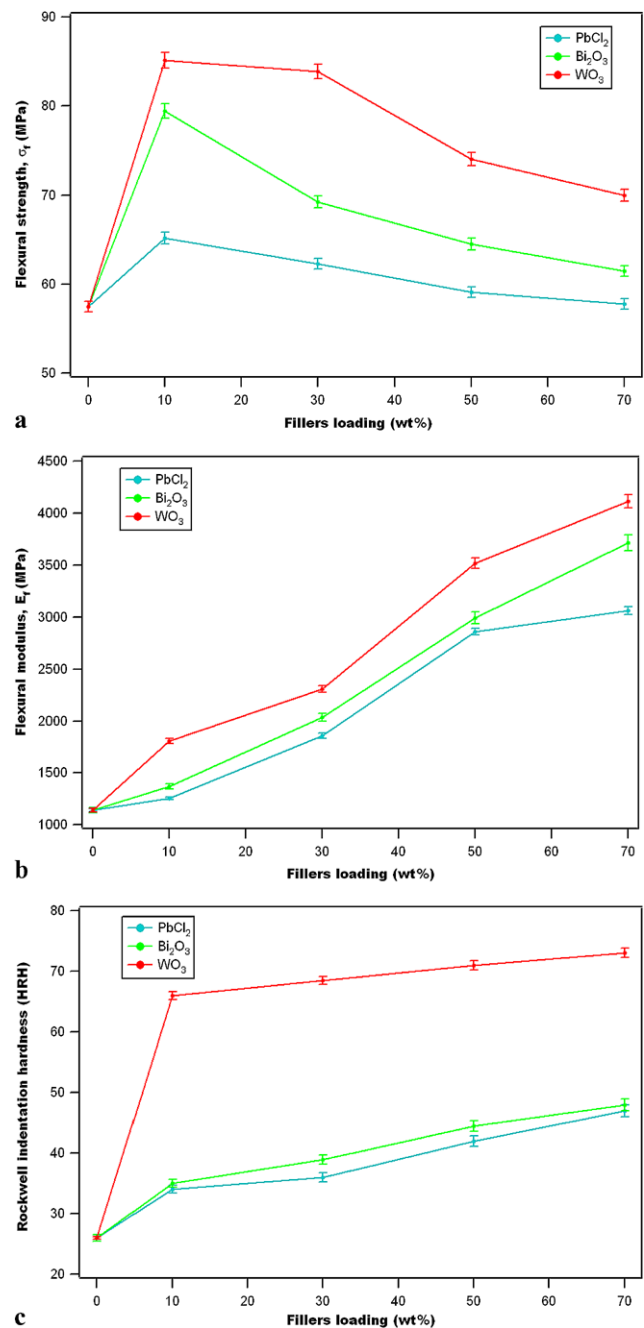


**Fig. 4** The effect of filler loading on (a) flexural strength; (b) flexural modulus and (c) hardness of epoxy-composites

glass is still superior to epoxy. For the hardness results, they show that an increase in the filler loading resulted in a modest increase in hardness of the composite. In comparison, the Rockwell hardness of lead glass is  $\sim$ HRC 043 [24].

The mechanical properties obtained in this work are adequate for the optimum sample (i.e. 70 wt%  $\text{Bi}_2\text{O}_3$ -epoxy composite) in x-ray shielding of radiological rooms since it is comparable with lead glass in terms of x-ray transmission although it shows lower flexural properties than lead glass.



In particular, the mechanical properties of the composite did not change even after being repeatedly exposed to the x-ray beam of highest x-ray tube voltage. Although these flexural properties are inferior when compared to lead glass, this limitation can be overcome by increasing the thickness of the 70 wt% Bi<sub>2</sub>O<sub>3</sub>-epoxy composite.

#### 4 Conclusions

It may be concluded that:

- PbCl<sub>2</sub>, Bi<sub>2</sub>O<sub>3</sub> or WO<sub>3</sub>-epoxy composites have good x-ray shielding ability, and hence they can be considered as candidate materials for x-ray shielding of radiological rooms.
- The 8-mm-thick Bi<sub>2</sub>O<sub>3</sub>-epoxy composite with 70 wt% Bi<sub>2</sub>O<sub>3</sub> is comparable with a 10-mm-thick commercial lead glass which contains 56 wt% Pb.
- The 8-mm-thick PbCl<sub>2</sub>- and WO<sub>3</sub>-epoxy composites were not comparable with the 10-mm-thick lead glass unless they were prepared with a thickness greater than 10 mm.
- Both flexural modulus and hardness of composites increased with increasing filler loading, but the flexural strength decreased markedly when the filler loading was equal to or greater than 30 wt%.

**Acknowledgements** The collection of synchrotron powder diffraction data was funded by the Australian Synchrotron (PD5075).

#### References

1. A. Holmes-Siedle, L. Adams, *Hand Book of Radiation Effects*, 2nd edn. (Oxford University Press, London, 2002)
2. F. El Haber, G. Froyer, *J. Univ. Chem. Technol. Metall.* **43**, 283 (2008)
3. E. Schmid, W. Panzer, H. Schlattl, H. Eder, *J. Radiol. Prot.* **32**, 129 (2012)
4. D.G. Sutton, C.J. Martin, D. Peet, J.R. Williams, *J. Radiol. Prot.* **32**, 117 (2012)
5. P. Sprawls, *The Physical Principles of Medical Imaging* (Aspen Publishers, Gaithersburg, 1993)
6. S. Arjula, A. Harsha, M. Ghosh, *J. Mater. Sci.* **43**, 1757 (2008)
7. K. Dworecki, M. Drabik, T. Hasegawa, S. Wąsik, *Nucl. Instrum. Methods Phys. Res., Sect. B, Beam Interact. Mater. Atoms* **225**, 483 (2004)
8. G.K. Hubler, *Nucl. Instrum. Methods Phys. Res.* **191**, 101 (1981)
9. M.R.F. Soares, P. Alegaonkar, M. Behar, D. Fink, M. Müller, *Nucl. Instrum. Methods Phys. Res., Sect. B, Beam Interact. Mater. Atoms* **218**, 300 (2004)
10. J.K. Kim, R.E. Robertson, *J. Mater. Sci.* **27**, 161 (1992)
11. S. Daren, Polymer versus glass, POLYMICRO newsletter, <http://www.polymicro-cc.com>. Accessed 16 July 2010
12. E.H. Lee, G.R. Rao, M.B. Lewis, L. Mansur K, *Nucl. Instrum. Methods Phys. Res., Sect. B, Beam Interact. Mater. Atoms* **74**, 326 (1993)
13. A.G. Andreopoulos, G.C. Papanicolaou, *J. Mater. Sci.* **22**, 3417 (1987)
14. V. Harish, N. Nagaiah, T.N. Prabhu, K.T. Varughese, *J. Appl. Polym. Sci.* **112**, 1503 (2009)
15. M.M. Abdel-Aziz, A.S. Badran, A.A. Abdel-Hakem, F.M. Helaly, A.B. Moustafa, *J. Appl. Polym. Sci.* **42**, 1073 (1991)
16. V.I. Pavlenko, V.M. Lipkanskii, P.N. Yastrebinskii, *J. Eng. Phys. Thermophys.* **77**, 11 (2004)
17. W. Osei-Mensah, J.J. Fletcher, K.A. Danso, *Int. J. Sci. Technol.* **2**, 455 (2012)
18. L. Liu, L. He, C. Yang, W. Zhang, R.-G. Jin, L.-Q. Zhang, *Macromol. Rapid Commun.* **25**, 1197 (2004)
19. Premac lead acrylic, part of the Wardray Premise total radiation shielding package, Wardray Premise Ltd., <http://wardray-premise.com/structural/materials/premac.html>. Accessed 4 May 2011
20. L.S. Limited (ed.), *Radiation Safety & Consumable Products*. (Lablogic, Sheffield, 2009). [http://www.lablogic.com/moreinfo/PDF/consumables/lablogic\\_consumables\\_brochure.pdf](http://www.lablogic.com/moreinfo/PDF/consumables/lablogic_consumables_brochure.pdf). Accessed 9 June 2010.
21. N.Z. Noor Azman, S.A. Siddiqui, R. Hart, I.M. Low, *Appl. Radiat. Isot.* **71**, 62 (2013)
22. Australian Standards 1774.5, Method 5. The determination of density, porosity and water absorption (1989)
23. ASTM, *Annual Book of ASTM Standards*, vol. 08.01 (2005)
24. Data sheet lead glass (X-ray protection), UQG optics, <http://www.uqgoptics.com/pdf/Lead%20Glass.pdf>. Accessed 9 November 2012

## 4. PARTICLE SIZE EFFECT ON THE X-RAY ATTENUATION ABILITY OF WO<sub>3</sub> FILLER-EPOXY COMPOSITES

---

Chapter 4 reveals the effect of particle size, filler loadings and X-ray tube voltage or X-ray energy on the X-ray transmission in WO<sub>3</sub>-epoxy composites fabricated by melt-mixing method. The X-ray attenuation ability of the samples was investigated by a mammography unit, a radiography unit and an X-ray Absorption Spectroscopy (XAS) unit respectively. In addition, the equivalent energy for the X-ray tube voltages operated by the mammography and radiography unit were determined by comparing the X-ray transmission of the samples at the X-ray tube voltages with the X-ray transmission results found from XAS synchrotron radiation energies.

## 4.1 Effect of Particle Size, Filler Loadings and X-ray Energy on the X-ray Attenuation Ability of Tungsten Oxide – Epoxy Composites

---

The effect of particle size, filler loadings and X-ray tube voltage on the X-ray transmission in WO<sub>3</sub>-epoxy composites fabricated by melt-mixing method was investigated as published in the *Applied Radiation and Isotopes*, volume 71, pages 62-67 in the year 2013.

For this study, a mammography unit and a diagnostic radiology machine were used; they comprised variable X-ray tube voltages 25- 120 kV.

### **Key findings:**

- For the same WO<sub>3</sub> loading, nano-sized WO<sub>3</sub>-epoxy composite attenuate more X-ray beams at lower tube voltages (25–35kV) when compared with the micro-sized WO<sub>3</sub>-epoxy.
- The role of particle size in X-ray shielding was insignificant at the higher tube voltages range (40–120 kV).
- The X-ray transmission by either nano-sized or micro-sized WO<sub>3</sub>-epoxy composite at 40 kV of mammography unit is not the same as at 40 kV of radiography unit.



## Effect of particle size, filler loadings and x-ray tube voltage on the transmitted x-ray transmission in tungsten oxide—epoxy composites

N.Z. Noor Azman<sup>a,b</sup>, S.A. Siddiqui<sup>a</sup>, R. Hart<sup>c</sup>, I.M. Low<sup>a,\*</sup>

<sup>a</sup> Department of Imaging and Applied Physics, Curtin University, GPO Box U1987, Perth, WA 6845, Australia

<sup>b</sup> School of Physics, Universiti Sains Malaysia, 11800 Penang, Malaysia

<sup>c</sup> Royal Perth Hospital, East Perth, WA 6001, Australia

### HIGHLIGHTS

- Investigated the effect of particle size of WO<sub>3</sub> on the x-ray attenuation ability.
- Nano-sized WO<sub>3</sub> has a better ability to attenuate lower x-ray energies (22–49 kV<sub>p</sub>).
- Particle size has negligible effect at the higher x-ray energy range (40–120 kV<sub>p</sub>).

### ARTICLE INFO

#### Article history:

Received 19 June 2012

Received in revised form

7 September 2012

Accepted 18 September 2012

Available online 25 September 2012

#### Keywords:

Micro-sized WO<sub>3</sub>-epoxy composites

Nano-sized WO<sub>3</sub>-epoxy composites

Transmission

X-ray tube voltage

Filler loading

### ABSTRACT

The effect of particle size, filler loadings and x-ray tube voltage on the x-ray transmission in WO<sub>3</sub>-epoxy composites has been investigated using the mammography unit and a general radiography unit. Results indicate that nano-sized WO<sub>3</sub> has a better ability to attenuate the x-ray beam generated by lower tube voltages (25–35 kV) when compared to micro-sized WO<sub>3</sub> of the same filler loading. However, the effect of particle size on x-ray transmission was negligible at the higher x-ray tube voltages (40–120 kV).

© 2012 Published by Elsevier Ltd. All rights reserved.

## 1. Introduction

Use of nano-particles in designing advanced materials has attracted much attraction amongst the researchers because of superior physical and mechanical properties that can be achieved. For instance, recent studies have shown that nano-sized filler reinforced polymer composites provided much improvement in chemical, physical and mechanical properties by virtue of better dispersion of the nano-particles within the polymer matrix (Chapman and Mulvaney, 2001; Karim et al., 2002; Ohno et al., 2002; Schmidt and Malwitz, 2003). The main improvement of nanoparticles as a filler assembly over conventional materials is the maximization of the surface/volume ratio of the fillers (Fabiani et al., 2010). For example, nanoparticles improved the electrochemical capacitance of  $\alpha$ -Ni(OH)<sub>2</sub> in alkali solutions as compared to

micro-sized particles of the same hydroxide due to the greater surface/volume ratio of the nanoparticles (Jayalakshmi et al., 2006).

Additionally, this size-effect also becomes one of the virtues in designing materials for shielding of ionizing radiations. Some x-ray technologists believe that this effect will improve the x-ray attenuation ability of the composite since nano-sized fillers are able to disperse more uniformly within the polymer matrix with less agglomeration as compared to micro-sized fillers (Botelho et al., 2011; El Haber and Froyer, 2008; Steinhart, 2004). A recent study by Botelho et al. (2011) found that nanostructured copper oxide (CuO) is more effective in attenuation of lower x-ray beam energy (26 and 30 kV) and no significant variation in x-ray attenuation at higher x-ray beam energy (60 and 102 kV). Künzel and Okuno (2012) also provided similar results, which show that the x-ray absorption is higher for a nanostructured CuO compound compared to the microstructured counterpart for low energy x-ray beams (25 and 30 kV) for all CuO concentrations incorporated into polymeric resin.

In general, the attenuation of photons (x-rays/gamma-rays) is dependent upon three factors: density, elemental composition,

\* Corresponding author. Tel.: +618 9266 7544; fax: +618 9266 2377.

E-mail address: [j.low@curtin.edu.au](mailto:j.low@curtin.edu.au) (I.M. Low).

and thickness of the absorbing material (Sprawls, 1993). Even though lead (Pb) or lead compounds provide good x-ray shielding properties, their usage as the shielding materials has increasingly become a sensitive issue due to its hazardous nature. As a result, much research has been focusing on developing new x-ray shielding materials which are safer and easier to handle (Robert, 2005; Spinks and Wood, 1976).

The aim of this work was to develop new x-ray shielding materials based on tungsten oxide–epoxy composites with either nano-sized or micro-sized fillers. The effect of filler size on the x-ray transmission in the diagnostic imaging energy range (25–120 kV) has been investigated. The filler size effect in x-ray shielding ability is discussed.

## 2. Experimental procedure

### 2.1. Samples preparation

Nano-sized (< 100 nm) and micro-sized (~20 μm) tungsten oxide (WO<sub>3</sub>) were used as filler for synthesizing WO<sub>3</sub>-epoxy composites. The former were obtained from Sigma-Aldrich and the latter (FR251) from Fiberglass and Resin Sales.

To prepare WO<sub>3</sub>-epoxy composite samples, WO<sub>3</sub> powder was added into the FR251 epoxy resin (Bisphenol-A diglycidyl ether polymer) before the FR251 hardener (Isophoronediamine) was mixed into it. The ratio of epoxy resin to hardener used was 2:1. The mixing of WO<sub>3</sub> powder in epoxy resin was done through gentle stirring using a stirring machine at constant speed for 15 min to ensure uniform dispersion of the powder in epoxy matrix. The well-mixed mixture was then cast in a 4 cm × 6 cm rectangular silicon rubber mold with a thickness of 7 mm and was allowed to set overnight at room temperature. The list of prepared samples with different weight percentages of WO<sub>3</sub> are shown in Table 1.

### 2.2. Measurement of the x-ray transmission

This work was done using two different sets of equipment. For the lower x-ray energy range, a mammography unit (brand: Siemens AG, model: 2403951-4G.E Health Care) was used while a general diagnostic x-ray machine (brand: Shimadzu, model: Circlex 0.6/1.2 P364DK-100SF) was used for the higher x-ray energy range. The initial x-ray beam intensity ( $I_0$ ) was determined by directly measuring x-rays with the DIADOS diagnostic detector connected to DIADOS diagnostic dosimeter (PTW-Freiburg, Germany) in the absence of the sample. The dosimeter is a universal dosimeter for measuring simultaneous dose and dose rate for radiography, fluoroscopy, mammography, dental X-ray and CT with a minimal dose sensitivity of  $8.7 \times 10^{-8}$  milliGray (mGy) and also has a claimed sensitive range of x-rays energy of 25 kV to 150 kV.

**Table 1**  
List of prepared samples with different weight fractions of filler (WO<sub>3</sub>) and epoxy resin.

Composite by weight fraction (wt %)	
Filler (WO <sub>3</sub> )	Epoxy resin
5	95
10	90
20	80
30	70
35	65

Meanwhile the transmitted x-ray beam intensity ( $I$ ) was taken with the sample placed on the detector. The distance between the x-rays' tube and the detector was set to 86 cm since this is the maximum distance that can be adjusted for the mammography unit, and the x-ray beam was well collimated to the size of the sample.

The exposure was set at 10 mAs to obtain meaningful readings for this type of detector. The x-ray beams generated in the range of 25–49 kV tube voltage was selected from mammography unit since the machine can go only within this range for lower x-ray energy. On the other hand, the x-ray beams generated in the range of 40–120 kV tube voltage was chosen from the general diagnostic x-ray machine because this range is the normal range of the x-ray tube voltage used in general diagnostic imaging purposes.

For each composite, the measurements were performed three times. The performance of micro-sized and nano-sized WO<sub>3</sub>-epoxy composite was compared from a log-linear scale graph of x-ray transmission ( $I/I_0$ ) as a function of filler loading for each x-ray tube voltage.

## 3. Results and discussion

Three different anode/filter combinations (Table 2) were used for lower x-ray tube voltage generated from the mammography machine, since the combination was operated by the machine itself. The x-ray beams generated by these anode/filter combinations composed mainly of the characteristic x-ray energies of molybdenum (17.5 keV and 19.6 keV) or rhodium (20.2 keV and 22.7 keV). For WO<sub>3</sub> of 5 wt% and 10 wt%, the exit dose reading was observed at 25 kV x-ray tube voltage while for 20 wt%–35 wt%, the dose reading was initiated at 30 kV x-ray tube voltage due to the zero reading of the dosimeter at 25 kV x-ray tube voltages.

Fig. 1 clearly showed a big difference of x-ray transmission between micro-sized WO<sub>3</sub>-epoxy composite and nano-sized WO<sub>3</sub>-epoxy composite for x-ray beams generated for 25–49 kV tube voltages by the mammography unit at the same filler loading. The ratio of the x-ray transmission for micro-sized WO<sub>3</sub>-epoxy composite ( $T_m$ ) to the x-ray transmission for nano-sized WO<sub>3</sub>-epoxy composite ( $T_n$ ) was in the range 1.3–3.0. The ratio ( $T_m/T_n$ ) was larger at the x-ray tube voltages 25–35 kV and was dropping as the x-ray tube voltage was increased ( $\geq 40$  kV) as can be seen in Fig. 1. Meanwhile, the ratio ( $T_m/T_n$ ) is  $\approx 1.0$ , for the diagnostic x-ray tube voltages range (40–120 kV) generated by the general radiography unit, which provided that  $T_m \approx T_n$ . Thus, the effect of WO<sub>3</sub> particle sized reinforced epoxy composite was negligible at the x-ray beam produced by higher x-ray tube voltage (Fig. 2).

**Table 2**  
Anode/filter combination operated by mammography machine.

X-ray tube voltage (kV)	Anode/filter combination
22	Mo/Mo <sup>a</sup>
25	
30	
35	Mo/Rh <sup>b</sup>
40	
45	Rh/Rh <sup>c</sup>
49	

<sup>a</sup> Mo/Mo stands for molybdenum anode/molybdenum filter.

<sup>b</sup> Mo/Rh stands for molybdenum anode/rhodium filter.

<sup>c</sup> Rh/Rh stands for rhodium anode/rhodium filter.

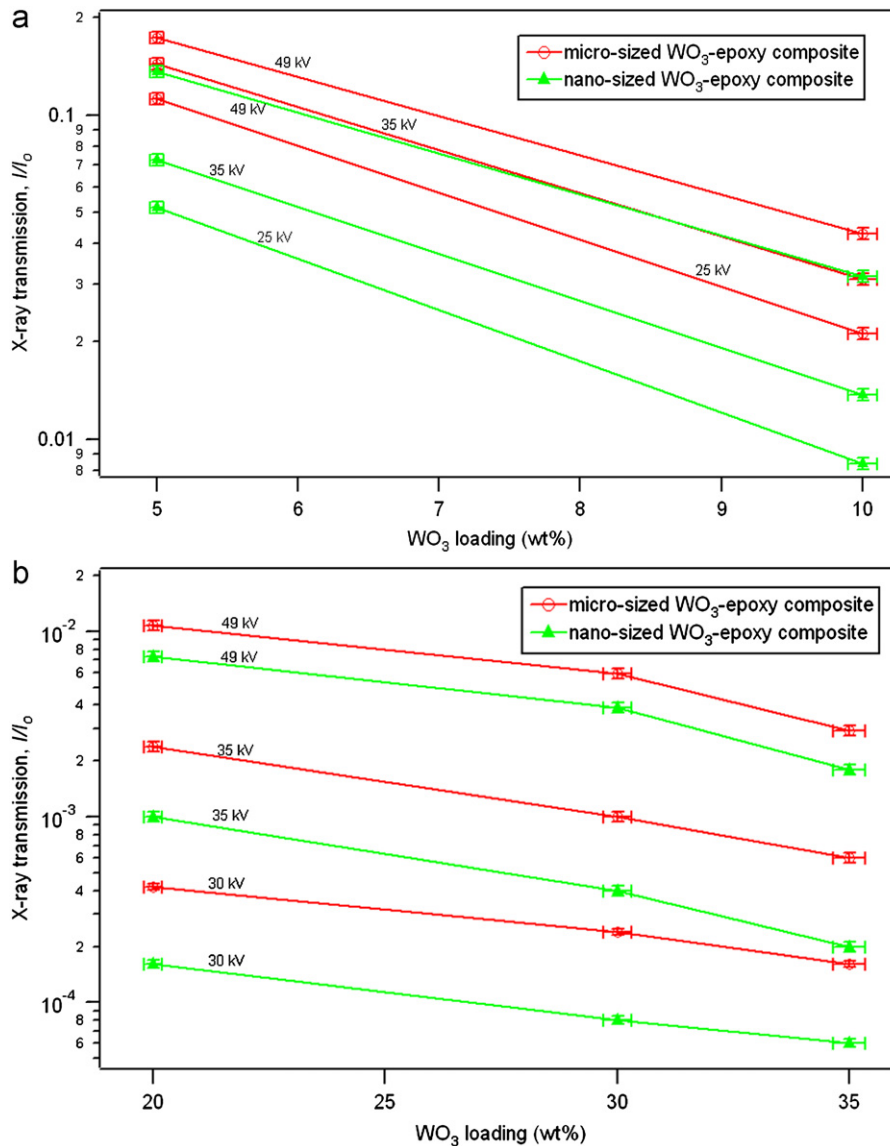


**Fig. 1.** X-ray transmission as a function of filler loading of (a) 5 and 10 wt% of the nano-sized  $WO_3$ -epoxy composite for x-ray tube voltage of 25, 35 and 49 kV generated by mammography unit and (b) 20–35 wt% of the nano-sized  $WO_3$ -epoxy composite as compared to the micro-sized  $WO_3$ -epoxy composite for x-ray tube voltage of 30, 35 and 49 kV generated by mammography unit.

Besides that, Fig. 3 showed that even though the x-ray tube voltage selected from the mammography unit, and general radiography unit is same (40 kV), the value of x-ray transmission by the nano-sized  $WO_3$  epoxy composite is lower for the x-ray photon generated by the mammography unit. A similar result was also obtained from micro-sized  $WO_3$  epoxy composite. This outcome proved that the general radiography unit comprised of a continuous spectrum of x-ray energy, which is having higher equivalent energies as compared to the characteristic x-ray energies produced from the mammography unit (17.5–22.7 keV).

Generally, photoelectric absorption dominates at lower photon (x-ray) energy range. A photon is completely absorbed by the atom of the material, and a photoelectron is ejected in the process. The ejected photoelectrons may undergo single- or multiple-scattering events with neighboring atoms, which can alter the mass attenuation coefficient of an element relative to the bulk material when considered over a small range of x-ray energies together with slight fluctuations in the probability of emission of Auger electron and fluorescent photons. The

probability of the photoelectric interaction is approximately dependent on  $Z^3/E^3$  where  $Z$  is the atomic number of the absorbing material and  $E$  is the photon energy. Furthermore, the number of W particles/gram in the nano-sized  $WO_3$ -epoxy composite is higher than that for the micro-sized  $WO_3$ -epoxy composite. Thus, the probability of an x-ray photon generated by lower tube voltage to interact and to be absorbed may be higher for nano-sized  $WO_3$ -epoxy composite rather than micro-sized  $WO_3$ -epoxy composite.

As photon energy increases, the probability of Compton scattering increases and hence the attenuation by the material decreases since this interaction was weakly dependent on  $Z$  and  $E$ . Hence, the probability of an x-ray photon generated by higher tube voltage to interact and to be absorbed may be similar for nano-sized and micro-sized  $WO_3$ -epoxy composite.

To support our investigation on an x-ray photon generated by lower tube voltage, we have repeated the procedure to measure the x-ray transmission of a  $WO_3$  compact disc of the same mass for 20 wt% (31% porosity) and 35 wt% (34% porosity) of  $WO_3$



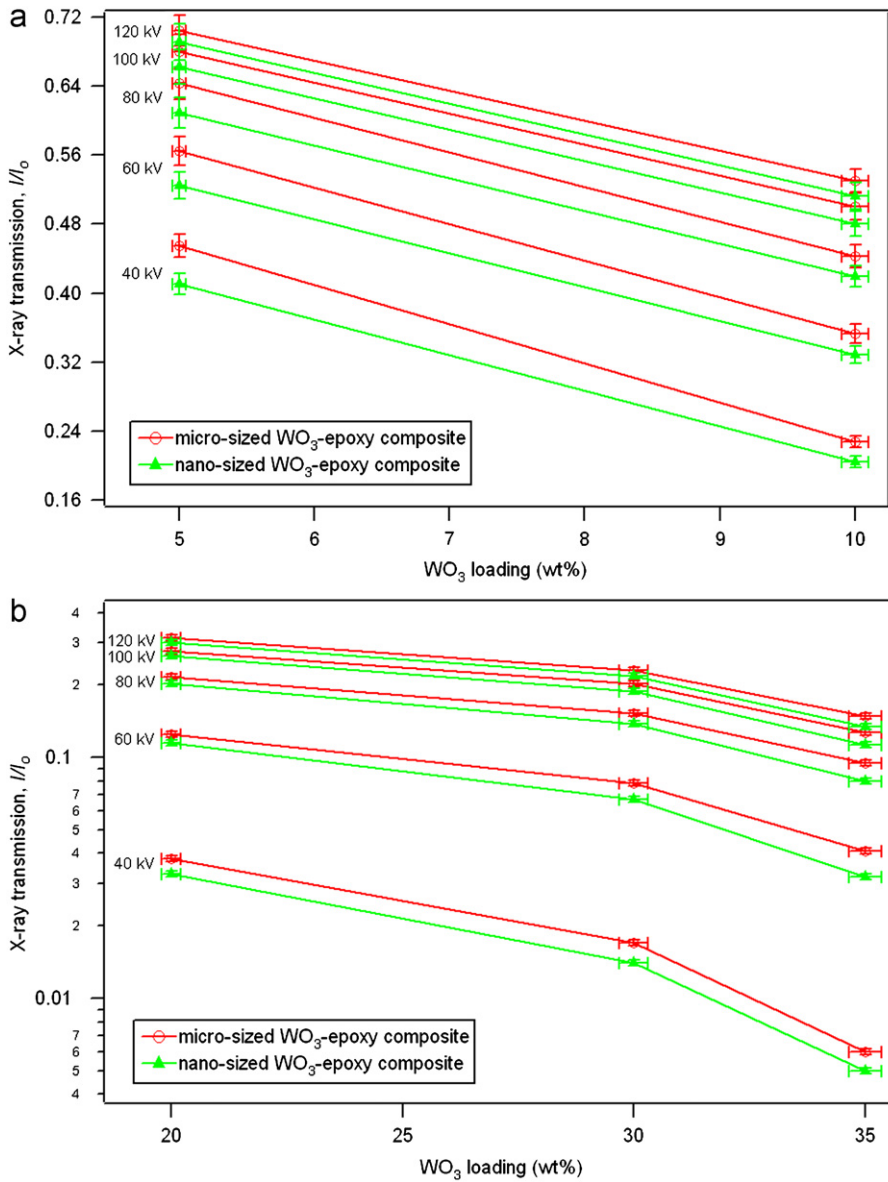


Fig. 2. X-ray transmission as a function of filler loading of (a) 5 and 10 wt% and (b) 20–35 wt% of the nano-sized  $WO_3$ -epoxy composite as compared to the micro-sized  $WO_3$ -epoxy composite for x-ray tube voltage of 40–120 kV generated by general radiography unit.

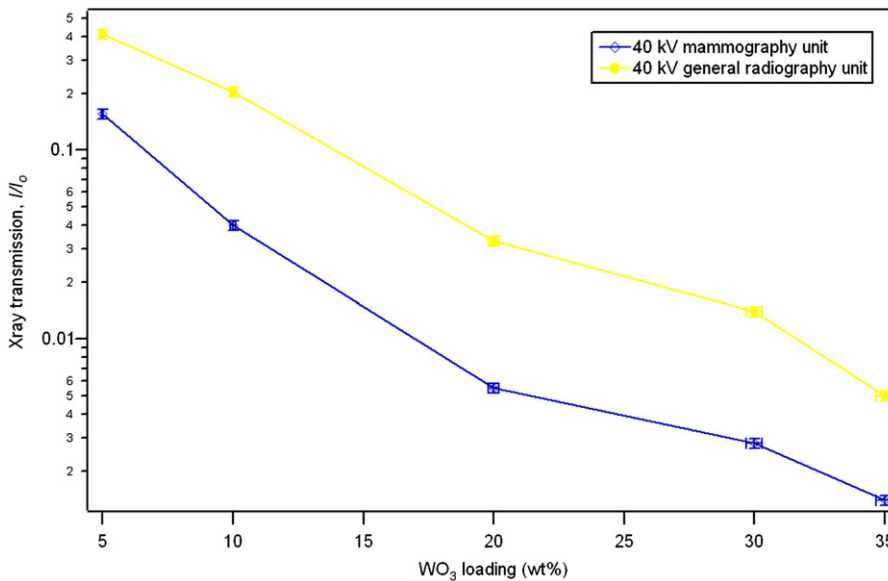
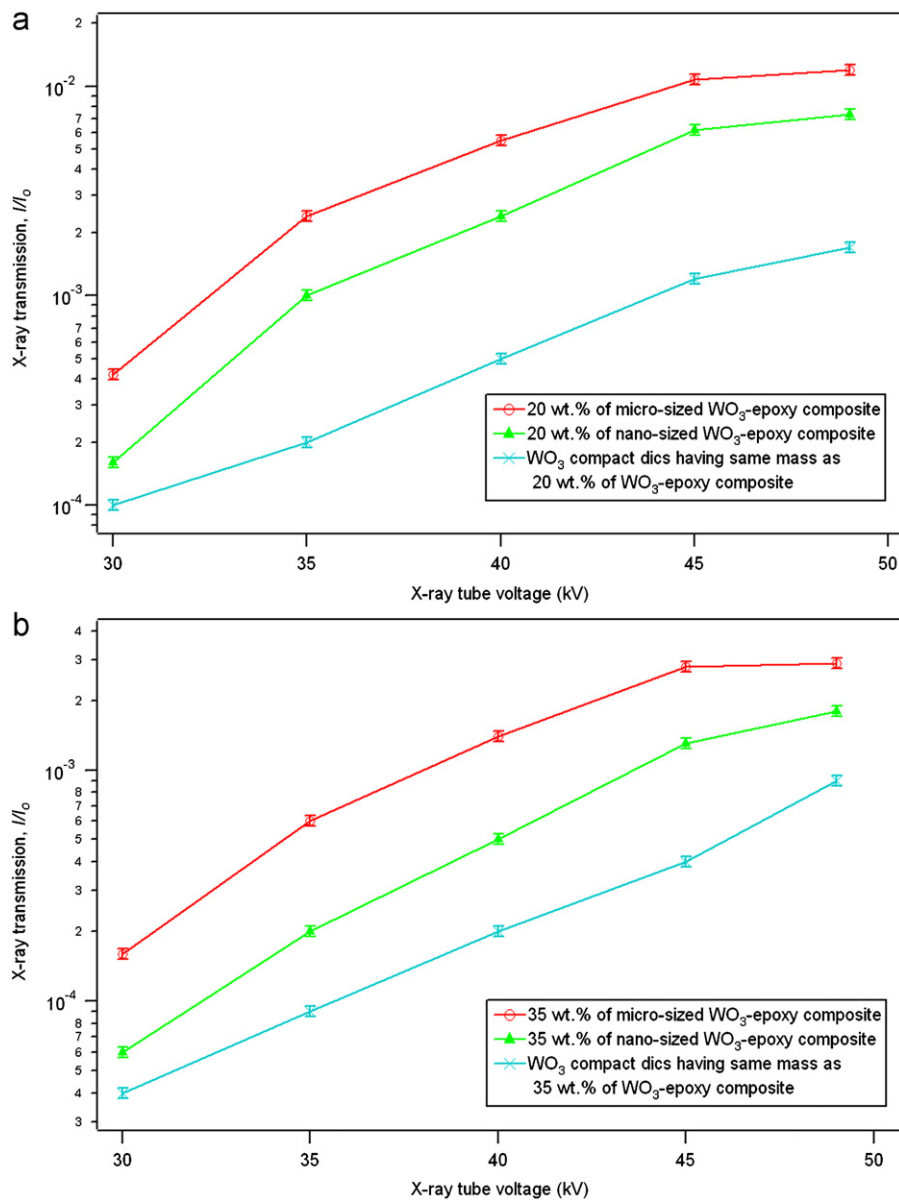


Fig. 3. Comparison of x-ray transmission values for all nano-sized  $WO_3$  wt% loading in the epoxy sample for operating tube voltage of 40 kV used by the mammography unit and the general radiography unit.



**Fig. 4.** X-ray transmission for WO<sub>3</sub> compact disc as compared to both micro-sized and nano-sized WO<sub>3</sub>-epoxy composite of the same mass of (a) 20 wt% and (b) 35 wt% of WO<sub>3</sub> loading in epoxy sample for x-ray tube voltage range (30–49 kV) generated by mammography unit.

loading in the epoxy sample. Fig. 4 proved that the WO<sub>3</sub> compact disc has the lowest x-ray transmission as compared to both micro-sized and nano-sized WO<sub>3</sub>-epoxy composites of the same mass since WO<sub>3</sub> particles have been compressed to be close together (even though they have high porosity) rather than being dispersed.

Hence, the results obtained in this work are in good agreement with the work of Künzel and Okuno, (2012) which showed that nano-sized fillers are superior to micro-sized fillers for attenuating the x-ray beams generated for lower tube voltages but the effect is the same for the x-ray beams generated for higher tube voltages.

#### 4. Conclusions

The results of this work showed that for the same WO<sub>3</sub> loading, nano-sized WO<sub>3</sub>-epoxy composite has better attenuating ability to attenuate the x-ray beams generated for lower tube voltages (25–35 kV) when compared to the micro-sized WO<sub>3</sub>-epoxy

composite. However, the role of particle size in x-ray shielding was insignificant at the higher tube voltages range (40–120 kV).

#### References

- Botelho, M.Z., Künzel, R., Okuno, E., Levenhagen, R.S., Basegio, T., Bergmann, C.P., 2011. X-ray transmission through nanostructured and microstructured CuO materials. *Appl. Radiat. Isot.* 69, 527–530.
- Chapman, R., Mulvaney, P., 2001. Electro-optical shifts in silver nanoparticle films. *Chem. Phys. Lett.* 349, 358–362.
- El Haber, F., Froyer, G., 2008. Transparent polymers embedding nanoparticles for x-rays attenuation (Review). *J. Univ. Chem. Technol. Metallurgy* 43, 283–290.
- Fabiani, D., Montanari, G.C., Krivda, A., Schmidt, L.E., Hollertz, R., 2010. Epoxy Based Materials Containing Micro- and Nano-Sized Fillers for Improved Electrical Characteristics, International Conference on Solid Dielectrics. IEEE, Potsdam, Germany, pp. 1–4.
- Jayalakshmi, M., Mohan Rao, M., Kim, K.B., 2006. Effect of particle size on the electrochemical capacitance of  $\alpha$ -Ni(OH)<sub>2</sub> in alkali solutions. *Int. J. Electrochem. Sci.* 1, 324–333.
- Karim, A., Amis, E., Yurekli, K., Krishnamoorti, R., Meredith, C., 2002. Combinatorial methods for polymer materials science: phase behavior of nanocomposite blend films. *Polym. Eng. Sci.* 42, 1836–1840.



- Künzel, R., Okuno, E., 2012. Effects of the particle sizes and concentrations on the X-ray absorption by CuO compounds. *Appl. Radiat. Isot.* 70, 781–784.
- Ohno, K., Koh, K.M., Tsujii, Y., Fukuda, T., 2002. Synthesis of gold nanoparticles coated with well-defined, high-density polymer brushes by surface-initiated living radical polymerization. *Macromolecules* 35, 8989–8993.
- Robert, R.D., 2005. High Density Composites Replace Lead. Ecomass Technologies, Austin, Texas, USA.
- Schmidt, G., Malwitz, M.M., 2003. Properties of polymer-nanoparticle composites. *Curr. Opin. Colloid Interface Sci.* 8, 103–108.
- Spinks, J.W.T., Wood, R.J., 1976. An introduction to radiation chemistry, 2nd ed. Wiley-Interscience, New York.
- Sprawls, P., 1993. The Physical Principles of Medical Imaging, 2nd ed. Aspen Publishers, Gaithersburg, Md.
- Steinhart, M., 2004. Introduction to Nanotechnology. By Charles P. Poole, Jr. and Frank J. Owens. *Angewandte Chemie International Edition* 43, 2196–2197.

## 4.2 Characterisation of Micro-sized and Nano-sized Tungsten Oxide-Epoxy Composites for Radiation Shielding of Diagnostic X-rays

---

This work is the continuous analysis of Chapter 4.1, which provides the X-ray transmission results from XAS and also discussions on mechanical and microstructural analyses of the composites. This work is still under review for the second time after the first revision was made in the *Materials Science and Engineering C*, In press.

### Key findings:

- For the same  $\text{WO}_3$  loading, nano-sized  $\text{WO}_3$ -epoxy composite is superior in attenuating X-ray at the synchrotron energy of 10-25 keV when compared with their micro-sized counterparts.
- At higher synchrotron energy (i.e. 30-40 keV), the X-ray transmission was similar with no size effect for both nano-sized and micro-sized  $\text{WO}_3$ -epoxy composites.
- The equivalent X-ray energies for X-ray tube voltages operated by mammography unit (25-49 kV) was in the range 15-25 keV.
- For the general radiology unit of 40-60 kV, the range was 25-40 keV and for voltages greater than 60 kV (i.e. 70-100 kV), the equivalent energy was in excess of 40 keV.
- The mechanical properties of epoxy composites increased initially with an increase in the filler loading; then deteriorated with a further increase in the  $\text{WO}_3$  loading.



Contents lists available at ScienceDirect

## Materials Science and Engineering C

journal homepage: [www.elsevier.com/locate/msec](http://www.elsevier.com/locate/msec)

## Characterisation of micro-sized and nano-sized tungsten oxide-epoxy composites for radiation shielding of diagnostic X-rays

N.Z. Noor Azman<sup>a,b</sup>, S.A. Siddiqui<sup>a</sup>, I.M. Low<sup>a,\*</sup>

<sup>a</sup> Department of Imaging and Applied Physics, Curtin University, GPO Box U1987, Perth, WA 6845 Australia

<sup>b</sup> School of Physics, Universiti Sains Malaysia, 11800 Penang, Malaysia

## ARTICLE INFO

## Article history:

Received 6 May 2013

Received in revised form 5 August 2013

Accepted 18 August 2013

Available online xxxxx

## Keywords:

X-ray shielding

Micro-sized WO<sub>3</sub>-epoxy composites

Nano-sized WO<sub>3</sub>-epoxy composites

X-ray transmission

Filler loading

## ABSTRACT

Characteristics of X-ray transmissions were investigated for epoxy composites filled with 2–10 vol% WO<sub>3</sub> loadings using synchrotron X-ray absorption spectroscopy (XAS) at 10–40 keV. The results obtained were used to determine the equivalent X-ray energies for the operating X-ray tube voltages of mammography and radiology machines. The results confirmed the superior attenuation ability of nano-sized WO<sub>3</sub>-epoxy composites in the energy range of 10–25 keV when compared to their micro-sized counterparts. However, at higher synchrotron radiation energies (i.e., 30–40 keV), the X-ray transmission characteristics were similar with no apparent size effect for both nano-sized and micro-sized WO<sub>3</sub>-epoxy composites. The equivalent X-ray energies for the operating X-ray tube voltages of the mammography unit (25–49 kV) were in the range of 15–25 keV. Similarly, for a radiology unit operating at 40–60 kV, the equivalent energy range was 25–40 keV, and for operating voltages greater than 60 kV (i.e., 70–100 kV), the equivalent energy was in excess of 40 keV. The mechanical properties of epoxy composites increased initially with an increase in the filler loading but a further increase in the WO<sub>3</sub> loading resulted in deterioration of flexural strength, modulus and hardness.

Crown Copyright © 2013 Published by Elsevier B.V. All rights reserved.

### 1. Introduction

Hitherto, numerous analytical methods have been developed to investigate the effect of the particle size of a material on the X-ray attenuation for various incoming X-ray energies including scattered gamma-rays and X-rays [1–11]. It is widely believed that nano-sized particles are able to disperse more uniformly within the matrix with less agglomerations when compared to micro-sized particles, thus improving the X-ray attenuation ability of the material [6,12,13]. For instance, Hołyńska (1969) found that the intensity of scattered radiations increased with increases in the grain size of a material. This size effect has been observed in a sand matrix and for samples containing heavy elements such as iron or barium [4].

Filler-reinforced polymers have gained increasing attention from X-ray technologists in radiation shielding since polymers have great potential in many important applications by virtue of their unique properties, such as low density, the ability to form intricate shapes, optical transparency, low manufacturing cost and toughness. One of the filler-reinforced polymers commonly used for radiation shielding is lead acrylic [14–16]. Moreover, some researchers have also tried to synthesise nano-sized filler-reinforced polymers for radiation shielding by virtue of the size effect in X-ray attenuation [2,6,17]. For instance, a recent study by Botelho et al. [13] revealed that the attenuation for

X-ray beams generated from low tube voltages (i.e., 26–30 kV) in nanostructured copper oxide (CuO) was better than microstructured CuO. However, no significant difference in attenuation was observed for X-rays generated from higher tube voltages (i.e., 60–102 kV). A similar conclusion on this size effect in X-ray attenuation was made by Kunzel et al. [18] for a nanostructured CuO-polymer system.

In a recent work on WO<sub>3</sub>-filled epoxy composites [19], we investigated the effect of nano-sized and micro-sized WO<sub>3</sub> filler-epoxy composites on X-ray attenuation in the X-ray tube voltage range of 22–127 kV generated by a mammography unit and a general radiography unit. The equivalent X-ray energies for the various X-ray tube voltages used were in the range of 17.5–60 keV, which conformed to our expectation since the equivalent X-ray energies for a mammography unit were 17.5, 19.6, 20.2 and 22.7 keV, which are the characteristic energies of molybdenum and rhodium, while the equivalent X-ray energy for a radiology unit is about one-third of the X-ray tube voltage used. The results showed that nano-sized WO<sub>3</sub> was more effective than micro-sized WO<sub>3</sub> in X-ray attenuation only in the low X-ray tube voltage range of 22–35 kV, but this size effect was not apparent at the higher X-ray operating tube voltage range of 40–120 kV [19]. Hence, the aim of this work was to verify our previous work on X-ray transmission in WO<sub>3</sub>-filled epoxy composites by using synchrotron radiations as the X-ray source for the characteristic (monochromatic) X-ray energy range of 10–40 keV. The results obtained were compared with those of previous work [19] to determine the equivalent energy range of the previous machines used (a mammography unit and a radiology unit).

\* Corresponding author. Tel.: +61 8 9266 7544; fax: +61 8 9266 2377.

E-mail address: [j.low@curtin.edu.au](mailto:j.low@curtin.edu.au) (I.M. Low).

## 2. Experimental procedure

### 2.1. Sample preparation

Nano-sized (<100 nm) tungsten oxide and micro-sized (~20 μm) tungsten oxide (WO<sub>3</sub>) were used as the filler for synthesising WO<sub>3</sub>-epoxy composites. The former was obtained from Sigma-Aldrich and the latter (FR251) from Fibreglass and Resin Sales. The particle sizes were provided by Sigma-Aldrich.

Details about the preparation of the WO<sub>3</sub>-epoxy composite samples are available in [19]. For the current work, the thickness of the samples was set at 2.0 mm. The list of the prepared samples with the different volume percentages of WO<sub>3</sub> is shown in Table 1.

### 2.2. Measurements of X-ray transmission

This work was done using the X-ray absorption spectroscopy (XAS) beamline at the Australian Synchrotron located in Melbourne. Experiments were carried out in the energy range of 10–40 keV using a Si (311) monochromator and a beam size on the sample of about 0.25 × 0.25 mm<sup>2</sup> and a photon flux of about 10<sup>11</sup> ph/s. Data on X-ray transmission ( $I/I_0$ ) were collected in an ionisation chamber after the sample and compared to the incident beam flux. For each sample, 20 readings were recorded at each energy level. To normalise the data collected, readings were also recorded for an empty sample holder. The average  $I/I_0$  was calculated and plotted as a function of filler loadings (WO<sub>3</sub> vol%) for each synchrotron radiation energy. The X-ray transmission ( $I/I_0$ ) was related to the linear attenuation coefficient ( $\mu$ ) and the thickness of the samples ( $t$ ) through Eq. (1):

$$(I/I_0) = \exp(-\mu t) \quad (1)$$

Next, all the samples were examined again with a mammography unit and a radiology unit according to previous experiments [19].

### 2.3. Powder diffraction

Powder diffraction (PD) measurements were conducted to identify the crystallite size of the WO<sub>3</sub>. This was done at the Australian Synchrotron in Melbourne, on the Powder Diffraction beamline. Mythen detectors were used to record the diffraction patterns in the 2θ range of 0°–60° at a fixed wavelength of 1.13 Å. The crystallite size ( $L$ ) of the nano-sized WO<sub>3</sub> was determined using the Scherrer equation as follows (Eq. (2)):

$$L = \frac{k\lambda}{(\text{FWHM}) \cos\theta} \quad (2)$$

where  $k$  is a constant depending upon the crystal shape and size ( $k = 0.90$ ),  $\lambda$  is the wavelength, FWHM is the full-width half maximum of the peak and 2θ is the diffraction angle of the strongest peak.

**Table 1**

Compositions of WO<sub>3</sub>-epoxy composites with different volume fractions of filler WO<sub>3</sub> and epoxy resin.

Composite by volume fraction (vol%)	
Filler (WO <sub>3</sub> )	Epoxy resin
2	98
4	96
6	94
8	92
10	90

### 2.4. Flexural tests

Three-point bending tests were used to determine the flexural strength and modulus of the WO<sub>3</sub>-epoxy composites containing different loadings of nano-sized and micro-sized WO<sub>3</sub>. Specimens with dimensions 60 mm × 10 mm × 2 mm were prepared for the test according to the ASTM D790-03 standard [20] on a universal testing machine (LLOYD Instruments). A minimum of three samples was tested for each composite and the average results were taken. In these measurements, the samples were tested to the applied load with the results calculated by the NEXYGEN Plus software.

### 2.5. Indentation hardness test

The hardness values of polished WO<sub>3</sub>-epoxy composites were determined using a Rockwell hardness tester with scale H. The hardness measurements were conducted using an indentation load of 588.4 N and ball diameter of 0.3 cm. Five measurements were conducted for each sample in order to obtain an average value.

## 3. Results and discussion

### 3.1. Characteristics of X-ray transmissions

Since the synchrotron radiations of the XAS beam line contain a large range of energies (i.e., 10–40 keV), the thickness of the samples was set at 2 mm to ensure that the detector was able to obtain a meaningful X-ray transmission reading for the lower energy range without being totally absorbed by the samples. As shown in Fig. 1, there was an obvious difference in X-ray transmissions between the micro-sized WO<sub>3</sub>-epoxy and nano-sized WO<sub>3</sub>-epoxy composites of the same WO<sub>3</sub> vol% at the energy range of 10–20 keV. With a further increase of synchrotron energy to greater than 20 keV, there was no difference in X-ray transmissions between these two composites, thus indicating the absence of size effect at play. The results show that for all the WO<sub>3</sub> loadings in an epoxy matrix, the ratio of the X-ray transmission of the micro-sized WO<sub>3</sub>-epoxy composite ( $(I/I_0)_m$ ) relative to the nano-sized WO<sub>3</sub>-epoxy composite ( $(I/I_0)_n$ ),  $(I/I_0)_m/(I/I_0)_n$  remained at ~1.0 for the synchrotron energy range of 25–40 keV. On the other hand, the ratio  $(I/I_0)_m/(I/I_0)_n$  was 1.15–2.3 for all WO<sub>3</sub> loadings (see Fig. 2). The values determined for  $(I/I_0)_m/(I/I_0)_n$  at these energy ranges indicate that the nano-sized WO<sub>3</sub>-epoxy samples absorbed more low energy X-rays than their micro-sized WO<sub>3</sub>-epoxy counterparts.

Further investigations were conducted to verify our previous results [19] obtained from a mammography unit and a radiography unit. In this investigation, all the same measurements from the previous work were repeated with samples of 2 mm in thickness. Since a mammography

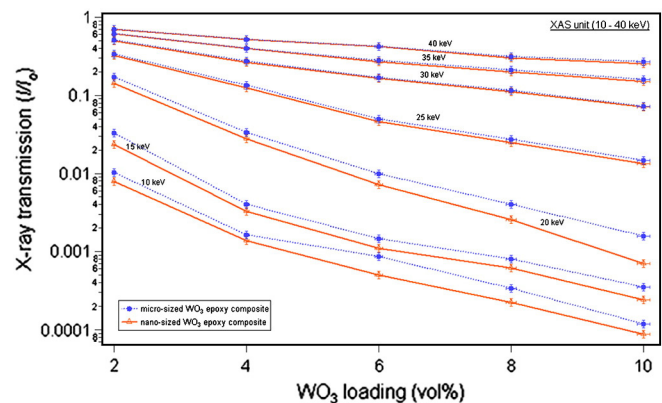


**Fig. 1.** Comparisons of X-ray transmission comparison in nano-sized and micro-sized WO<sub>3</sub>-epoxy composites for synchrotron radiation generated by the XAS unit for energy of 10–40 keV.

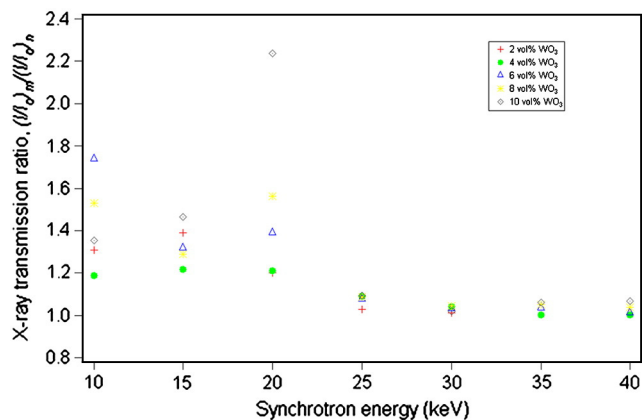


**Fig. 2.** The X-ray transmission ratio of micro-sized  $\text{WO}_3$ -epoxy composite  $(I/I_0)_m$  to the X-ray transmission for nano-sized  $\text{WO}_3$ -epoxy composite  $(I/I_0)_n$ ,  $(I/I_0)_m/(I/I_0)_n$  for synchrotron energies (10–40 keV).

unit generates characteristic X-ray energies of molybdenum (17.5 keV and 19.6 keV) or rhodium (20.2 keV and 22.7 keV), it is much easier to compare with the XAS results (see Fig. 3). In the results presented in Fig. 3, it is clearly shown that the X-ray transmission results for the mammography unit sat between the results of 15–25 keV for the XAS beam energies. In contrast, for the radiography unit, the operated X-ray tube voltages generated a broad spectrum (polychromatic X-ray beam). Thus, the equivalent energies for the X-ray tube voltages of the radiography unit were estimated from the XAS results by superimposing their data together (see Fig. 4). As can be seen in Fig. 4, the X-ray transmissions of samples for X-ray tube voltages of 40–60 kV were sitting between 25 and 40 keV while the others were sitting above 40 keV. Hence, the X-ray tube voltages of 40–60 kV operated by the radiography unit produced the equivalent X-ray energies in the range of 25–40 keV while the X-ray tube voltages of  $\geq 60$  kV had an equivalent energy of  $\geq 40$  keV.

Fig. 5 shows the comparison of X-ray transmissions for samples with different thicknesses. Samples of 7 mm thickness were used in our previous study [19], whereas 2-mm-thick samples were used in this study. Fig. 5a and b provide the results for the mammography unit only on samples with 4 vol% and 6 vol% loading of  $\text{WO}_3$ , respectively. As shown in these figures, the differences in the X-ray transmission between the micro-sized and nano-sized  $\text{WO}_3$ -epoxy became larger for thicker samples (7 mm). In contrast, Fig. 5c shows insignificant differences in X-ray transmission between nano-sized and micro-sized  $\text{WO}_3$ -epoxy composites for radiography tube voltages only for samples with a loading of 4 vol%  $\text{WO}_3$ . This trend was also observed for all the other loadings (i.e., 2, 6, 8 and 10 vol%  $\text{WO}_3$ ). These findings are in good agreement with the work by Künzel and Okuno (2012), which also showed that

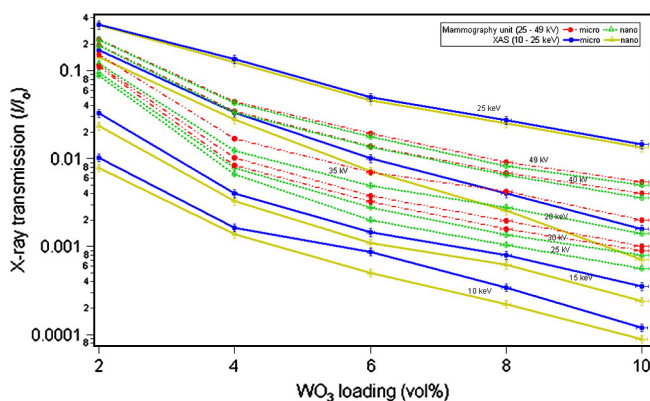


**Fig. 3.** Comparisons of X-ray transmission in nano-sized and micro-sized  $\text{WO}_3$ -epoxy composites for synchrotron radiation generated by the XAS unit for energies of 10–25 keV and mammography unit tube voltages of 25–49 kV.

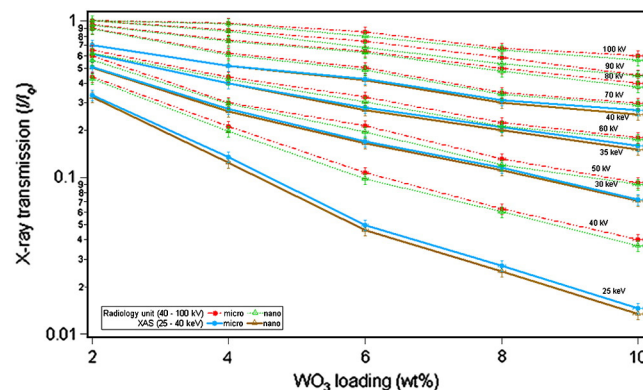


**Fig. 4.** Comparisons of X-ray transmission in nano-sized and micro-sized  $\text{WO}_3$ -epoxy composites for synchrotron radiation generated by the XAS unit for energies of 25–40 keV and radiography unit tube voltages of 40–100 kV.

the grain size effect increased with the increase of the sample thickness at low energy X-ray beams (25 kV and 30 kV) but remained unchanged over the material thickness for higher energy X-ray beams (60 kV) [18].

In general, the photoelectric effect is the most likely interaction to occur within a matter at a lower photon (X-ray) energy range. In this interaction, a photon will transfer its entire energy to an electron in the material on which it impinges. The electron thereby acquires enough energies to free itself from the material to which it is bound and then may undergo single or multiple-scattering events with neighboring atoms. In addition, there is also a slight fluctuation in the probability of emission of Auger electrons and fluorescent photons may form during this interaction. This phenomenon can contribute to the alteration of the mass attenuation coefficient of an element relative to the bulk material when considered over a small range of X-ray energies. The probability of photoelectric interaction is directly proportional to the cube of the atomic number of the absorbing material  $Z^3$  and inversely proportional to the cube of the X-ray energy  $(1/E)^3$ .

Moreover, nano-sized  $\text{WO}_3$ -epoxy composites consist of a higher number of  $\text{WO}_3$  particles/gram when compared to micro-sized  $\text{WO}_3$ -epoxy composites. Therefore, the distribution of the nano-sized  $\text{WO}_3$  in the resin should also be different from that presented by micro-sized  $\text{WO}_3$ , thus resulting in a more uniform dispersion in the resin. As a consequence, the chances of an X-ray photon with lower energy to interact and be absorbed by  $\text{WO}_3$  particles may be higher in nano-sized  $\text{WO}_3$ -epoxy composites than in micro-sized  $\text{WO}_3$ -epoxy composites. Fig. 6 shows the back-scattered images of the same loading of  $\text{WO}_3$  (4 vol%) within nano-sized  $\text{WO}_3$ -epoxy and micro-sized  $\text{WO}_3$ -epoxy composites using the Zeiss Evo 40XVP scanning electron microscope. The  $\text{WO}_3$  particles were seen to be more closely dispersed in the nano-sized  $\text{WO}_3$ -epoxy composite (Fig. 6a) as compared to its micro-sized counterpart (Fig. 6b). Thus, the probability for the lower energy photons to interact with the  $\text{WO}_3$  particles and be absorbed is higher for the nano-sized  $\text{WO}_3$ -epoxy composite.

As the photon energy increases, the photon (X-ray) penetration through the absorbing material without interaction increases, and hence, less photoelectric effect relative to the Compton effect occurs. Thus, the X-ray attenuation by the absorbing material decreased since the Compton interaction was weakly dependent on  $Z$  and  $E$  and this interaction only took place between the incident photon and one of the outer shell electrons of an atom in the absorbing material.

In order to discover the X-ray shielding ability of the composites, the results were compared to commercial lead (Pb) sheets (model RAS20 Calibrated Absorber Set) of four different thicknesses (i.e., 0.81, 1.63, 3.18 and 6.35 mm) (see Fig. 7) using a radiography unit of tube voltages 40–100 kV. The results show that although the lead sheets gave the lowest X-ray transmissions at each tube voltage when compared to all compositions of  $\text{WO}_3$ -epoxy composites, the latter with 10 vol% of either micro-sized or nano-sized  $\text{WO}_3$ , can be a substitute for Pb in



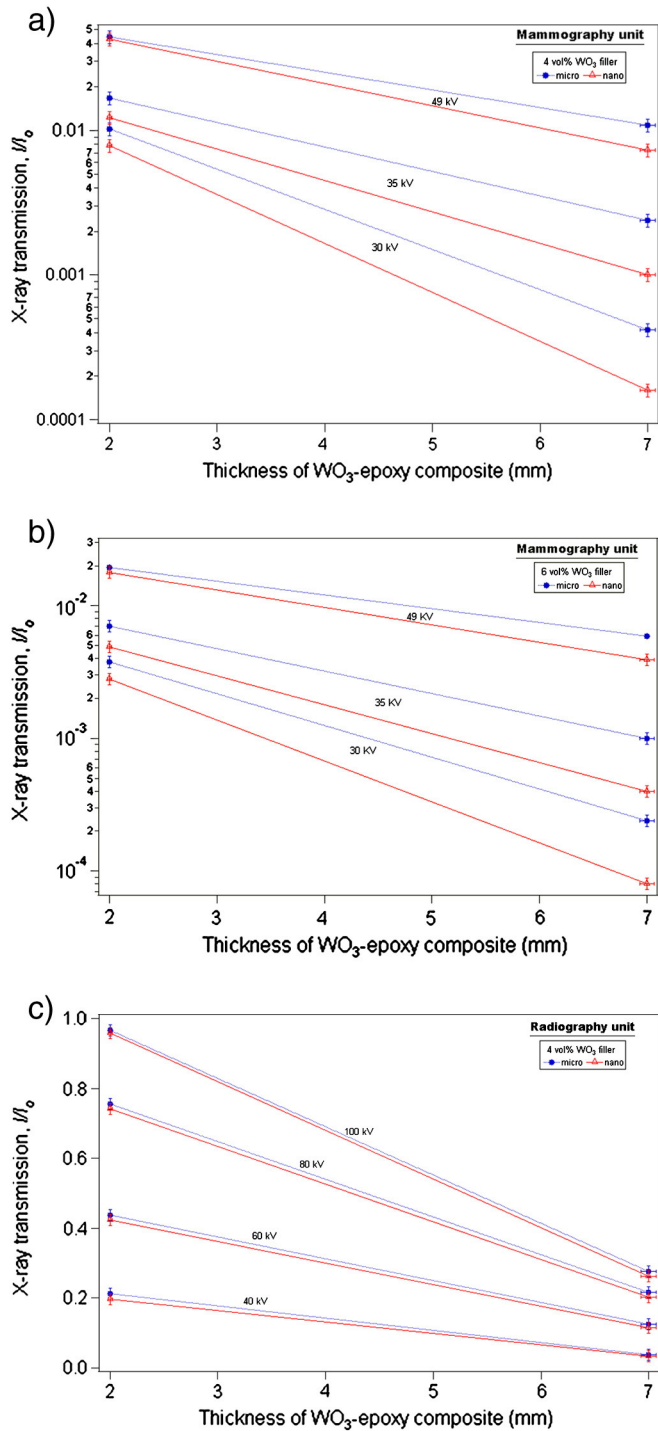


Fig. 5. X-ray transmission comparison for different thickness of the sample for (a) 4 vol% of  $WO_3$  filler epoxy composites for mammography unit tube voltages of 30, 35 and 49 kV; (b) 6 vol% of  $WO_3$  filler epoxy composites for mammography unit tube voltages of 30, 35 and 49 kV; and (c) 4 vol% of  $WO_3$  filler epoxy composites for radiography unit tube voltages of 40, 60, 80 and 100 kV.

X-ray shielding by increasing the sample thickness to  $\geq 7$  mm. Hence, the usage of lead in X-ray shielding can be substituted by  $WO_3$  whereby W is lighter and less toxic compared to Pb.

3.2. Crystallite size

The reference for fitting the peaks was taken from the International Centre for Diffraction Data PDF-4 + 2009 database. The wavelength for

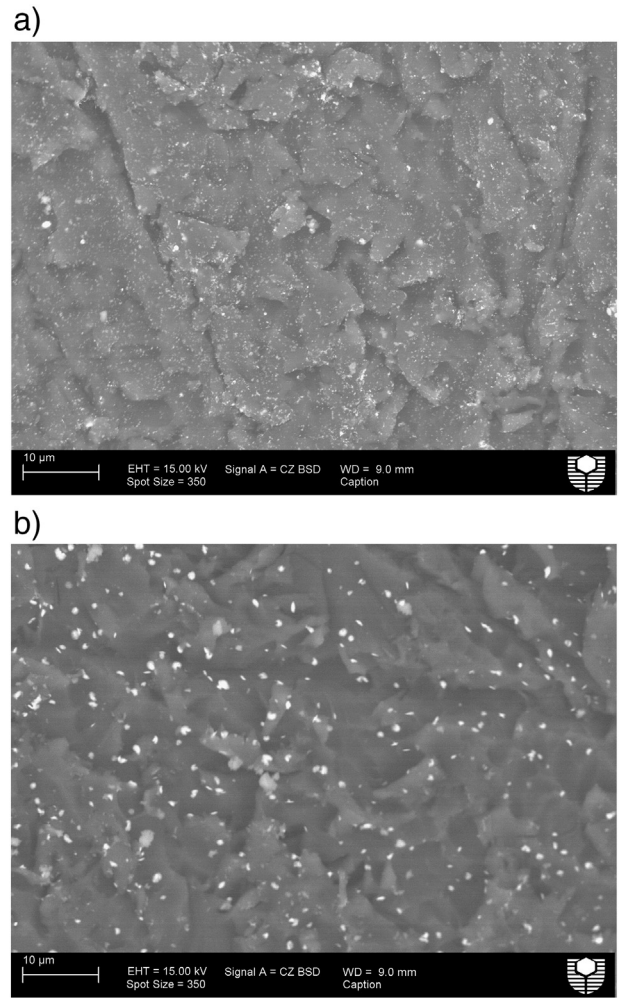


Fig. 6. SEM images for epoxy composites filled with (a) 4 vol% nano-sized  $WO_3$  and (b) 4 vol% of micro-sized  $WO_3$ .

all of these databases was chosen to be the same as the wavelength of the synchrotron radiation used. The diffraction peaks shown in Fig. 8 belong to monoclinic  $WO_3$  (PDF file 00-043-1035). These results indicate that both the micro-sized  $WO_3$  and the nano-sized  $WO_3$  were single-phase pure without impurities.

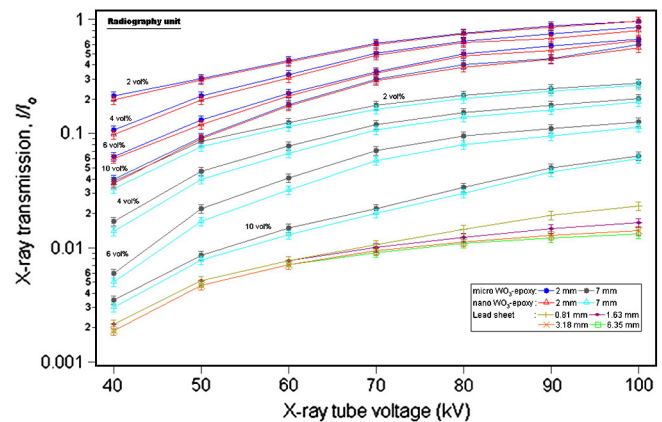


Fig. 7. X-ray transmission as a function of radiography unit X-ray tube voltage (40–100 kV) for all micro-sized and nano-sized  $WO_3$ -epoxy composites and commercial lead sheets.

The diffraction patterns were plotted only in the  $2\theta$  range of  $9^\circ$ – $15^\circ$  to clearly show the size difference of the peaks for each micro-sized and nano-sized  $\text{WO}_3$ . As shown in Fig. 8, the broad peaks belonged to nanometer-sized  $\text{WO}_3$  crystallite whereas the well-defined crystalline peaks belonged to micrometer-sized  $\text{WO}_3$ . The crystallite size determined from the Scherrer equation for nano-sized  $\text{WO}_3$  was 51.5 nm. These nano-crystallites were significantly smaller than the particle sizes provided by Sigma-Aldrich, thus indicating that at least 2 crystallites were present in each  $\text{WO}_3$  particle of 100 nm in size.

### 3.3. Mechanical properties

Fig. 9 shows the effect of filler loading on the flexural strength, flexural modulus and Rockwell hardness of the epoxy composites. The flexural strength was found to decrease with increased  $\text{WO}_3$  filler size while it had little or no effect on flexural modulus. Similar results were reported by Park [21], who observed an increase in flexural strength with decreased particle size in silica-reinforced epoxy composites. However, Moloney et al. [22] reported a negligible effect of particle size on flexural modulus in their epoxy composites filled with silica.

From Fig. 9a, it can be seen that the flexural strength of pure epoxy was 49.9 MPa, but increased to a maximum value of 64 MPa for the composite containing 4 vol% nano-sized  $\text{WO}_3$ . However, a further increase in the filler loading beyond 4 vol% resulted in a decrease in flexural strength whereby the composite containing 10 vol% nano-sized  $\text{WO}_3$  exhibited the lowest flexural strength of 52.6 MPa. Similarly for micro-sized  $\text{WO}_3$ -epoxy composites, the maximum flexural strength was obtained for a filler loading of 2 vol%. A reduction in flexural strength was again observed when the filler loading was increased beyond 2 vol% due to non-uniform dispersion of the filler within the matrix. The resultant agglomeration of the fillers acted as stress-concentrators which served to reduce the strength of the composites.

The flexural modulus of the composites increased with an increase in the filler loading for both the nano-sized and micro-sized  $\text{WO}_3$ , which may indicate that the stiffness of these composites obeyed the well-known rule-of-mixtures (Fig. 9b).

Finally, the hardness results presented in Fig. 9c indicate that an increase in the  $\text{WO}_3$  filler loading resulted in an initial increase in the hardness of the composite, but a further increase in filler loading at 10 vol% caused a reduction in hardness probably due to the undesirable agglomeration of the fillers. The initial increase in the hardness of the composites observed for both the nano-fillers and the micro-fillers may be attributed to their uniform dispersion within the epoxy matrix,

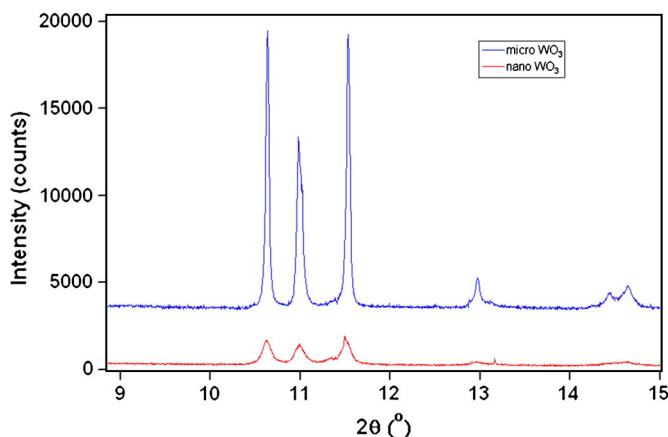


Fig. 8. Typical powder diffraction patterns for micro-sized and nano-sized  $\text{WO}_3$  loading in epoxy composites.

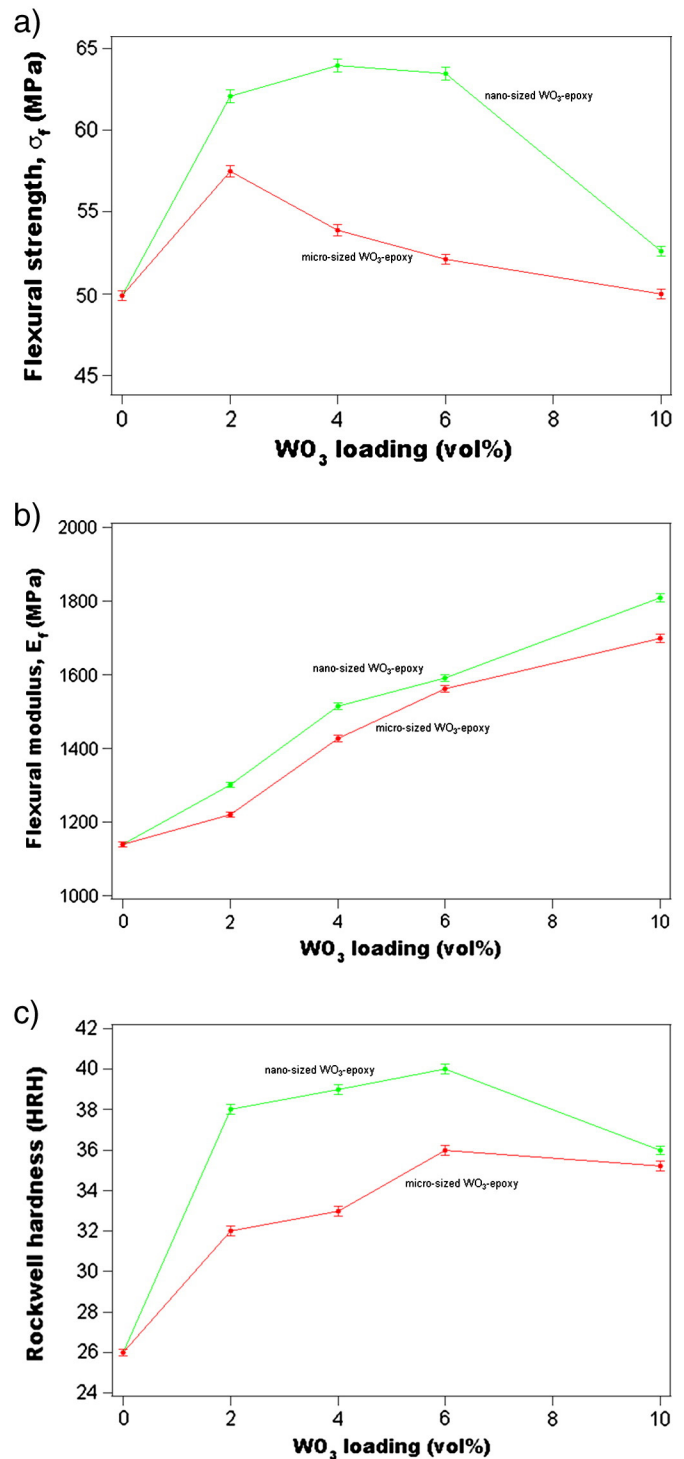


Fig. 9. Mechanical properties of epoxy composites showing: (a) flexural strength as a function of  $\text{WO}_3$  filler loading; (b) flexural modulus as a function of  $\text{WO}_3$  filler loading; and (c) Rockwell hardness as a function of  $\text{WO}_3$  filler loading.

together with their strong interaction with the epoxy chains to form good interfacial bonding.

### 4. Conclusion

The size effect of  $\text{WO}_3$  particles on the X-ray transmission in nano-sized and micro-sized  $\text{WO}_3$ -epoxy composites has been investigated at various synchrotron radiation energies (i.e., 10–40 keV). The results

presented in this work demonstrated that the size effect on X-ray attenuation was profoundly dependent on the energy of the synchrotron radiations. The particle size effect was more pronounced at lower synchrotron radiation energies (10–20 keV) since the X-ray transmission in nano-sized WO<sub>3</sub>-epoxy composites was less than in their micro-sized counterparts. However, this size effect became insignificant at higher energies of 20–40 keV because the X-ray transmissions in both nano-sized and micro-sized WO<sub>3</sub>-epoxy composites were very similar. The X-ray transmission results for the mammography unit sat between the results of 15–25 keV for XAS beam energies. Meanwhile, the X-ray transmissions in samples for X-ray tube voltages of 40–60 kV of the radiography unit sat between 25 and 40 keV. In addition, for composites with the same filler loading, but with increasing sample thickness, the size effect in X-ray transmission was most prominent for X-ray tube voltages of 25–35 kV but was negligible at 35–100 kV. As the filler loading of the WO<sub>3</sub> increased, the mechanical properties showed an initial optimum improvement, but a further increase in the filler loading caused these properties to deteriorate.

### Acknowledgements

The collection of X-ray absorption spectroscopy (XAS) data was funded by the Australian Synchrotron (AS123/XAS5341). We thank Dr. Bernt Johannessen of the Australian Synchrotron and our colleagues Dr. C. Ng and A/Prof. Z. Sun for assistance with XAS data collection. Also, we would like to thank Carolyn Madeley of Breast Assessment Centre,

Royal Perth Hospital, Western Australia for giving us the opportunity to use the mammography unit.

### References

- [1] C.R. Patra, R. Bhattacharya, D. Mukhopadhyay, P. Mukherjee, *Adv. Drug Deliv. Rev.* 62 (2010) 346–361.
- [2] F. Van Den Heuvel, J.P. Locquet, S. Nuyts, *Phys. Med. Biol.* 55 (2010) 4509–4520.
- [3] T. Wang, Z. Liu, M. Lu, B. Wen, Q. Ouyang, Y. Chen, C. Zhu, P. Gao, C. Li, M. Cao, L. Qi, *J. Appl. Phys.* 113 (2013) 024314–024318.
- [4] B. Holyńska, *Spectrochim. Acta B At. Spectrosc.* 24 (1969) 85–93.
- [5] A. Granmayeh Rad, H. Abbasi, M.H. Afzali, *Phys. Procedia* 22 (2011) 203–208.
- [6] F. El Haber, G. Froyer, *J. Univ. Chem. Technol. Metall.* 43 (2008) 283–290.
- [7] P. Jackson, S. Periasamy, V. Bansal, M. Geso, *Australas. Phys. Eng. Sci. Med.* 34 (2011) 243–249.
- [8] X. Huang, M.A. El-Sayed, *J. Adv. Res.* 1 (2010) 13–28.
- [9] P.D. Sahare, R. Ranju, S. Numan, S.P. Lochab, *J. Phys. D Appl. Phys.* 40 (2007) 759.
- [10] A. Popov, *SPIE Newsroom* 24 (2009) 1–2.
- [11] S.-S. Chen, H.-C. Chen, W.-C. Wang, C.-Y. Lee, I.N. Lin, J. Guo, C.-L. Chang, *J. Appl. Phys.* 113 (2013) 113704–113710.
- [12] M. Steinhart, *Angew. Chem. Int. Ed.* 43 (2004) 2196–2197.
- [13] M.Z. Botelho, R. Künzel, E. Okuno, R.S. Levenhagen, T. Basesio, C.P. Bergmann, *Appl. Radiat. Isot.* 69 (2011) 527–530.
- [14] Lablogic, in: L.S. Limited (Ed.), Lablogic, Sheffield, United Kingdom, 2009.
- [15] S. Daren, *POLYMICRO Newsletter*, 2004.
- [16] Premac Lead Acrylic, Part of the Wardray Premise Total Radiation Shielding Package, Wardray Premise Ltd., Surrey, United Kingdom, 2005–2011.
- [17] M. Faccini, C. Vaquero, D. Amantia, *J. Nanomater.* 2012 (2012) 1–9.
- [18] R. Künzel, E. Okuno, *Appl. Radiat. Isot.* 70 (2012) 781–784.
- [19] N.Z. Noor Azman, S.A. Siddiqui, R. Hart, I.M. Low, *Appl. Radiat. Isot.* 71 (2013) 62–67.
- [20] *Annual Book of ASTM Standards*, vol. 08.01, ASTM, 2005.
- [21] J.J. Park, *Trans. Electr. Electron. Mater.* 14 (2013) 39–42.
- [22] A.C. Moloney, H.H. Kausch, T. Kaiser, H.R. Beer, *J. Mater. Sci.* 22 (1987) 381–393.



## **5. FILLER DISPERSION WITHIN EPOXY, ACRYLIC AND GLASS BY ION-IMPLANTATION METHOD**

---

This chapter describes the fabrication of filler (Pb, Au and W) reinforced epoxy, acrylic and glass composites using ion-implantation method. A comparative study of the near surface composition depth profiling of the samples was performed using ion beam analysis (Rutherford backscattering spectroscopy). Moreover, the comparative X-ray attenuation analysis of the samples was performed using a calibrated general diagnostic radiology machine.

## 5.1 Synthesis and Characterization of Ion-Implanted Epoxy Composites for X-ray Shielding

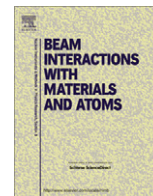
---

This work reports on the fabrication of filler-epoxy composite using ion-implantation, as published in the *Nuclear Instruments and Methods in Physics Research B: Beam Interactions with Materials and Atoms*, volume 287, pages 120-123 in the year 2012.

Pb, W and Au ions were implanted on the epoxy matrix since they are well-known candidates for X-ray shielding. A comparative study of the near surface composition depth profiling of the samples was performed using ion beam analysis (Rutherford backscattering spectroscopy). Moreover, the comparative X-ray attenuation analysis of the samples was performed using a calibrated general diagnostic radiology machine.

### **Key findings:**

- A higher nominal dose resulted in a higher implanted ion concentration in the epoxy.
- For a small concentration of implanted elements, the variation of the mass attenuation coefficient with the X-ray tube voltage is similar to the result for pure epoxy.
- For higher concentrations of implanted elements, there is a noticeable increase of the mass attenuation coefficient above the result for pure epoxy.



## Synthesis and characterisation of ion-implanted epoxy composites for X-ray shielding

N.Z. Noor Azman<sup>a,b</sup>, S.A. Siddiqui<sup>a</sup>, M. Ionescu<sup>c</sup>, I.M. Low<sup>a,\*</sup>

<sup>a</sup> Department of Imaging and Applied Physics, Faculty of Science and Engineering, Curtin University, GPO Box U1987, Perth, WA 6845, Australia

<sup>b</sup> School of Physics, Universiti Sains Malaysia, 11800 Penang, Malaysia

<sup>c</sup> Australian Nuclear Science and Technology Organisation (ANSTO), Lucas Heights, NSW 2234, Australia

### ARTICLE INFO

#### Article history:

Received 4 May 2012

Received in revised form 6 June 2012

Available online 17 June 2012

#### Keywords:

Ion-implantation

Nominal dose

Implanted dose

Implanted ions

X-ray mass attenuation coefficient

X-ray shielding

### ABSTRACT

The epoxy samples were implanted with heavy ions such as tungsten (W), gold (Au) and lead (Pb) to investigate the attenuation characteristics of these composites. Near-surface composition depth profiling of ion-implanted epoxy systems was studied using Rutherford Backscattering Spectroscopy (RBS). The effect of implanted ions on the X-ray attenuation was studied with a general diagnostic X-ray machine with X-ray tube voltages from 40 to 100 kV at constant exposure 10 mAs. Results show that the threshold of implanted ions above which X-ray mass attenuation coefficient,  $\mu_m$  of the ion-implanted epoxy composite is distinguishably higher than the  $\mu_m$  of the pure epoxy sample is different for W, Au and Pb.

Crown Copyright © 2012 Published by Elsevier B.V. All rights reserved.

### 1. Introduction

X-ray shielding requirements have become more stringent as standards for exposure of personnel and general public have been re-assessed. X-rays technologists practice the ALARA principle (as-low-as-reasonably-achievable) dose when dealing with harmful ionizing radiation in order to continuously minimize the dose received by personnel and general public [1–5].

Moreover, the application of polymers in X-ray shielding technology is increasing steadily. This is due to a number of advantages such as the choice of fillers into the polymer matrix, the improved dispersion of fillers which enable the formation of mechanically stable hard coating materials and the possibility to modify both chemical composition and the related physical properties of polymers by easy-to-control fabrication parameters [6–11].

In addition, other surface modification tools such as ion implantation has also become increasingly used due to the ease and readability to process some parameters during the irradiation such as the choice of ions, the ion fluence, the depth of ion implantation, etc., which can further improve the X-ray absorption capacity of shielding materials, including polymers [7,9,12–14]. The main advantage of ion-implantation technology is the capability of accurately controlling the number of implanted dopant atoms and the dopant's depth distribution profile [15]. In addition, the

ion-implantation is well established and well understood technology as shown in applications for modifying the surface properties of metals, semiconductors and ceramics. More recently, the ion implantation technology has been applied to the surface modification of polymers to enhance their mechanical and electrical properties without changing the bulk properties [10,11,16–19]. Promising results on ion-implanted ultra high molecular weight polyethylene (UHMWPE) have been shown by Chen et al. where improved hardness and Young's modulus could be obtained through nitrogen ion-implantation [14].

In addition, an epoxy system is a thermoset polymer which is generally stronger and better suited to higher temperatures than thermoplastics so it can withstand the high energetic ion during the implantation process [20]. Hence, the purpose of the present study is to synthesize and characterize the X-ray attenuation property, microstructure and near-surface composition of epoxy composites which have been implanted with heavy ions such as tungsten (W), gold (Au) and lead (Pb).

### 2. Experimental procedure

#### 2.1. Sample preparation

Pure epoxy samples were prepared by mixing one part of FR251 hardener (Isophoronediamine) with two parts of FR251 epoxy resin (Bisphenol-A diglycidyl ether polymer). The mixing of epoxy resin and hardener was done through gentle stirring using a

\* Corresponding author. Tel.: +61 92667544.

E-mail address: [j.low@curtin.edu.au](mailto:j.low@curtin.edu.au) (I.M. Low).

stirring machine (2 level of speed) within a beaker with constant level 1 speed for 10 min to ensure the uniformity of the mixture. Then, the mixture was cast in cylindrical Fixiform moulds (diameter of 25 mm) with a thickness of 2 mm and allowed to set overnight. The cured epoxy samples were polished using diamond pastes from 15  $\mu\text{m}$  to 1.0  $\mu\text{m}$  to obtain flat and mirror-like surface finishes.

## 2.2. Ion-implantation

For this preliminary investigation of the X-ray attenuation characteristics of ion-implanted composites, we started with lower implanted dose in order to prevent possible melting and/or decomposition of the epoxy samples during ion implantation.

Polished epoxy samples were implanted with tungsten (W), gold (Au) and lead (Pb), produced by a metal evaporation and direct extraction ion source. For this type of ion source, the charge distribution of positive ions was measured previously by RBS and they are:  $W^{+1} = 1\%$ ,  $W^{+2} = 16\%$ ,  $W^{+3} = 58\%$ ,  $W^{+4} = 25\%$ ,  $Au^{+1} = 12\%$ ,  $Au^{+2} = 78\%$ ,  $Au^{+3} = 9\%$ ,  $Au^{+4} = 1\%$  and  $Pb^{+1} = 35\%$ ,  $Pb^{+2} = 64\%$ ,  $Pb^{+3} = 1\%$ . These values are close to the theoretical prediction using the Debye–Huckel approximation of non-ideal plasma [13]. The RBS measured values of charge distribution result in an average charge of  $W^{+3.07}$ ,  $Au^{+1.99}$  and  $Pb^{+1.66}$ . Thus, the ion acceleration of 40 kV used in this work afforded an average implantation energy of  $W = 122.8$  keV,  $Au = 79.6$  keV and  $Pb = 66.4$  keV, and a projected range in epoxy of 80 nm, 59 nm and 54 nm, respectively. The beam size was close to 20  $\text{cm}^2$ , and the beam current used in this experiment was around 30  $\mu\text{A}$ . The ion fluence was monitored by converting the ion target current into pulses using a current-to-frequency convertor. In this work all three ions were implanted at nominal doses between  $7 \times 10^{14}$  ions/ $\text{cm}^2$  and  $1.4 \times 10^{15}$  ions/ $\text{cm}^2$ , measured by RBS, after the implantation process, and converted in [at.%] for ease of comparison.

## 2.3. Ion beam analysis and Rutherford Backscattering Spectroscopy (RBS)

The near surface composition depth profiling of ion-implanted epoxy samples was characterized by ion beam analysis and RBS using a beam of 1.8 MeV  $\text{He}^{1+}$  ions beam at the Australian Nuclear Science and Technology Organisation. The information obtained was processed using SIMNRA code [21] which allowed calculation of depth distribution of implanted species and the implanted dose, which was converted in concentration. For these particular samples, a depth resolution of the order of 10 nm was achieved for the implanted heavy element.

## 2.4. Measurement of X-ray mass attenuation coefficient ( $\mu_m$ )

This work was done using a general diagnostic X-ray machine (brand: Shimadzu, model: Circlex 0.6/1.2 P364DK-100SF). The initial X-ray dose ( $D_0$ ) was determined by directly measuring X-rays with the DIADOS diagnostic detector connected to DIADOS diagnostic dosimeter (PTW-Freiburg, Germany) in the absence of the sample. The dosimeter is a universal dosimeter for measuring simultaneous dose and dose rate for radiography, fluoroscopy, mammography, dental X-ray and CT. Meanwhile the exit dose ( $D$ ) was taken with the sample placed on the detector. The distance between the X-rays tube and the detector was set to 100 cm and the X-ray beam was well collimated to the size of the sample. The exposure was set at 10 mAs to obtain meaningful reading for this type of detector while the tube voltage was increased from 40 kV to 100 kV in step of 10 kV for each dose measurement. The range of X-ray tube voltage (40–100 kV) was selected because this range is the normal range of X-ray tube voltage used for general

diagnostic imaging purposes. The mass attenuation coefficient,  $\mu_m = \mu/\rho_{comp}$  for each sample was determined from Eq. (1) where  $x$  is the thickness of the sample and  $\rho_{comp}$  is the apparent density of the composite sample. The value of  $\rho_{comp}$  was measured and calculated according to Archimedes' method [22]:

$$\mu_m = -\frac{\ln\left(\frac{D}{D_0}\right)}{x(\rho_{comp})} \quad (1)$$

## 3. Results and discussion

### 3.1. Rutherford Backscattering Spectroscopy (RBS)

The RBS results in Fig. 1 shows the yield versus channel number for samples B1, B3 and B5 implanted with W, Au and Pb, respectively. The list of samples with the different amount of implanted ions is shown in Table 1. These results confirm that a higher nominal dose resulted in a higher implanted concentration in the samples. For example, for Au-implanted sample B3, a maximum Au concentration of 0.13 at.% has been implanted in epoxy down to a depth of about 600 mono layers (ML) and it drops to 0.06 at.% for the next 800 ML. For sample B4 a maximum Au concentration of 0.23 at.% has been implanted in epoxy down to a depth of about 700 ML and then it drops to about 0.08 at.% for the next 900 ML. This small difference in the implantation depth of Au in epoxy is attributed to the small differences in the local density of the hand-made epoxy polymer.

A similar depth-profile RBS results was obtained for samples implanted with W and Pb.

### 3.2. X-ray mass attenuation coefficient

Fig. 2 shows the mass attenuation coefficient,  $\mu_m$  as a function of X-ray tube voltage for pure epoxy sample and for samples implanted with all three ions at various concentrations, as determined by RBS. The results illustrate the typical decrease of  $\mu_m$  with the increase of X-ray tube excitation voltage, due to a higher energy bremsstrahlung. In addition, a small increase of  $\mu_m$  is noticed with the change of the implanted elements (W, Au and Pb). For small concentrations of implanted elements, the variation of  $\mu_m$  with the X-ray tube voltage is similar with the result of  $\mu_m$  for pure epoxy. However, for higher concentration of implanted elements, there is a noticeable increase of  $\mu_m$  above the  $\mu_m$  of pure epoxy,

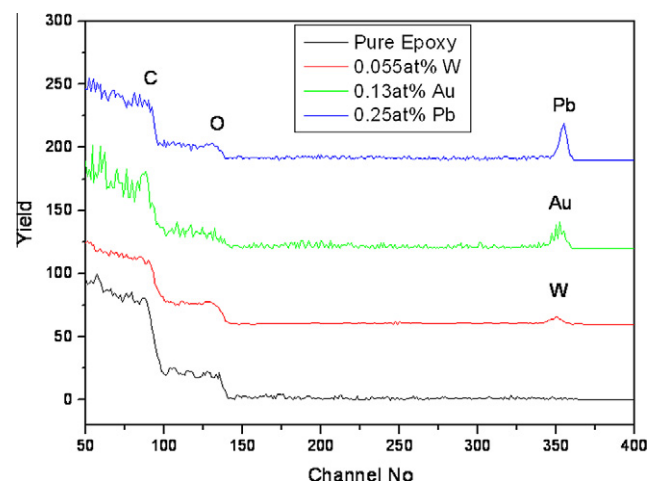


Fig. 1. RBS result for pure epoxy sample and implanted samples B1 (0.055 at.% W), B3 (0.13 at.% Au) and B5 (0.25 at.% Pb).

**Table 1**  
List of samples prepared with different implanted ions, average charge and RBS concentration of implanted ion.

Sample ID	Implanted ion	Average charge	RBS concentration (at.%)
B1	W	+3.07	0.055
B2	W		0.115
B3	Au	+1.99	0.130
B4	Au		0.230
B5	Pb	+1.66	0.250
B6	Pb		0.402

**Table 2**  
Relative increase of  $\mu_m$  with the excitation of the X-ray tube for a relative increase in the concentration of implanted ions of: W = 109.1%; Au = 76.9% and Pb = 60.8%.

X-ray tube excitation voltage (kV)	W (%)	Au (%)	Pb (%)
40	4.18	4.95	5.55
60	1.45	2.69	3.01
100	1.64	1.59	2.09

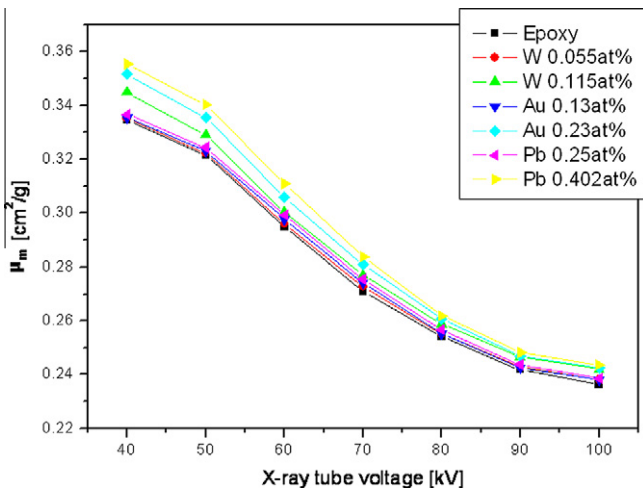


**Fig. 2.** Comparison of  $\mu_m$  versus X-ray tube voltage for pure epoxy sample and all implanted samples.

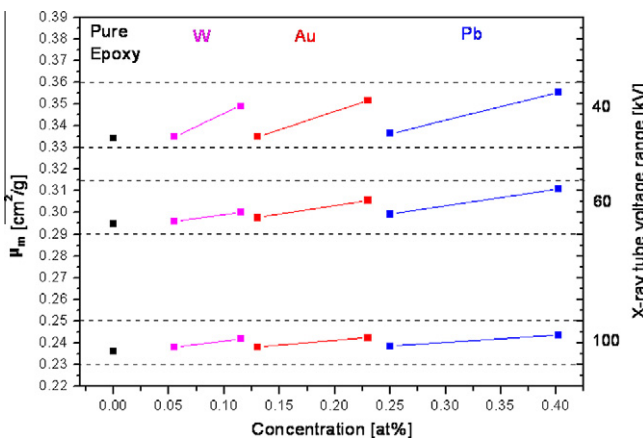


**Fig. 3.** Variation of  $\mu_m$  with concentration of implanted ion, the type of implanted ion and the excitation energy of the X-ray tube.

at each X-ray tube voltage, but this increase is higher at lower excitation voltages (energies). This is better illustrated in Fig. 3, where we capture the variation of  $\mu_m$  with concentration of implanted ion, the type of implanted ion and the excitation energy of the X-ray tube. In addition, with the decreasing of  $\mu_m$  with the increased of X-ray energy, we note the increase of  $\mu_m$  with the concentration of implanted element and with type of implanted element. For the same energy of X-rays, the heavier the implanted ion or in other word the higher the atomic number of implanted ion, the higher is the value of  $\mu_m$ . These were due to the photoelectric interaction dominates in the low X-ray energy range and high atomic number of absorbing material. The probability of the photoelectric

interaction is approximately dependent on  $Z^3/E^3$  where  $Z$  is atomic number of the absorbing material (implanted ions) and  $E$  is the photon energy [23].

Fig. 3 also shows that for the same excitation voltage, the increase of  $\mu_m$  is more effective and that small additions of W afford a reasonable increase. For example (see Table 1) for comparable concentrations of 0.115 at.% W (sample B2) and 0.13 at.% Au (sample B3), the W appears to be more effective in increasing the  $\mu_m$  which is contrary to what we expect since the atomic number of W is lower than the atomic number of Au. A possible explanation could be that at these concentrations, Au and Pb is agglomerating to a higher degree than W, but this is yet to be verified by cross section TEM. However, in terms of the relative increase in the concentration of implanted ions, the increase of  $\mu_m$  is higher for Pb, as shown in Table 2. Table 2 also shows that within the range used for the excitation voltage of the X-ray tube, the doping threshold where  $\mu_m$  of the composite starts to be larger than the  $\mu_m$  of the pure epoxy is around 0.1 at.% for W, 0.2 at.% for Au and 0.25 at.% for Pb.

**4. Conclusions**

The ion-implantation technique has been successfully used to implant epoxy resin with W, Au and Pb at various concentrations, and the X-ray mass attenuation coefficient of the composite has been measured in a range of 40–100 kV of the excitation voltage for the X-ray tube. It has been shown that the threshold of implanted ions above which  $\mu_m$  of the ion-implanted epoxy composite is distinguishably higher than the  $\mu_m$  of the pure epoxy is different for W, Au and Pb. The practical concentrations of W, Au and Pb in epoxy composite which could provide good X-ray attenuation properties and could be considered as candidates for effective X-ray shielding in diagnostic radiology is higher than the concentrations used in this report, and further work is considered.

**Acknowledgements**

The work on ion-implantation and ion-beam analysis was conducted at the Australian Nuclear Science and Technology Organisation with financial support from AINSE under grant AINGRA 11-135.

**References**

- [1] A.A. Okunade, Comparison of lead attenuation and lead hardening equivalence of materials used in respect of diagnostic X-ray shielding, *Appl. Radiat. Isot.* 57 (2002) 819–824.
- [2] A.A. Okunade, Numerical models for the determination of primary structural barriers for diagnostic X-ray facilities, *Med. Phys.* 31 (2004) 513–520.
- [3] B.R. Archer, Recent history of the shielding of medical X-ray imaging facilities, *Health Phys.* 88 (2005) 579–586.
- [4] R.L. Dixon, D.J. Simpkin, Primary shielding barriers for diagnostic X-ray facilities: a new model, *Health Phys.* 74 (1998) 181–189.
- [5] A. Hessenbruch, A brief history of X-rays, *Endeavour* 26 (2002) 137–141.
- [6] Y. Wu, T. Zhang, H. Zhang, X. Zhang, Z. Deng, G. Zhou, Electrical properties of polymer modified by metal ion implantation, *Nucl. Instrum. Methods Phys. Res. Sect. B* 169 (2000) 89–93.

- [7] K. Dworecki, M. Drabik, T. Hasegawa, S. Wąsik, Modification of polymer membranes by ion implantation, *Nucl. Instrum. Methods Phys. Res. Sect. B* 225 (2004) 483–488.
- [8] G.K. Hubler, Use of ion beam analysis in metal modification by means of ion implantation, *Nucl. Instrum. Methods Phys. Res.* 191 (1981) 101–113.
- [9] M.R.F. Soares, P. Alegaonkar, M. Behar, D. Fink, M. Müller,  $6\text{Li}^+$  ion implantation into polystyrene, *Nucl. Instrum. Methods Phys. Res. Sect. B* 218 (2004) 300–307.
- [10] E.H. Lee, G.R. Rao, M.B. Lewis, L.K. Mansur, Ion beam application for improved polymer surface properties, *Nucl. Instrum. Methods Phys. Res. Sect. B* 74 (1993) 326–330.
- [11] W. Yuguang, Z. Tonghe, Z. Huixing, Z. Xiaoji, D. Zhiwei, Polymer modification by MEVVA source deposited and ion implantation, *Surf. Coat. Technol.* 131 (2000) 520–524.
- [12] C.M. Lopatin, T.L. Alford, V.B. Pizziconi, M. Kuan, T. Laursen, Ion-beam densification of hydroxyapatite thin films, *Nucl. Instrum. Methods Phys. Res. Sect. B* 145 (1998) 522–531.
- [13] A. Anders, *Phys. Rev. E* 55 (1997) 969.
- [14] J.S. Chen, S.P. Lau, Z. Sun, B.K. Tay, G.Q. Yu, F.Y. Zhu, D.Z. Zhu, H.J. Xu, Structural and mechanical properties of nitrogen ion implanted ultra high molecular weight polyethylene, *Surf. Coat. Technol.* 138 (2001) 33–38.
- [15] <<http://www.ece.gatech.edu/research/labs/vc/theory/ionimplant.html#depth>> (22/6/2010).
- [16] E.V. Kozlov, A.I. Ryabchikov, Y.P. Sharkeev, I.B. Stepanov, S.V. Fortuna, D.O. Sivin, I.A. Kurzina, T.S. Prokopova, I.A. Mel'nik, Formation of intermetallic layers at high intensity ion implantation, *Surf. Coat. Technol.* 158–159 (2002) 343–348.
- [17] P.J. Evans, J. Hyvarinen, M. Samandi, Surface modification of austenitic stainless steel by titanium ion implantation, *Surf. Coat. Technol.* 71 (1995) 151–158.
- [18] V. Ashworth, W.A. Grant, R.P.M. Procter, E.J. Wright, The effect of ion implantation on the corrosion behavior of pure iron-IV. Lead ion implantation, *Corros. Sci.* 18 (1978) 681–685.
- [19] C. Wang, Y.X. Tao, The influence of boron ion-implantation on silica and lead glasses, *J. Non-Cryst. Solids* 71 (1985) 397–402.
- [20] Archos LLC, <[http://www.archos-llc.com/Material\\_Guide\\_2.html](http://www.archos-llc.com/Material_Guide_2.html)> (6/10/2011).
- [21] M. Mayer, in: J.L. Duggan, I.L. Morgan (Eds.), *Proceedings of the 15th International Conference on the Application of Accelerators in Research and Industry*, American Institute of Physics Conference Proceedings vol. 475, 1999, p. 541.
- [22] Australian Standards 1774.5, Method 5. The Determination of Density, Porosity and Water Absorption, 1989.
- [23] P. Sprawls, *The Physical Principles of Medical Imaging*, second ed., Aspen Publishers, Gaithersburg, Md, 1993.

## 5.2 A Comparative Study of X-ray Shielding Capability in Ion-Implanted Acrylic and Glass

---

This work details the fabrication of acrylic and glass with Pb and W using the similar ion-implantation process as described in Chapter 5.1. It was published in the *Radiation Physics and Chemistry*, volume 85, pages 102-106 in the year 2013.

This work studied the similar characterization analyses reported in the previous chapter which comprised a comparative study of the near surface composition depth profiling using RBS and the comparative X-ray attenuation. The final results were compared with the results reported for the implanted epoxy mentioned in Chapter 5.1.

### **Key findings:**

- The range of implanted ions is inversely proportional to the atomic number ( $Z$ ) of the implanted ion (Pb=82, W=74) and with the density of the matrix.
- A higher nominal dose resulted in a higher implanted ion concentration in the matrix.
- Glass has a lower projected range/depth profile as compared with acrylic and epoxy, hence has a shorter RBS depth profile.
- There is a high possibility of acrylic being altered by the energetic ions when they bombard the surface and cause bond breaking along the ion tracks.
- For a small concentration of implanted elements, the variation of the linear attenuation coefficient with the X-ray tube voltage is similar to that of the result for pure matrix.
- For higher concentrations of implanted elements, there is a noticeable increase of the linear attenuation coefficient above that of the result for pure matrix.
- The ion-implanted glass shows the highest attenuation compared with acrylic and epoxy (Chapter 5.1) since it is denser and has the highest RBS ion concentration of the same ion.





ELSEVIER

Contents lists available at [SciVerse ScienceDirect](http://www.sciencedirect.com)

# Radiation Physics and Chemistry

journal homepage: [www.elsevier.com/locate/radphyschem](http://www.elsevier.com/locate/radphyschem)

## A comparative study of X-ray shielding capability in ion-implanted acrylic and glass

N.Z. Noor Azman<sup>a,b</sup>, S.A. Siddiqui<sup>a</sup>, M. Ionescu<sup>c</sup>, I.M. Low<sup>a,\*</sup><sup>a</sup> Department of Imaging and Applied Physics, Curtin University, Perth, WA 6845, Australia<sup>b</sup> School of Physics, Universiti Sains Malaysia, Penang 11800, Malaysia<sup>c</sup> Australian Nuclear Science and Technology Organization, Sydney, NSW 2232, Australia

### HIGHLIGHTS

- ▶ Synthesis of ion-implanted acrylic and glass for X-ray attenuation.
- ▶ X-ray attenuation of implanted samples increase with dose of ions.
- ▶ Implanted glass has the best X-ray attenuation property.
- ▶ A higher dose through prolonged time is necessary for implanted acrylic.

### ARTICLE INFO

#### Article history:

Received 22 November 2012

Accepted 22 December 2012

Available online 31 December 2012

#### Keywords:

Sample matrix

Nominal dose

RBS ion concentration

Depth profile

Implanted ions

X-ray linear attenuation coefficient

### ABSTRACT

Samples of acrylic and glass were implanted with tungsten (W) and lead (Pb) to investigate their X-ray attenuation characteristics. The near-surface composition depth profiles of ion-implanted acrylic and glass samples were studied using ion-beam analysis (Rutherford backscattering spectroscopy—RBS). The effect of implanted ions on the X-ray attenuation ability was studied using a conventional laboratory X-ray machine with X-ray tube voltages ranging from 40 to 100 kV at constant exposure 10 mAs. The results were compared with previous work on ion-implanted epoxy. As predicted, the RBS results and X-ray attenuation for both ion-implanted acrylic and glass increase with the type of implanted ions when compared to the controls. However, since the glass is denser than epoxy or acrylic, it has provided the higher X-ray attenuation property and higher RBS ion concentration implanted with a shorter range of the ion depth profile when compared to epoxy and acrylic. A prolonged time is necessary for implanting acrylic with a very high nominal dose to minimize a high possibility of acrylic to melt during the process.

Crown Copyright © 2012 Published by Elsevier Ltd. All rights reserved.

### 1. Introduction

Hitherto, the application of ion implantation has become increasingly used due to the capability of accurate control on the number of implanted ions and the implanted depth distribution profile. This enables scientists to further improve the X-ray absorption capacity of shielding materials such as glass and polymers (Anders, 1997; Chen et al., 2001; Dworecki et al., 2004; Evans et al., 1995; Hubler, 1981; Kozlov et al., 2002; Lee et al., 1993; Lopatin et al., 1998; Soares et al., 2004; Wu et al., 2000; Yuguang et al., 2000). For example, a recent research by Rodríguez et al. (2007) has shown that ion implantation is an effective technology for implanting elements into polymers for surface modification to improve their mechanical

properties such as hardness and elastic modulus. In addition, promising material comprising Cu nanoparticles in a ZnO matrix for exhibiting the phenomenon of self-defocusing and possessing a high nonlinear absorption coefficient for the usage as an active light intensity limiter in the visible spectral range was successfully obtained by the ion implantation technique by Stepanov et al. (2004). Furthermore, our previous work on epoxy implanted with lead, tungsten and gold ions showed a higher X-ray attenuation of when compared to pure epoxy (Noor Azman et al., 2012).

Glass is one example of materials used in shielding of ionizing radiations, especially for X-rays and gamma-rays, but it is heavy, expensive and very brittle. So, it is not surprising that the application of polymers in X-ray shielding technology is increasing steadily. This is due to a number of advantages that glass could not meet because of their unique properties, such as low manufacturing cost and rugged shatter-resistant material (Dworecki et al., 2004; Soares et al., 2004). But due to its high density as compared to polymer, glass

\* Corresponding author. Tel.: +618 9266 7544; fax: +618 9266 2377.

E-mail address: [j.low@curtin.edu.au](mailto:j.low@curtin.edu.au) (I.M. Low).



is still in use for ionizing radiation shielding purposes since it can provide higher attenuation than polymer of the same thickness (Chanthima et al., 2011).

The aim of the present work was to synthesize, characterize and compare the X-ray attenuation properties and near-surface composition profiles of acrylic and glass implanted with tungsten and lead for X-ray shielding purposes. These results were also compared with our previous work done on ion-implanted epoxy (Noor Azman et al., 2012).

## 2. Materials and methods

The works of ion-implantation and the ion beam analysis by Rutherford backscattering spectroscopy (RBS) was conducted at Australian Nuclear Science and Technology Organization. As a continuation of our study to improve the X-ray shielding materials, we used here as base materials a commercial acrylic and a commercial glass. Both these materials were implanted with tungsten and lead. For reasons of comparing all different materials, we used the same nominal doses that were used in our previous work on ion-implanted epoxy, which for tungsten (W) was ( $7 \times 10^{14}$  ions/cm<sup>2</sup>) and for lead (Pb) was between ( $7 \times 10^{14}$  ions/cm<sup>2</sup>) and ( $1.4 \times 10^{15}$  ions/cm<sup>2</sup>) in order to prevent possible melting and/or decomposition of the polymer sample matrix during implantation. The ions were produced by a metal evaporation and a direct extraction ion source. The charge distribution of positive ions of W and Pb as measured previously by RBS are:  $W^{+1}=1\%$ ,  $W^{+2}=16\%$ ,  $W^{+3}=58\%$ ,  $W^{+4}=25\%$ , and  $Pb^{+1}=35\%$ ,  $Pb^{+2}=64\%$ ,  $Pb^{+3}=1\%$  which are nearly the same as the theoretical prediction by the Debye–Huckel approximation of non-ideal plasma (Anders, 1997). The RBS measured values of the charge distribution provided an average charge of  $W^{+3.07}$  and  $Pb^{+1.66}$ . With these values and the nominal acceleration voltage of 40 kV used in this study, an average implantation energy of  $W=122.8$  keV and  $Pb=66.4$  keV was afforded to the ions prior to implantation. The beam size was close to 20 cm<sup>2</sup>, and the beam current used in this experiment was around 30  $\mu$ A. The ion fluence was monitored by converting the ion target current into pulses using a current-to-frequency convertor.

A beam of 1.8 MeV  $He^{+1}$  ions beam was used for RBS, and the information gathered was processed with SIMNRA code (Mayer, 1999) to obtain the calculation of the depth distribution of implanted species, which was then converted in concentration [at%]. These results were compared with the previous results on ion-implanted epoxy samples (Noor Azman et al., 2012).

For the work on the X-ray shielding capability of these implanted samples, a general diagnostic X-ray machine (Make: Shimadzu, Model: Circlex 0.6/1.2 P364DK-100SF), a DIADOS diagnostic detector and a DIADOS diagnostic dosimeter (PTW-Freiburg, Germany) were used. The DIADOS dosimeter is a universal dosimeter for measuring simultaneous dose and dose rate for radiography, fluoroscopy, mammography, dental X-ray and CT with a minimal dose sensitivity of 0.01 microRoentgen ( $\mu$ R). The incident X-ray dose ( $D_0$ ) was measured by placing the detector directly below the X-ray tube at a distance of 100 cm. The exit dose ( $D$ ) was measured by placing the sample on the detector. The X-ray beam was well collimated to the size of the sample and the exposure was set at 10 mAs to receive significant readings for this type of detector. The range of X-ray tube voltage (40–100 kV) was selected for this investigation since this range is the normal range of X-ray tube voltage used for the general diagnostic imaging purposes. The linear attenuation coefficient,  $\mu$  (unit: cm<sup>-1</sup>) for each sample was determined from Eq. (1) where  $x$  is the thickness of the sample.

$$\mu = \frac{\ln(D_0/D)}{x} \quad (1)$$

## 3. Results and discussion

The list of samples implanted with different ions is shown in Table 1. Fig. 1 shows the RBS results plotted as the yield versus channel number for acrylic and glass samples (B1–C3) implanted with W and Pb.

The RBS composition of acrylic and glass was used to calculate the range of implanted ions, using Monte Carlo simulation (SRIM 2010). The range of 122.8 keV W in acrylic is 84 nm and in glass is

**Table 1**

List of polymer composites and glass prepared with different implanted ions and their concentrations. For comparison reasons, we included previous results on the epoxy.

Sample ID	Matrix	Nominal dose [ions/cm <sup>2</sup> ]	Implanted Ion	RBS ion concentration [at%]
A1	Epoxy	$7.0 \times 10^{14}$	W	0.055
A2		$7.0 \times 10^{14}$	Pb	0.250
A3		$1.4 \times 10^{15}$	Pb	0.390
B1	Acrylic	$7.0 \times 10^{14}$	W	0.050
B2		$7.0 \times 10^{14}$	Pb	0.200
B3	Glass	$1.4 \times 10^{15}$	Pb	0.430
C1		$7.0 \times 10^{14}$	W	0.100
C2		$7.0 \times 10^{14}$	Pb	0.290
C3		$1.4 \times 10^{15}$	Pb	0.850

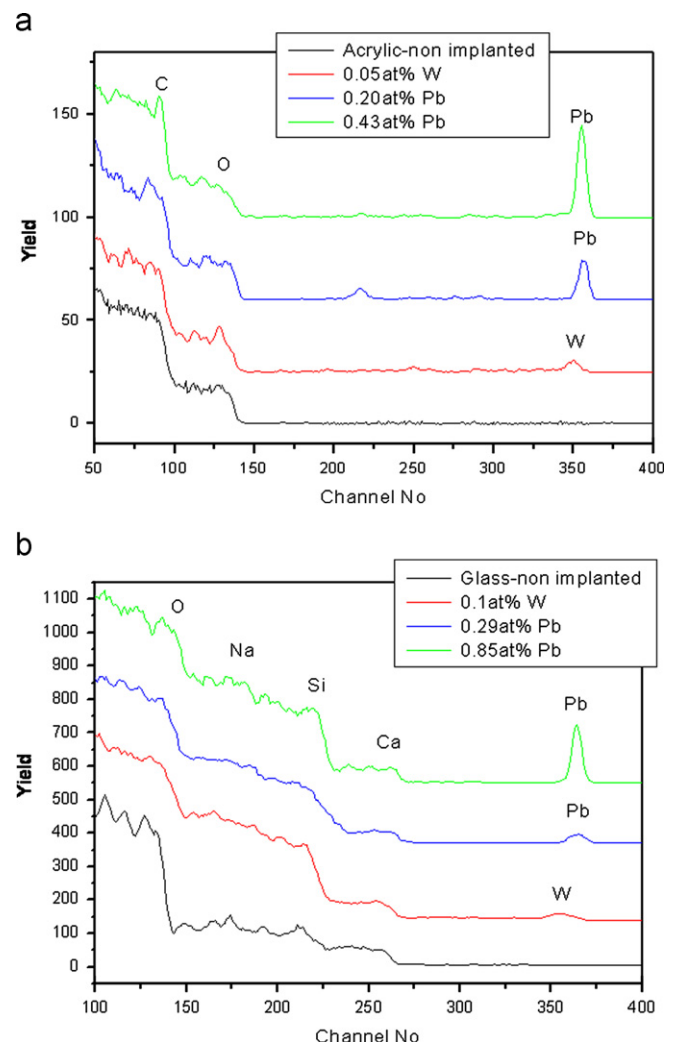


**Fig. 1.** RBS result for (a) acrylic implanted samples B1 (W), B2 and B3 (Pb); and (b) glass implanted samples C1 (W), C2 and C3 (Pb).

48 nm, and the range of 66.4 keV Pb in acrylic is 56 nm and in glass is 32 nm. These values are similar with the depth distribution calculated from RBS results and shown in Fig. 2, where for comparison reasons we also show the results of depth distribution of W and Pb in epoxy.

The results confirmed that the range of implanted ions is inversely proportional with the atomic number ( $Z$ ) of implanted ion (Pb=82, W=74) and with the density of the matrix. In addition, RBS shows specific variations in range and concentration of implanted ions, which are the result of specific sample matrix inhomogeneity. For example (Fig. 2), for W-implanted acrylic (B1), a maximum W concentration of 0.05 at% has been implanted down to a depth of about 1000 mono layers (ML) and then it drops to about 0.025 at% for the next 200 ML. For W-implanted glass (C1), a maximum W concentration of 0.1 at% has been implanted down to a depth of about 1000 ML, and as the density of glass is higher than the density of acrylic, one would expect the W implantation depth to be smaller than the W implantation depth in acrylic, but this is not the case due to local inhomogeneities. Even for the same sample matrix (acrylic), the same ion may have a different depth profile, and this again, is attributed to the differences in the local density of the acrylic itself. Similar depth profile RBS results were also obtained for composite samples of glass as a matrix base and also our previously epoxy samples (Noor Azman et al., 2012).

In Table 1, the differences between the measured RBS concentration of W and Pb ion at the same nominal implantation dose are explained by two factors: the different sputtering properties of the two ions, and the uncertainty in the dose measurement between different implantation runs. The glass is a denser ( $2.45 \text{ g/cm}^3$ ) matrix when compared to the acrylic or epoxy and contains heavier elements (Si, Na) hence it has a higher stopping power to slow down the ions as they travel within it. Further, a denser material has a lower projected range/depth profile (because ions have a greater chance of colliding with the atoms within the material especially near the surface). In contrast, epoxy and acrylic have nearly the same density (average  $1.15 \text{ g/cm}^3$ ) and hence they do not show significant differences in the RBS concentration between them. These statements are supported by the results in Fig. 2 since Pb-implanted glass (C3) has a shorter depth profile as compared to Pb-implanted epoxy (A3) and Pb-implanted acrylic (B3) of the same nominal dose of  $1.4 \times 10^{15} \text{ ions/cm}^2$ .

Besides, there is a huge difference in ion concentration between sample A3 or B3 with C3 when we double the nominal dose ( $1.4 \times 10^{15} \text{ ions/cm}^2$ ) as shown in Table 1. After the ions entering a matrix, the energy that an ion loses is converted to heat when slowing down within the material as the atoms dissipate

the kinetic energy in a series of collisions. Moreover, the melting point of acrylic or epoxy is  $\sim 160^\circ\text{C}$  while for the glass is  $> 1000^\circ\text{C}$ . So there is a high possibility of acrylic being altered (Fig. 3) by the energetic ions (with average velocity around  $2.0 \times 10^5 \text{ m/s}$ ) when they bombard the surface and cause bond breaking along the ion tracks, some of the matrix atoms (H, O) could be lost and escape by diffusion. These altered regions of the polymer may play an additional role in absorbing the X-ray, but this is yet to be tested in a future experiment.

Fig. 4 shows the linear attenuation coefficient,  $\mu$  as a function of X-ray tube voltage for all samples listed in Table 1, and for non-implanted samples of each material used for ion implantation. The result of  $\mu$  for W-implanted acrylic and glass with the nominal dose of  $7.0 \times 10^{14} \text{ ions/cm}^2$  is nearly the same with the result of  $\mu$  for non-implanted material, at each X-ray tube voltage. Meanwhile, with the decreasing of  $\mu$  with the increasing of X-ray tube voltage we noticed that  $\mu$  is also increasing with the atomic number of implanted element. For the same X-ray tube voltage, the heavier the implanted ion or in other words the higher the atomic number of implanted ion, the higher is the value of  $\mu$  and can be differentiated from the  $\mu$  for pure matrix composite especially at lower X-ray tube voltage (40–70 kV). This showed that the attenuation of the primary X-ray beam by the absorbing material is highly dependent on the atomic number of the absorbing material itself. Notice that the

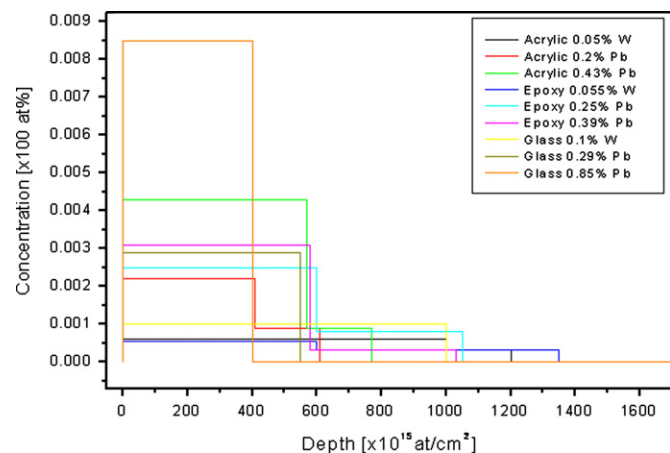


Fig. 2. RBS depth profile of implanted elements, for samples listed in Table 1. For comparison reasons we included the previous results on epoxy.

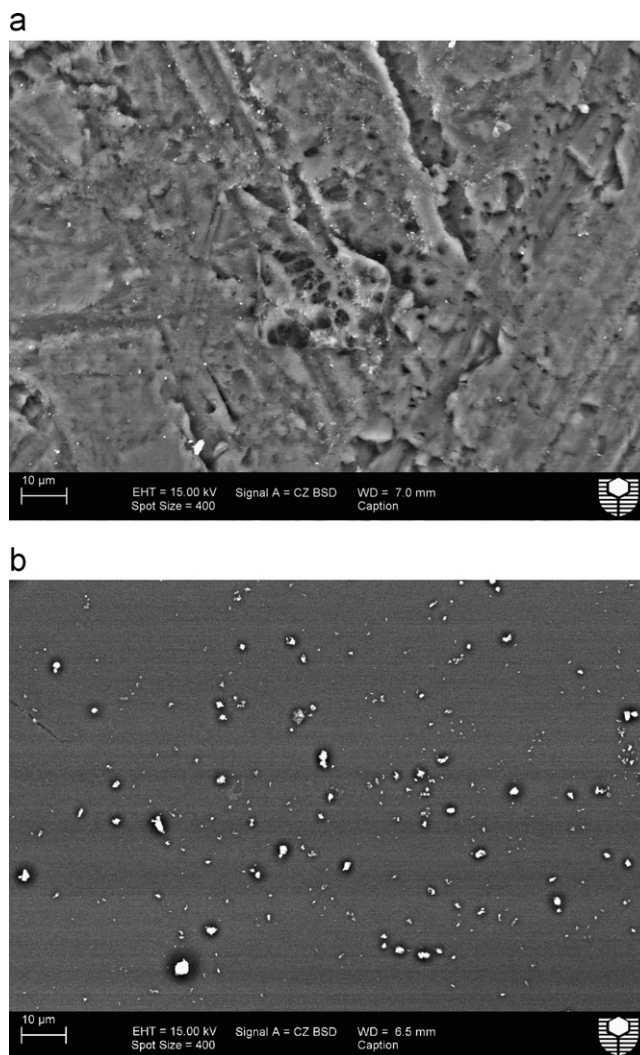


Fig. 3. SEM image of the surface of a) acrylic implanted with Pb (sample B3) showing the region being melted during the higher nominal dose of implantation; and b) glass implanted with Pb (sample C3).

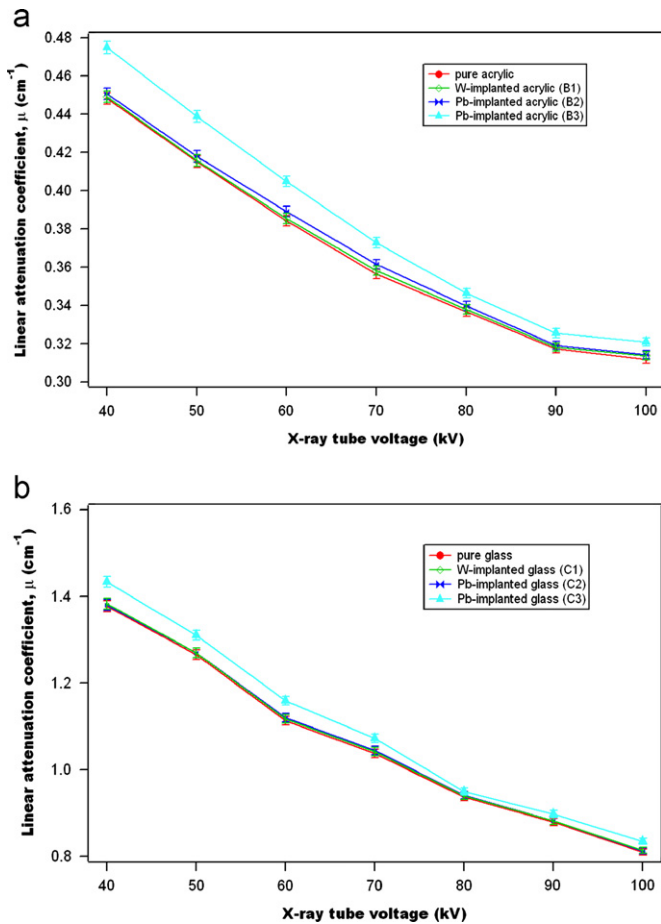


Fig. 4. Comparison of  $\mu$  versus X-ray tube voltage for (a) pure acrylic and acrylic implanted samples B1 (W), B2 and B3(Pb); and (b) pure glass and glass implanted samples C1 (W), C2 and C3 (Pb).

atoms of higher atomic number absorbing material present larger targets for the radiation to strike and hence the chances of interactions via the photoelectric interaction is relatively high. Hence, the attenuation should therefore be relatively large. Meanwhile, in the case of lower atomic number absorbing material however the individual atoms are smaller and hence the chances of interactions are reduced. In other words the radiation has a greater probability of being transmitted through the absorbing material and the attenuation is consequently lower than in the high atomic number case. The photoelectric interaction usually dominates in the lower X-ray energy range and also for the high atomic number of absorbing material (implanted ions). The probability for the photoelectric interaction to occur is dependent on  $Z^3/E^3$  where  $Z$  is the atomic number of the absorbing material, and  $E$  is the photon (X-ray/gamma-ray) energy (Sprawls, 1993). Additionally, the ion-implanted glass shows the highest attenuation compared to acrylic/epoxy since it is denser and has the highest RBS ion concentration of the same ion (Fig. 5) because more primary X-ray beam being attenuated by a denser absorbing material than a lower density absorbing material since the chances of an interaction between the radiation and the atoms of the absorbing material are relatively higher. In most cases, high density absorbing materials are more effective than low density alternatives for blocking or reducing the intensity of radiation. However, low density absorbing materials can compensate for the disparity with increased thickness, which is as significant as density in shielding applications.

From the above analyses, glass is still the best candidate for implanting with high RBS ion concentration and thus able to

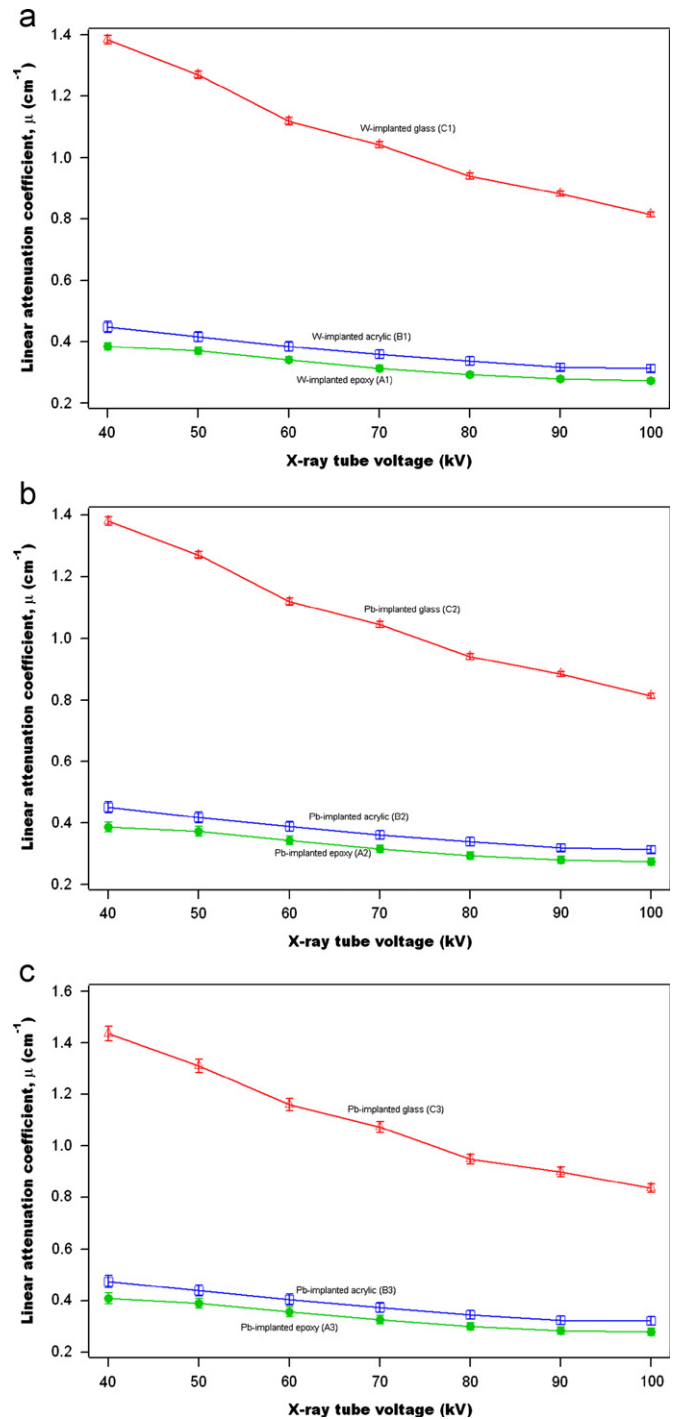


Fig. 5. Comparison of  $\mu$  versus X-ray tube voltage for (a) W-implanted epoxy (A1), acrylic (B1) and glass (C1); (b) Pb-implanted epoxy (A2), acrylic (B2) and glass (C2); and (c) Pb-implanted epoxy (A3), acrylic (B3) and glass (C3).

attenuate more X-rays as compared to pure acrylic/epoxy but it is fragile and easy to break; thus we need to handle it carefully for using as X-ray shielding. In contrast, even though acrylic is inferior in terms of density, melting point and seems not an ideal applicant but an implanted acrylic can still be chosen as a candidate for X-ray shielding because it is tougher and lighter as compared to glass but prolonged time is needed when implanted it with a high nominal dose to prevent it to melt during the implantation process. Besides, it also can provide similar X-ray attenuation like glass with increased thickness, which is as significant as density in shielding applications.

#### 4. Conclusions

Ion-implantation has been successfully used to modify the near-surface of acrylic and glass with W and Pb ions to improve X-ray attenuation for X-ray shielding for diagnostic radiology purposes. The X-ray attenuation is higher for the composite with the denser sample matrix and the composite having the higher RBS ion concentration. However, the amount of implanted doses will need to be significantly increased so that this approach can be feasible for designing new shielding materials for the X-ray technologists. Even though glass provided the best results for both RBS ion concentration and X-ray attenuation, its usage as X-ray shielding needs extra care since it is easy to break. In contrast, implanted acrylic can be a good candidate for X-ray shielding but much time is needed when implanted acrylic with a very high nominal dose since it has a low melting point and by increasing its thickness.

#### Acknowledgements

The work on ion-implantation and ion-beam analysis was conducted at the Australian Nuclear Science and Technology Organization with financial support from AINSE (AINGRA 11-135).

#### References

- Anders, A., 1997. Ion charge state distributions of vacuum arc plasmas: The origin of species. *Phys. Rev. E* 55, 969–981.
- Chanthima, N., Kaekwkhao, J., Kedkaew, C., Chewpraditkul, W., Pokaipisit, A., Limsuwan, P., 2011. Study on interaction of Bi<sub>2</sub>O<sub>3</sub>, PbO and BaO in silicate glass system at 662 keV for development of gamma-rays shielding materials. *Prog. Nucl. Sci. Technol.* 1, 106–109.
- Chen, J.S., Lau, S.P., Sun, Z., Tay, B.K., Yu, G.Q., Zhu, F.Y., Zhu, D.Z., Xu, H.J., 2001. Structural and mechanical properties of nitrogen ion implanted ultra high molecular weight polyethylene. *Surf. Coat. Technol.* 138, 33–38.
- Dworecki, K., Drabik, M., Hasegawa, T., Wasik, S., 2004. Modification of polymer membranes by ion implantation. *Nucl. Instrum. Methods Phys. Res., Sect. B* 225, 483–488.
- Evans, P.J., Hyvarinen, J., Samandi, M., 1995. Surface modification of austenitic stainless steel by titanium ion implantation. *Surf. Coat. Technol.* 71, 151–158.
- Hubler, G.K., 1981. Use of ion beam analysis in metal modification by means of ion implantation. *Nucl. Instrum. Methods Phys. Res.* 191, 101–113.
- Kozlov, E.V., Ryabchikov, A.I., Sharkeev, Y.P., Stepanov, I.B., Fortuna, S.V., Sivin, D.O., Kurzina, I.A., Prokopova, T.S., Mel'nik, I.A., 2002. Formation of intermetallic layers at high intensity ion implantation. *Surf. Coat. Technol.* 158–159, 343–348.
- Lee, E.H., Rao, G.R., Lewis, M.B., Mansur, L., K., 1993. Ion beam application for improved polymer surface properties. *Nucl. Instrum. Methods Phys. Res., Sect. B* 74, 326–330.
- Lopatin, C.M., Alford, T.L., Pizziconi, V.B., Kuan, M., Laursen, T., 1998. Ion-beam densification of hydroxyapatite thin films. *Nucl. Instrum. Methods Phys. Res., Sect. B* 145, 522–531.
- Mayer, M., 1999. Proceedings of the 15th International Conference on the Application of Accelerators in Research and Industry, J. L. Duggan and I.L. Morgan (Eds.), American Institute of Physics Conference Proceedings 475, 541.
- Noor Azman, N.Z., Siddiqui, S.A., Ionescu, M., Low, I.M., 2012. Synthesis and characterisation of ion-implanted epoxy composites for X-ray shielding. *Nucl. Instrum. Methods Phys. Res., Sect. B* 287, 120–123.
- Rodríguez, R.J., Medrano, A., García, J.A., Fuentes, G.G., Martínez, R., Puertolas, J.A., 2007. Improvement of surface mechanical properties of polymers by helium ion implantation. *Surf. Coat. Technol.* 201, 8146–8149.
- Soares, M.R.F., Alegaonkar, P., Behar, M., Fink, D., Müller, M., 2004. 6Li<sup>+</sup> ion implantation into polystyrene. *Nucl. Instrum. Methods Phys. Res., Sect. B* 218, 300–307.
- Sprawls, P., 1993. *The Physical Principles of Medical Imaging*, second ed. Aspen Publishers, Gaithersburg, Md.
- Stepanov, A.L., Khaibullin, R.I., Can, N., Ganeev, R.A., Ryasnyansky, A.I., Buchal, C., Uysal, S., 2004. Application of ion implantation for synthesis of copper nanoparticles in a zinc oxide matrix for obtaining new nonlinear optical materials. *Tech. Phys. Lett.* 30, 846–849.
- Wu, Y., Zhang, T., Zhang, H., Zhang, X., Deng, Z., Zhou, G., 2000. Electrical properties of polymer modified by metal ion implantation. *Nucl. Instrum. Methods Phys. Res., Sect. B* 169, 89–93.
- Yuguang, W., Tonghe, Z., Huixing, Z., Xiaoji, Z., Zhiwei, D., 2000. Polymer modification by MEVVA source deposited and ion implantation. *Surf. Coat. Technol.* 131, 520–524.

## 6. CHARACTERISTICS OF X-RAY ATTENUATION IN ELECTROSPUN BISMUTH OXIDE/POLY-LACTIC ACID NANOFIBRE MATS

---

This chapter is the final episode of this thesis and presents a novel electrospinning method to fabricate the filler-nanofibre mats. It was appeared in the *Journal of Synchrotron Radiation*, volume 20, pages 741-748 in the year 2013.

Poly lactic acid (PLA) was used as the matrix for nanofibre mat synthesis due to the advantages of PLA for the electrospinning process. This work presents the performance of PLA mat together with different particle sizes for X-ray transmission. A better understanding was gained by the comparative study using a solution casting method to synthesize the same composites but in a thin film form.

### Key findings:

- The apparent density of the electrospun Bi<sub>2</sub>O<sub>3</sub>/PLA nanofibre mats underestimated the theoretical values.
- The density of the electrospun Bi<sub>2</sub>O<sub>3</sub>/PLA nanofibre mat increased with the filler loading, except for the electrospun Bi<sub>2</sub>O<sub>3</sub>/PLA nanofibre mat of 38 wt% Bi<sub>2</sub>O<sub>3</sub> loading; a sudden decrease in the density occurred.
- The porosity of both electrospun n- and m- Bi<sub>2</sub>O<sub>3</sub>/PLA nanofibre mats was >70%.
- The difference in linear attenuation coefficient between electrospun n- Bi<sub>2</sub>O<sub>3</sub>/PLA and m- Bi<sub>2</sub>O<sub>3</sub>/PLA nanofibre mats becomes higher as the Bi<sub>2</sub>O<sub>3</sub> loading increased at all the synchrotron energy ranges and mammography unit tube voltages.
- The average nanofibre diameter was increased by the increment of filler (Bi<sub>2</sub>O<sub>3</sub>) loadings within the PLA solution except for 38 wt% Bi<sub>2</sub>O<sub>3</sub> increment; there was a sudden decrease in average nanofibre diameter.

\*\*On page 84 line 3, the photon energy is 511 keV; not 611 keV.



## Characteristics of X-ray attenuation in electrospun bismuth oxide/poly(lactic acid) nanofibre mats

Nurul Z. Noor Azman, Salim A. Siddiqui, Hazim J. Haroosh, Hani M. M. Albetran, Bernt Johannessen, Yu Dong and It M. Low

*J. Synchrotron Rad.* (2013). **20**, 741–748

Copyright © International Union of Crystallography

Author(s) of this paper may load this reprint on their own web site or institutional repository provided that this cover page is retained. Reproduction of this article or its storage in electronic databases other than as specified above is not permitted without prior permission in writing from the IUCr.

For further information see <http://journals.iucr.org/services/authorrights.html>



Synchrotron radiation research is rapidly expanding with many new sources of radiation being created globally. Synchrotron radiation plays a leading role in pure science and in emerging technologies. The *Journal of Synchrotron Radiation* provides comprehensive coverage of the entire field of synchrotron radiation research including instrumentation, theory, computing and scientific applications in areas such as biology, nanoscience and materials science. Rapid publication ensures an up-to-date information resource for scientists and engineers in the field.

# Characteristics of X-ray attenuation in electrospun bismuth oxide/polylactic acid nanofibre mats

Nurul Z. Noor Azman,<sup>a,b</sup> Salim A. Siddiqui,<sup>a</sup> Hazim J. Haroosh,<sup>c</sup>  
Hani M. M. Albetran,<sup>a</sup> Bernt Johannessen,<sup>d</sup> Yu Dong<sup>e</sup> and It M. Low<sup>a\*</sup>

<sup>a</sup>Department of Imaging and Applied Physics, Curtin University, GPO Box U1987, Perth, WA 6845, Australia, <sup>b</sup>School of Physics, Universiti Sains Malaysia, Pulau Pinang 11800, Malaysia, <sup>c</sup>Department of Chemical Engineering, Curtin University, GPO Box U1987, Perth, WA 6845, Australia, <sup>d</sup>The Australian Synchrotron, Melbourne, VIC 3168, Australia, and <sup>e</sup>Department of Mechanical Engineering, Curtin University, GPO Box U1987, Perth, WA 6845, Australia.  
E-mail: j.low@curtin.edu.au

The characteristics of the X-ray attenuation in electrospun nano(n)- and micro(m)-Bi<sub>2</sub>O<sub>3</sub>/polylactic acid (PLA) nanofibre mats with different Bi<sub>2</sub>O<sub>3</sub> loadings were compared as a function of energy using mammography (*i.e.* tube voltages of 22–49 kV) and X-ray absorption spectroscopy (XAS) (7–20 keV). Results indicate that X-ray attenuation by electrospun n-Bi<sub>2</sub>O<sub>3</sub>/PLA nanofibre mats is distinctly higher than that of m-Bi<sub>2</sub>O<sub>3</sub>/PLA nanofibre mats at all energies investigated. In addition, with increasing filler loading (n-Bi<sub>2</sub>O<sub>3</sub> or m-Bi<sub>2</sub>O<sub>3</sub>), the porosity of the nanofibre mats decreased, thus increasing the X-ray attenuation, except for the sample containing 38 wt% Bi<sub>2</sub>O<sub>3</sub> (the highest loading in the present study). The latter showed higher porosity, with some beads formed, thus resulting in a sudden decrease in the X-ray attenuation.

**Keywords:** electrospun nano-Bi<sub>2</sub>O<sub>3</sub>/PLA nanofibre mat; electrospun micro-Bi<sub>2</sub>O<sub>3</sub>/PLA nanofibre mat; nano-Bi<sub>2</sub>O<sub>3</sub>/PLA thin films; micro-Bi<sub>2</sub>O<sub>3</sub>/PLA thin films; X-ray attenuation; porosity.

© 2013 International Union of Crystallography  
Printed in Singapore – all rights reserved

## 1. Introduction

Nanoparticles, *i.e.* nanometre-sized particles, have attracted much attention amongst researchers in different fields of physics, chemistry, material science, medicine and biology because of their unique and often superior electronic, magnetic, optical, mechanical, physical and chemical properties (Patra *et al.*, 2010; Huang & El-Sayed, 2010; Granmayeh Rad *et al.*, 2011; Sahare *et al.*, 2007; Lines, 2008; Haiwen *et al.*, 2006; Popov, 2009). For example, in the medical field, nanoparticles have been widely used in diagnosis, tissue engineering and also as drug delivery devices (Storrie & Mooney, 2006). Gold nanoparticles are one of the most useful nanoparticles in industry and medicine (Granmayeh Rad *et al.*, 2011). For instance, in the medical field, gold nanoparticles show significant improvement in the treatment of cancers by enhancing the sensitivity of radiation from a radiotherapy unit with minimal adverse effects on surrounding normal tissues (Patra *et al.*, 2010; Huang & El-Sayed, 2010).

Additionally, this size effect has also become one of the virtues in designing materials for shielding of ionizing radiations. Some X-ray technologists believe that this effect will improve the X-ray attenuation ability of composites since nano-sized fillers can be dispersed more uniformly within a matrix with fewer agglomerations compared with micro-sized

fillers and consequently affect the density and composition that modify the total attenuation coefficient of the composite (Botelho *et al.*, 2011; El Haber & Froyer, 2008). The latest work by Buyuk *et al.* (2012) proved that decreasing the titanium diboride particle size in titanium diboride reinforced boron-carbide–silicon-carbide composites results in a higher linear attenuation coefficient for the energy of 0.662 MeV emitted by a Cs-137 gamma source (Buyuk *et al.*, 2012). In a complementary finding, a recent study by Botelho *et al.* (2011) showed that nanostructured copper oxide (CuO) is more effective in attenuating lower X-ray beam energies (tube voltages of 26 and 30 kV), whilst no significant variation in the X-ray attenuation at higher energies (tube voltages of 60 and 102 kV) were observed. Künzel & Okuno (2012) also provided similar results, showing that the X-ray beam attenuation is greater for a nanostructured CuO compound compared with its microstructured counterpart for low energies (tube voltages of 25 and 30 kV) for a wide range of CuO concentrations incorporated into polymeric resins.

Electrospinning is a well established polymer processing technique which has proven to be a flexible and effective method for fabricating multilayers of microscale (>1 µm) to nanoscale (<1000 nm) fibres from different types of polymers used in a wide range of applications, such as in drug delivery, tissue engineering and protective clothing (Faccini *et al.*, 2012;

Prabhakaran *et al.*, 2008; Sill & von Recum, 2008; Russo & Lamberti, 2011; Huang *et al.*, 2012; Haroosh *et al.*, 2012; Yiin-Kuen & Li-Chih, 2013; Rajeswari *et al.*, 2012; Hu *et al.*, 2010; Yu *et al.*, 2009). This technique provides many benefits to industry with perhaps the most important being its versatility and simplicity, which means it is a very time efficient way to fabricate a variety of continuous nanofibrous structures. It is advantageous to use nanofibre webs in a layered structure together with a suited substrate material such that the final product offers sufficient strength and durability. Besides, the nanofibre layers should be flexible and also have a good adherence to the substrates without easily being broken or delaminated (Faccini *et al.*, 2012; Lee & Obendorf, 2007; Brettmann *et al.*, 2012). Moreover, some researchers have shown that electrospinning can improve the dispersion of nanoparticles within the polymer matrix thereby improving the properties of nanocomposites (Demir *et al.*, 2004; Shanshan *et al.*, 2010).

Poly(lactic acid) (PLA) fibres are polymeric in nature and provide the inherent performance of fibres together with the positive environmental advantages of being renewable and recyclable. In addition, production of PLA emits less CO<sub>2</sub> compared with other petroleum-based fibres. Disposal of PLA not only fits within the existing disposal systems but also includes the additional option of composting (Farrington *et al.*, 2005). Meanwhile, Bi<sub>2</sub>O<sub>3</sub> is non-hazardous and is also a relatively environmentally friendly compound that is used as a substitute for toxic lead oxide which is widely used in the production of lead glass. For example, Bi<sub>2</sub>O<sub>3</sub>-based glasses have gained fascination among glass researchers because of their non-linear optical properties which are important for the development of optical information processing technology (An *et al.*, 2006). Thus, they have played an important role in the replacement of lead glass by radiation shielding glass (Chanthima *et al.*, 2011).

In the present study, given the simplicity of the electrospinning technique, it is investigated whether electrospinning can also be used to produce nanofibre mats for the efficient shielding of ionizing radiation. In a recent work on WO<sub>3</sub>-filled epoxy composites (Noor Azman *et al.*, 2013), we investigated the X-ray attenuation effect of nano- and micro-sized fillers in epoxy composites over an X-ray tube voltage range of 22–127 kV. Our results showed that nano-sized WO<sub>3</sub> was more effective than its micro-sized counterpart in attenuation of low X-ray tube voltages (22–35 kV). This is explained by the domination of photoelectric interactions at low photon energy and also the number of W particles per gram in the nano-sized WO<sub>3</sub>-epoxy composite being greater than that of the micro-sized WO<sub>3</sub>-epoxy composite. The size effect was not apparent in the higher X-ray tube voltage range of 40–120 kV. Hence, the objective of our present study is to synthesize new radiation shielding materials using the electrospinning technique with the preparation of well dispersed Bi<sub>2</sub>O<sub>3</sub> of different particle sizes in PLA fibre mats. The effectiveness of electrospun nano-Bi<sub>2</sub>O<sub>3</sub>/PLA nanofibre mats in radiation protection during diagnostic imaging using low X-ray energies is also reported, with the ultimate goal of offering a new approach to

**Table 1**

Prepared electrospun Bi<sub>2</sub>O<sub>3</sub>/PLA nanofibre mats with different weight fractions (wt%) of filler (Bi<sub>2</sub>O<sub>3</sub>) and PLA.

Filler (Bi <sub>2</sub> O <sub>3</sub> ) (wt%)	PLA (wt%)
24	76
28	72
34	66
38	62

radiation protection, based on nanotechnology and the electrospinning technique to produce composites that are environmentally friendly.

## 2. Experimental procedure

### 2.1. Materials

Bismuth (III) oxide (Bi<sub>2</sub>O<sub>3</sub>) particles of sizes 90–210 nm and 10 µm were used as a filler for synthesizing electrospun Bi<sub>2</sub>O<sub>3</sub>/poly(lactic acid) (PLA) nanofibre mats and Bi<sub>2</sub>O<sub>3</sub>/PLA thin films. Bi<sub>2</sub>O<sub>3</sub>, chloroform and methanol were obtained from Sigma-Aldrich. Meanwhile, PLA (3051D) pellets, with molecular weight  $M_n = 93500 \text{ g mol}^{-1}$  and glass transition temperature  $T_g = 338.50 \text{ K}$  were supplied by NatureWorks USA.

### 2.2. Sample preparation

Electrospinning was carried out using 9% wt/v PLA solution by mixing with 8 ml of chloroform and 2 ml of methanol as solvents. The micro(m)-Bi<sub>2</sub>O<sub>3</sub> and nano(n)-Bi<sub>2</sub>O<sub>3</sub> suspension was added at 24–38 wt% to the polymer solution and was homogenized for 45 min under ultrasonication. For the electrospinning process, the solutions were transferred to a 10 ml syringe pump with 25-G needles. The flow rate of the polymer solution was 1 ml h<sup>-1</sup>, and the applied positive voltage was ~19 kV. The distance between the needle tip and the target was set at 12 cm. The resulting nanofibre mats were collected on a flat aluminium foil over ~2 h to achieve an acceptable thickness for X-ray attenuation experiments. The nanofibre mats were removed from the aluminium foil and cut to a dimension of 2.0 cm × 1.5 cm or were folded together before cutting so that they had an acceptable thickness for a reliable X-ray attenuation experiment. Three sets of the same nanofibre mats were prepared. A list of prepared electrospun Bi<sub>2</sub>O<sub>3</sub>/PLA nanofibre mats with different Bi<sub>2</sub>O<sub>3</sub> weight percentages are shown in Table 1.

The solution casting method was performed to prepare Bi<sub>2</sub>O<sub>3</sub>/PLA thin films for verifying the X-ray attenuation results obtained for the electrospun Bi<sub>2</sub>O<sub>3</sub>/PLA fibre mats. In this method, PLA was mixed with chloroform without methanol (since methanol was only used in the electrospinning process to increase the conduction of the solution and will totally evaporate during the process) of the same amount as in the electrospinning process and was homogenized for 45 min under ultrasonication. Then, the solution was poured into a 5 cm-diameter beaker and left in a fume cupboard for 24 h to dry. Next, the thin film was removed from the beaker



and three sets of the same thin film were cut into 2.0 cm × 1.5 cm pieces for X-ray attenuation experiments. The list of prepared Bi<sub>2</sub>O<sub>3</sub>/PLA thin films with different weight percentages of Bi<sub>2</sub>O<sub>3</sub> are the same as those shown in Table 1.

### 2.3. Measurements of sample thickness and porosity

Since it is inherently difficult to produce all the electrospun fibre mats with a uniform thickness, which is an important factor in X-ray attenuation comparison, the nanofibre mat thickness for each sample was measured by determining the weight and surface area. The average thickness ( $t_{ave}$ ) of the mats was then determined from equation (1), where  $m$  is the mass,  $A$  is the surface area and  $\rho$  is the apparent density of the electrospun mats,

$$t_{ave} = m/A\rho. \quad (1)$$

The apparent density ( $\rho$ ) was accurately measured using the density bottle method (ASTM D854) and an average of three measurements were taken for each mat. The porosity of the mats was calculated using equation (2). A calibrated single-pan electrical balance and distilled water were used for this purpose,

$$\text{Porosity (\%)} = 1 - (\rho/\rho_{\text{theory}}), \quad (2)$$

where  $\rho_{\text{theory}}$  is the bulk density of the Bi<sub>2</sub>O<sub>3</sub>/PLA composite.

Meanwhile, for the thin films the average thickness  $t_{ave}$  was measured using a vernier caliper. The apparent density ( $\rho$ ) of the thin films was calculated using (1) with  $m$  and  $A$  being the film mass and surface area, respectively.

### 2.4. Measurement of X-ray attenuation

Two separate methods were used to characterize the X-ray attenuation of the samples. The first involved the use of the X-ray absorption spectroscopy beamline at the Australian Synchrotron. Experiments were carried out in the energy range 7–20 keV using a Si (311) monochromator, a beam size on the sample of about 0.25 mm × 0.25 mm and a photon flux of about 10<sup>9</sup> photons s<sup>-1</sup>. Transmission data were collected using ionization chambers before and after the sample. For each sample, 20 readings were recorded at each energy. To normalize the data, readings were also recorded for beam passing through the air.

The second method used a mammography unit (Siemens AG, model 2403951-4, GE Health Care) at Royal Perth Hospital, Western Australia. For the work with this mammography unit, the exposure was set at 10 mAs to obtain meaningful readings for the DIADOS diagnostic detector connected to the diagnostic dosimeter (PTW-Freiburg, Germany), and the X-ray tube voltage range 22–49 kV was selected. The dosimeter was a universal dosimeter for measuring simultaneous dose and dose rate for radiography, fluoroscopy, mammography, dental X-ray and computed tomography with a sensitivity of 0.01 microRoentgen ( $\mu\text{R}$ ). Three different anode/filter combinations (Table 2) were used for filtering the X-ray beam produced by the chosen X-ray tube voltages used for the mammography machine, since the

**Table 2**

Anode/filter combination operated by the mammography machine.

X-ray tube voltage (kV)	Anode/filter combination
22	Mo/Mo†
25	
30	
35	Mo/Rh‡
40	
45	Rh/Rh§
49	

† Molybdenum anode/molybdenum filter. ‡ Molybdenum anode/rhodium filter. § Rhodium anode/rhodium filter.

combination was controlled by the machine itself. The X-ray beams generated by these anode/filter combinations were mainly of the characteristic X-ray energies of molybdenum (17.5 keV and 19.6 keV) or rhodium (20.2 keV and 22.7 keV). For each sample the measurements were performed three times. The detector was placed 86 cm below the X-ray tube since this is the maximum distance that can be adjusted for the mammography unit, and the X-ray beam was collimated to the size of the sample to minimize the scattered X-rays produced by the sample.

The incident intensity  $I_0$  and transmitted intensity  $I$  (normalized to the case without a sample) were measured; the X-ray transmission ( $T = I/I_0$ ) is related to the linear attenuation coefficient ( $\mu$ ) through equation (3),

$$T = (I/I_0) = \exp(-\mu t_{ave}). \quad (3)$$

Hence, equation (3) can be re-written as

$$\mu = \frac{-\ln T}{t_{ave}}, \quad (4)$$

where the X-ray transmission  $T$  is determined by  $\mu$  which is the total linear attenuation coefficient of a PLA nanofibre mat or PLA thin film with Bi<sub>2</sub>O<sub>3</sub> particles and pores expressed as  $(\mu_{\text{mat or film}})x + (\mu_{\text{Bi}_2\text{O}_3})y + (\mu_{\text{pores}})z$ , where  $x + y + z = 1$  is the weighted fraction contributions of the individual components.

A graph of the X-ray linear attenuation coefficient ( $\mu$ ) as a function of X-ray energy was plotted for each sample.

### 2.5. Scanning electron microscopy (SEM)

The depth profile of the samples was examined using a Zeiss Evo 40XVP scanning electron microscope at a voltage of 15 kV with the working distance between 8.0 and 9.0 mm. Both secondary electron and backscattered electron techniques coupled with an energy-dispersive X-ray spectroscopy (EDS) probe were performed after standard coating with platinum to minimize charging in order to show the difference between the images due to the different atomic number of PLA and Bi. A pure electrospun PLA nanofibre mat was also examined as a benchmark.

**Table 3**

Density of electrospun Bi<sub>2</sub>O<sub>3</sub>/PLA nanofibre mats and Bi<sub>2</sub>O<sub>3</sub>/PLA thin films.

Filler (Bi <sub>2</sub> O <sub>3</sub> ) weight fraction (wt%)	Density (g cm <sup>-3</sup> )				
	Electrospun nanofibre mat			Thin films	
	Theoretical	Nano	Micro	Nano	Micro
24	1.56	0.27	0.25	1.54	1.50
28	1.63	0.40	0.37	1.59	1.52
34	1.75	0.49	0.45	1.69	1.64
38	1.84	0.30	0.24	1.77	1.72

### 3. Results and discussion

#### 3.1. Thickness and porosity measurement

The average thicknesses  $t_{ave}$  for all the electrospun Bi<sub>2</sub>O<sub>3</sub>/PLA nanofibre mats measured were in the range 0.006–0.014 cm while for Bi<sub>2</sub>O<sub>3</sub>/PLA thin films they were in the range 0.04–0.08 cm. All of these  $t_{ave}$  measurements will be used in equation (4) to calculate the value of  $\mu$  for each sample.

From Table 3, the apparent density  $\rho$  of each thin film (the last two columns in the table) of the same filler (Bi<sub>2</sub>O<sub>3</sub>) category increased by the increment of filler content in the PLA solution. The density found in the thin films illustrates that m-Bi<sub>2</sub>O<sub>3</sub>/PLA thin films have a lower density compared with n-Bi<sub>2</sub>O<sub>3</sub>/PLA thin films though neither are significantly different from their theoretical value. However, the apparent density of the electrospun Bi<sub>2</sub>O<sub>3</sub>/PLA nanofibre mats underestimated the theoretical values due to the nanofibres being highly porous, randomly oriented and aligned. As can be seen, the density of the electrospun Bi<sub>2</sub>O<sub>3</sub>/PLA nanofibre mat increased with the filler loading except for the electrospun Bi<sub>2</sub>O<sub>3</sub>/PLA nanofibre mat of 38 wt% Bi<sub>2</sub>O<sub>3</sub> loading; there is a sudden decrease in the density due to the higher porosity found (Table 4) and also the formation of PLA beads.

Porosity is an important parameter when preparing the absorbing material for X-ray attenuation experiments. As can be seen from Table 4, the porosity of both electrospun n- and m-Bi<sub>2</sub>O<sub>3</sub>/PLA nanofibre mats was >70%. This is likely to be caused by the entangled structure of the randomly oriented nanofibres, indicating that they were highly porous and thus not ideally suited for X-ray attenuation, especially with the filler  $\geq$  38 wt%. Further increases to filler loading, beyond 38 wt%, was not performed owing to the decreased density and increased porosity, which is unlikely to give any advantages for future X-ray transmission experiments. The porosity found from the control electrospun PLA nanofibre mat was 88.8%. Thus, if a further investigation was performed for greater filler loadings the electrospun Bi<sub>2</sub>O<sub>3</sub>/PLA nanofibre mat would probably have similar or even higher porosity than this controlled sample.

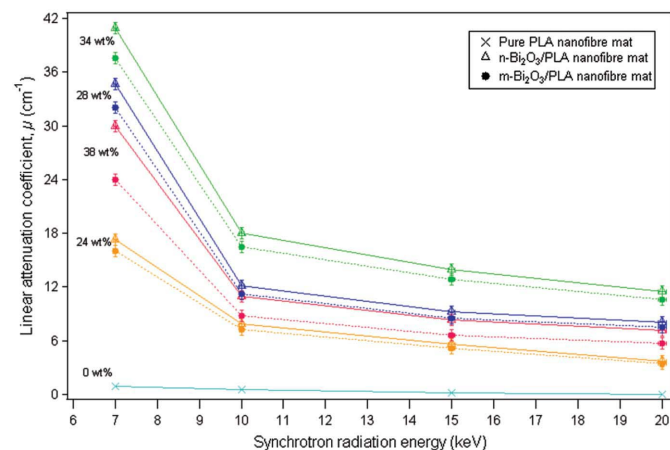
#### 3.2. X-ray attenuations

Fig. 1 shows the XAS linear attenuation coefficient ( $\mu$ ) results of electrospun nanofibre mats for an X-ray energy of 7–20 keV for 0–38 wt% Bi<sub>2</sub>O<sub>3</sub> loading. It clearly shows a big

**Table 4**

Porosity of electrospun Bi<sub>2</sub>O<sub>3</sub>/PLA nanofibre mats.

Filler (Bi <sub>2</sub> O <sub>3</sub> ) weight fraction (wt%)	Porosity (%)	
	Nano-Bi <sub>2</sub> O <sub>3</sub> /PLA nanofibre mat	Micro-Bi <sub>2</sub> O <sub>3</sub> /PLA nanofibre mat
0	88.8	88.8
24	83.0	84.0
28	75.4	77.0
34	72.1	74.3
38	83.6	87.0



**Figure 1**

Linear attenuation coefficient as a function of synchrotron radiation energy operated by XAS (7–20 keV) for all Bi<sub>2</sub>O<sub>3</sub> loading (0–38 wt%) of the electrospun n-Bi<sub>2</sub>O<sub>3</sub>/PLA and m-Bi<sub>2</sub>O<sub>3</sub>/PLA nanofibre mats.

difference in  $\mu$  between electrospun n-Bi<sub>2</sub>O<sub>3</sub>/PLA nanofibre mats and electrospun m-Bi<sub>2</sub>O<sub>3</sub>/PLA nanofibre mats at the same filler loadings as the X-ray energy increased. Additionally, Fig. 2 also shows a distinct difference in  $\mu$  between electrospun n-Bi<sub>2</sub>O<sub>3</sub>/PLA nanofibre mats and electrospun m-Bi<sub>2</sub>O<sub>3</sub>/PLA nanofibre mats at the same filler loadings as the X-ray energy increased, which is related to the mammography X-ray effective energy operated at an X-ray tube voltage of 22–49 kV (Fig. 3). These effective energies were determined

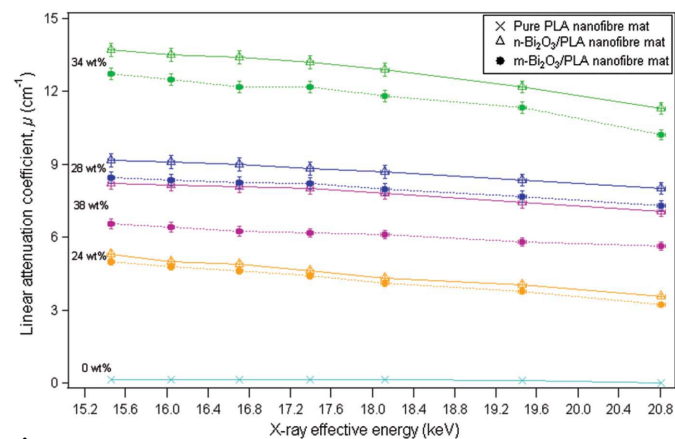


**Figure 2**

Linear attenuation coefficient as a function of effective energy operated by various X-ray tube voltages of the mammography unit (22–49 kV) for all Bi<sub>2</sub>O<sub>3</sub> loading (0–38 wt%) of the electrospun n-Bi<sub>2</sub>O<sub>3</sub>/PLA and m-Bi<sub>2</sub>O<sub>3</sub>/PLA nanofibre mats.

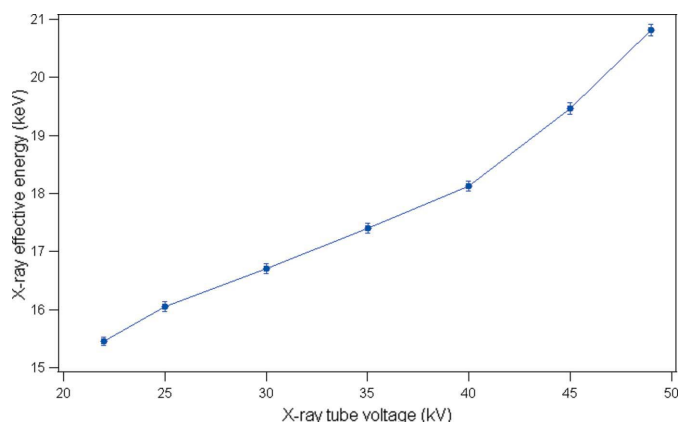


**Figure 3** Effective energy as a function of the X-ray tube voltages operated by the mammography unit determined from half-value layer measurements.

using half-value layer (HVL) experiments (Suk *et al.*, 2012) on the mammography unit. With kilovoltage X-rays, determination of the HVL of the X-ray beam can be used to characterize the effective energy by converting the measured HVL to the linear attenuation coefficient. The effective energy of a polyenergetic beam is equal to the energy of a monoenergetic X-ray beam that is attenuated at the same rate as the polyenergetic beam which can be determined from tabulated data (Berger *et al.*, 2010).

As can be seen from both Figs. 1 and 2,  $\mu$  increased with an increase of the filler loading within the PLA matrix for both electrospun n-Bi<sub>2</sub>O<sub>3</sub>/PLA and m-Bi<sub>2</sub>O<sub>3</sub>/PLA nanofibre mats, except for the 38 wt% Bi<sub>2</sub>O<sub>3</sub> loading where there is a sudden decrease in  $\mu$ . However, the difference in  $\mu$  between electrospun n-Bi<sub>2</sub>O<sub>3</sub>/PLA and m-Bi<sub>2</sub>O<sub>3</sub>/PLA nanofibre mats becomes higher as the Bi<sub>2</sub>O<sub>3</sub> loading increased. These findings support the density and porosity results discussed previously, including the 38 wt% of Bi<sub>2</sub>O<sub>3</sub>/PLA nanofibre mats which showed low density and high porosity, thus leading to decreased  $\mu$ . Meanwhile, a comparison of thin films between m-Bi<sub>2</sub>O<sub>3</sub>/PLA and n-Bi<sub>2</sub>O<sub>3</sub>/PLA does not totally support the results found from this study for the electrospun Bi<sub>2</sub>O<sub>3</sub>/PLA nanofibre mats. From Fig. 4, as the X-ray effective energy increased to >17.4 keV (*i.e.* X-ray tube voltages > 35 kV), for the same wt% of Bi<sub>2</sub>O<sub>3</sub> filler within this thin film sample,  $\mu$  for m-Bi<sub>2</sub>O<sub>3</sub>/PLA thin film and  $\mu$  by n-Bi<sub>2</sub>O<sub>3</sub>/PLA thin film become comparable. They only show significant differences in  $\mu$  for lower X-ray effective energy, <17.4 keV (*i.e.* X-ray tube voltage 22–35 kV), operated from the mammography unit.

As in our previous study for the comparison of different sizes of WO<sub>3</sub> particles–epoxy composites (Noor Azman *et al.*, 2013), we also obtain similar results for electrospun Bi<sub>2</sub>O<sub>3</sub>/PLA nanofibre mats which showed that the attenuation by electrospun n-Bi<sub>2</sub>O<sub>3</sub>/PLA nanofibre mats is higher than the attenuation by electrospun m-Bi<sub>2</sub>O<sub>3</sub>/PLA nanofibre mats with the same filler loading in the low-energy regime (22–35 kV operated from the mammography unit). However, by increasing the X-ray tube voltage beyond 35 kV (*i.e.* X-ray effective energy > 17.4 keV), the attenuation by electrospun n-Bi<sub>2</sub>O<sub>3</sub>/PLA nanofibre mats is still higher than the attenua-

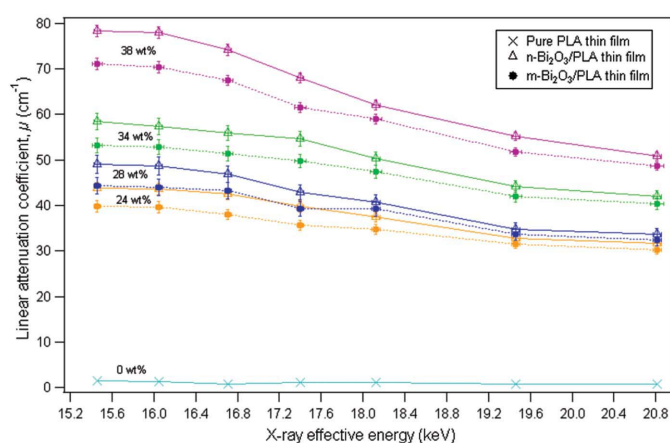


**Figure 4** Linear attenuation coefficient as a function of the effective energy operated by various X-ray tube voltages of the mammography unit (22–49 kV) for all Bi<sub>2</sub>O<sub>3</sub> loading (0–38 wt%) of the n-Bi<sub>2</sub>O<sub>3</sub>/PLA and m-Bi<sub>2</sub>O<sub>3</sub>/PLA thin films.

tion by electrospun m-Bi<sub>2</sub>O<sub>3</sub>/PLA nanofibre mats. In contrast, in our previous work, the differences in the attenuation by micro-sized WO<sub>3</sub>–epoxy composites and nano-sized WO<sub>3</sub>–epoxy composites become indistinguishable when the X-ray tube voltage was increased beyond 35 kV (Noor Azman *et al.*, 2013). Only Bi<sub>2</sub>O<sub>3</sub>/PLA thin film has a good agreement with our previous results for X-ray tube voltages greater than 35 kV, which shows the indistinguishability in attenuation between m-Bi<sub>2</sub>O<sub>3</sub>/PLA thin film and n-Bi<sub>2</sub>O<sub>3</sub>/PLA thin film.

Fig. 5 presents the value of  $\mu$  for electrospun n-Bi<sub>2</sub>O<sub>3</sub>/PLA nanofibre mats for all the X-ray beam energies generated by XAS and the mammography unit. The results found from XAS were correlated with those from the mammography unit since the mammography unit produced effective energies of 15–21 keV with the Mo and Rh anode/filter characteristic X-ray energies of 17.5–22.7 keV, while the X-ray energy used with XAS was ~7–20 keV.

In essence, the total X-ray attenuation by the absorbing material is determined by three energy-dissipative mechanisms, namely the photoelectric effect, Compton scattering and

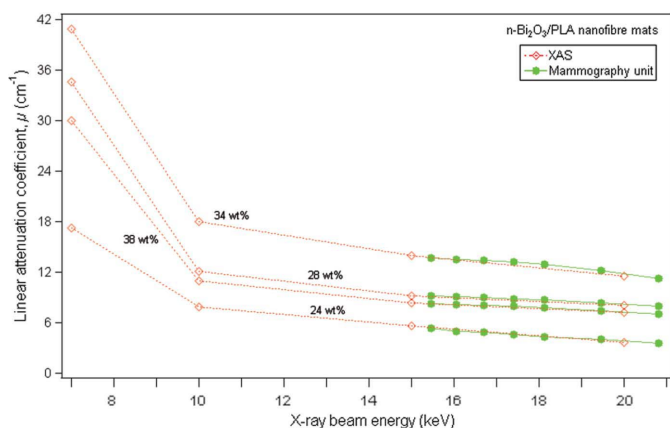


**Figure 5** Comparison of the linear attenuation coefficient for the electrospun n-Bi<sub>2</sub>O<sub>3</sub>/PLA nanofibre mats for all X-ray beam energies generated by XAS and the mammography unit.

pair production. Pair production was not considered in this study because this mechanism will only occur when the photon energy is beyond 611 keV. In the photoelectric absorption process, a photon undergoes an interaction with an absorber atom in which the photon completely disappears. In its place, an energetic photoelectron is ejected from one of the bound shells of the atom. The photoelectric process is the predominant mode of photon interaction at relatively low photon energies and high atomic number  $Z$ , *i.e.*  $(Z/E)^3$ . Meanwhile, Compton scattering takes place between the incident photon and one of the outer-shell electrons of an atom in the absorbing material. The probability of Compton scattering is almost independent of atomic number  $Z$  and X-ray energy  $E$ . It is most dominant as the photon energy increases due to a concomitant decrease in the photoelectric effect.

In addition, the number of Bi particles per gram in both n-Bi<sub>2</sub>O<sub>3</sub>/PLA fibre mats and thin films is higher than their micro-sized counterparts. Hence, the probability of X-rays with lower energies (*i.e.* 7–20 keV and 22–35 kV) interacting and being absorbed by n-Bi<sub>2</sub>O<sub>3</sub> filler is higher when compared with their micro-sized counterparts since the photons interact with the absorbing materials mainly by the photoelectric effect.

As a consequence, electrospun n-Bi<sub>2</sub>O<sub>3</sub>/PLA nanofibre mats are superior to their micro-sized counterparts in terms of X-ray attenuation for all the X-ray beam energies (*i.e.* 7–20 keV and 22–49 kV generated by XAS and mammography, respectively). In contrast, n-Bi<sub>2</sub>O<sub>3</sub>/PLA thin films are a good X-ray shielding candidate only for the mammography unit at 22–35 kV when compared with m-Bi<sub>2</sub>O<sub>3</sub>/PLA thin films. Both can be chosen as X-ray shielding materials for voltages greater than 35 kV. The observed similarity in the attenuation results for PLA thin films of n-Bi<sub>2</sub>O<sub>3</sub> and m-Bi<sub>2</sub>O<sub>3</sub> at the X-ray tube voltage of the mammography unit of more than 35 kV may be attributed to: (a) the decrease of the photoelectric effect, and (b) the domination of the Compton scattering effect when the photon energy increases. The latter effect results in less interaction and absorption of the photons by Bi particles of these thin films; thus the X-ray attenuation of the films is similar. In contrast, electrospun n-Bi<sub>2</sub>O<sub>3</sub>/PLA nanofibre mats are superior to their micro-sized counterparts in terms of X-ray attenuation at the same energy range. The observed large differences in

X-ray attenuation of these fibre mats may be explained by the difference in uniformity of dispersion between nano- and micro-sized Bi particles within the PLA matrix where large agglomerations tend to occur in the latter, thus affecting the final density of the composite.

Hence, the electrospun n-Bi<sub>2</sub>O<sub>3</sub>/PLA nanofibre mats of all filler loadings (24–38 wt%) are potential candidates in X-ray shielding for all the incident X-ray energies studied either by XAS (7–20 keV) or mammography (22–49 kV) when compared with their micro-sized counterparts. However, the latter may still be a suitable candidate for X-ray attenuator of scattered radiation which requires lower energy. These electrospun Bi<sub>2</sub>O<sub>3</sub>/PLA nanofibre mats can be used as a coating material for X-ray shielding because PLA nanofibres provide many benefits such as higher tenacity, resistance to degradation and mechanical properties (Farrington *et al.*, 2005;

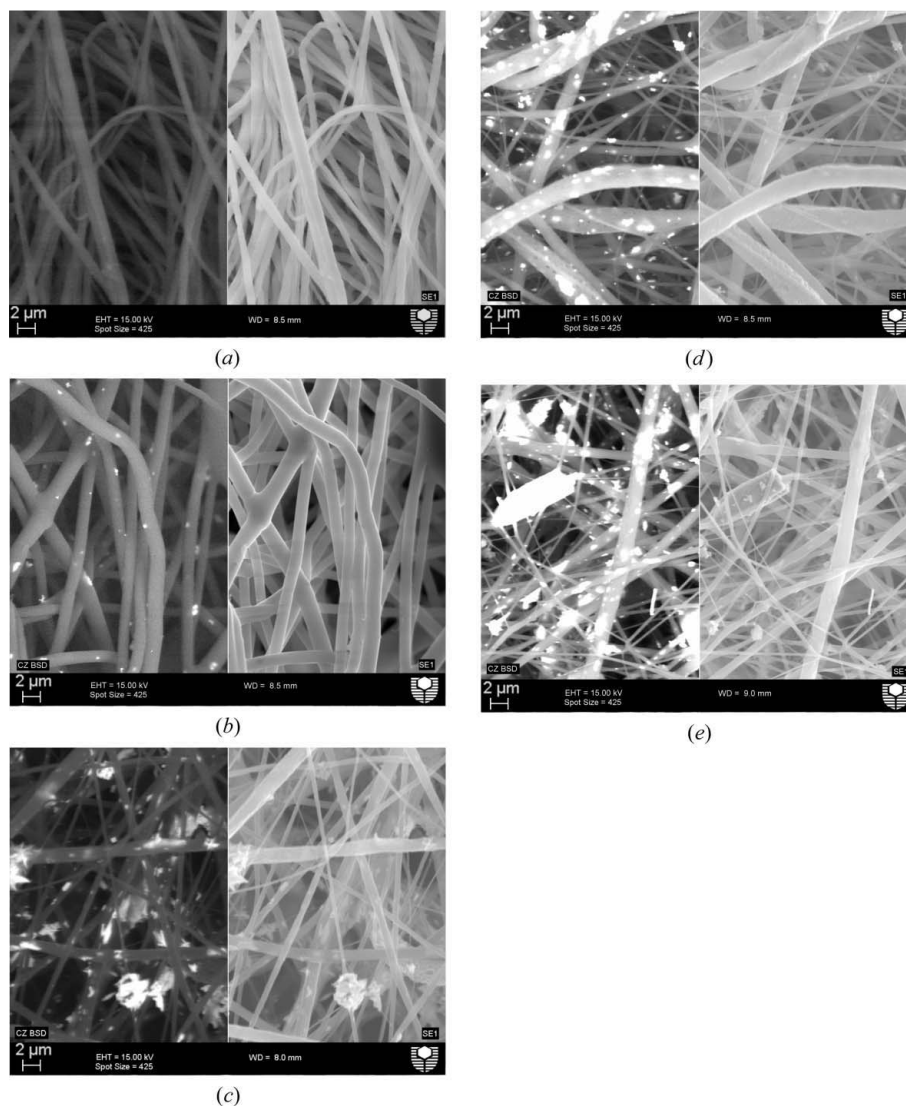


**Figure 6** SEM images using, for each figure, the backscattered electron technique (left) and the secondary electron technique (right) for (a) the control electrospun PLA nanofibres without any particles (0 wt% of Bi<sub>2</sub>O<sub>3</sub>); (b) 28 wt% Bi<sub>2</sub>O<sub>3</sub> of electrospun n-Bi<sub>2</sub>O<sub>3</sub>/PLA nanofibres; (c) 28 wt% Bi<sub>2</sub>O<sub>3</sub> of electrospun m-Bi<sub>2</sub>O<sub>3</sub>/PLA nanofibres; (d) 38 wt% Bi<sub>2</sub>O<sub>3</sub> of electrospun n-Bi<sub>2</sub>O<sub>3</sub>/PLA nanofibres; and (e) 38 wt% Bi<sub>2</sub>O<sub>3</sub> of electrospun m-Bi<sub>2</sub>O<sub>3</sub>/PLA nanofibres.



Haroosh *et al.*, 2012). Besides, since PLA has a higher tenacity, these electrospun  $\text{Bi}_2\text{O}_3/\text{PLA}$  nanofibre mats can be fabricated as gloves to be worn by radiation workers when holding radioactive materials or waste (non-clinical use), or used as a liner on examination tables to help attenuate scattered X-rays coming out from patients during medical diagnosis or therapy (using higher X-ray or  $\gamma$ -ray energies in the MeV range) performed by specialist radiographers and radiologists (clinical use).

Meanwhile, n- $\text{Bi}_2\text{O}_3/\text{PLA}$  thin films are good X-ray shielding candidates only for mammography at 25–35 kV, when compared with m- $\text{Bi}_2\text{O}_3/\text{PLA}$  thin films. Both can be chosen as X-ray shielding materials for X-ray tube voltages greater than 35 kV.

### 3.3. Microstructure analyses

Microstructure analysis of the electrospun nanofibres was performed using both backscattered electrons and secondary electrons to clearly show the difference between the PLA polymer and the embedded Bi elements. Fig. 6(a) shows a SEM image of the control electrospun PLA nanofibres without any  $\text{Bi}_2\text{O}_3$  filler. The average diameter of these fibres was  $854 \pm 35$  nm. The average diameter of PLA nanofibres increased when 24–34 wt%  $\text{Bi}_2\text{O}_3$  was added to the PLA solution. For instance, Fig. 6(b) shows the homogeneous nanofibres of 28 wt% n- $\text{Bi}_2\text{O}_3$  filler with an average diameter of  $971 \pm 22$  nm. Meanwhile, in Fig. 6(c) the average diameter of 28 wt% m- $\text{Bi}_2\text{O}_3/\text{PLA}$  nanofibres is  $911 \pm 41$  nm with a large variation in fibre diameter and particle agglomerations can be observed.

This indicates that, by increasing the solution viscosity while both the conductivity and the surface tension decreased with the increment of filler ( $\text{Bi}_2\text{O}_3$ ) loadings within the PLA solution, the average nanofibre diameter was increased. The significant increase in the viscosity of the solution with increasing filler loadings was due to the increased molecular entanglement which enabled the charged jet to withstand a larger stretching force (from the Coulombic repulsion) resulting in the coarsening of the nanofibres.

In contrast, a further increase of  $\text{Bi}_2\text{O}_3$  loading to 38 wt% caused a decrease in the average diameter to  $496 \pm 32$  nm for n- $\text{Bi}_2\text{O}_3/\text{PLA}$  nanofibres which have a maximum diameter of  $2.06 \pm 0.49$   $\mu\text{m}$  and a minimum of  $114 \pm 2$  nm (Fig. 6d). Meanwhile, the average diameter of m- $\text{Bi}_2\text{O}_3/\text{PLA}$  nanofibres is  $406 \pm 71$  nm with a maximum diameter of  $1.13 \pm 0.23$   $\mu\text{m}$  and a minimum of  $111 \pm 2$  nm (Fig. 6e). The unexpected decrease in the average fibre diameter may be attributed to the domination of electrical conductivity when filler loading or viscosity of solution increases. As a result, this leads to the production of fibres with non-uniform diameters, as well as formation of beads and particle agglomerations.

Figs. 7(a)–7(c) illustrate the EDS results for the electrospun n- $\text{Bi}_2\text{O}_3/\text{PLA}$  nanofibre mat with 34 wt% filler loading which confirms the existence of the Bi element from the filler together with elements C and O from the PLA matrix. SEM images of m- $\text{Bi}_2\text{O}_3/\text{PLA}$  and n- $\text{Bi}_2\text{O}_3/\text{PLA}$  thin films with

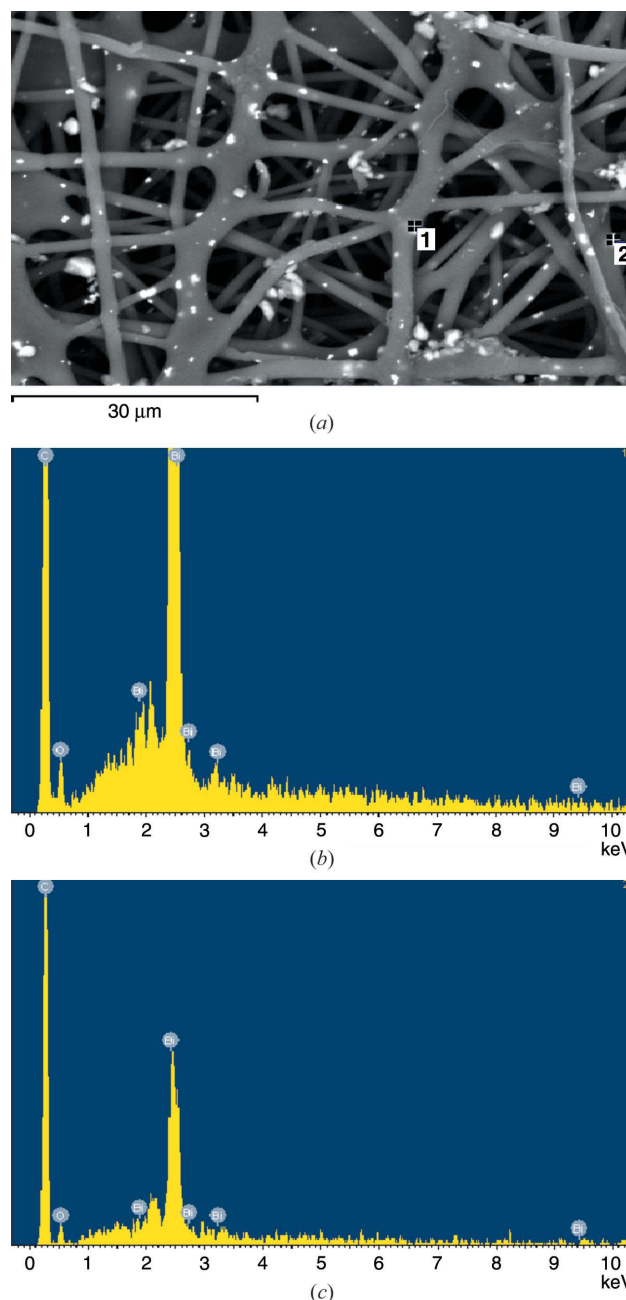


**Figure 7**  
(a) SEM image used for EDS analyses on 34 wt%  $\text{Bi}_2\text{O}_3$  of the electrospun n- $\text{Bi}_2\text{O}_3/\text{PLA}$  nanofibres to prove that only Bi particles are detected other than C and O which is the composition of PLA. (b) EDS analyses for point 1 and (c) for point 2 marked in (a).

28 wt% filler loading are shown in Fig. 8, indicating the presence of agglomerations within the PLA matrix.

## 4. Conclusions

Electrospun nanofibre mats of n- $\text{Bi}_2\text{O}_3/\text{PLA}$  and m- $\text{Bi}_2\text{O}_3/\text{PLA}$  with filler loadings of 24–38 wt% have been successfully fabricated. From the analyses, the electrospun n- $\text{Bi}_2\text{O}_3/\text{PLA}$  nanofibre mats of all filler loadings were found to be superior in attenuating X-rays compared with their micro-sized counterparts because n- $\text{Bi}_2\text{O}_3$  may provide more uniform materials

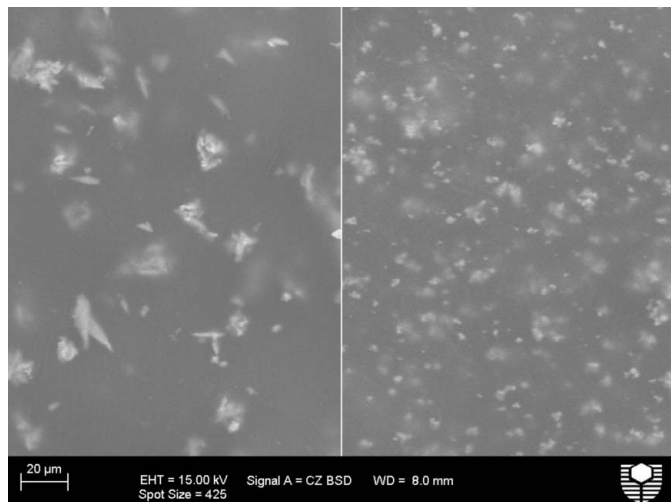


**Figure 8**  
SEM images of a thin film of 28 wt%  $\text{Bi}_2\text{O}_3$  for m- $\text{Bi}_2\text{O}_3/\text{PLA}$  on the left (clear agglomerations can be seen) and n- $\text{Bi}_2\text{O}_3/\text{PLA}$  on the right.

since the particle size can affect the microstructure and consequently the density and composition that will then modify the attenuation coefficient of the composite. However, the electrospun  $\text{Bi}_2\text{O}_3/\text{PLA}$  nanofibre mats with 38 wt% loading are not recommended for X-ray shielding because of higher porosity compared with the lower filler loadings. The n- $\text{Bi}_2\text{O}_3/\text{PLA}$  thin films are good X-ray shielding candidates only for the mammography unit at 22–35 kV when compared with the m- $\text{Bi}_2\text{O}_3/\text{PLA}$  thin films. The particle size effect on X-ray attenuation diminished as the X-ray tube voltage exceeded 35 kV.

Part of this research was undertaken on the XAS beamline at the Australian Synchrotron, Victoria, Australia. We thank our colleagues Dr C. Ng and Associate Professor Z. Sun for assistance with XAS data collection. Also, we would like to thank Carolyn Madeley of the Breast Assessment Centre, Royal Perth Hospital, Western Australia, for giving us the opportunity to use the mammography unit.

## References

An, J.-S., Park, J.-S., Kim, J.-R. & Hong, K. S. (2006). *J. Am. Ceram. Soc.* **89**, 3658–3661.  
Berger, M. J., Hubbell, J. H., Seltzer, S. M., Chang, J., Coursey, J. S., Sukumar, R., Zucker, D. S. & Olsen, K. (2010). *XCOM: Photon Cross Section Database*, <http://physics.nist.gov/xcom>.  
Botelho, M. Z., Künzel, R., Okuno, E., Levenhagen, R. S., Basegio, T. & Bergmann, C. P. (2011). *Appl. Radiat. Isot.* **69**, 527–530.

Brettmann, B. K., Tsang, S., Forward, K. M., Rutledge, G. C., Myerson, A. S. & Trout, B. L. (2012). *Langmuir*, **28**, 9714–9721.  
Buyuk, B., Tugrul, A. B., Akarsu, A. C. & Addemir, A. O. (2012). *J. Nano Electron. Phys.* **4**, 01010.  
Chanthima, N., Kaekwkhao, J., Kedkaew, C., Chewpraditkul, W., Pokaipisit, A. & Limsuwan, P. (2011). *Prog. Nucl. Sci. Technol.* **1**, 106–109.  
Demir, M. M., Gulgun, M. A., Menciloglu, Y. Z., Erman, B., Abramchuk, S. S., Makhaeva, E. E., Khokhlov, A. R., Matveeva, V. G. & Sulman, M. G. (2004). *Macromolecules*, **37**, 1787–1792.  
El Haber, F. & Froyer, G. (2008). *J. Univ. Chem. Technol. Metall.* **43**, 283–290.  
Faccini, M., Vaquero, C. & Amantia, D. (2012). *J. Nanomater.* **2012**, 1–9.  
Farrington, D. W., Lunt, J., Davies, S. & Blackburn, R. S. (2005). *Poly (Lactic Acid) Fibers*, pp. 191–220. Cambridge: Woodhead Publishing Series in Textiles.  
Granmayeh Rad, A., Abbasi, H. & Afzali, M. H. (2011). *Phys. Proc.* **22**, 203–208.  
Haiwen, X., Kai-Zhong, G., Yiming, S. & Song, X. (2006). *J. Phys. D.* **39**, 4746.  
Harooosh, H. J., Chaudhary, D. S. & Dong, Y. (2012). *J. Appl. Polym. Sci.* **124**, 3930–3939.  
Hu, W., Huang, Z. M. & Liu, X. Y. (2010). *Nanotechnology*, **21**, 315104.  
Huang, S., Kang, X., Cheng, Z., Ma, P., Jia, Y. & Lin, J. (2012). *J. Colloid Interface Sci.* **387**, 285–291.  
Huang, X. & El-Sayed, M. A. (2010). *J. Adv. Res.* **1**, 13–28.  
Künzel, R. & Okuno, E. (2012). *Appl. Radiat. Isot.* **70**, 781–784.  
Lee, S. & Obendorf, S. K. (2007). *Text. Res. J.* **77**, 696–702.  
Lines, M. G. (2008). *J. Alloys Compd.* **449**, 242–245.  
Noor Azman, N. Z., Siddiqui, S. A., Hart, R. & Low, I. M. (2013). *Appl. Radiat. Isot.* **71**, 62–67.  
Patra, C. R., Bhattacharya, R., Mukhopadhyay, D. & Mukherjee, P. (2010). *Adv. Drug Deliv. Rev.* **62**, 346–361.  
Popov, A. (2009). *SPIE Newsroom*, **24**, 1–2.  
Prabhakaran, M. P., Venugopal, J., Chan, C. K. & Ramakrishna, S. (2008). *Nanotechnology*, **19**, 455102.  
Rajeswari, R., Jayarama Reddy, V., Subramanian, S., Shayanti, M., Radhakrishnan, S. & Seeram, R. (2012). *Nanotechnology*, **23**, 385102.  
Russo, G. & Lamberti, G. (2011). *J. Appl. Polym. Sci.* **122**, 3551–3556.  
Sahare, P. D., Ranjan, R., Salah, N. & Lochab, S. P. (2007). *J. Phys. D.* **40**, 759–764.  
Shanshan, B., Jayaram, S. H. & Cherney, E. A. (2010). *2010 Annual Report Conference on Electrical Insulation and Dielectric Phenomena (CEIDP)*, pp. 1–4.  
Sill, T. J. & von Recum, H. A. (2008). *Biomaterials*, **29**, 1989–2006.  
Storrie, H. & Mooney, D. J. (2006). *Adv. Drug Deliv. Rev.* **58**, 500–514.  
Suk, C. C., Wei, L. J. & Harun, A. Z. (2012). *Malays. J. Med. Sci.* **19**, 22–28.  
Yiin-Kuen, F. & Li-Chih, L. (2013). *Nanotechnology*, **24**, 055301.  
Yu, D. G., Shen, X. X., Branford-White, C., White, K., Zhu, L. M. & Bligh, S. W. (2009). *Nanotechnology*, **20**, 055104.

## 7. CONCLUSIONS AND FUTURE WORK

---

### 7.1 Conclusions

This research was conducted with the specific novel approach to design technologically viable new radiation shielding materials providing a high potential of applications for shielding of X-rays for use in medical X-ray imaging facilities. These materials would be ideally based upon the dispersion of heavy element fillers into polymeric materials by different filler dispersion methods. In relation to the specific objectives of the research, the following concluding remarks can be made:

#### 7.1.1 Filler dispersion within epoxy resins by melt-mixing method

**a) Dispersion of the micro-sized filler into the epoxy matrix on their X-ray attenuation ability**

- i. The fillers ( $\text{PbO}$ ,  $\text{Pb}_3\text{O}_4$ ,  $\text{PbCl}_2$ ,  $\text{Bi}_2\text{O}_3$  and  $\text{WO}_3$ ) can be seen to be dispersed uniformly in the epoxy matrix with low filler loading. As the filler loading increased, some filler agglomerations within the epoxy matrix could be seen, thus affecting the density and composition of the composites. As a consequence, the effect of filler agglomerations will then modify the X-ray attenuation ability of the composite since it was dependent on the filler loading and composite density. In addition, the effect also influenced the flexural modulus, flexural strength and hardness of composites.
- ii. Even though the composites fabricated have shown some agglomeration at high filler loading, they still show good X-ray attenuation properties and could be considered as a potential candidate for radiation shielding in diagnostic radiology purposes. For example, the lead oxide-epoxy composites in this study are superior to the lead oxide-isophthalate resin composite previously investigated by other researchers. This has resulted since, with the same wt% of lead oxide, lead oxides-epoxy composite provides better attenuation on the Gamma- rays of energy 0.662 MeV emitted from Cs-137 point source than

lead oxide-isophthalate. Hence, the usage of lead oxides can be minimal in the fabrication of lead oxide-epoxy composites to provide similar attenuation ability with the lead oxide-isophthalate, thus reducing the health risks associated with lead oxides.

- iii. Furthermore, the 8 mm thick  $\text{Bi}_2\text{O}_3$ -epoxy composite with 70 wt%  $\text{Bi}_2\text{O}_3$  is comparable to a 10 mm thick commercial lead glass which contains 56 wt% Pb; while the 8 mm thickness of 70 wt%  $\text{PbCl}_2$ - or  $\text{WO}_3$ -epoxy composites were not comparable with the lead glass unless they were prepared with a thickness greater than 10 mm. Both flexural modulus and hardness of composites escalated with increasing filler loading; however, the flexural strength decreased markedly when the filler loading was equal to or greater than 30 wt%.

**b) Particle size effect on the X-ray attenuation ability of  $\text{WO}_3$  filler-epoxy composites**

- i. Nano-sized  $\text{WO}_3$ -epoxy composite has provided better attenuation ability to attenuate the X-ray beams generated by lower tube voltages (25–35 kV) operated by a mammography unit when compared to the micro-sized  $\text{WO}_3$ -epoxy composite. As the X-ray tube voltage selected is greater than 40–49 kV, they attenuate a similar amount of X-ray beams or, in other words, the attenuation ability of the nano-sized and micro-sized  $\text{WO}_3$  reinforced epoxy is indistinguishable. Meanwhile, the role of particle size in X-ray shielding was also insignificant at all X-ray tube voltage ranges (40–120 kV) for the radiography unit.
- ii. The particle size-effect of  $\text{WO}_3$ -epoxy composite on the X-ray attenuation was profoundly dependent on the energy of synchrotron radiations. The particle size-effect was more obvious at lower synchrotron radiation energies (10–20 keV) since X-ray transmission in nano-sized  $\text{WO}_3$ -epoxy composite was less than their micro-sized counterparts. In contrast, this size-effect became insignificant at higher energies between 20 and 40 keV because the X-ray



transmissions in both nano-sized and micro-sized WO<sub>3</sub>-epoxy composites were very similar.

- iii. The equivalent energy for X-ray tube voltages operated by a mammography unit (25-49 kV) are in the range of 15-25 keV of synchrotron radiation energies. Similarly, for a radiography unit, the X-ray tube voltages of 40 – 60 kV are equivalent to 25-40 keV synchrotron radiation energies. For tube voltages greater than 60 kV (i.e., 70-100 kV), the equivalent energy was in excess of 40 keV.
- iv. The particle size-effect on the X-ray attenuation tested with the mammography and radiography unit showed a similar trend in results as the composite of the same WO<sub>3</sub> loading thickness increased.
- v. Meanwhile, the effect of WO<sub>3</sub> loading on the mechanical properties showed an initial optimum improvement but a further increase in the filler loading caused these properties to deteriorate.

### **7.1.2 Filler dispersion within epoxy, acrylic and glass by ion-implantation method**

- a) Epoxy samples implanted with W, Au and Pb at various concentrations showed that the threshold of implanted ions above which the mass attenuation coefficient,  $\mu_m$  of the ion-implanted epoxy composite is distinguishably higher than the  $\mu_m$  of the pure epoxy, differs for different ion types. The practical concentrations of W, Au and Pb in epoxy composite which could provide good X-ray attenuation properties could be considered as candidates for effective X-ray shielding in diagnostic radiology by increasing the ion concentration rather than using the one illustrated in this work. Further work is needed for better explanation as to how ion implanted epoxy resins could be fabricated into a useful X-ray shielding material given that the range of the implanted ions is only around i.e. 50-80 nm providing that the thickness of the material for a useful shield is of the order of mm-cm.

- b) Acrylic and glass implanted with W and Pb ions showed higher X-ray attenuation for the composite, with the denser sample matrix and the composite having the higher RBS ion concentration. However, the amount of implanted doses should be significantly increased so that this approach can be feasible for designing new shielding materials for the X-ray technologists. Even though glass provided the best results for both RBS ion concentration and X-ray attenuation, its usage for X-ray shielding needs extra care since it is easy to break. In contrast, implanted acrylic can be a good candidate for X-ray shielding, however much time is needed when working with implanted acrylic having a very high nominal dose since it has a low melting point.

### **7.1.3 Filler dispersion within PLA nanofibre mats by electrospinning method**

PLA nanofibre mats dispersed with n-Bi<sub>2</sub>O<sub>3</sub> and m-Bi<sub>2</sub>O<sub>3</sub> showed that the electrospun n-Bi<sub>2</sub>O<sub>3</sub>/PLA nanofibre mats of all filler loadings (24-38 wt%) were found to be superior in attenuating X-rays compared with their micro-sized counterparts. This has resulted because the use of n-Bi<sub>2</sub>O<sub>3</sub> provides the fabrication of more uniform materials, since the particle size can affect the microstructure and consequently the density and composition that will then modify the attenuation coefficient of the composite. However, the electrospun Bi<sub>2</sub>O<sub>3</sub>/PLA nanofibre mats with 38 wt% loading are not recommended for X-ray shielding because of higher porosity compared with the lower filler loadings. Meanwhile, the n-Bi<sub>2</sub>O<sub>3</sub>/PLA thin films are good X-ray shielding candidates only for the mammography unit at tube voltages of 22–35 kV when compared to the m-Bi<sub>2</sub>O<sub>3</sub>/PLA thin films. The particle size effect on X-ray attenuation diminished as the X-ray tube voltage exceeded 35 kV.

## 7.2 Recommendations for Future Work

The primary objectives of this research have been achieved. The use of viable processing methodologies for designing new material with nanotechnology advances approach to enhance radiation shielding purposes to meet the safety requirements for use in medical X-ray imaging facilities was succeeding. However, only a very limited and slight amount of information was obtained from this project. This leaves a wide scope for future investigations. Therefore, some recommendations for further research are detailed as follows:

1. Since the relationship between the mass attenuation coefficient and particle size of lead oxide remains unknown, as mentioned in Chapter 3, further study should be undertaken to reveal their relationship, since lead oxide was the familiar compound used as radiation shielding in the past.
2. The dispersion of the nano-fillers by melt-mixing method was fairly homogeneous with some particle agglomerations having the use of only high speed mixture. However, obtaining perfect dispersion for nano-fillers in polymer matrices is still challenging. Therefore, different ways of mixing as well as curing is required to be investigated deeply in order to improve the nano-filler dispersion by melt-mixing method.
3. Deeper testing of the physical and mechanical properties of the composites should be considered so that the composites are able to be used practically as an X-ray shielding for long periods of time.
4. The practical concentrations of W, Au and Pb ions implanted into an epoxy, acrylic or glass composite should be increased to a higher rate than the concentrations used in this report in order to provide good X-ray attenuation properties. They could be considered as candidates for effective X-ray shielding in diagnostic radiology.

5. Since Bi has a greater atomic number, is classified as non-hazardous and is also a relatively environmentally-friendly compound compared to toxic Pb, the implantation of Bi ions into the epoxy, acrylic or glass should be considered to provide good X-ray attenuation properties. They could be considered as candidates for effective X-ray shielding in diagnostic radiology.
6. Deeper investigations should be considered in order to characterize the implanted composites. However, the higher implanted ion concentrations are required so that the characterization analyses on the composites could succeed.
7. The fabrication of nanofiller-nanofibre polymer by electrospinning should be tested with different filler and polymer types from the one used in this report. These are also a good candidate for attenuating X-rays.
8. Deeper investigations on the physical and mechanical properties of the electrospun nanofiller/nanofibre PLA should be considered for X-ray shielding practical purposes.

## 8. APPENDICES

---

### 8.1 APPENDIX A

---

#### Supplementary Information for Publication

##### 8.1.1 Appendix A-1: Supplementary Information for Chapter 5.1

Noor Azman, N.Z., Siddiqui, S.A., Ionescu, M., Low, I.M., Synthesis and characterization of ion-implanted epoxy composites for X-ray shielding, *Nuclear Instruments and Methods in Physics Research B: Beam Interactions with Materials and Atoms*, 287 (2012) 120–123.

##### Microstructure analyses

The image in Figure 8.1 shows the typical surface microstructures of the epoxy sample after being implanted with W at the dose of  $1.4 \times 10^{15}$  ions/cm<sup>2</sup>. Figure 8.2 shows that at the surface, W was detected only in accumulations like the bright white spot in Figure 8.1 using EDS. Meanwhile, Figure 8.3 provides EDS analysis of another part of the image which does not have any W elements. The surface macro-particles particles are due to the ion source working characteristics and they provide a small surface coverage (estimated at 5 μm).

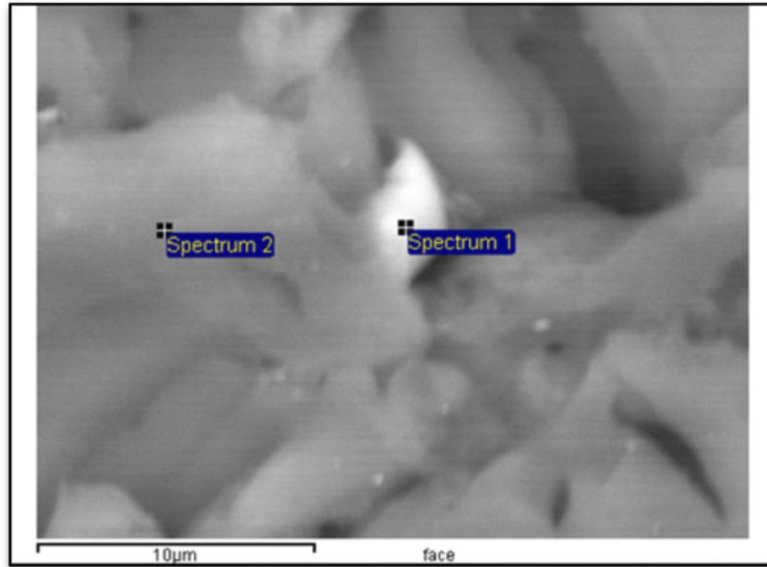


**Figure 8.1:** Backscattered micrograph for epoxy implanted with W (white patches) at  $1.4 \times 10^{15}$  ions/cm<sup>2</sup> (Sample B2).

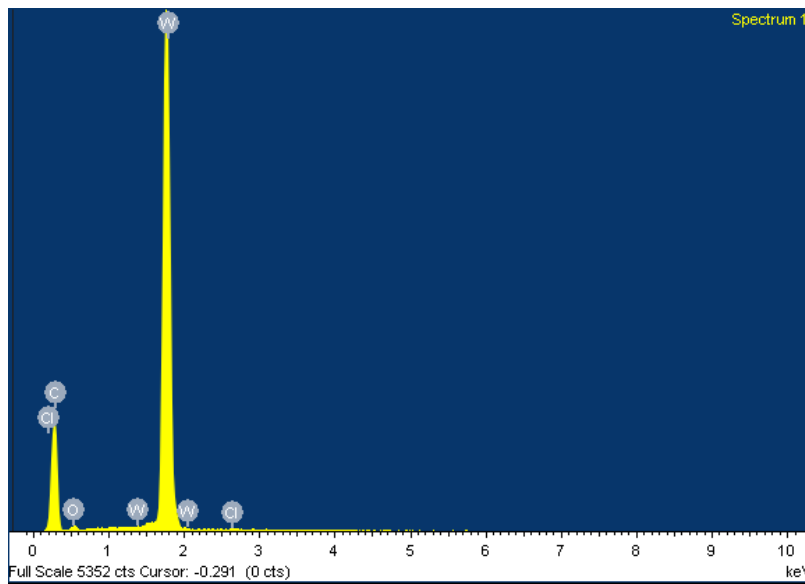


**Figure 8.2:** EDS result of Spectrum 1 obtained from Figure 8.1.

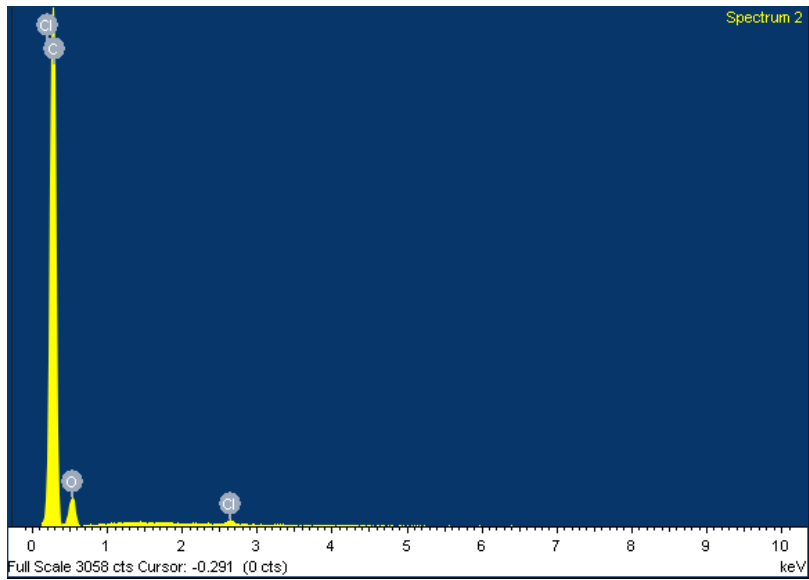


**Figure 8.3:** EDS result of Spectrum 2 obtained from Figure 8.1.

Meanwhile, Figure 8.4 illustrates the cross-sectional view of the implanted sample with Pb (bright white spot as confirmed from EDS analysis) at the same dose which also shows that the implanted element detected coalesce similar to small agglomerations at a certain depth.

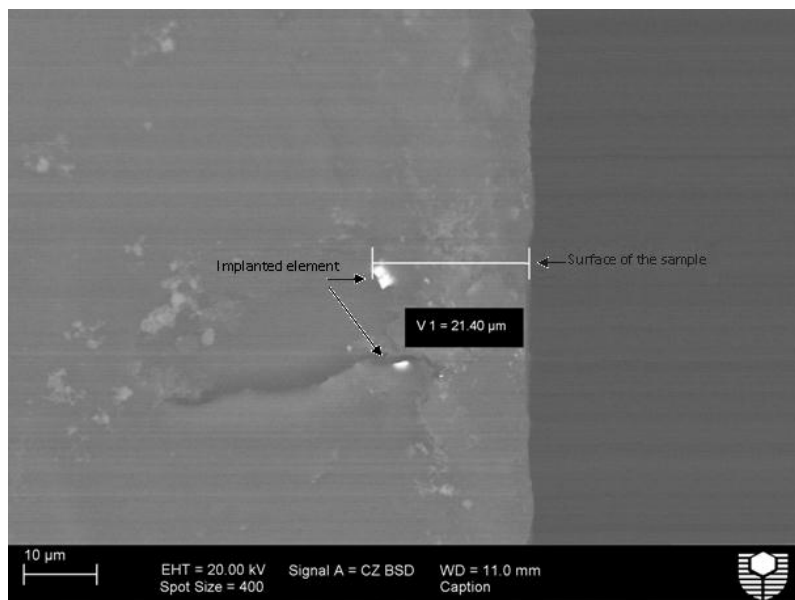


**Figure 8.4:** Backscattered micrograph for epoxy implanted with Pb at  $1.4 \times 10^{15}$  ions/cm<sup>2</sup> (side view) (Sample B6).

### 8.1.2 Appendix A-2: Supplementary Information for Chapter 6

Noor Azman, N.Z., Siddiqui, S.A., Haroosh, H.J., Albetran, H.M.M., Johannessen, B., Dong, Y., Low, I.M., Characteristics of X-ray attenuation in electrospun bismuth oxide / poly-lactic acid nanofibre mats, *Journal of Synchrotron Radiation*, 20 (2013) 741-748.

#### Electrospinning experimental set up and final product

Figure 8.5 shows the set up for the electrospinning process to fabricate Bi<sub>2</sub>O<sub>3</sub>/PLA nanofibre mats. The solution of Bi<sub>2</sub>O<sub>3</sub>/PLA mixed with chloroform and methanol held in a syringe is fed to a metal needle. The high voltage supply is connected to the needle, producing a fine jet of Bi<sub>2</sub>O<sub>3</sub>/PLA solution. This dries out in transit, resulting in fine nanofibres which are collected on the aluminium foil at the collector target. The final product of nanofibre mats collected is shown in Figure 8.6. The white mat belongs to the control PLA nanofibre, while the yellow mat belongs to Bi<sub>2</sub>O<sub>3</sub>/PLA nanofibre.



**Figure 8.5:** Electrospinning experimental set up to perform the electrospinning process.





**Figure 8.6:** Final product collected on the aluminium foil after the process was completed. The product on the left side is the control PLA nanofibre mat; while at the right side is the Bi<sub>2</sub>O<sub>3</sub>/PLA nanofibre mat.

## 8.2 APPENDIX B

---

### Statement of Contributions of Others

8.2.1 Appendix B-1: Statement of Contribution of Others for “Microstructured design of lead oxide-epoxy composites for radiation shielding purposes”.

---

Statement of Contribution of Others for “Microstructured design of lead oxide-epoxy composites for radiation shielding purposes”.

28<sup>th</sup> July 2013

To Whom It May Concern

I, Dr. S.A. Siddiqui, contributed by specialist technical advice and instrument usage (general diagnostic radiology machine at Department of Imaging and Applied Physics, Curtin University) and also manuscript editing to the paper/publication entitled

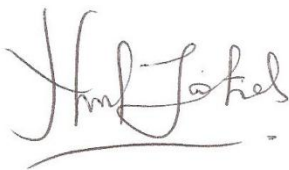
**Noor Azman, N.Z.**, Siddiqui, S.A., Hart, R., Low, I.M., Microstructured design of lead oxide-epoxy composites for radiation shielding purposes, *Journal of Applied Polymer Science*, 128 (2013) 3213-3219

Undertaken with Nurul Zahirah Binti Noor Azman



(Signature of Co-Author)

S.A. Siddiqui



(Signature of First Author)

Nurul Zahirah Binti Noor Azman

Statement of Contribution of Others for “Microstructured design of lead oxide-epoxy composites for radiation shielding purposes”.

28<sup>th</sup> July 2013

To Whom It May Concern

I, Dr. R. Hart, contributed by specialist technical service advice and instrument usage (general radiography and mammography unit at Royal Perth Hospital) as well as manuscript editing to the paper/publication entitled

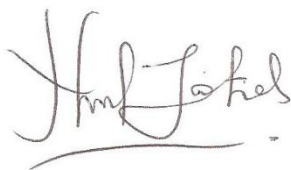
**Noor Azman, N.Z.,** Siddiqui, S.A., Hart, R., Low, I.M., Microstructured design of lead oxide-epoxy composites for radiation shielding purposes, *Journal of Applied Polymer Science*, 128 (2013) 3213-3219

Undertaken with Nurul Zahirah Binti Noor Azman



(Signature of Co-Author)

R. Hart



(Signature of First Author)

Nurul Zahirah Binti Noor Azman

Statement of Contribution of Others for “Microstructured design of lead oxide-epoxy composites for radiation shielding purposes”.

28<sup>th</sup> July 2013

To Whom It May Concern

I, Prof. I.M. Low, contributed by project supervision and manuscript editing to the paper/publication entitled

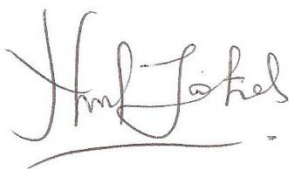
**Noor Azman, N.Z.**, Siddiqui, S.A., Hart, R., Low, I.M., Microstructured design of lead oxide-epoxy composites for radiation shielding purposes, *Journal of Applied Polymer Science*, 128 (2013) 3213-3219

Undertaken with Nurul Zahirah Binti Noor Azman

A handwritten signature in black ink that reads "I.M. Low". The letters are cursive and somewhat stylized.

(Signature of Co-Author)

I. M. Low

A handwritten signature in black ink that reads "Nurul Zahirah Binti Noor Azman". The signature is highly stylized and cursive.

(Signature of First Author)

Nurul Zahirah Binti Noor Azman

8.2.2 Appendix B-2: Statement of Contribution of Others for “Synthesis and characterization of epoxy composites filled with Pb, Bi or W compound for shielding of diagnostic X-rays”.

---

Statement of Contribution of Others for “Synthesis and characterization of epoxy composites filled with Pb, Bi or W compound for shielding of diagnostic X-rays”.

28<sup>th</sup> July 2013

To Whom It May Concern

I, Dr. S.A. Siddiqui, contributed by specialist technical advice and instrument usage (general diagnostic radiology machine at Department of Imaging and Applied Physics, Curtin University) and also manuscript editing to the paper/publication entitled

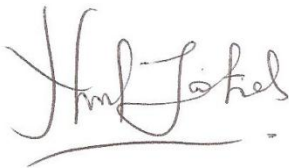
**Noor Azman, N.Z.,** Siddiqui, S.A., Low, I.M., Synthesis and characterization of epoxy composites filled with Pb, Bi or W compound for shielding of diagnostic X-rays, *Applied Physics A: Materials Science & Processing*, 110 (2013) 137-144

Undertaken with Nurul Zahirah Binti Noor Azman



(Signature of Co-Author)

S.A. Siddiqui



(Signature of First Author)

Nurul Zahirah Binti Noor Azman

Statement of Contribution of Others for “Synthesis and characterization of epoxy composites filled with Pb, Bi or W compound for shielding of diagnostic X-rays”.

28<sup>th</sup> July 2013

To Whom It May Concern

I, Prof. I.M. Low, contributed by project supervision and manuscript editing to the paper/publication entitled

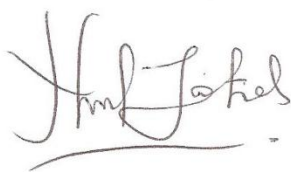
**Noor Azman, N.Z.**, Siddiqui, S.A., Low, I.M., Synthesis and characterization of epoxy composites filled with Pb, Bi or W compound for shielding of diagnostic X-rays, *Applied Physics A: Materials Science & Processing*, 110 (2013) 137-144

Undertaken with Nurul Zahirah Binti Noor Azman



(Signature of Co-Author)

I. M. Low



(Signature of First Author)

Nurul Zahirah Binti Noor Azman



8.2.3 Appendix B-3: Statement of Contribution of Others for “Effect of particle size, filler loadings and X-ray energy on the X-ray attenuation ability of tungsten oxide – epoxy composites”.

---

Statement of Contribution of Others for “Effect of particle size, filler loadings and X-ray energy on the X-ray attenuation ability of tungsten oxide – epoxy composites”.

28<sup>th</sup> July 2013

To Whom It May Concern

I, Dr. S.A. Siddiqui, contributed by specialist technical advice and instrument usage (general diagnostic radiology machine at Department of Imaging and Applied Physics, Curtin University) and also manuscript editing to the paper/publication entitled

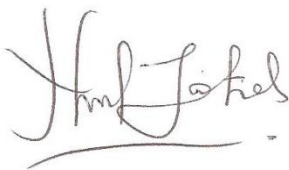
**Noor Azman, N.Z., Siddiqui, S.A., Hart, R., Low, I.M.,** Effect of particle size, filler loadings and X-ray energy on the X-ray attenuation ability of tungsten oxide – epoxy composites, *Applied Radiation and Isotopes*, 71 (2013) 62-67

Undertaken with Nurul Zahirah Binti Noor Azman



(Signature of Co-Author)

S.A Siddiqui



(Signature of First Author)

Nurul Zahirah Binti Noor Azman

Statement of Contribution of Others for “Effect of particle size, filler loadings and X-ray energy on the X-ray attenuation ability of tungsten oxide – epoxy composites”.

28<sup>th</sup> July 2013

To Whom It May Concern

I, Dr. R. Hart, contributed by specialist technical service advice and instrument usage (general radiography and mammography unit at Royal Perth Hospital) as well as manuscript editing to the paper/publication entitled

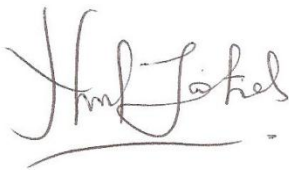
**Noor Azman, N.Z., Siddiqui, S.A., Hart, R., Low, I.M.,** Effect of particle size, filler loadings and X-ray energy on the X-ray attenuation ability of tungsten oxide – epoxy composites, *Applied Radiation and Isotopes*, 71 (2013) 62-67

Undertaken with Nurul Zahirah Binti Noor Azman



(Signature of Co-Author)

R. Hart



(Signature of First Author)

Nurul Zahirah Binti Noor Azman

Statement of Contribution of Others for “Effect of particle size, filler loadings and X-ray energy on the X-ray attenuation ability of tungsten oxide – epoxy composites”.

28<sup>th</sup> July 2013

To Whom It May Concern

I, Prof. I.M. Low, contributed by project supervision and manuscript editing to the paper/publication entitled

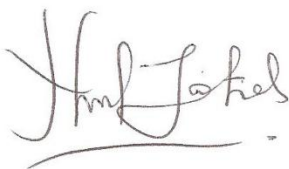
**Noor Azman, N.Z.**, Siddiqui, S.A., Hart, R., Low, I.M., Effect of particle size, filler loadings and X-ray energy on the X-ray attenuation ability of tungsten oxide – epoxy composites, *Applied Radiation and Isotopes*, 71 (2013) 62-67

Undertaken with Nurul Zahirah Binti Noor Azman



(Signature of Co-Author)

I. M. Low



(Signature of First Author)

Nurul Zahirah Binti Noor Azman

8.2.4 Appendix B-4: Statement of Contribution of Others for “Characterisation of micro-sized and nano-sized tungsten oxide-epoxy composites for radiation shielding of diagnostic X-rays”.

---

Statement of Contribution of Others for “Characterisation of micro-sized and nano-sized tungsten oxide-epoxy composites for radiation shielding of diagnostic X-rays”.

28<sup>th</sup> July 2013

To Whom It May Concern

I, Dr. S.A. Siddiqui, contributed by specialist technical advice and instrument usage (general diagnostic radiology machine at Department of Imaging and Applied Physics, Curtin University) and also manuscript editing to the paper/publication entitled

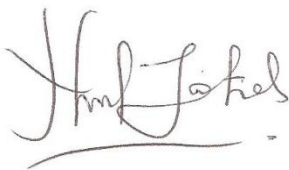
**Noor Azman, N.Z.**, Siddiqui, S.A., Low, I.M., Characterisation of micro-sized and nano-sized tungsten oxide-epoxy composites for radiation shielding of diagnostic X-rays, *Materials Science and Engineering C*, In press

Undertaken with Nurul Zahirah Binti Noor Azman



(Signature of Co-Author)

S.A. Siddiqui



(Signature of First Author)

Nurul Zahirah Binti Noor Azman

Statement of Contribution of Others for “Characterisation of micro-sized and nano-sized tungsten oxide-epoxy composites for radiation shielding of diagnostic X-rays”.

28<sup>th</sup> July 2013

To Whom It May Concern

I, Prof. I.M. Low, contributed by specialist technical advice and instrument usage (general diagnostic radiology machine at Department of Imaging and Applied Physics, Curtin University) and also manuscript editing to the paper/publication entitled

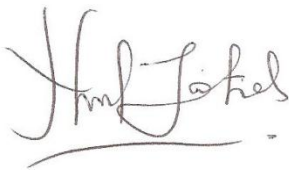
**Noor Azman, N.Z.**, Siddiqui, S.A., Low, I.M., Characterisation of micro-sized and nano-sized tungsten oxide-epoxy composites for radiation shielding of diagnostic X-rays, *Materials Science and Engineering C*, In press

Undertaken with Nurul Zahirah Binti Noor Azman



(Signature of Co-Author)

I.M. Low



(Signature of First Author)

Nurul Zahirah Binti Noor Azman

8.2.5 Appendix B-5: Statement of Contribution of Others for “Synthesis and characterization of ion-implanted epoxy composites for X-ray shielding”.

---



Statement of Contribution of Others for “Synthesis and characterization of ion-implanted epoxy composites for X-ray shielding”.

28<sup>th</sup> July 2013

To Whom It May Concern

I, Dr. S.A. Siddiqui, contributed by specialist technical advice and instrument usage (general diagnostic radiology machine at Department of Imaging and Applied Physics, Curtin University) and also manuscript editing to the paper/publication entitled

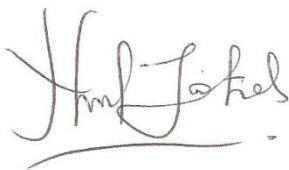
**Noor Azman, N.Z.**, Siddiqui, S.A., Ionescu, M., Low, I.M., Synthesis and characterization of ion-implanted epoxy composites for X-ray shielding, *Nuclear Instruments and Methods in Physics Research B: Beam Interactions with Materials and Atoms*, 287 (2012) 120–123

Undertaken with Nurul Zahirah Binti Noor Azman



(Signature of Co-Author)

S.A. Siddiqui



(Signature of First Author)

Nurul Zahirah Binti Noor Azman

Statement of Contribution of Others for “Synthesis and characterization of ion-implanted epoxy composites for X-ray shielding”.

28<sup>th</sup> July 2013

To Whom It May Concern

I, Dr. M. Ionescu, contributed by specialist technical service advice and instrument usage (ion-implantation, IBA and RBS at ANSTO) and manuscript editing to the paper/publication entitled

**Noor Azman, N.Z.**, Siddiqui, S.A., Ionescu, M., Low, I.M., Synthesis and characterization of ion-implanted epoxy composites for X-ray shielding, *Nuclear Instruments and Methods in Physics Research B: Beam Interactions with Materials and Atoms*, 287 (2012) 120–123

Undertaken with Nurul Zahirah Binti Noor Azman



(Signature of Co-Author)

M. Ionescu



(Signature of First Author)

Nurul Zahirah Binti Noor Azman

Statement of Contribution of Others for “Synthesis and characterization of ion-implanted epoxy composites for X-ray shielding”.

28<sup>th</sup> July 2013

To Whom It May Concern

I, Prof. I.M. Low, contributed by project supervision and manuscript editing to the paper/publication entitled

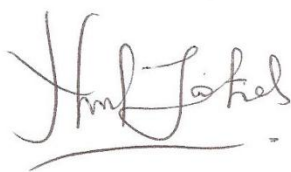
**Noor Azman, N.Z.**, Siddiqui, S.A., Ionescu, M., Low, I.M., Synthesis and characterization of ion-implanted epoxy composites for X-ray shielding, *Nuclear Instruments and Methods in Physics Research B: Beam Interactions with Materials and Atoms*, 287 (2012) 120–123

Undertaken with Nurul Zahirah Binti Noor Azman



(Signature of Co-Author)

I. M. Low



(Signature of First Author)

Nurul Zahirah Binti Noor Azman

8.2.6 Appendix B-6: Statement of Contribution of Others for “A comparative study of X-ray shielding capability in ion-implanted acrylic and glass”.

---

Statement of Contribution of Others for “A comparative study of X-ray shielding capability in ion-implanted acrylic and glass”.

28<sup>th</sup> July 2013

To Whom It May Concern

I, Dr. S.A. Siddiqui, contributed by specialist technical advice and instrument usage (general diagnostic radiology machine at Department of Imaging and Applied Physics, Curtin University) and also manuscript editing to the paper/publication entitled

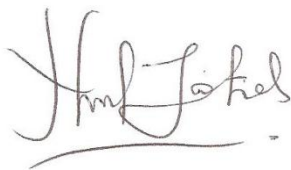
**Noor Azman, N.Z.**, Siddiqui, S.A., Ionescu, M., Low, I.M., A comparative study of X-ray shielding capability in ion-implanted acrylic and glass, *Radiation Physics and Chemistry*, 85 (2013) 102-106

Undertaken with Nurul Zahirah Binti Noor Azman



(Signature of Co-Author)

S.A. Siddiqui



(Signature of First Author)

Nurul Zahirah Binti Noor Azman

Statement of Contribution of Others for “A comparative study of X-ray shielding capability in ion-implanted acrylic and glass”.

28<sup>th</sup> July 2013

To Whom It May Concern

I, Dr. M. Ionescu, contributed by specialist technical service advice and instrument usage (ion-implantation, IBA and RBS at ANSTO) and manuscript editing to the paper/publication entitled

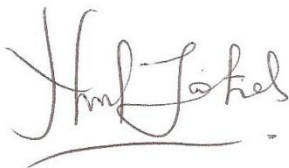
**Noor Azman, N.Z.**, Siddiqui, S.A., Ionescu, M., Low, I.M., A comparative study of X-ray shielding capability in ion-implanted acrylic and glass, *Radiation Physics and Chemistry*, 85 (2013) 102-106

Undertaken with Nurul Zahirah Binti Noor Azman

A handwritten signature in blue ink, appearing to read 'M. Ionescu'.

(Signature of Co-Author)

M. Ionescu

A handwritten signature in black ink, appearing to read 'Noor Azman'.

(Signature of First Author)

Nurul Zahirah Binti Noor Azman

Statement of Contribution of Others for “A comparative study of X-ray shielding capability in ion-implanted acrylic and glass”.

28<sup>th</sup> July 2013

To Whom It May Concern

I, Prof. I.M. Low, contributed by project supervision and manuscript editing to the paper/publication entitled

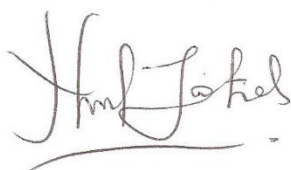
**Noor Azman, N.Z.**, Siddiqui, S.A., Ionescu, M., Low, I.M., A comparative study of X-ray shielding capability in ion-implanted acrylic and glass, *Radiation Physics and Chemistry*, 85 (2013) 102-106

Undertaken with Nurul Zahirah Binti Noor Azman



(Signature of Co-Author)

I. M. Low



(Signature of First Author)

Nurul Zahirah Binti Noor Azman

8.2.7 Appendix B-7: Statement of Contribution of Others for “Characteristics of X-ray attenuation in electrospun bismuth oxide / poly-lactic acid nanofibre mats”.

---



Statement of Contribution of Others for “Characteristics of X-ray attenuation in electrospun bismuth oxide / poly-lactic acid nanofibre mats”.

28<sup>th</sup> July 2013

To Whom It May Concern

I, Dr. S.A. Siddiqui, contributed by specialist technical advice and instrument usage (general diagnostic radiology machine at Department of Imaging and Applied Physics, Curtin University) and also manuscript editing to the paper/publication entitled

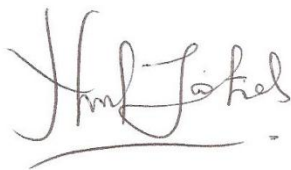
**Noor Azman, N.Z.**, Siddiqui, S.A., Haroosh, H.J., Albetran, H.M.M., Johannessen, B., Dong, Y., Low, I.M., Characteristics of X-ray attenuation in electrospun bismuth oxide / poly-lactic acid nanofibre mats, *Journal of Synchrotron Radiation*, 20 (2013) 741-748

Undertaken with Nurul Zahirah Binti Noor Azman



(Signature of Co-Author)

S.A. Siddiqui



(Signature of First Author)

Nurul Zahirah Binti Noor Azman

Statement of Contribution of Others for “Characteristics of X-ray attenuation in electrospun bismuth oxide / poly-lactic acid nanofibre mats”.

28<sup>th</sup> July 2013

To Whom It May Concern

I, H.J. Haroosh, contributed by specialist technical service advice and samples for electrospinning experiments to the paper/publication entitled

**Noor Azman, N.Z.**, Siddiqui, S.A., Haroosh, H.J., Albetran, H.M.M., Johannessen, B., Dong, Y., Low, I.M., Characteristics of X-ray attenuation in electrospun bismuth oxide / poly-lactic acid nanofibre mats, *Journal of Synchrotron Radiation*, 20 (2013) 741-748

Undertaken with Nurul Zahirah Binti Noor Azman



(Signature of Co-Author)

H.J. Haroosh



(Signature of First Author)

Nurul Zahirah Binti Noor Azman

Statement of Contribution of Others for “Characteristics of X-ray attenuation in electrospun bismuth oxide / poly-lactic acid nanofibre mats”.

28<sup>th</sup> July 2013

To Whom It May Concern

I, H.M.M. Albetran, contributed by specialist technical service advice and samples for electrospinning experiments to the paper/publication entitled

**Noor Azman, N.Z.**, Siddiqui, S.A., Haroosh, H.J., Albetran, H.M.M., Johannessen, B., Dong, Y., Low, I.M., Characteristics of X-ray attenuation in electrospun bismuth oxide / poly-lactic acid nanofibre mats, *Journal of Synchrotron Radiation*, 20 (2013) 741-748

Undertaken with Nurul Zahirah Binti Noor Azman



(Signature of Co-Author)

H.M.M. Albetran



(Signature of First Author)

Nurul Zahirah Binti Noor Azman

Statement of Contribution of Others for “Characteristics of X-ray attenuation in electrospun bismuth oxide / poly-lactic acid nanofibre mats”.

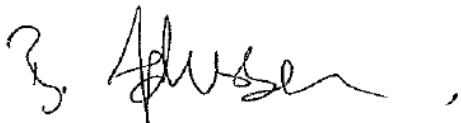
28<sup>th</sup> July 2013

To Whom It May Concern

I, Dr. B. Johannessen, contributed by specialist technical service advice and instrument usage (XAS at Australian Synchrotron) and also manuscript editing to the paper/publication entitled

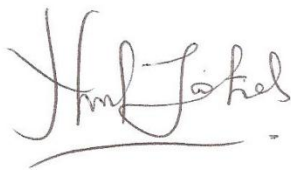
**Noor Azman, N.Z.**, Siddiqui, S.A., Haroosh, H.J., Albetran, H.M.M., Johannessen, B., Dong, Y., Low, I.M., Characteristics of X-ray attenuation in electrospun bismuth oxide / poly-lactic acid nanofibre mats, *Journal of Synchrotron Radiation*, 20 (2013) 741-748

Undertaken with Nurul Zahirah Binti Noor Azman



(Signature of Co-Author)

B. Johannessen



(Signature of First Author)

Nurul Zahirah Binti Noor Azman

Statement of Contribution of Others for “Characteristics of X-ray attenuation in electrospun bismuth oxide / poly-lactic acid nanofibre mats”.

28<sup>th</sup> July 2013

To Whom It May Concern

I, Dr. Y. Dong, contributed by specialist technical service advice and instrument usage (electrospinning machine) as well as manuscript editing to the paper/publication entitled

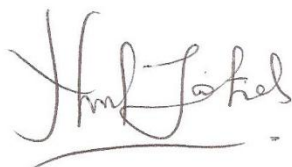
**Noor Azman, N.Z.**, Siddiqui, S.A., Haroosh, H.J., Albetran, H.M.M., Johannessen, B., Dong, Y., Low, I.M., Characteristics of X-ray attenuation in electrospun bismuth oxide / poly-lactic acid nanofibre mats, *Journal of Synchrotron Radiation*, 20 (2013) 741-748

Undertaken with Nurul Zahirah Binti Noor Azman

A handwritten signature in black ink, appearing to read 'dong' followed by a stylized flourish.

(Signature of Co-Author)

Y. Dong

A handwritten signature in black ink, appearing to read 'Nurul Zahirah Binti Noor Azman'.

(Signature of First Author)

Nurul Zahirah Binti Noor Azman

Statement of Contribution of Others for “Characteristics of X-ray attenuation in electrospun bismuth oxide / poly-lactic acid nanofibre mats”.

28<sup>th</sup> July 2013

To Whom It May Concern

I, Prof. I.M. Low, contributed by project supervision and manuscript editing to the paper/publication entitled

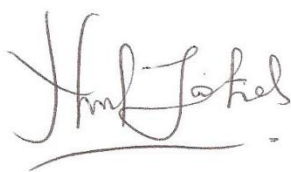
**Noor Azman, N.Z.**, Siddiqui, S.A., Haroosh, H.J., Albetran, H.M.M., Johannessen, B., Dong, Y., Low, I.M., Characteristics of X-ray attenuation in electrospun bismuth oxide / poly-lactic acid nanofibre mats, *Journal of Synchrotron Radiation*, 20 (2013) 741-748

Undertaken with Nurul Zahirah Binti Noor Azman



(Signature of Co-Author)

I. M. Low



(Signature of First Author)

Nurul Zahirah Binti Noor Azman

### Copyright Forms

#### 8.3.1 Appendix C-1: Elsevier Journal Articles

---

Copyright information relating to;

**Noor Azman, N.Z.**, Siddiqui, S.A., Hart, R., Low, I.M., Effect of particle size, filler loadings and X-ray energy on the X-ray attenuation ability of tungsten oxide – epoxy composites, *Applied Radiation and Isotopes*, 71 (2013) 62-67.

**Noor Azman, N.Z.**, Siddiqui, S.A., Ionescu, M., Low, I.M., Synthesis and characterization of ion-implanted epoxy composites for X-ray shielding, *Nuclear Instruments and Methods in Physics Research B: Beam Interactions with Materials and Atoms*, 287 (2012) 120–123.

**Noor Azman, N.Z.**, Siddiqui, S.A., Ionescu, M., Low, I.M., A comparative study of X-ray shielding capability in ion-implanted acrylic and glass, *Radiation Physics and Chemistry*, 85 (2013) 102-106.

**Noor Azman, N.Z.**, Siddiqui, S.A., Low, I.M., Characterisation of micro-sized and nano-sized tungsten oxide-epoxy composites for radiation shielding of diagnostic X-rays, *Materials Science and Engineering C*, In press.

Available on

<http://www.elsevier.com/journal-authors/author-rights-and-responsibilities>

## Rights & responsibilities

At Elsevier, we request transfers of copyright, or in some cases exclusive rights, from our journal authors in order to ensure that we have the rights necessary for the proper administration of electronic rights and online dissemination of journal articles. Authors and their employers retain (or are granted/transferred back) significant scholarly rights in their work. We take seriously our responsibility as the steward of the online record to ensure the integrity of scholarly works and the sustainability of journal business models, and we actively monitor and pursue unauthorized and unsubscribed uses and re-distribution (for subscription models).

In addition to [authors' scholarly rights](#), authors have certain responsibilities for their work, particularly in connection with [publishing ethics issues](#). View our webinar on [Ethics for Authors](#) for a useful resource of information.

As a journal author, you have rights for a large range of uses of your article, including use by your employing institute or company. These rights can be exercised without the need to obtain specific permission.

### How authors can use their own journal articles

Authors publishing in Elsevier journals have wide rights to use their works for teaching and scholarly purposes without needing to seek permission.

**Table of Authors' Rights**

	Preprint version (with a few exceptions- see below *)	Accepted Author Manuscript	Published Journal Articles
Use for classroom teaching by author or author's institution and presentation at a meeting or	Yes	Yes with full acknowledgement of final article	Yes with full acknowledgement of final article



<b>conference and distributing copies to attendees</b>			
<b>Use for internal training by author's company</b>	Yes	Yes with full acknowledgement of final article	Yes with full acknowledgement of final article
<b>Distribution to colleagues for their research use</b>	Yes	Yes	Yes
<b>Use in a subsequent compilation of the author's works</b>	Yes	Yes with full acknowledgement of final article	Yes with full acknowledgement of final article
<b>Inclusion in a thesis or dissertation</b>	Yes	Yes with full acknowledgement of final article	Yes with full acknowledgement of final article
<b>Reuse of portions or extracts from the article in other works</b>	Yes	Yes with full acknowledgement of final article	Yes with full acknowledgement of final article
<b>Preparation of derivative works (other than for commercial purposes)</b>	Yes	Yes with full acknowledgement of final article	Yes with full acknowledgement of final article
<b>Preprint servers</b>	Yes	Yes with the specific written permission of Elsevier	No
<b>Voluntary posting on open web sites operated by author or author's institution for scholarly purposes</b>	Yes (author may later add an appropriate bibliographic citation, indicating subsequent publication by Elsevier and journal title)	Yes, with appropriate bibliographic citation and a link to the article once published	Only with the specific written permission of Elsevier
<b>Mandated deposit or deposit in or posting to subject-oriented or centralized repositories</b>	Yes under specific agreement between Elsevier and the repository	Yes under specific agreement between Elsevier and the repository**	Yes under specific agreement between Elsevier and the repository
<b>Use or posting for commercial gain or to substitute for services</b>	Only with the specific written permission of Elsevier	Only with the specific written permission of	Only with the specific written permission of

provided directly by journal		Elsevier	Elsevier
------------------------------	--	----------	----------

### 8.3.2 Appendix C-2: John Wiley and Sons Articles

---

Copyright information relating to;

**Noor Azman, N.Z.**, Siddiqui, S.A., Hart, R., Low, I.M., Microstructured design of lead oxide-epoxy composites for radiation shielding purposes, *Journal of Applied Polymer Science*, 128 (2013) 3213-3219.

**JOHN WILEY AND SONS LICENSE  
TERMS AND CONDITIONS**

Jun 28, 2013

This is a License Agreement between Nurul Noor Azman ("You") and John Wiley and Sons ("John Wiley and Sons") provided by Copyright Clearance Center ("CCC"). The license consists of your order details, the terms and conditions provided by John Wiley and Sons, and the payment terms and conditions.

**All payments must be made in full to CCC. For payment instructions, please see information listed at the bottom of this form.**

License Number	3177600573501
License date	Jun 28, 2013
Licensed content publisher	John Wiley and Sons
Licensed content publication	Journal of Applied Polymer Science
Licensed content title	Microstructural design of lead oxide epoxy composites for radiation shielding purposes
Licensed copyright line	Copyright © 2012 Wiley Periodicals, Inc.
Licensed content author	Nurul Zahirah Noor Azman,Salim Ahmed Siddiqui,Robin Hart,It Meng Low
Licensed content date	Sep 20, 2012
Start page	3213
End page	3219
Type of use	Dissertation/Thesis
Requestor type	Author of this Wiley article
Format	Print and electronic
Portion	Full article
Will you be translating?	No
Total	0.00 USD
Terms and Conditions	

**TERMS AND CONDITIONS**

This copyrighted material is owned by or exclusively licensed to John Wiley & Sons, Inc. or one of its group companies (each a "Wiley Company") or a society for whom a Wiley Company has exclusive publishing rights in relation to a particular journal (collectively "WILEY"). By clicking "accept" in connection with completing this licensing transaction, you agree that the following terms and conditions apply to this transaction (along with the billing and payment terms and conditions established by the Copyright Clearance Center Inc., ("CCC's Billing and Payment terms and conditions"), at the time that you opened your RightsLink account (these are available at any time at <http://myaccount.copyright.com>).

### 8.3.3 Appendix C-3: Springer

---

Copyright information relating to;

**Noor Azman, N.Z.**, Siddiqui, S.A., Low, I.M., Synthesis and characterization of epoxy composites filled with Pb, Bi or W compound for shielding of diagnostic X-rays, *Applied Physics A: Materials Science & Processing*, 110, (2013) 137-144.

**SPRINGER LICENSE  
TERMS AND CONDITIONS**

Jun 28, 2013

This is a License Agreement between Nurul Noor Azman ("You") and Springer ("Springer") provided by Copyright Clearance Center ("CCC"). The license consists of your order details, the terms and conditions provided by Springer, and the payment terms and conditions.

**All payments must be made in full to CCC. For payment instructions, please see information listed at the bottom of this form.**

License Number	3177600427826
License date	Jun 28, 2013
Licensed content publisher	Springer
Licensed content publication	Applied Physics A: Materials Science & Processing
Licensed content title	Synthesis and characterization of epoxy composites filled with Pb, Bi or W compound for shielding of diagnostic x-rays
Licensed content author	Nurul Z. Noor Azman
Licensed content date	Jan 1, 2012
Volume number	110
Issue number	1
Type of Use	Thesis/Dissertation
Portion	Full text
Number of copies	4
Author of this Springer article	Yes and you are the sole author of the new work
Order reference number	
Title of your thesis / dissertation	Design of Nanostructured Polymeric Materials for Radiation Shielding of Ionizing Radiations
Expected completion date	Sep 2013
Estimated size(pages)	150
Total	0.00 USD

**Terms and Conditions**

**Introduction**

The publisher for this copyrighted material is Springer Science + Business Media. By clicking "accept" in connection with completing this licensing transaction, you agree that the following terms and conditions apply to this transaction (along with the Billing and Payment terms and conditions established by Copyright Clearance Center, Inc. ("CCC"), at the time that you opened your Rightslink account and that are available at any time at <http://myaccount.copyright.com>).

**Limited License**

With reference to your request to reprint in your thesis material on which Springer Science

#### 8.3.4 Appendix C-4: (IUCr) Synchrotron Radiation Online

---

Copyright information relating to;

**Noor Azman, N.Z.**, Siddiqui, S.A., Haroosh, H.J., Albetran, H.M.M., Johannessen, B., Dong, Y., Low, I.M., Characteristics of X-ray attenuation in electrospun bismuth oxide / poly-lactic acid nanofibre mats, *Journal of Synchrotron Radiation*, 20 (2013) 741-748.

Available on

<http://journals.iucr.org/s/services/authorservices.html>

Synchrotron  
**Radiation**  
Online



Journals **Online**  
search  
help  
subscribe

supplementary files  
contact us  
terms of use  
site index

## copyright policy

Authorship of a scientific article is associated with certain intellectual property rights, protected within the framework of copyright laws. Under the most widespread international agreement, the Berne Convention, copyright in an article automatically belongs to the creator or creators of the article, except for works performed 'for hire', in which case the employer or funding body may own the copyright in the work. Often that copyright is formally transferred to the publisher in the case of a scientific article accepted for publication. This allows the publisher to manage permissions and other functions on behalf of the author; the author, however, retains extensive rights of fair use to the original material. Sometimes, however, the author (or the author's employer or funding body) retains copyright, and licenses the publisher to discharge certain specific rights of dissemination and redistribution. Also, especially for the results of government-funded research, copyright is sometimes waived.

## Author rights after acceptance

### IUCr copyright

Articles for which the authors have transferred copyright to the IUCr carry a statement

© International Union of Crystallography

on their initial page.

Provided that a full bibliographic reference to the article as published in an IUCr journal is made, **authors** of such articles may, without needing to seek permission from the IUCr:

- share print or electronic copies of the article with colleagues;
- use all or part of the article and abstract, without revision or modification, in personal compilations or other publications of their own work;
- use the article within their employer's institution or company for educational or research purposes, including use in course packs;
- post an [authorised electronic reprint](#) of the article on their own personal website, on their employer's website/repository and on free public servers in their subject area.

**Readers** of such articles may, without needing to seek permission from the IUCr:



- save to hard disk a local copy of the article for their personal use;
- print off one or more copies of individual articles for their personal use (they may **not** systematically download multiple articles or disseminate copies to third parties);
- include brief extracts from the article or abstract, without revision or modification, in their own publications so long as the original source is acknowledged and a full bibliographic reference given.

For all other uses, please see the page "[Permissions requests](#)".

### Supplementary materials and supporting data

It is the practice of IUCr journals to provide free access to all supplementary materials and supporting data files deposited with a published article. Copyright in supplementary materials that represent an author's creative work (*e.g.* mathematical appendices, extended discussion, additional figures) will follow that of the primary article, *i.e.* transferred to the IUCr or reserved by the author. Copyright protection is not extended to files of scientific data (*e.g.* structural data CIFs, structure factors, primary diffraction images), and such data sets may be used for *bona fide* research purposes within the scientific community so long as proper attribution is given to the source from which they were obtained.

### Useful links

- [Transfer of Copyright Agreement](#)
- [Licence to Publish Agreement](#)
- [Detailed statement of author rights](#)
- [Permissions requests](#)
- [Obtaining copyright permission for published works](#)

---

The International Union of Crystallography is a non-profit scientific union serving the world-wide interests of crystallographers and other scientists employing crystallographic methods.

**Crystallography Journals** [Online partners](#) and [site credits](#).

Copyright © International Union of Crystallography  
[IUCr Webmaster](#)

## BIBLIOGRAPHY

---

Abdel-Aziz, M.M., Badran, A.S., Abdel-Hakem, A.A., Helaly, F.M. & Moustafa, A.B. 1991, 'Styrene–butadiene rubber/lead oxide composites as gamma radiation shields', *Journal of Applied Polymer Science*, vol. 42, no. 4, pp. 1073-80.

Abdel-Rahman, W. & Podgorsak, E.B. 2010, 'Energy transfer and energy absorption in photon interactions with matter revisited: A step-by-step illustrated approach', *Radiation Physics and Chemistry*, vol. 79, no. 5, pp. 552-66.

Akkurt, I., Mavi, B., Akkurt, A., Basyigit, C., Kilincarslan, S. & Yalim, H.A. 2005, 'Study on dependence of partial and total mass attenuation coefficients', *Journal of Quantitative Spectroscopy and Radiative Transfer*, vol. 94, no. 3–4, pp. 379-85.

Al-Maamori, M.H., Al-Bodairy, O.H. & Saleh, N.A. 2012, 'Effect of PbO with rubber composite on transmission of (X-ray)', *Academic Research International*, vol. 3, no. 3, pp. 113-9.

An, J.S., Park, J.S., Kim, J.R. & Hong, K.S. 2006, 'Effects of Bi<sub>2</sub>O<sub>3</sub> and Na<sub>2</sub>O on the thermal and dielectric properties of zinc borosilicate glass for plasma display panels', *Journal of the American Ceramic Society*, vol. 89, pp. 3658-61.

Anders, A. 1997, 'Ion charge state distributions of vacuum arc plasmas: The origin of species', *Physical Review E*, vol. 55, no. 1, pp. 969-81.

Andreopoulos, A.G. & Papanicolaou, G.C. 1987, 'Rubber-modified polymer composites', *Journal of Materials Science*, vol. 22, no. 9, pp. 3417-20.

*Annual Book of ASTM Standards Vol. 08.01, ASTM*. 2005.

Archer, B.R. 1995, 'History of the shielding of diagnostic X-ray facilities.', *Health Phys*, vol. 69, no. 5, pp. 750-8.

Archer, B.R. 2005, 'Recent history of the shielding of medical X-ray imaging facilities.', *Health Phys*, vol. 88, no. 6, pp. 579-86.

Archer, B.R., Thornby, J.I. & Bushong, S.C. 1983, 'Diagnostic X-ray shielding design based on an empirical model of photon attenuation.', *Health Phys*, vol. 44, no. 5, pp. 507-17.

Arjula, S., Harsha, A. & Ghosh, M. 2008, 'Solid-particle erosion behavior of high-performance thermoplastic polymers', *Journal of Materials Science*, vol. 43, no. 6, pp. 1757-68.

Attix, F.H. 1986, *Introduction to Radiological Physics and Radiation Dosimetry*, John Wiley and Sons, New York, United States.

Australian Standards 1774.5 1989, *Method 5. The determination of density, porosity and water absorption*.

Baltaş, H., Çelik, Ş., Çevik, U. & Yanmaz, E. 2007, 'Measurement of mass attenuation coefficients and effective atomic numbers for superconductor using X-ray energies', *Radiation Measurements*, vol. 42, no. 1, pp. 55-60.

Baltaş, H., Çevik, U., Tıraşoğlu, E., Ertuğral, B., Apaydın, G. & Kobya, A.İ. 2005, 'Mass attenuation coefficients of YBaCuO and BiPbSrCaCuO superconductors at 511, 661 and 1274 keV energies', *Radiation Measurements*, vol. 39, no. 1, pp. 33-7.

Berger, M.J., Hubbell, J.H., Seltzer, S.M., Chang, J., Coursey, J.S., Sukumar, R., Zucker, D.S. & Olsen, K. 2010, *XCOM: Photon Cross Section Database (version 1.5)*, National Institute of Standards and Technology, Gaithersburg, MD., <<http://physics.nist.gov/xcom>>.

*Bismuth oxide*, 2013, Chemicalland21, viewed 1 May 2013,

<<http://chemicalland21.com/lifescience/uh/BISMUTH%20OXIDE.htm>>.

Botelho, M.Z., Künzel, R., Okuno, E., Levenhagen, R.S., Basegio, T. & Bergmann, C.P. 2011, 'X-ray transmission through nanostructured and microstructured CuO materials', *Applied Radiation and Isotopes*, vol. 69, no. 2, pp. 527-30.

Brettmann, B.K., Tsang, S., Forward, K.M., Rutledge, G.C., Myerson, A.S. & Trout, B.L. 2012, 'Free surface electrospinning of fibres containing microparticles', *Langmuir*, vol. 28, no. 25, pp. 9714-21.

Buyuk, B., Tugrul, A.B., Akarsu, A.C. & Addemir, A.O. 2012, 'Investigation on the effects of titanium diboride particle size on radiation shielding properties of titanium diboride reinforced boron carbide-silicon carbide composites', *J. Nano- and Electronic Physics*, vol. 4, no. 1, pp. 01010(1)-(4).

Chanthima, N., Kaekwkhao, J., Kedkaew, C., Chewpraditkul, W., Pokaipisit, A. & Limsuwan, P. 2011, 'Study on interaction of Bi<sub>2</sub>O<sub>3</sub>, PbO and BaO in silicate glass system at 662 keV for development of gamma-rays shielding materials', *Progress in Nuclear Science and Technology*, vol. 1, pp. 106-9.

Chapman, R. & Mulvaney, P. 2001, 'Electro-optical shifts in silver nanoparticle films', *Chemical Physics Letters*, vol. 349, no. 5–6, pp. 358-62.

*Chapter 6 Modern Technology*, 2012, viewed 22 May 2013,  
<<http://www.physics.hku.hk/~phys0607/lectures/chap06.html>>.

Chen, J.S., Lau, S.P., Sun, Z., Tay, B.K., Yu, G.Q., Zhu, F.Y., Zhu, D.Z. & Xu, H.J. 2001, 'Structural and mechanical properties of nitrogen ion implanted ultra high molecular weight polyethylene', *Surface and Coatings Technology*, vol. 138, no. 1, pp. 33-8.

Chen, S.S., Chen, H.C., Wang, W.C., Lee, C.Y., Lin, I.N., Guo, J. & Chang, C.L. 2013, 'Effects of high energy Au-ion irradiation on the microstructure of diamond films', *Journal of Applied Physics*, vol. 113, no. 11, pp. 113704-10.

Chowdhury, M. & Stylios, G. 2010, 'Effect of experimental parameters on the morphology of electrospun Nylon 6 fibres', *International Journal of Basic & Applied Sciences*, vol. 10, no. 06, pp. 116-31.

*Control Windows*, 2000-2010, viewed 31 May 2013,  
<[http://www.raybar.com/cntrl\\_wndws.htm#clr\\_acryl](http://www.raybar.com/cntrl_wndws.htm#clr_acryl)>.

Daren, S. 2004, *Polymer versus Glass*, POLYMICRO Newsletter, viewed 16 July 2011,  
< <http://www.polymicro-cc.com>>

*Data sheet lead glass (X-ray protection)*, UQG Optics, viewed 31 May 2013,  
<<http://www.uqgoptics.com/pdf/Lead%20Glass.pdf>>.

Deitzel, J.M., Kleinmeyer, J., Harris, D. & Beck Tan, N.C. 2001, 'The effect of processing variables on the morphology of electrospun nanofibres and textiles', *Polymer*, vol. 42, no. 1, pp. 261-72.

Demir, M.M., Gulgun, M.A., Menciloglu, Y.Z., Erman, B., Abramchuk, S.S., Makhaeva, E.E., Khokhlov, A.R., Matveeva, V.G. & Sulman, M.G. 2004, 'Palladium nanoparticles by electrospinning from poly(acrylonitrile-co-acrylic acid)-PdCl<sub>2</sub> solutions. Relations between preparation conditions, particle size, and catalytic activity', *Macromolecules*, vol. 37, pp. 1787-92.

Di Girolamo, G., Massaro, M., Piscopiello, E., Pesce, E., Esposito, C., Tapfer, L. & Vittori Antisari, M. 2008, 'Strain sensitivity in ion-implanted polymers', *MRS Online Proceedings Library*, vol. 1134, pp. 1134-BB08-13.

Di Girolamo, G., Massaro, M., Piscopiello, E. & Tapfer, L. 2010, 'Metal ion implantation in inert polymers for strain gauge applications', *Nuclear Instruments and Methods in Physics Research Section B: Beam Interactions with Materials and Atoms*, vol. 268, no. 19, pp. 2878-82.

Dworecki, K., Drabik, M., Hasegawa, T. & Wąsik, S. 2004, 'Modification of polymer membranes by ion implantation', *Nuclear Instruments and Methods in Physics Research Section B: Beam Interactions with Materials and Atoms*, vol. 225, no. 4, pp. 483-8.

El Haber, F. & Froyer, G. 2008, 'Transparent polymers embedding nanoparticles for X-rays attenuation (Review)', *Journal of the University of Chemical Technology and Metallurgy*, vol. 43, no. 3, pp. 283-90.

Erdem, M., Baykara, O., Dogru, M. & Kuluozturk, F. 2010, 'A novel shielding material prepared from solid waste containing lead for gamma ray', *Radiation Physics and Chemistry*, vol. 79, no. 9, pp. 917-22.

Evans, P.J., Hyvarinen, J. & Samandi, M. 1995, 'Surface modification of austenitic stainless steel by titanium ion implantation', *Surface and Coatings Technology*, vol. 71, pp. 151-8.

Edward, W.W. 1966, 'Experiments with medium- Z materials for shielding against low-energy X rays', *Radiology*, vol. 86, p. 146.

Fabiani, D., Montanari, G.C., Krivda, A., Schmidt, L.E. & Hollertz, R. 2010, 'Epoxy based materials containing micro and nano sized fillers for improved electrical characteristics', paper presented to 2010 International Conference on Solid Dielectrics, Potsdam, Germany.

Faccini, M., Vaquero, C. & Amantia, D. 2012, 'Development of protective clothing against nanoparticle based on electrospun nanofibres', *J. Nanomaterials*, vol. 2012, pp. 1-9.

Farrington, D.W., Lunt, J., Davies, S. & Blackburn, R.S. 2005, 'Biodegradable and sustainable fibres', in *Poly (lactic acid) fibres*, Woodhead Publishing Series in Textiles, Cambridge, United Kingdom, pp. 191-220, <[http://jimluntllc.com/pdfs/polylactic\\_fibres.pdf](http://jimluntllc.com/pdfs/polylactic_fibres.pdf)>.

Fuh, Y.K. & Lien, L.C. 2013, 'Pattern transfer of aligned metal nano/microwires as flexible transparent electrodes using an electrospun nanofibre template', *Nanotechnology*, vol. 24, no. 5, p. 055301.

Gerward, L. 1992, 'Theoretical upper and lower limits to experimental X-ray attenuation coefficients', *Nuclear Inst. and Methods in Physics Research, B*, vol. 69, no. 4, pp. 407-12.

Gowda, S., Krishnaveni, S., Yashoda, T., Umesh, T.K. & Gowda, R. 2004, 'Photon mass attenuation coefficients, effective atomic numbers and electron densities of some thermoluminescent dosimetric compounds', *Pramana - Journal of Physics*, vol. 63, no. 3, pp. 529-41.

Granmayeh Rad, A., Abbasi, H. & Afzali, M.H. 2011, 'Gold nanoparticles: synthesizing, characterizing and reviewing novel application in recent years', *Physics Procedia*, vol. 22, no. 0, pp. 203-8.

Haiwen, X., Kai-Zhong, G., Yiming, S. & Song, X. 2006, 'Precessional dynamics of single-domain magnetic nanoparticles driven by small ac magnetic fields', *Journal of Physics D: Applied Physics*, vol. 39, no. 22, p. 4746.

Harish, V., Nagaiah, N. & Harish Kumar, H.G. 2012, 'Lead oxide filled isophthalic resin polymer composites for gamma radiation shielding applications', *Indian Journal of Pure and Applied Physics*, vol. 50, pp. 847-50.

Harish, V., Nagaiah, N., Prabhu, T.N. & Varughese, K.T. 2009, 'Preparation and characterization of lead monoxide filled unsaturated polyester based polymer composites for gamma radiation shielding applications', *Journal of Applied Polymer Science*, vol. 112, no. 3, pp. 1503-8.

Haroosh, H.J., Chaudhary, D.S. & Dong, Y. 2012, 'Electrospun PLA/PCL fibres with tubular nanoclay: Morphological and structural analysis', *Journal of Applied Polymer Science*, vol. 124, no. 5, pp. 3930-9.

Hoheisel, M., Bernhardt, P., Lawaczeck, R. & Pietsch, H. 2006, 'Comparison of polychromatic and monochromatic X-rays for imaging', *Proceedings of the SPIE*, vol. 6142, pp. 71-8.

Holmes-Siedle, A. & Adams, L. 2002, *Hand Book of Radiation Effects*, 2<sup>nd</sup> ed., Oxford University Press: England.

Holyńska, B. 1969, 'Grain size effect in low energy gamma and X-ray scattering', *Spectrochimica Acta Part B: Atomic Spectroscopy*, vol. 24, no. 1, pp. 85-93.

Hu, W., Huang, Z.M. & Liu, X.Y. 2010, 'Development of braided drug-loaded nanofibre sutures', *Nanotechnology*, vol. 21, no. 31, p. 315104.

Huang, S., Kang, X., Cheng, Z., Ma, P., Jia, Y. & Lin, J. 2012, 'Electrospinning preparation and drug delivery properties of Eu<sup>3+</sup>/Tb<sup>3+</sup> doped mesoporous bioactive glass nanofibres', *J Colloid Interface Sci*, vol. 387, no. 1, pp. 285-91.

Huang, X. & El-Sayed, M.A. 2010, 'Gold nanoparticles: Optical properties and implementations in cancer diagnosis and photothermal therapy', *Journal of Advanced Research*, vol. 1, no. 1, pp. 13-28.

Hubler, G.K. 1981, 'Use of ion beam analysis in metal modification by means of ion implantation', *Nuclear Instruments and Methods in Physics Research*, vol. 191, no. 1-3, pp. 101-13.



Hussain, R., Haq, Z.-U. & Mohammad, D. 1997, 'A study of the shielding properties of poly ethylene glycol-lead oxide composite', *Journal of Islamic Academy of Sciences*, vol. 10, no. 3, pp. 81-4.

*Hybrid polymer X-ray shielding material*, 2010, viewed 24 June 2013, <<http://www.canlaser.com/en/XRay.aspx>>.

Içelli, O., Erzeneoglu, S. & Boncukçuoğlu, R. 2003, 'Measurement of mass attenuation coefficients of some boron compounds and the trommel sieve waste in the energy range 15.746-40.930 keV', *Journal of Quantitative Spectroscopy and Radiative Transfer*, vol. 78, no. 2, pp. 203-10.

Içelli, O., Erzeneoglu, S. & Boncukçuoğlu, R. 2004, 'Experimental studies on measurements of mass attenuation coefficients of boric acid at different concentration', *Annals of Nuclear Energy*, vol. 31, no. 1, pp. 97-106.

*Interaction of radiation with matter:attenuation coefficients*, 2010, viewed 31 May 20113, <[http://inst.nuc.berkeley.edu/NE107/Lectures/Interactions\\_NE107\\_Fall10.pdf](http://inst.nuc.berkeley.edu/NE107/Lectures/Interactions_NE107_Fall10.pdf)>.

*Interactions of photons with matter*, viewed 31 May 2013, <[http://ocw.mit.edu/courses/nuclear-engineering/22-01-introduction-to-ionizing-radiation-fall-2006/lecture-notes/energy\\_dep\\_photo.pdf](http://ocw.mit.edu/courses/nuclear-engineering/22-01-introduction-to-ionizing-radiation-fall-2006/lecture-notes/energy_dep_photo.pdf)>.

Jackson, P., Periasamy, S., Bansal, V. & Geso, M. 2011, 'Evaluation of the effects of gold nanoparticle shape and size on contrast enhancement in radiological imaging', *Australasian Physical & Engineering Science in Medicine*, vol. 34, no. 2, pp. 243-9.

Jayalakshmi, M., Mohan Rao, M. & Kim, K.B. 2006, 'Effect of particle size on the electrochemical capacitance of  $\alpha$ -Ni(OH)<sub>2</sub> in alkali solutions', *International Journal of Electrochemical Science*, no. 1, pp. 324-33.

Karim, A., Amis, E., Yurekli, K., Krishnamoorti, R. & Meredith, C. 2002, 'Combinatorial methods for polymer materials science: Phase behavior of nanocomposite blend films', *Polymer Engineering and Science*, vol. 42, no. 9, pp. 1836-40.

Kim, J.K. & Robertson, R.E. 1992, 'Toughening of thermoset polymers by rigid crystalline particles', *Journal of Materials Science*, vol. 27, no. 1, pp. 161-74.

Koen H.A., Janssens. R.E. & Van Grieken 2004, *Non-destructive microanalysis of cultural heritage materials*, Elsevier, Amsterdam, The Netherlands.

Kozlov, E.V., Ryabchikov, A.I., Sharkeev, Y.P., Stepanov, I.B., Fortuna, S.V., Sivin, D.O., Kurzina, I.A., Prokopova, T.S. & Mel'nik, I.A. 2002, 'Formation of intermetallic layers at high intensity ion implantation', *Surface and Coatings Technology*, vol. 158-159, pp. 343-8.

Künzel, R. & Okuno, E. 2012, 'Effects of the particle sizes and concentrations on the X-ray absorption by CuO compounds', *Applied Radiation and Isotopes*, vol. 70, no. 4, pp. 781-4.

Kurudirek, M., Özdemir, Y., Simsek, Ö. & Durak, R. 2010, 'Comparison of some lead and non-lead based glass systems, standard shielding concretes and commercial window glasses in terms of shielding parameters in the energy region of 1 keV-100 GeV: A comparative study', *Journal of Nuclear Materials*, vol. 407, no. 2, pp. 110-5.

Lablogic. 2009, *Radiation Safety & Consumable Products*, Lablogic, Sheffield, United Kingdom, brochure, viewed 31 January 2013, <[http://www.lablogic.com/moreinfo/PDF/consumables/lablogic\\_consumables\\_brochure.pdf](http://www.lablogic.com/moreinfo/PDF/consumables/lablogic_consumables_brochure.pdf)>.

*Lead Acrylic*, 2013, viewed 31 May 2013, <<http://marshield.com/medical-shielding/lead-acrylic/>>.

*Lead glass for X-ray / radiation shielding*, 2009, viewed 31 May 2013, <[http://www.afabxray.com/lead\\_glass.htm](http://www.afabxray.com/lead_glass.htm)>.

*Lead X-ray glass*, 2013, viewed 31 May 2013,  
<<http://www.radiationproducts.com/leaded-glass.htm>>.

*Lead X-ray glass vs. lead plastic acrylic*, 2013, viewed 31 May 2013,  
<<http://www.marshield.com/nuclear-shielding/leaded-x-ray-shielding-glass-and-acrylic>>.

*Leaded glass for X-ray shielding*, viewed 31 May 2013,  
<<http://www.drct.com/dss/shielding/leadglass.html>>.

Lee, E.H., Rao, G.R., Lewis, M.B. & Mansur, L., K. 1993, 'Ion beam application for improved polymer surface properties. ', *Nuclear Instruments and Methods in Physics Research Section B: Beam Interactions with Materials and Atoms*, vol. 74, pp. 326-30.

Lee, S. & Obendorf, S.K. 2007, 'Use of electrospun nanofibre web for protective textile materials as barriers to liquid penetration', *Textile Research Journal*, vol. 77, no. 9, pp. 696-702.

Lines, M.G. 2008, 'Nanomaterials for practical functional uses', *Journal of Alloys and Compounds*, vol. 449, no. 1-2, pp. 242-5.

Liu, L., He, L., Yang, C., Zhang, W., Jin, R.-G. & Zhang, L.-Q. 2004, 'In situ reaction and radiation protection properties of Gd(AA)<sub>3</sub>/NR composites', *Macromolecular Rapid Communications*, vol. 25, pp. 1197-202.

Lopatin, C.M., Alford, T.L., Pizziconi, V.B., Kuan, M. & Laursen, T. 1998, 'Ion-beam densification of hydroxyapatite thin films', *Nuclear Instruments and Methods in Physics Research Section B: Beam Interactions with Materials and Atoms*, vol. 145, no. 4, pp. 522-31.

Lu, X., Zhao, Y. & Ce, W. 2005, 'Fabrication of PbS nanoparticles in polymer-fibre matrices by electrospinning', *Advanced Materials*, vol. 17, pp. 2485-8.

Martínez Ripoll, M. & Félix Hernández, C. 2013, *X-rays*, viewed 04 June 2013,

<[http://www.xtal.iqfr.csic.es/Cristalografia/parte\\_02-en.html](http://www.xtal.iqfr.csic.es/Cristalografia/parte_02-en.html)>.

Mayer, M. 1999, *Proceedings of the 15th International Conference on the Application of Accelerators in Research and Industry*, J. L. Duggan and I.L. Morgan (eds.), American Institute of Physics Conference Proceedings 475, p. 541.

Molamma, P.P., Venugopal, J., Casey, K.C. & Ramakrishna, S. 2008, 'Surface modified electrospun nanofibrous scaffolds for nerve tissue engineering', *Nanotechnology*, vol. 19, no. 45, p. 455102.

Moloney, A.C., Kausch, H.H., Kaiser, T. & Beer, H.R. 1987, 'Review -Parameters determining the strength and toughness of particulate filled epoxide resins', *Journal of Materials Science*, vol. 22, pp. 381-93.

Nambiar, S., Osei, E. & Yeow, J. 2011, 'MO-F-BRA-01: Polymer Composite-Based Shielding of Diagnostic X-rays', *Medical physics*, vol. 38, no. 6, p. 3720.

Nambiar, S., Osei, E.K. & Yeow, J.T.W. 2013, 'Polymer nanocomposite-based shielding against diagnostic X-rays', *Journal of Applied Polymer Science*, vol. 127, no. 6, pp. 4939-46.

Ohno, K., Koh, K.M., Tsujii, Y. & Fukuda, T. 2002, 'Synthesis of gold nanoparticles coated with well-defined, high-density polymer brushes by surface-initiated living radical polymerization', *Macromolecules*, vol. 35, no. 24, pp. 8989-93.

Okunade, A.A. 2002, 'Comparison of lead attenuation and lead hardening equivalence of materials used in respect of diagnostic X-ray shielding', *Applied Radiation and Isotopes*, vol. 57, no. 6, pp. 819-24.

Osei-Mensah, W., John, J.F. & Danso, K.A. 2012, 'Assessment of radiation shielding properties of polyester steel composite using MCNP5 ', *International Journal of Science and Technology*, vol. 2, no. 2, pp. 455-61.

*Other ray-bar products*, 2000-2010, viewed 14 April 2013,  
<[http://www.raybar.com/other\\_prd.htm](http://www.raybar.com/other_prd.htm)>.

Park, J.J. 2013, 'Effect of particle size on the mechanical and electrical properties of epoxy/spherical silica composites', *Transactions On Electrical And Electronic Materials*, vol. 14, no. 1, pp. 39-42.

Patra, C.R., Bhattacharya, R., Mukhopadhyay, D. & Mukherjee, P. 2010, 'Fabrication of gold nanoparticles for targeted therapy in pancreatic cancer', *Advanced Drug Delivery Reviews*, vol. 62, no. 3, pp. 346-61.

Pavlenko, V.I., Lipkanskii, V.M. & Yastrebinskii, P.N. 2004, 'Calculations of the passage of gamma-quanta through a polymer radiation-protective composite', *Journal of Engineering Physics and Thermophysics*, vol. 77, pp. 11-4.

*Poly tungsten radiation shielding*, 1997-2013, viewed 31 May 2013,  
<<http://www.poly-tungsten.com/Tungsten-poly-radiation-shielding.html>>.

Popok, V.N. 2012, 'Ion implantation of polymers: formation of nanoparticulate materials', *Review Advanced Materials Science*, vol. 30, pp. 1-26.

Popov, A. 2009, 'Sun protection using nanoparticles', *SPIE Newsroom*, vol. 24, pp. 1-2.

Rajeswari, R., Jayarama Reddy, V., Subramanian, S., Shayanti, M., Radhakrishnan, S. & Seeram, R. 2012, 'Minimally invasive injectable short nanofibres of poly(glycerol sebacate) for cardiac tissue engineering', *Nanotechnology*, vol. 23, no. 38, p. 385102.

Robert, R.D. 2005, 'High density composites replace lead', *Ecomass Technologies*, viewed 6 July 2012,  
<<http://www.ecomass.com/pdf/High%20Density%20Composites%20Replace%20Lead.pdf>>.

Rodríguez, R.J., Medrano, A., García, J.A., Fuentes, G.G., Martínez, R. & Puertolas, J.A. 2007, 'Improvement of surface mechanical properties of polymers by helium ion implantation', *Surface and Coatings Technology*, vol. 201, no. 19–20, pp. 8146-9.

Russo, G. & Lamberti, G. 2011, 'Electrospinning of drug-loaded polymer systems: Preparation and drug release', *Journal of Applied Polymer Science*, vol. 122, no. 6, pp. 3551-6.

Sahare, P.D., Ranju, R., Numan, S. & Lochab, S.P. 2007, ' $K_3Na(SO_4)_2$ : Eu nanoparticles for high dose of ionizing radiation', *Journal of Physics D: Applied Physics*, vol. 40, no. 3, p. 759.

Schmid, E., Panzer, W., Schlattl, H. & Eder, H. 2012, 'Emission of fluorescent x-radiation from non-lead based shielding materials of protective clothing: a radiobiological problem?', *Journal of Radiological Protection*, vol. 32, no. 3, p. N129.

Shanshan, B., Jayaram, S.H. & Cherney, E.A. 2010, 'Use of electrospinning to disperse nanosilica into silicone rubber', in *Electrical Insulation and Dielectric Phenomena (CEIDP), 2010 Annual Report Conference on*, pp. 1-4.

Sill, T.J. & von Recum, H.A. 2008, 'Electrospinning: Applications in drug delivery and tissue engineering', *Biomaterials*, vol. 29, no. 13, pp. 1989-2006.

Soares, M.R.F., Alegaonkar, P., Behar, M., Fink, D. & Müller, M. 2004, ' $^6Li^+$  ion implantation into polystyrene', *Nuclear Instruments and Methods in Physics Research Section B: Beam Interactions with Materials and Atoms*, vol. 218, no. 0, pp. 300-7.

Sprawls, P. 1993, *The Physical Principles of Medical Imaging*, 2nd edition edn, Interaction of Radiation with Matter, Aspen Publishers, Gaithersburg, Md.

Spinks, J.W.T. & Wood, R.J. 1976, *An introduction to radiation chemistry*, 2nd edition edn, Wiley-Interscience, New York.

Steinhart, M. 2004, 'Introduction to Nanotechnology. By Charles P. Poole, Jr. and Frank J. Owens', *Angewandte Chemie International Edition*, vol. 43, no. 17, pp. 2196-7.

Stepanov, A.L., Khaibullin, R.I., Can, N., Ganeev, R.A., Ryasnyansky, A.I., Buchal, C. & Uysal, S. 2004, 'Application of ion implantation for synthesis of copper nanoparticles in a zinc oxide matrix for obtaining new nonlinear optical materials', *Technical Physics Letters*, vol. 30, no. 10, pp. 846-9.

Storrie, H. & Mooney, D.J. 2006, 'Sustained delivery of plasmid DNA from polymeric scaffolds for tissue engineering', *Advanced Drug Delivery Reviews*, vol. 58, no. 4, pp. 500-14.

Suk, C.C., Wei, L.J. & Harun, A.Z. 2012, 'Evaluation of X-ray beam quality based on measurements and estimations using SpekCalc and Ipem78 models', *Malays J Med Sci.*, vol. 19, no. 3, pp. 22-8.

Sutton, D.G., Martin, C.J., Peet, D. & Williams, J.R. 2012, 'The characterization and transmission of scattered radiation resulting from X-ray beams filtered with zero to 0.99 mm copper', *Journal of Radiological Protection*, vol. 32, no. 2, p. 117.

Taylor, G. 1969, 'Electrically Driven Jets', *Proceedings of the Royal Society of London. A. Mathematical and Physical Sciences*, vol. 313, no. 1515, pp. 453-75.

*Technology: Electrospinning* 2007-2012, Neotherix Ltd., viewed 24 April 2013, <<http://www.neotherix.com/technology.php>>.

Teli, M.T., Nathuram, R. & Mahajan, C.S. 2000, 'Single-experiment simultaneous-measurement of elemental mass-attenuation coefficients of hydrogen, carbon and oxygen for 0.123–1.33 MeV gamma rays', *Radiation Measurements*, vol. 32, no. 4, pp. 329-33.

Thomas, S.C., James, E.D. & Robert, C.M. 1990, 'Basic interactions between X rays and matter', in *Christensen's physics of diagnostic radiology.-4th ed.*, Lippincott Williams & Wilkins, Philadelphia, Pennsylvania USA.

Tickner, J. 2000, 'Modelling detector responses to neutrons using MCNP', paper presented to Advanced Monte Carlo for Radiation Physics, Particle Transport Simulation and Applications, Proceedings of the Monte Carlo 2000 Conference, Lisbon, Spain, 23-26 Oct., 2000.

Tran, C.Q., Chantler, C.T. & Barnea, Z. 2003, 'X-ray mass attenuation coefficient of silicon: theory versus experiment', *Phys Rev Lett*, vol. 90, no. 25 Pt 1, p. 257401.

*Tungsten Products: Poly Tungsten*, viewed 14 April 2013,  
<<http://www.stanfordmaterials.com/poly-tungsten.html>>.

Umeda, N., Bandourko, V.V., Vasilets, V.N. & Kishimoto, N. 2003, 'Metal precipitation process in polymers induced by ion implantation of 60 keV Cu<sup>+</sup>', *Nuclear Instruments and Methods in Physics Research B*, vol. 206, pp. 657–62.

Van Den Heuvel, F., Locquet, J.P. & Nuyts, S. 2010, 'Beam energy considerations for gold nano-particle enhanced radiation treatment', *Physics in Medicine and Biology*, vol. 55, no. 16, pp. 4509-20.

Wang, T., Liu, Z., Lu, M., Wen, B., Ouyang, Q., Chen, Y., Zhu, C., Gao, P., Li, C., Cao, M. & Qi, L. 2013, 'Graphene-Fe<sub>3</sub>O<sub>4</sub> nanohybrids: Synthesis and excellent electromagnetic absorption properties', *Journal of Applied Physics*, vol. 113, no. 2, pp. 024314-8.

Wardray. 2005-2011, *Premac Lead Acrylic, Part of the Wardray Premise Total Radiation Shielding Package*, Wardray Premise Ltd., viewed 4 May 2011, <<http://wardray-premise.com/structural/materials/premac.html>>.

Wu, Y., Zhang, T., Zhang, H., Zhang, X., Deng, Z. & Zhou, G. 2000, 'Electrical properties of polymer modified by metal ion implantation', *Nuclear Instruments and Methods in Physics Research Section B: Beam Interactions with Materials and Atoms*, vol. 169, no. 1–4, pp. 89-93.



*X-ray absorption*, viewed 19 April 2013, <<http://www.helsinki.fi/~serimaa/xray-luento/xray-absorption.html>>.

*X-ray Interaction (Part I)*, viewed 31 January 2013, <<http://newton.ex.ac.uk/teaching/resources/jjm/pam2011/Lectures/X-ray%20Interaction%201.pdf>>.

*X-ray Interactions*, viewed 31 January 2013, <<http://whs.wsd.wednet.edu/faculty/busse/mathhomepage/busseclasses/radiationphysics/lecturenotes/chapter12/chapter12.html>>.

*X-rays 2012*, Australian Radiation Protection and Nuclear Safety Agency, viewed 16 April 2013, <<http://www.arpsansa.gov.au/radiationprotection/basics/xrays.cfm>>.

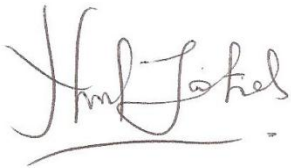
Wu, Y., Zhang, T., Zhang, H., Zhang, X. & Deng, Z. 2000, 'Polymer modification by MEVVA source deposited and ion implantation', *Surface and Coatings Technology*, vol. 131, no. 1–3, pp. 520-4.

Yu, D.G., Shen, X.X., Chris, B.W., Kenneth, W., Zhu, L.M. & Bligh, S.W.A. 2009, 'Oral fast-dissolving drug delivery membranes prepared from electrospun polyvinylpyrrolidone ultrafine fibres', *Nanotechnology*, vol. 20, no. 5, p. 055104.

“Every reasonable effort has been made to acknowledge the owners of copyright material. I would be pleased to hear from any copyright owner who has been omitted or incorrectly acknowledged.”

Nurul Zahirah Binti Noor Azman

Signature:

A handwritten signature in black ink, appearing to read 'Nurul Zahirah Binti Noor Azman', written in a cursive style. The signature is positioned above a horizontal line.

Date: 5<sup>th</sup> September 2013